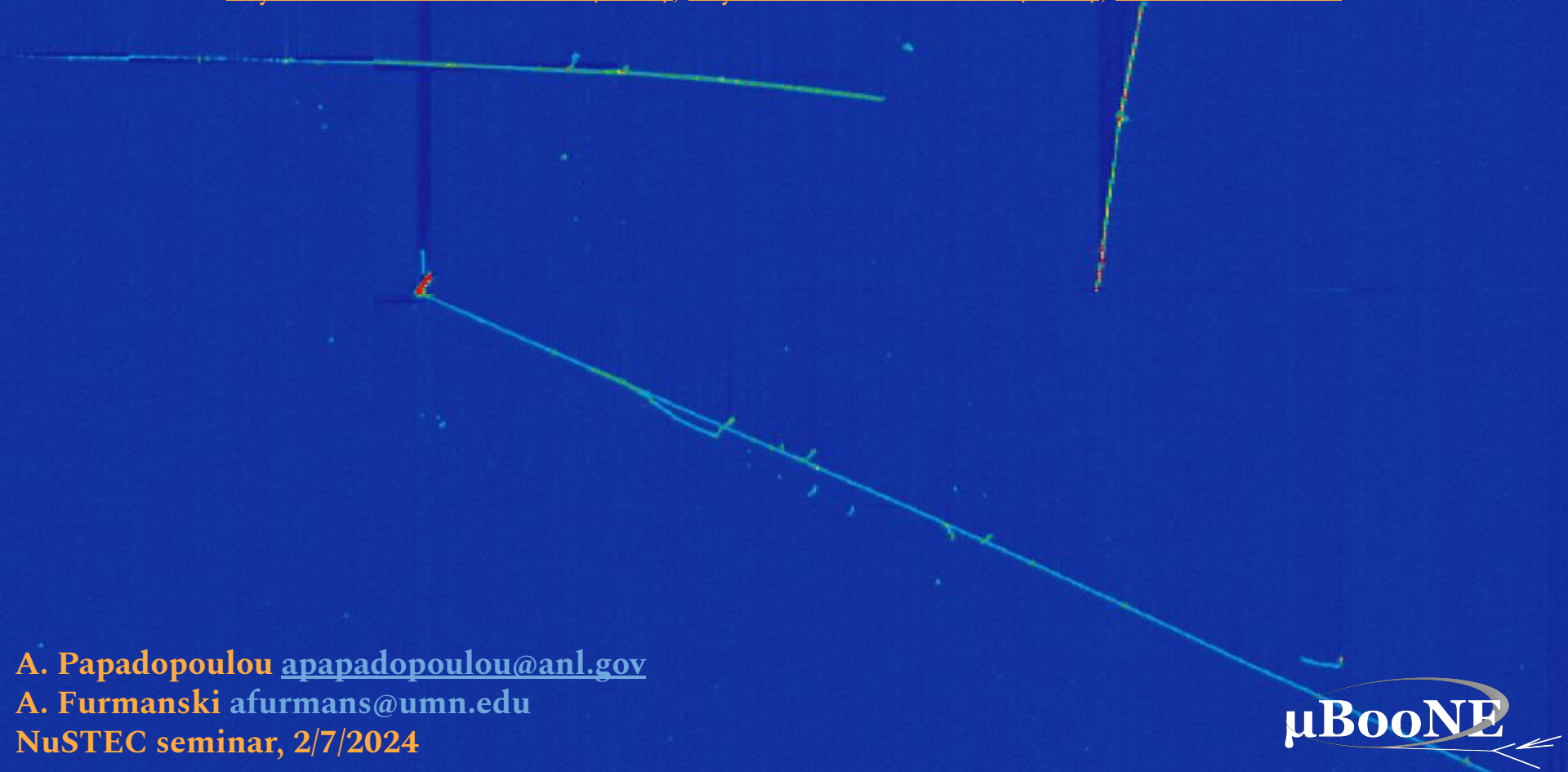


# Kinematic imbalance in neutrino-argon interactions at MicroBooNE

[Phys. Rev. Lett. 131, 101802 \(2023\)](#), [Phys. Rev. D 108, 053002 \(2023\)](#), [arXiv:2310.06082](#)



A. Papadopoulou [apapadopoulou@anl.gov](mailto:apapadopoulou@anl.gov)  
A. Furmanski [afurmans@umn.edu](mailto:afurmans@umn.edu)  
NuSTEC seminar, 2/7/2024

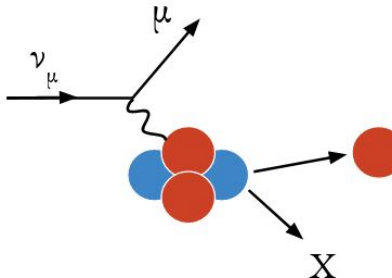
μBooNE

# Neutrino-Nucleus Modeling

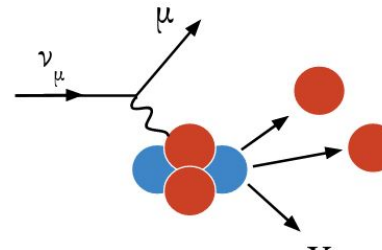
Challenging ...

- Broad neutrino spectra
- Various complex interaction mechanisms

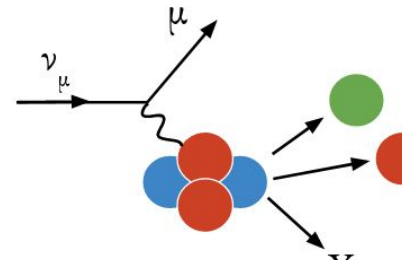
Any mismodeling in neutrino event generator simulation predictions can limit experimental sensitivity



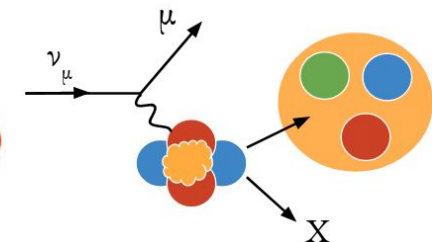
Quasi-elastic (QE)



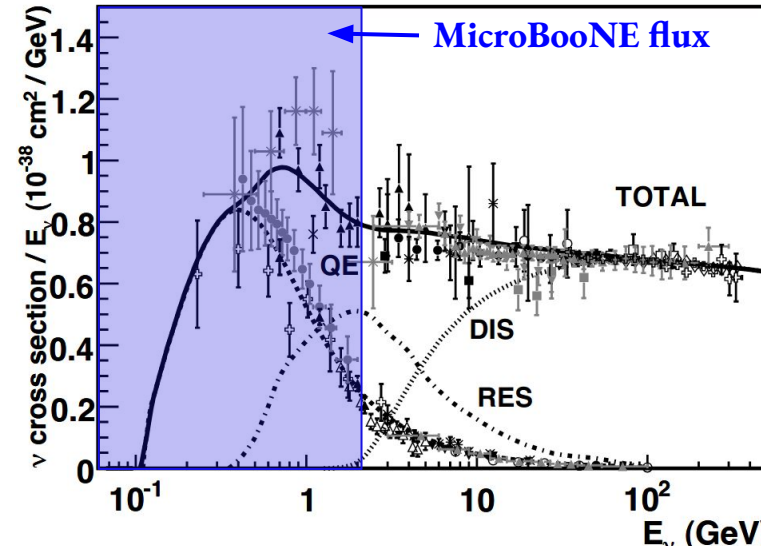
Meson Exchange Current (MEC)



Resonance (RES)

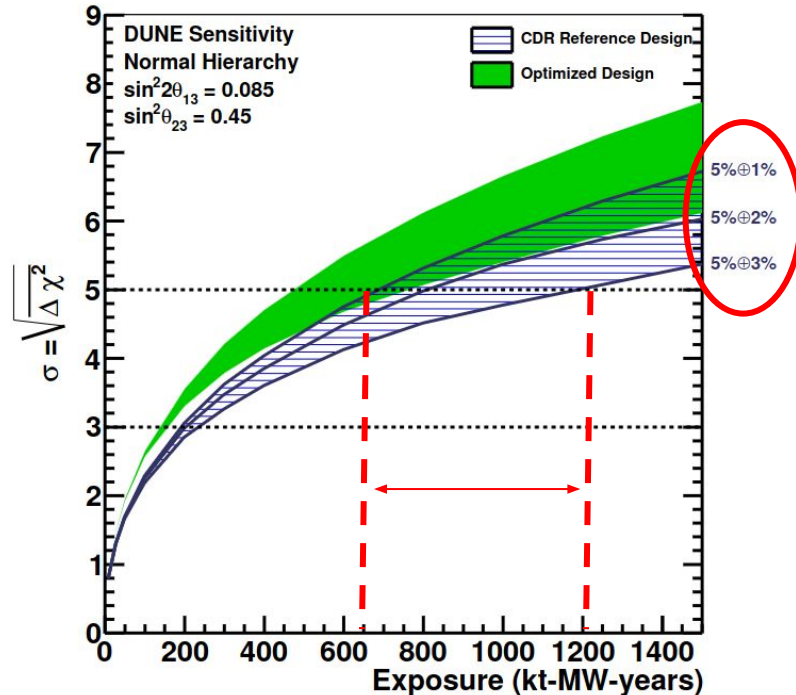


Deep Inelastic Scattering (DIS)



# Future Experiments

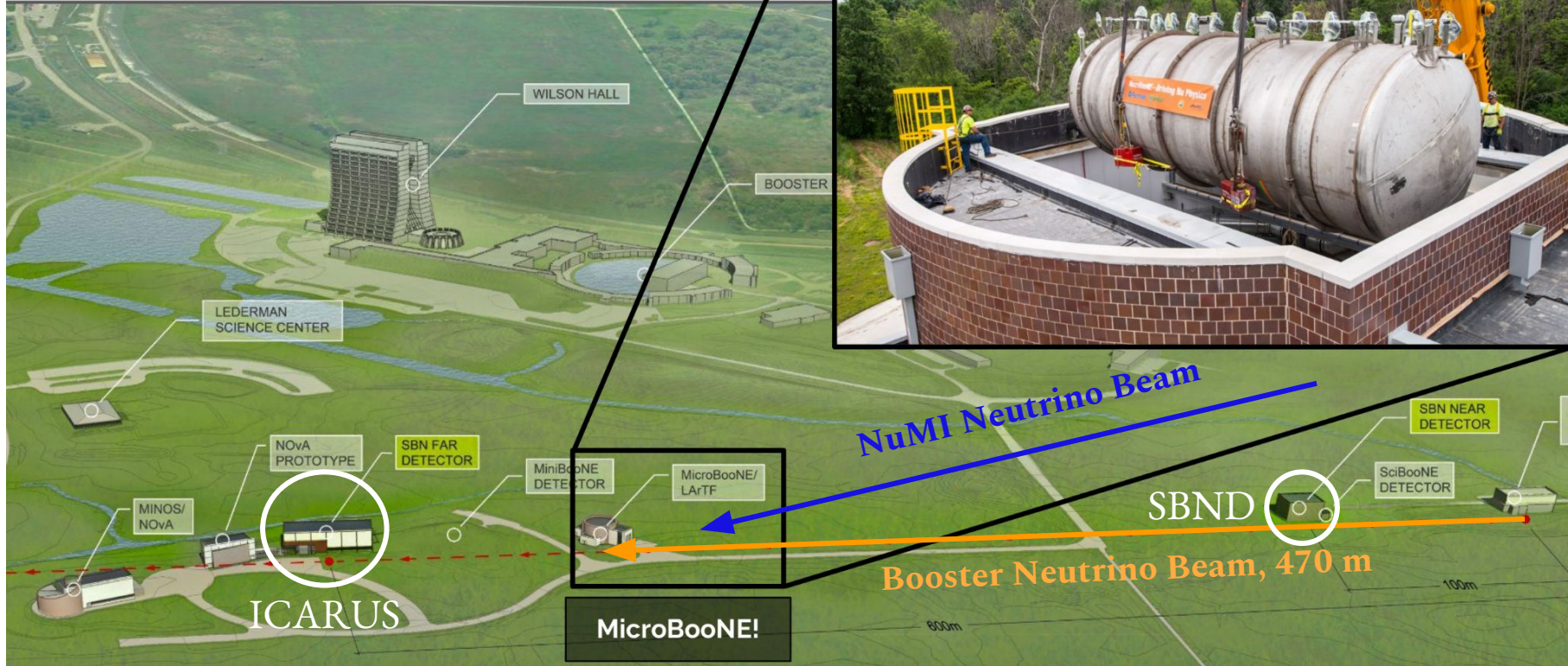
50% CP Violation Sensitivity



- Mismodeling can impact required run time of forthcoming flagship experiments
- But ... head start with Short-Baseline Neutrino (SBN) Program (MicroBooNE, SBND, ICARUS)

DUNE CDR, [arXiv:1512.06148](https://arxiv.org/abs/1512.06148)

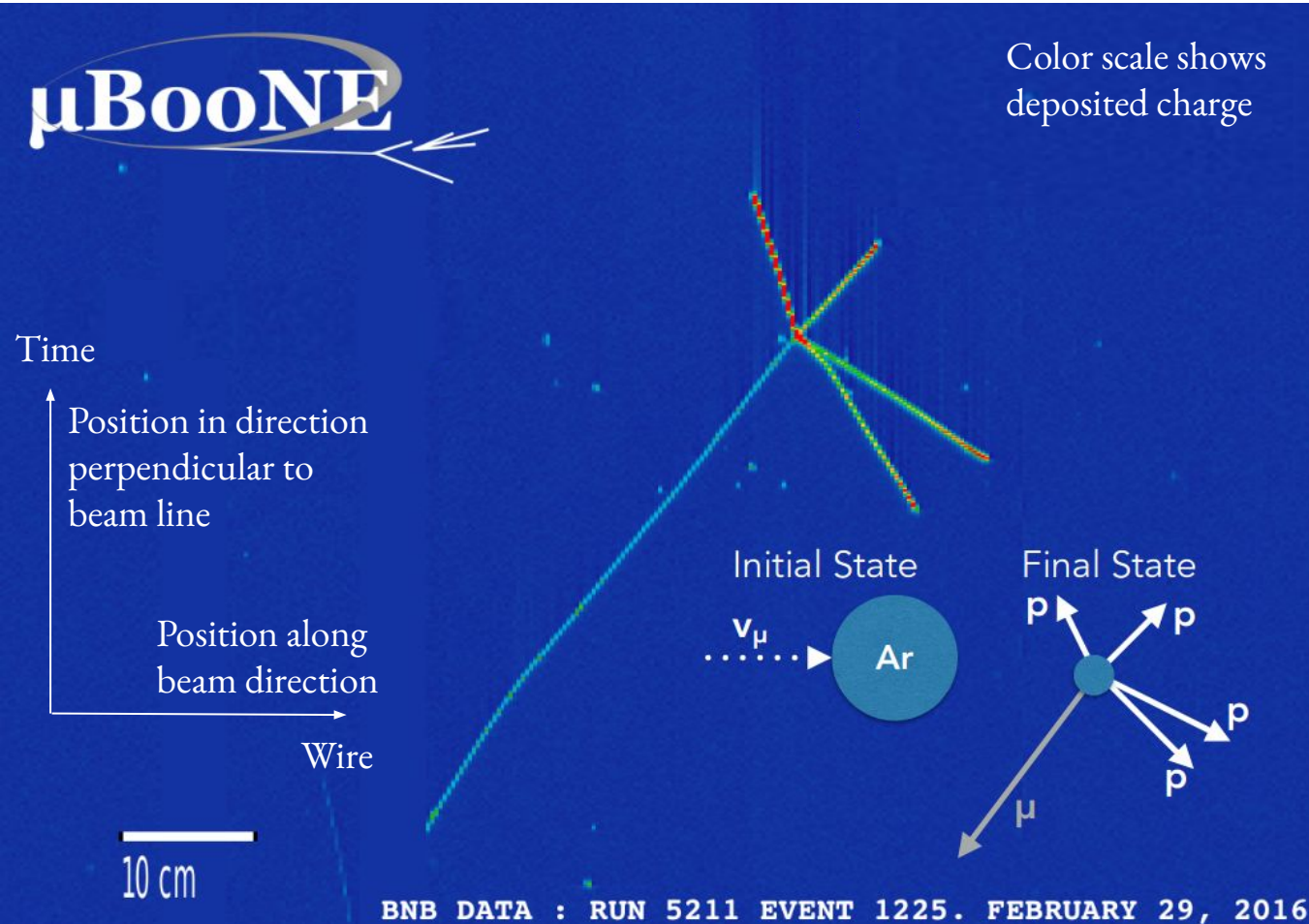
# MicroBooNE@FNAL



MicroBooNE being lowered into LArTF

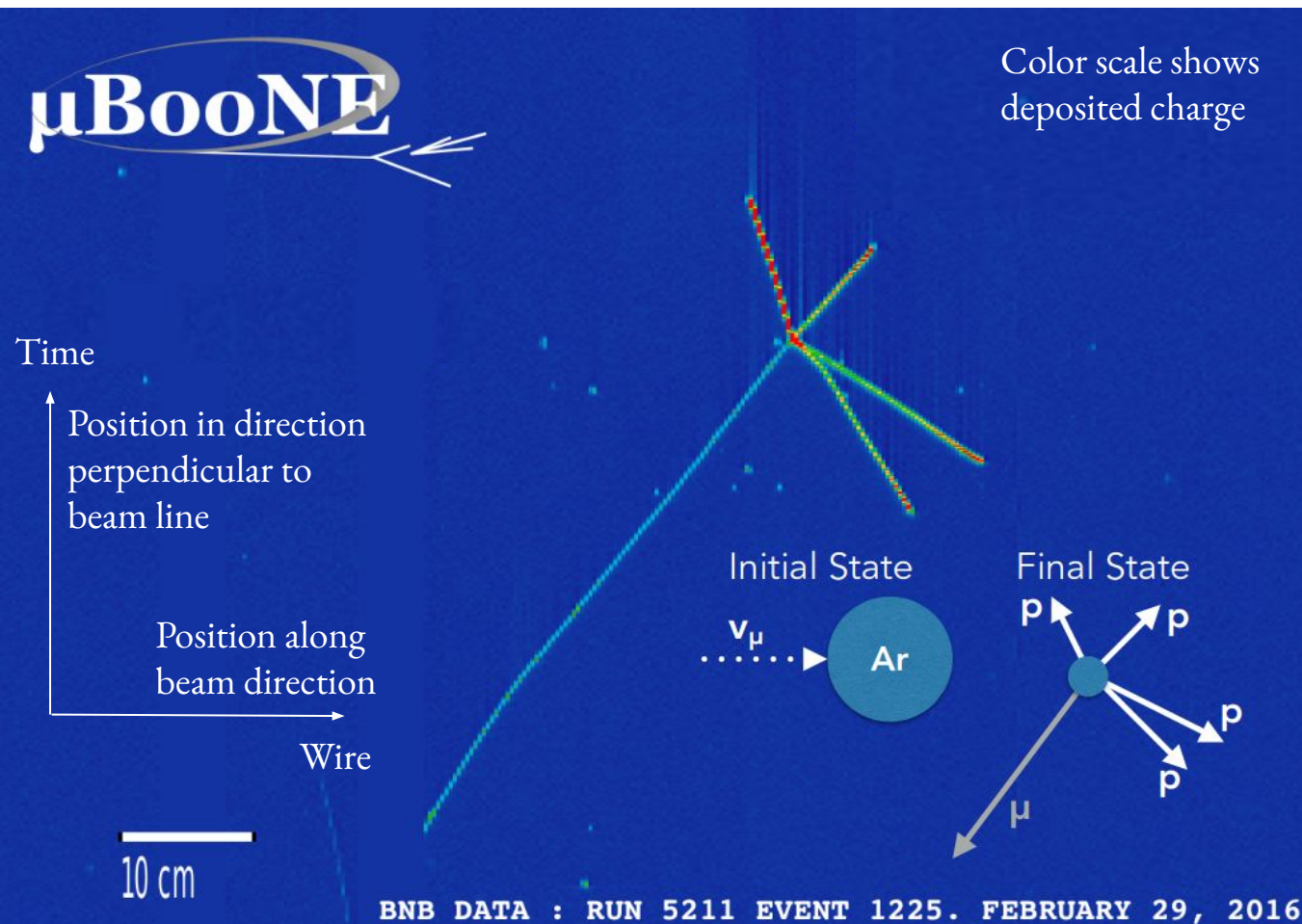
85 tonne Liquid Argon Time Projection Chamber (LArTPC)  
[JINST 12, P02017 \(2017\)](https://arxiv.org/abs/1702.07027)

# MicroBooNE Data Events



- Excellent spatial resolution
- Low detection thresholds
- Precise calorimetric information
- Powerful particle identification

# MicroBooNE Data Events



- Largest available neutrino-argon data set with ~500k recorded neutrino interactions
- 15 released and more than 30 active MicroBooNE cross section analyses
- Multiple topologies investigated

# Already Public Results

## CC inclusive

- 1D  $\nu_\mu$  CC inclusive @ BNB  
[Phys. Rev. Lett. 123, 131801 \(2019\)](#)
- 1D  $\nu_\mu$  CC  $E_\nu$  @ BNB  
[Phys. Rev. Lett. 128, 151801 \(2022\)](#)
- 3D CC  $E_\nu$  @ BNB  
[arXiv:2307.06413](#), submitted to PRL
- 1D  $\nu_e$  CC inclusive @ NuMI  
[Phys. Rev. D105, L051102 \(2022\)](#)  
[Phys. Rev. D104, 052002 \(2021\)](#)

## Pion production

- $\nu_\mu$  NC $\pi^0$  @ BNB  
[Phys. Rev. D 107, 012004 \(2023\)](#)

## Rare channels

- $\eta$  production @ BNB, submitted to PRL  
[arXiv:2305.16249](#)
- $\Lambda$  production @ NuMI  
[Phys. Rev. Lett. 130, 231802 \(2023\)](#)

## CC0 $\pi$

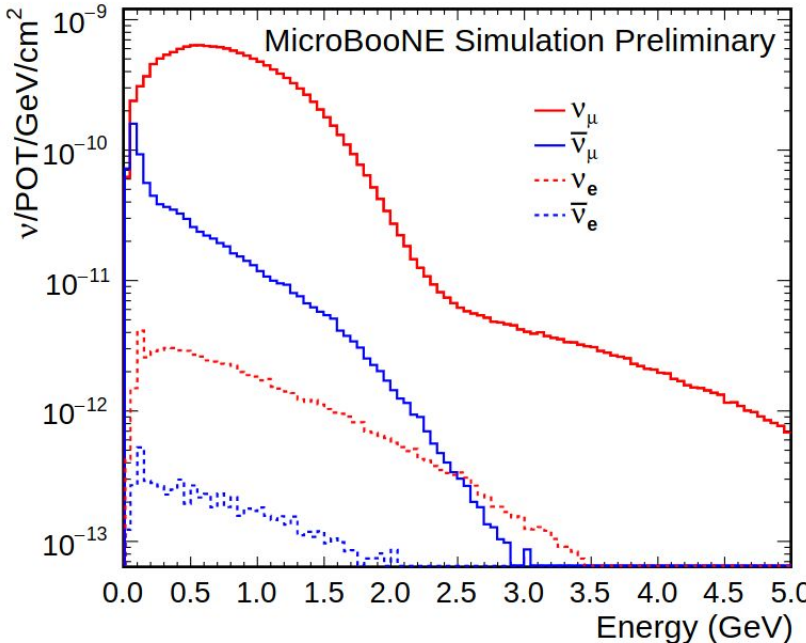
- 1D  $\nu_e$  CCNp0 $\pi$  @ BNB  
[Phys. Rev. D 106, L051102 \(2022\)](#)
- 1D & 2D  $\nu_\mu$  CC1p0 $\pi$  Transverse Imbalance @ BNB  
[Phys. Rev. Lett. 131, 101802 \(2023\)](#)  
[Phys. Rev. D 108, 053002 \(2023\)](#)
- 1D & 2D  $\nu_\mu$  CC1p0 $\pi$  Generalized Imbalance @ BNB  
[arXiv:2310.06082](#), accepted for publication in PRD
- 1D  $\nu_\mu$  CC1p0 $\pi$  @ BNB  
[Phys. Rev. Lett. 125, 201803 \(2020\)](#)
- 1D  $\nu_\mu$  CC2p @ BNB  
[arXiv:2211.03734](#)
- 1D  $\nu_\mu$  CCNp0 $\pi$  @ BNB  
[Phys. Rev. D102, 112013 \(2020\)](#)

15 cross section publications  
and way more to come!

# Today's Discussion



## Booster Neutrino Beam (BNB) flux



[Phys. Rev. D 79, 072002 \(2009\)](https://doi.org/10.1103/PhysRevD.79.072002)

- 1D & 2D  $\nu_\mu$  CC1p0 $\pi$  Transverse Imbalance @ BNB  
[Phys. Rev. Lett. 131, 101802 \(2023\)](https://doi.org/10.1103/PhysRevLett.131.101802)  
[Phys. Rev. D 108, 053002 \(2023\)](https://doi.org/10.1103/PhysRevD.108.053002)
- 1D & 2D  $\nu_\mu$  CC1p0 $\pi$  Generalized Imbalance @ BNB  
[arXiv:2310.06082](https://arxiv.org/abs/2310.06082), accepted for publication in PRD

Single- and double-differential muon-neutrino cross-section measurements in kinematic imbalance variables using BNB flux

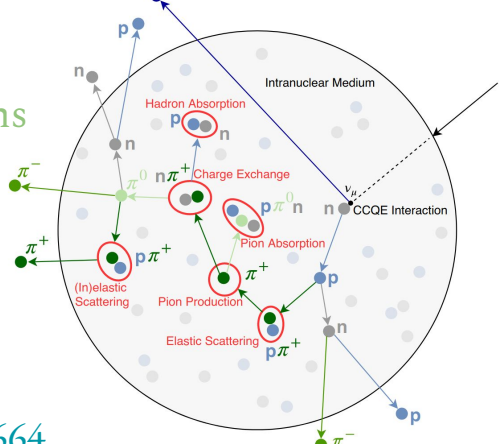
# Nuclear Effects

- Fermi motion
- Final state interactions
- Meson exchange currents
- ...

}

Known unknowns that need to be accurately simulated

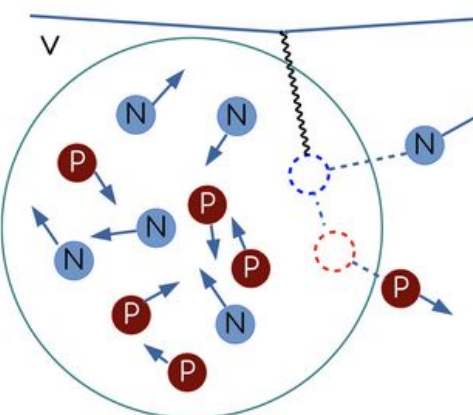
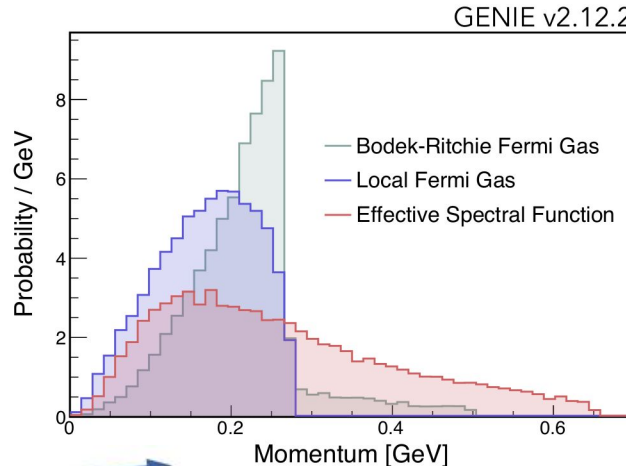
Hadron reinteractions



arXiv:2201.04664

[Rev. Mod. Phys. 89, 045002 \(2017\)](#)

Struck nucleon motion in argon



Nucleon-nucleon relative angle and momenta

[J. Wolcott](#)

[Wine & Cheese Seminar](#)

# CC1p0 $\pi$ Quasielastic-like Signal Definition

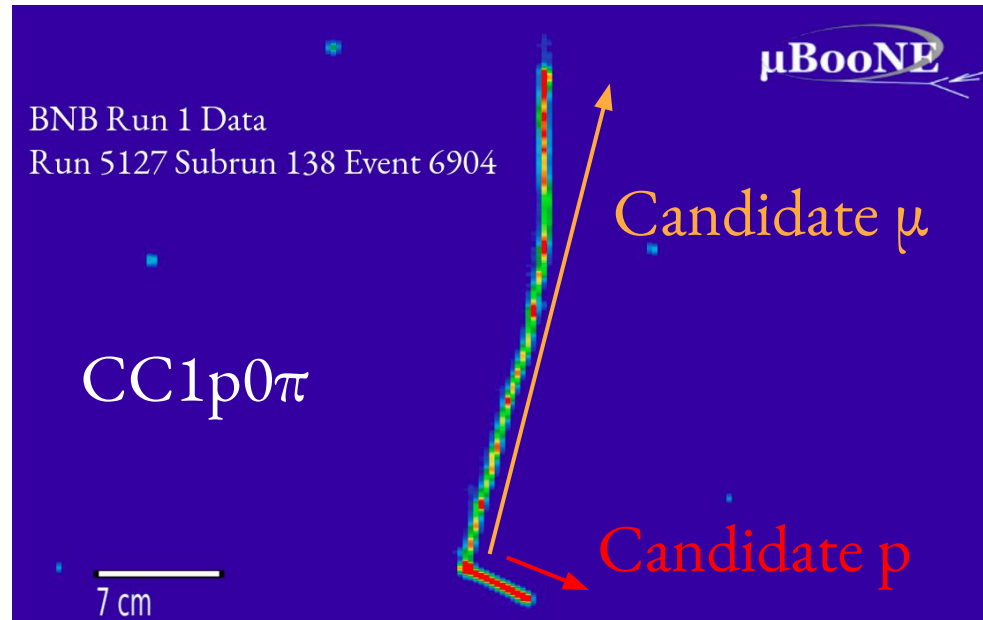
Ranges driven by minimum track length, track containment, hadronic reinteractions, and systematics

- 1 muon  
 $100 < P_\mu < 1200$  MeV/c
- 1 proton  
 $300 < P_p < 1000$  MeV/c
- No  $\pi^\pm$  with  $P_\pi > 70$  MeV/c
- No  $\pi^0$  or heavier mesons
- Any number of neutrons

9051 CC1p0 $\pi$  candidate data events

CC1p0 $\pi$  ~10% efficiency

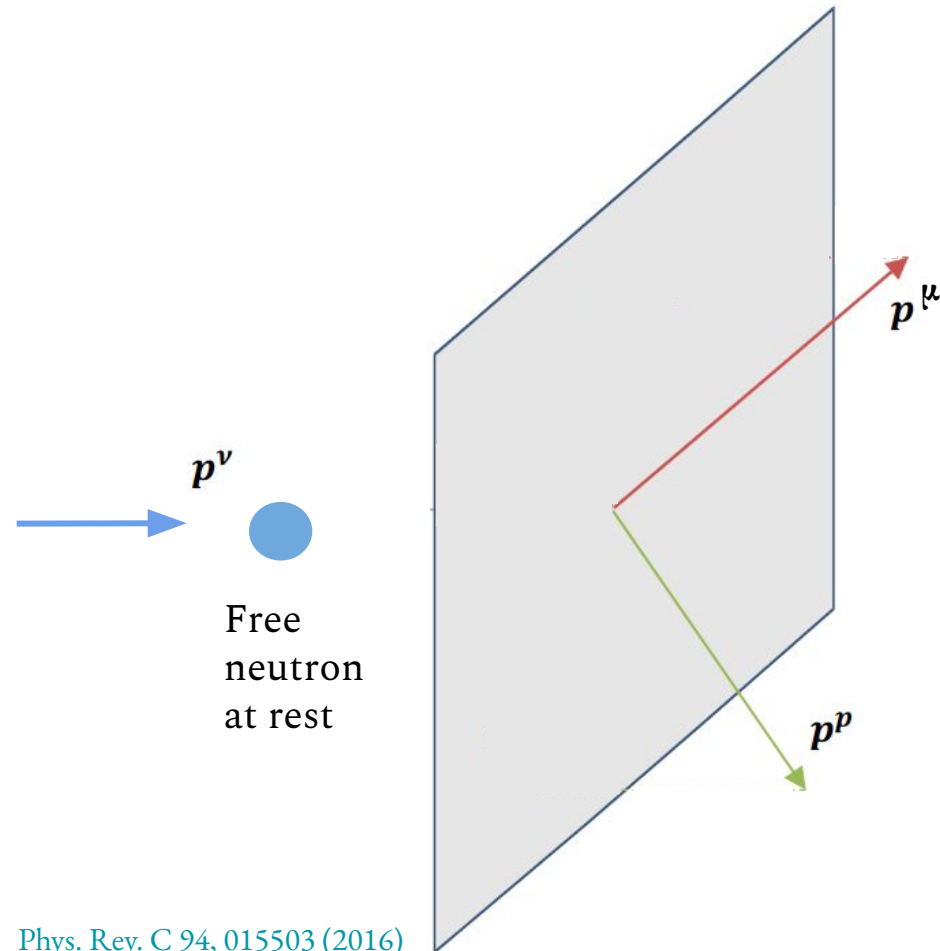
~70% purity



[Phys. Rev. Lett. 131, 101802 \(2023\)](#)  
[Phys. Rev. D 108, 053002 \(2023\)](#)  
[arXiv:2310.06082](#)

MC: GENIE v3.0.6 G18\_10a\_02\_11b + tune\*  
Nieves QE & MEC, Berger Sehgal RES  
\* [Phys. Rev. D 105, 072001 \(2022\)](#)

# Transverse Kinematic Imbalance (TKI)



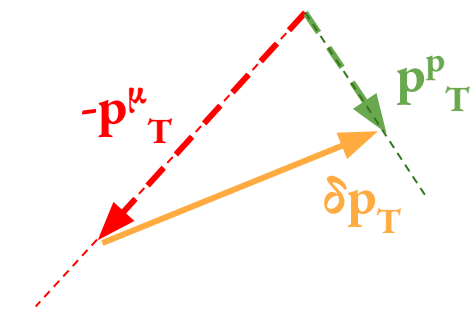
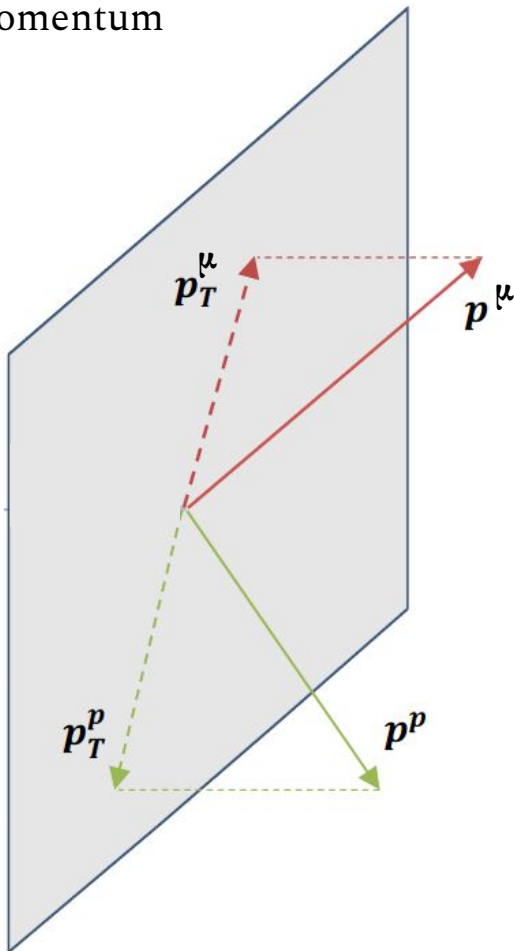
# Transverse Kinematic Imbalance (TKI)

Transverse missing momentum

$$\delta p_T = | p_T^\mu + p_T^p | = 0$$



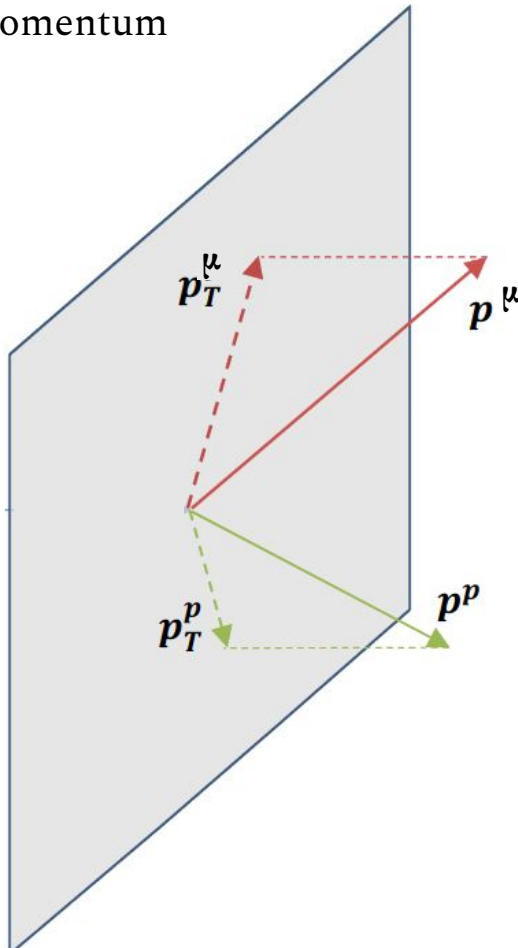
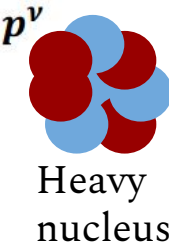
Free  
neutron  
at rest



# Transverse Kinematic Imbalance (TKI)

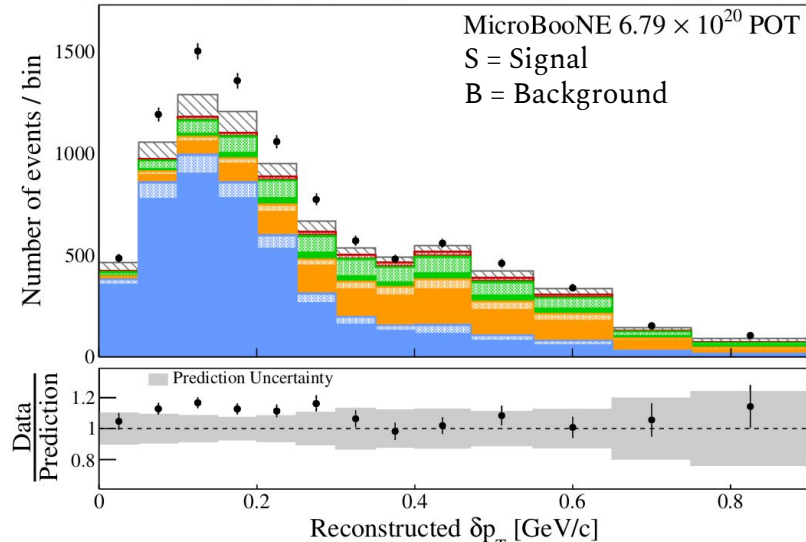
Transverse missing momentum

$$\delta p_T = | \mathbf{p}_T^\mu + \mathbf{p}_T^p | > 0$$



Sensitivity to ground state and final state interactions / multi-nucleon effects

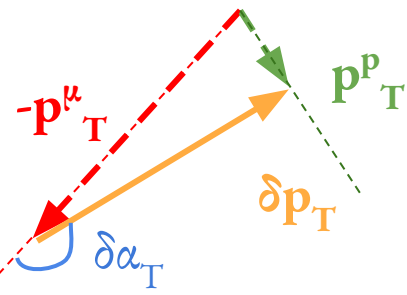
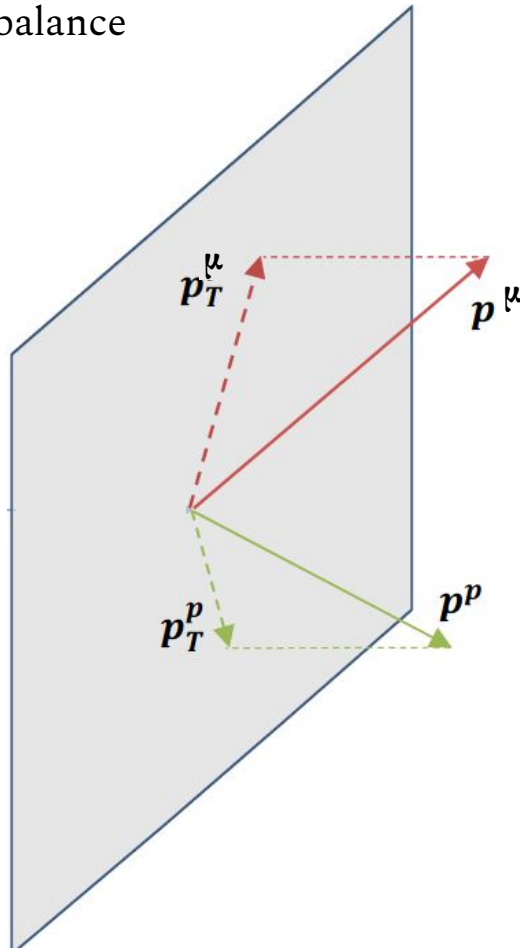
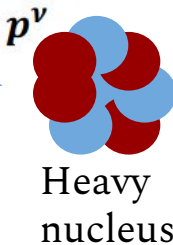
◆ BNB Data    █ S QE (51%)    █ S MEC (15%)    █ S RES (3%)    █ S DIS (0%)  
█ Cosmic (8%)    █ B QE (7%)    █ B MEC (4%)    █ B RES (9%)    █ B DIS (2%)



# Transverse Kinematic Imbalance (TKI)

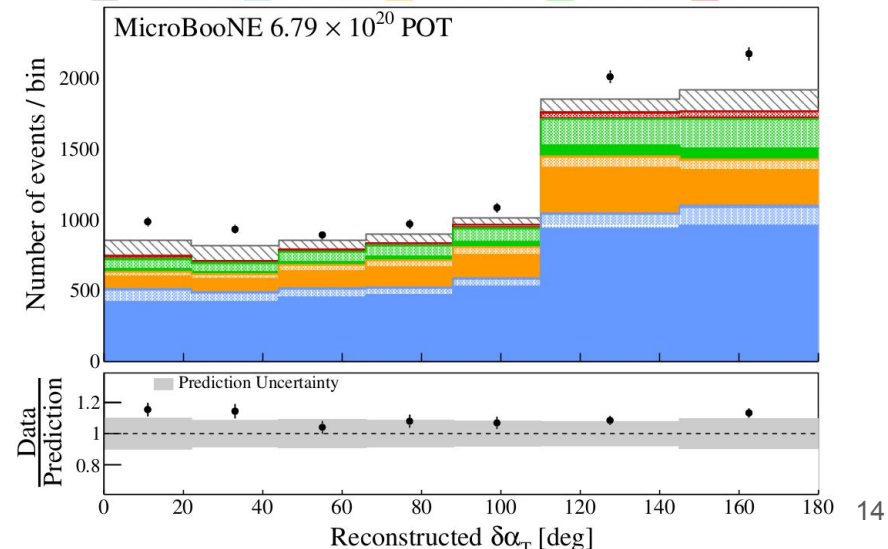
Orientation of the imbalance

$$\delta\alpha_T = \text{acos}(-\mathbf{p}_T^\mu \cdot \delta\mathbf{p}_T)$$



Sensitivity to final state interactions  
and multi-nucleon effects

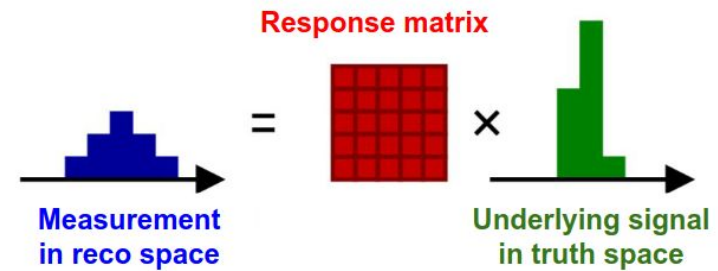
◆ BNB Data ◆ S QE (51%) ◆ S MEC (15%) ◆ S RES (3%) ◆ S DIS (0%)  
▨ Cosmic (8%) ▨ B QE (7%) ▨ B MEC (4%) ▨ B RES (9%) ▨ B DIS (2%)



# Unfolding & Regularization

- Nominal flux-averaged cross section unfolded with Wiener-SVD method [[JINST 12 P10002 \(2017\)](#)]
- Maximizes the overall signal to noise ratio through the application of the Wiener filter
- Reported covariance matrix includes all statistical and systematic model uncertainties
- Bias introduced in regularization captured in a (known) smearing matrix  $A_C$
- $A_C$  matrix is necessary ingredient to perform a comparison between reported cross sections and event generator predictions

$$M_i = \sum_j R_{ij} \cdot S_j + B_i$$

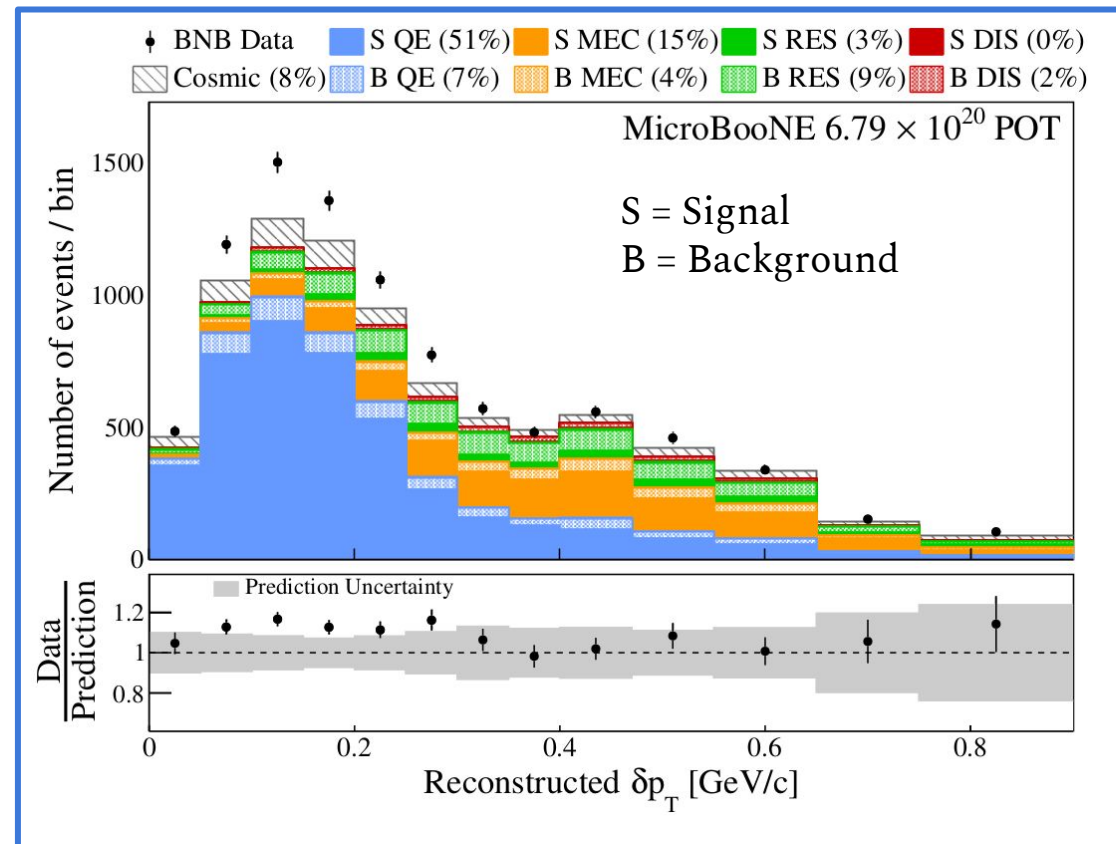


# Cross Section Extraction with Wiener SVD Unfolding

[JINST 12 P10002 \(2017\)](#)

## Input Quantities

- Measurement (Data)
- Background (Cosmics + MC)
- Response Matrix (MC)
- Total Covariance Matrix (MC)



[Phys. Rev. D 108, 053002 \(2023\)](#)

# Cross Section Extraction with Wiener SVD Unfolding

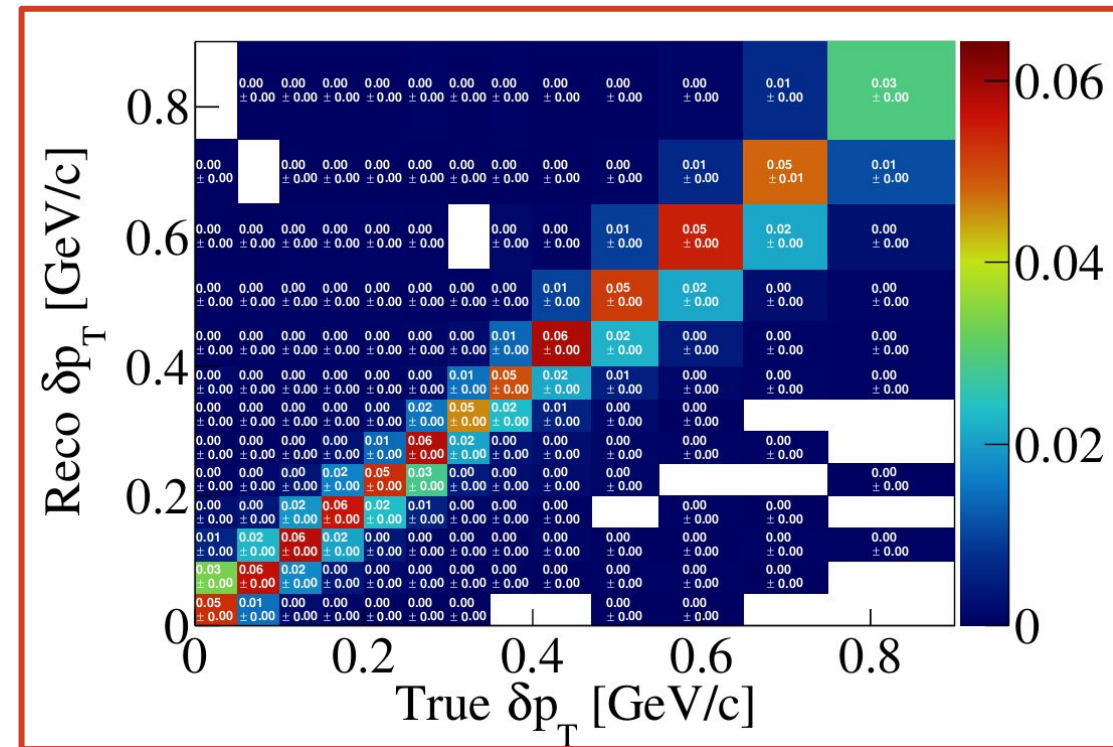
JINST 12 P10002 (2017)

## Input Quantities

- Measurement (Data)
- Background (MC)
- Response Matrix (MC)
- Total Covariance Matrix (MC)

Probability that a generated event is reconstructed and selected

Diagonal matrix with flat ~6% efficiency



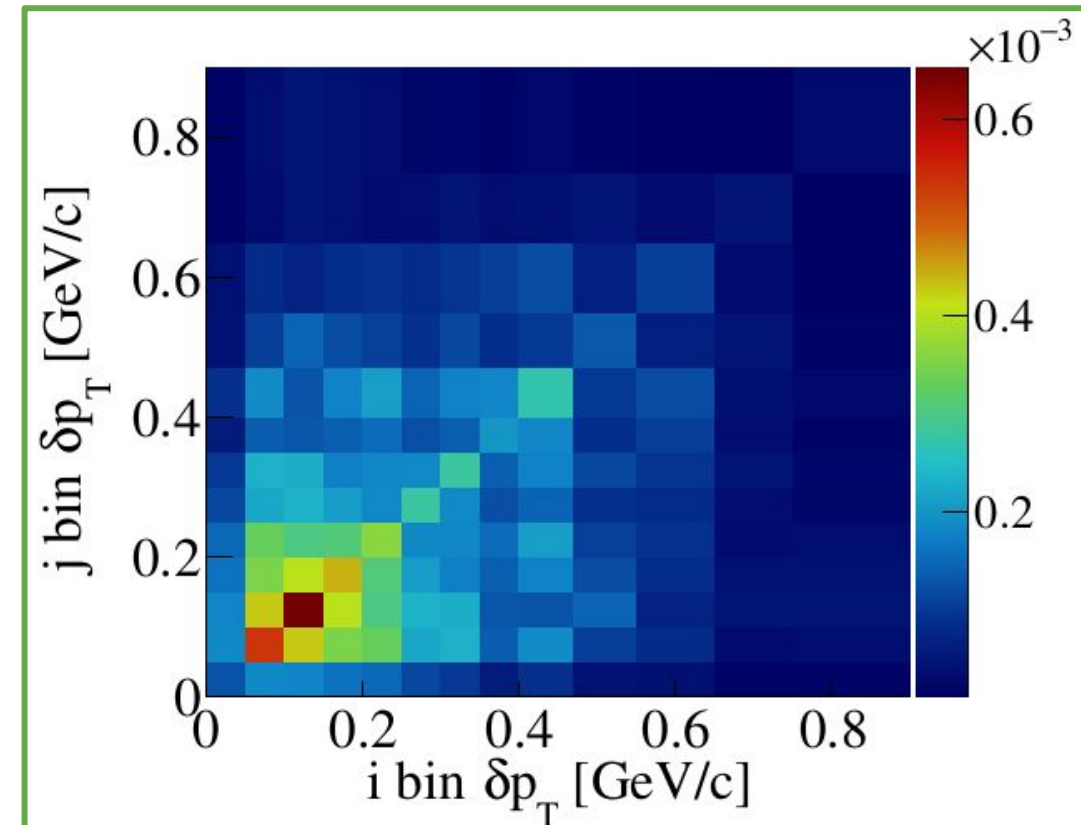
# Cross Section Extraction with Wiener SVD Unfolding

[JINST 12 P10002 \(2017\)](#)

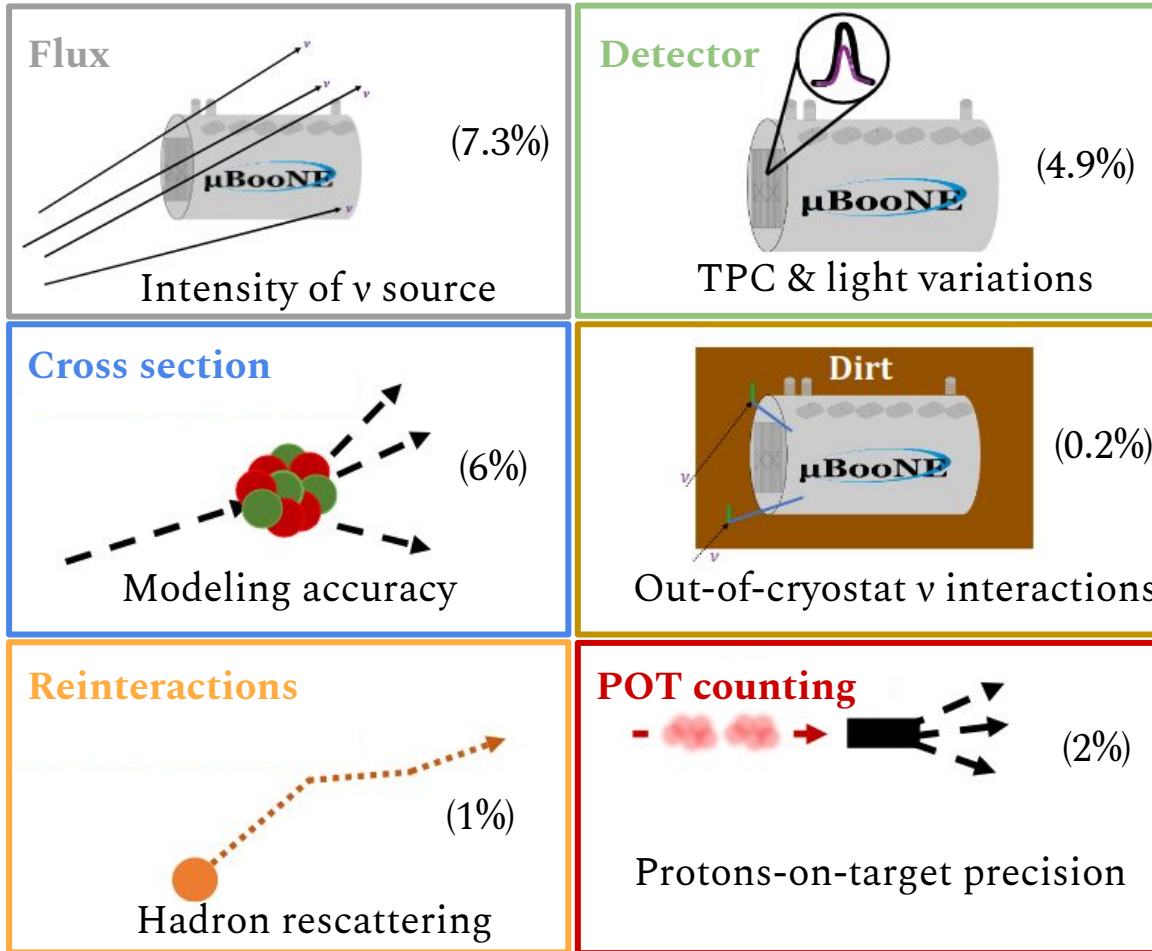
Input Quantities

- Measurement (Data)
- Background (MC)
- Response Matrix (MC)
- Total Covariance Matrix (MC)

Includes information on statistical  
and systematic model uncertainties



# Uncertainties



- + Statistical (1.5%)
- + Number of argon targets (1%)

**Total (11%)**

Systematics-dominated analysis

# Cross Section Extraction with Wiener SVD Unfolding

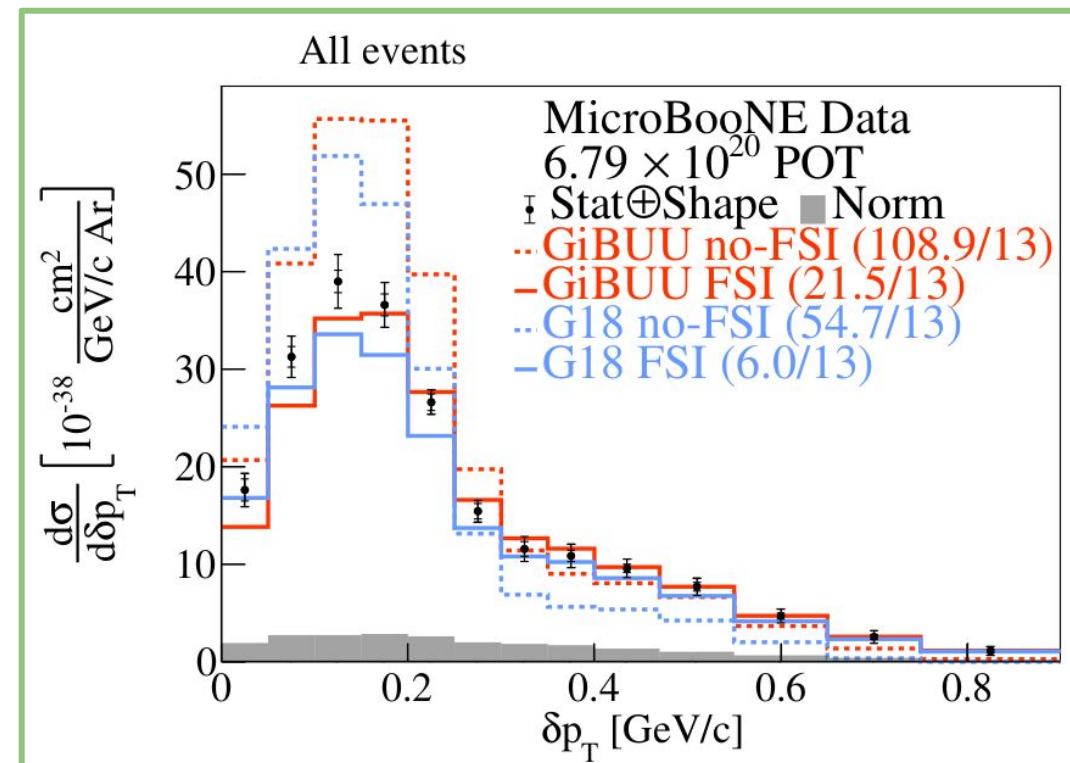
[JINST 12 P10002 \(2017\)](#)

Output quantities in  
regularized space

- Unfolded data spectrum

- Smearing Matrix  $A_C$

\*Applied on theory predictions  
and included in data release



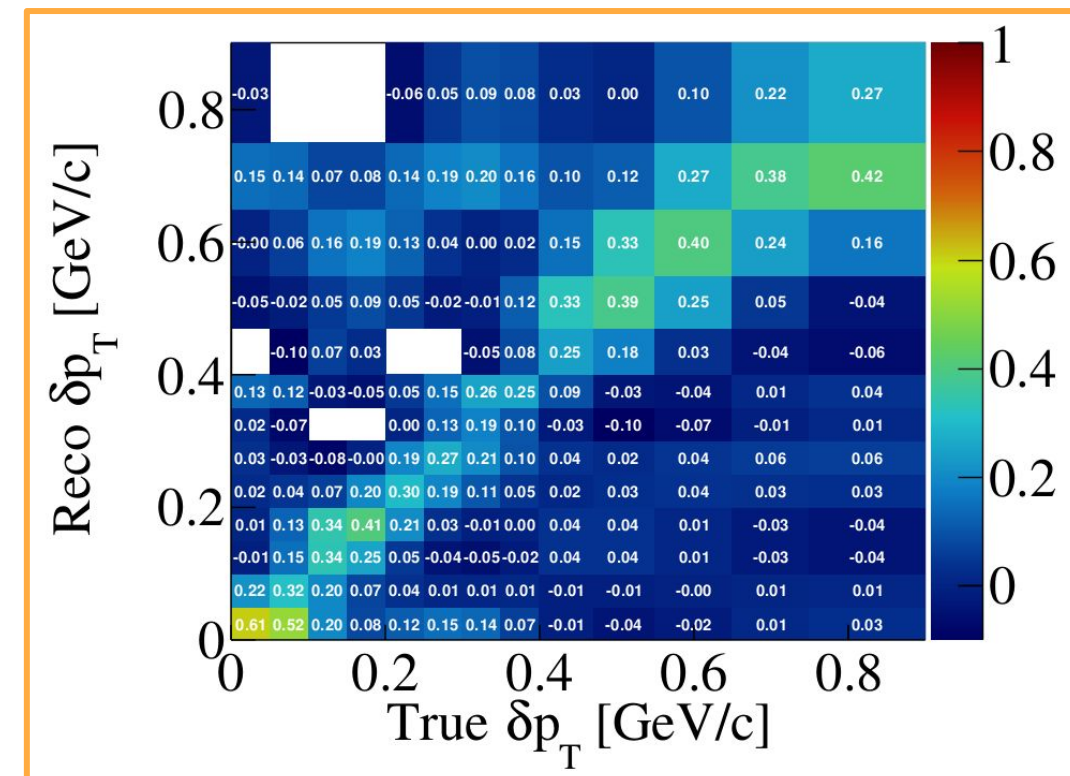
# Cross Section Extraction with Wiener SVD Unfolding

[JINST 12 P10002 \(2017\)](#)

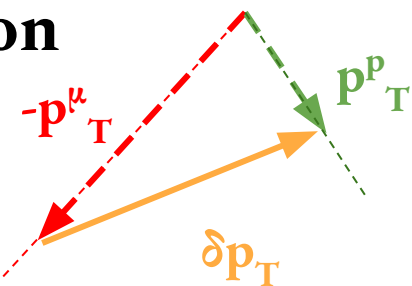
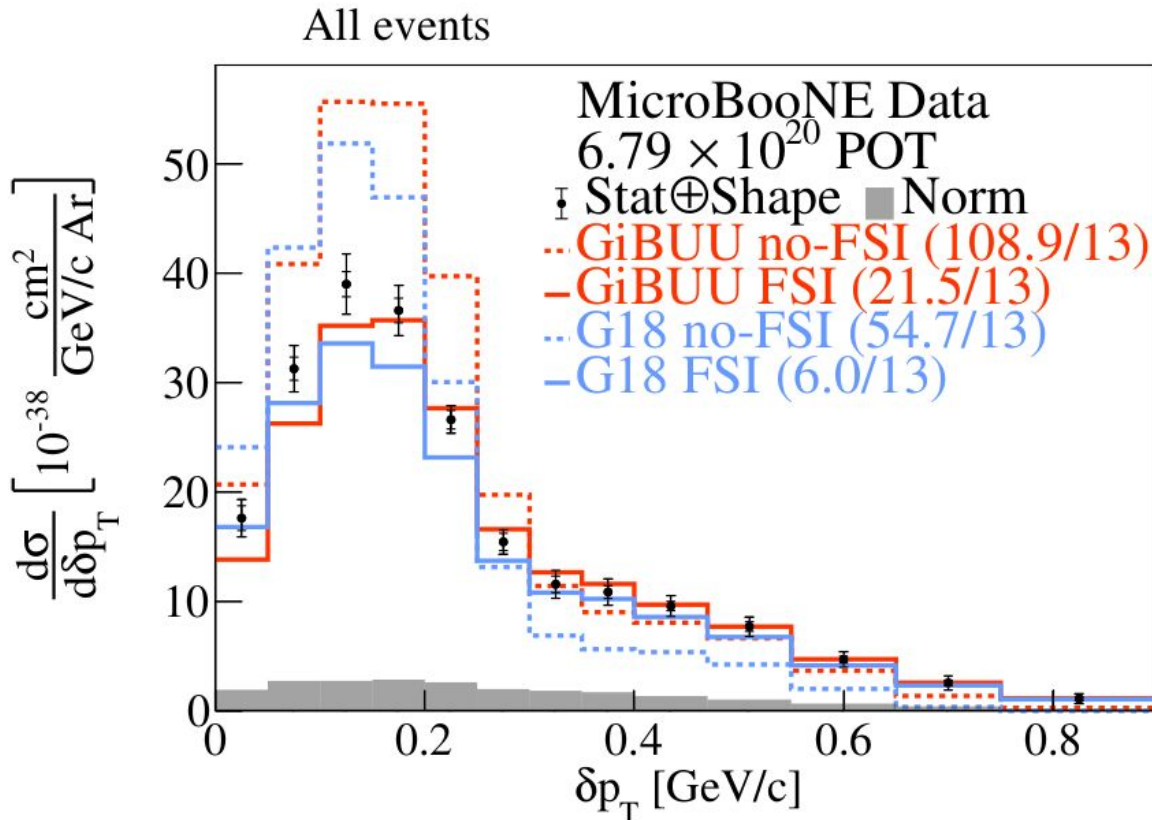
Output quantities in  
regularized space

- Unfolded data spectrum
- Smearing Matrix  $A_C$

\*Applied on theory predictions  
and included in data release



# Transverse Missing Momentum $\delta p_T$ Cross Section



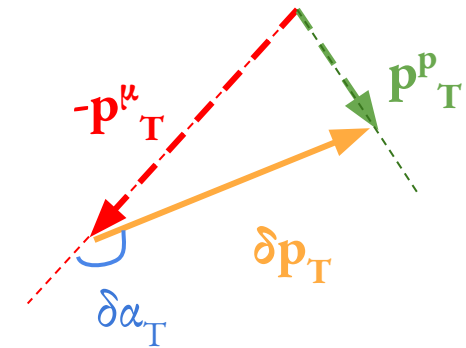
- First neutrino-argon differential cross section in  $\delta p_T$
- FSI reduces strength of the peak
- Small changes in the tail
- Data favors FSI addition

[Phys. Rev. Lett. 131, 101802 \(2023\)](#)  
[\\* Phys. Rev. D 105, 072001 \(2022\)](#)

G18 = GENIE v3.0.6 G18\_10a\_02\_11b + tune\*  
GiBUU = GiBUU 2021

# High Statistics→Into the Multiverse!

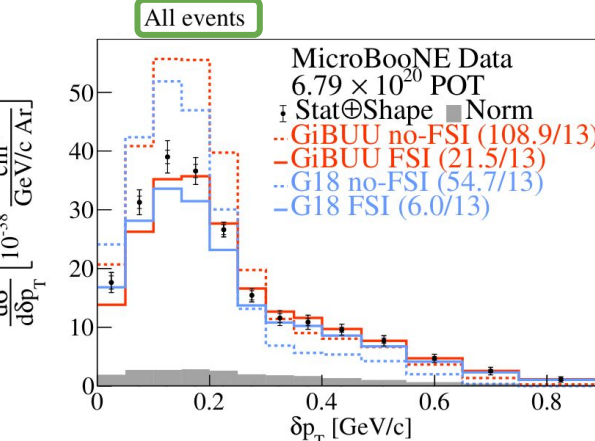
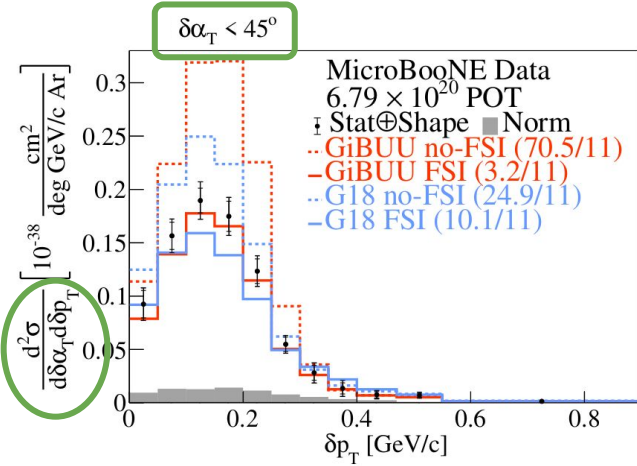
- Extension to 2D for the first time on argon
- Probe regions with greater model discrimination power



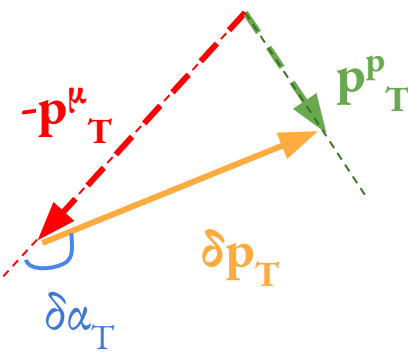
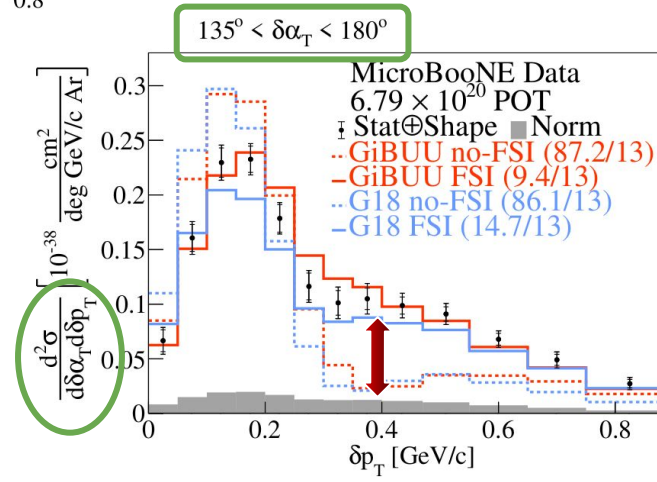
# High Statistics → Into the Multiverse!

- Extension to 2D for the first time on argon
- Probe regions with greater model discrimination power

QE-dominated

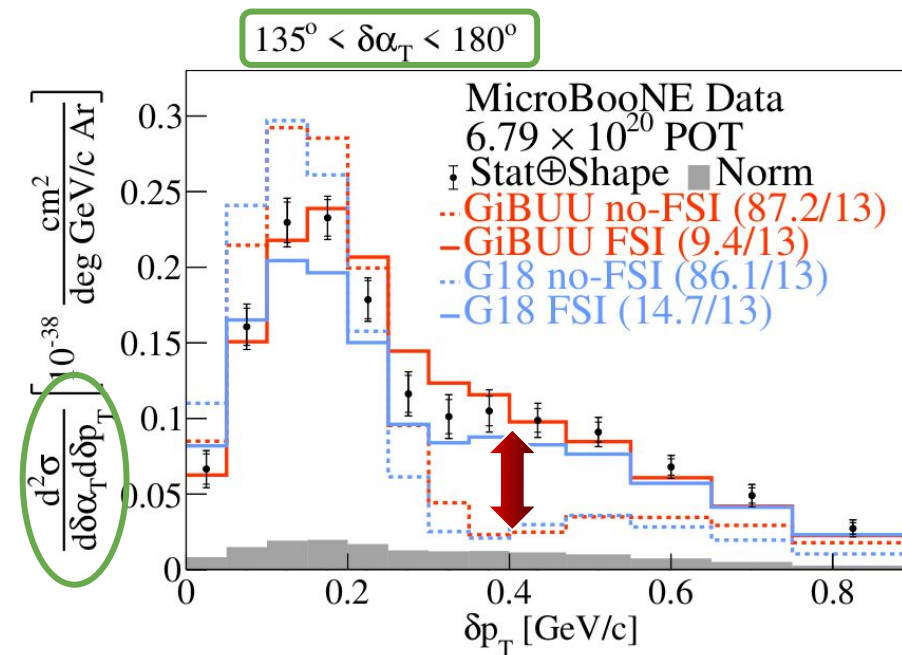
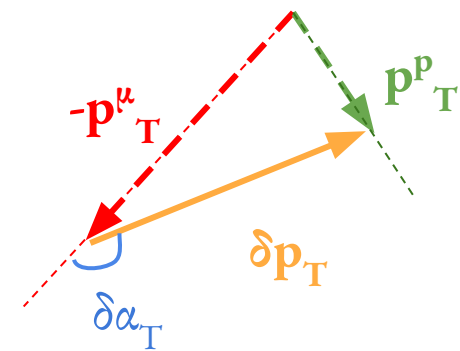


MEC/RES/FSI-dominated



# Zooming into the Multiverse!

MEC/RES/FSI-dominated

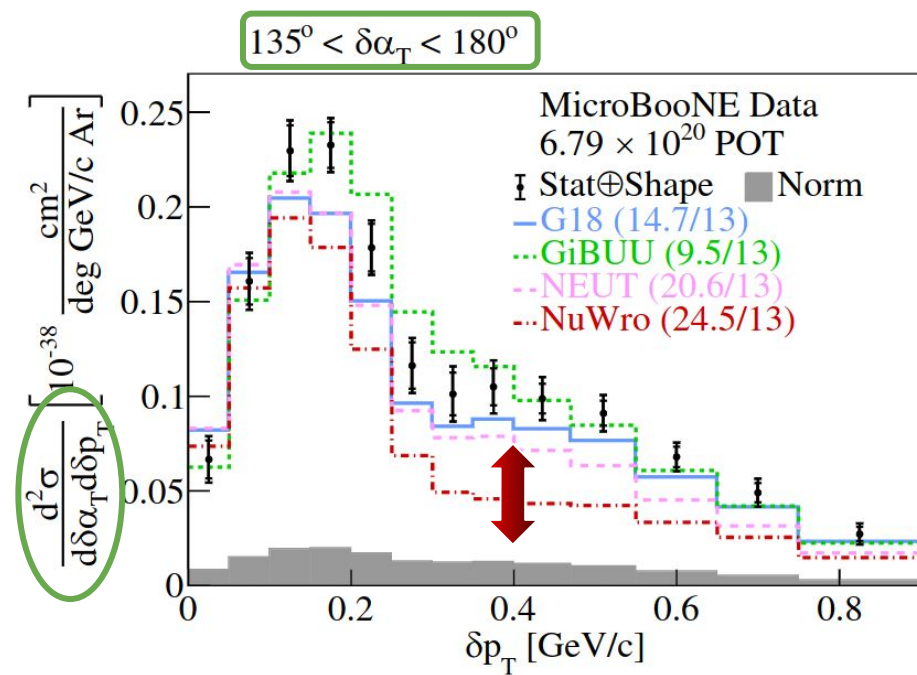


- FSI predictions in good agreement with data
- Minimal “no-FSI” contributions at high  $\delta p_T$
- High  $\delta\alpha_T$  & high  $\delta p_T$  part of phase-space ideal to test FSI / multinucleon effects

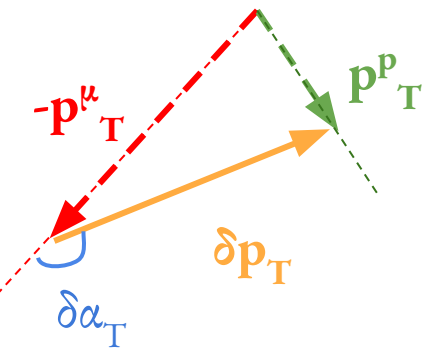
G18 = GENIE v3.0.6 G18\_10a\_02\_11b + tune\*

GiBUU = GiBUU 2021

# Multiple Generator Comparisons

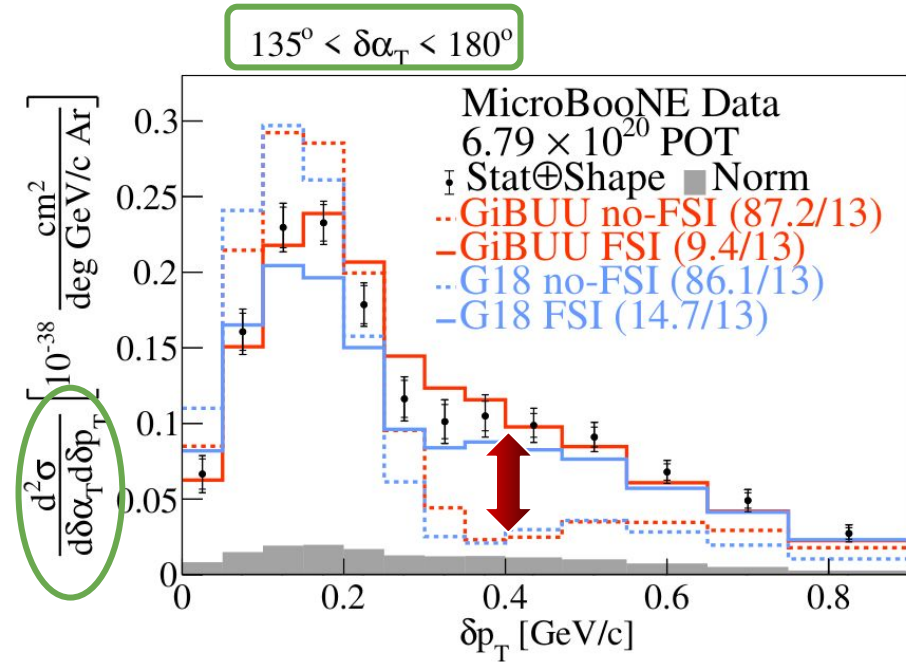


Name	Generator / Configuration
Gv2	GENIE v2.12.10
G18	GENIE v3.0.6 G18_10a_02_11a
G18T	G18 with tune
G21	GENIE v3.2.0 G21_11b_00_000
GiBUU	GiBUU 2021
NuWro	NuWro v19.02.1
NEUT	NEUT v5.4.0



# CC1p0 $\pi$ TKI Summary

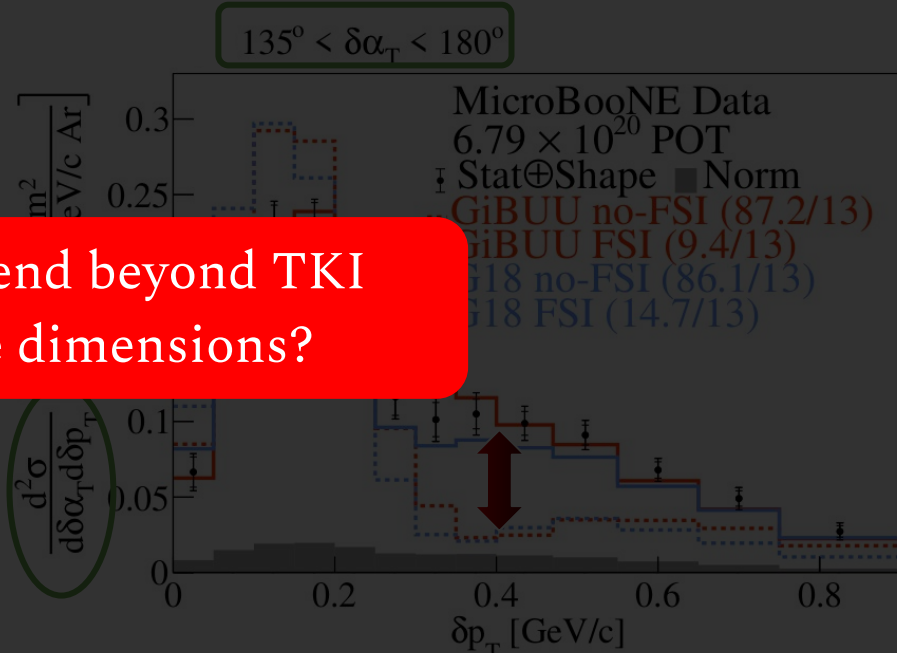
- First single- and double- differential neutrino-argon cross section measurements in TKI
- Identified parts of the phase-space with sensitivity to specific nuclear effects
- Way more single- and double-differential results in [Phys. Rev. Lett. 131, 101802 \(2023\)](#) and [Phys. Rev. D 108, 053002 \(2023\)](#)!



# CC1p0 $\pi$ TKI Summary

- First single- and double- differential neutrino-argon cross section measurements in TKI
- Fermi motion studied w in  $\delta p_T$  with  $\delta\alpha_T < 45^\circ$
- FSI & multinucleon effects studied with 2D measurement in  $\delta p_T$  with  $135^\circ < \delta\alpha_T < 180^\circ$
- Way more single- and double-differential results in [Phys. Rev. Lett. 131, 101802 \(2023\)](#) and [Phys. Rev. D 108, 053002 \(2023\)](#)!

But why not extend beyond TKI by using three dimensions?



# Generalized Kinematic Imbalance (GKI)

[Phys. Rev. C 95, 065501 \(2017\)](#)

[arXiv:2310.06082](#)

- Extension to 3D by considering longitudinal component of missing momentum and calorimetric assumption on the incoming energy

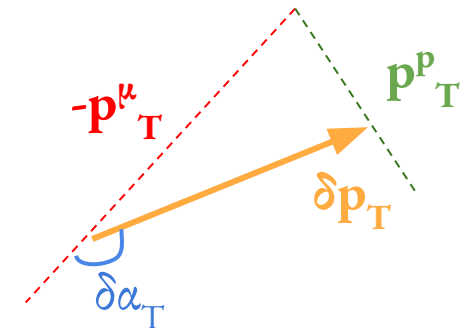
Start by considering the physical meaning of the TKI variables:

$\delta p_T$  is the transverse missing momentum

$-p^{\mu}_T$  is the transverse momentum transfer

$\delta\alpha_T$  is the angle between these two vectors

$\delta\phi_T$  is the angle between the proton momentum and  $q$



Can we find a way of identifying the longitudinal components of all of these vectors?

# Generalized Kinematic Imbalance (GKI)

[Phys. Rev. C 95, 065501 \(2017\)](#)

[arXiv:2310.06082](#)

- Extension to 3D by considering longitudinal component of missing momentum and calorimetric assumption on the incoming energy

$$B = 30.9 \text{ MeV}$$

- Assume we see all of the energy - now we know the neutrino energy
- Now we have the momentum transfer longitudinal component
- Difference between visible energy and net longitudinal momentum is the longitudinal missing momentum

$$E_{\text{cal}} = E_\mu + K_p + B$$

$$\vec{q} = E_{\text{cal}} \hat{z} - \vec{p}_\mu$$

$$p_L = p_L^\mu + p_L^p - E_{\text{cal}}$$

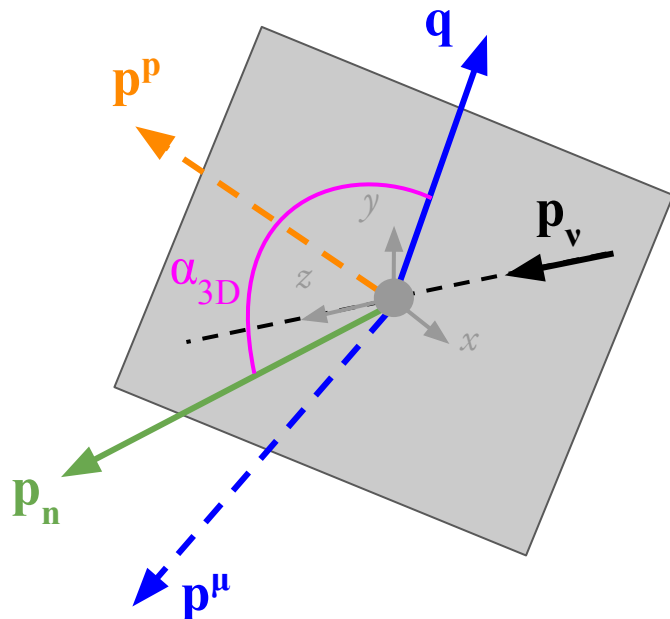
Note, this is numerically almost identical to the method in [Phys. Rev. C 95, 065501 \(2017\)](#) while being significantly simpler

# Generalized Kinematic Imbalance (GKI)

[Phys. Rev. C 95, 065501 \(2017\)](#)

[arXiv:2310.06082](#)

- Extension to 3D by considering longitudinal component of missing momentum and calorimetric assumption on the incoming energy



$$p_n = |\vec{p}_n| = \sqrt{p_L^2 + \delta p_T^2}$$

$$\alpha_{3D} = \cos^{-1} \left( \frac{\vec{q} \cdot \vec{p}_n}{|\vec{q}| |\vec{p}_n|} \right)$$

$$\phi_{3D} = \cos^{-1} \left( \frac{\vec{q} \cdot \vec{p}_p}{|\vec{q}| |\vec{p}_p|} \right)$$

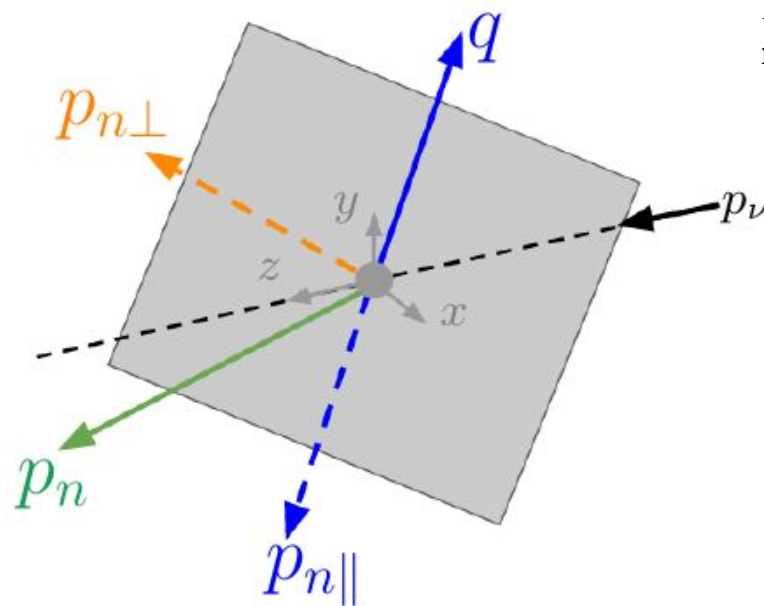
Assume missing momentum is all nuclear recoil,  $p_n$  measures the initial state neutron momentum,  $\alpha_{3D}$  measures it's direction relative to the momentum transfer

# Generalized Kinematic Imbalance (GKI)

[Phys. Rev. C 95, 065501 \(2017\)](#)

[arXiv:2310.06082](#)

- Extension to 3D by considering longitudinal component of missing momentum and calorimetric assumption on the incoming energy



Include projections of  $p_n$  parallel and perpendicular to the momentum transfer:

$$p_{n\perp,x} = (\hat{q}_T \times \hat{z}) \cdot \vec{p}_n,$$

$$p_{n\perp,y} = (\hat{q} \times (\hat{q}_T \times \hat{z})) \cdot \vec{p}_n,$$

$$p_{n\perp} = \sqrt{(p_{n\perp,x})^2 + (p_{n\perp,y})^2} = |p_n| \sin(\alpha_{3D}),$$

$$p_{n\parallel} = \hat{q} \cdot \vec{p}_n = |p_n| \cos(\alpha_{3D}).$$

# Generalized Kinematic Imbalance (GKI)

[Phys. Rev. C 95, 065501 \(2017\)](#)

[arXiv:2310.06082](#)

- Extension to 3D by considering longitudinal component of missing momentum and calorimetric assumption on the incoming energy

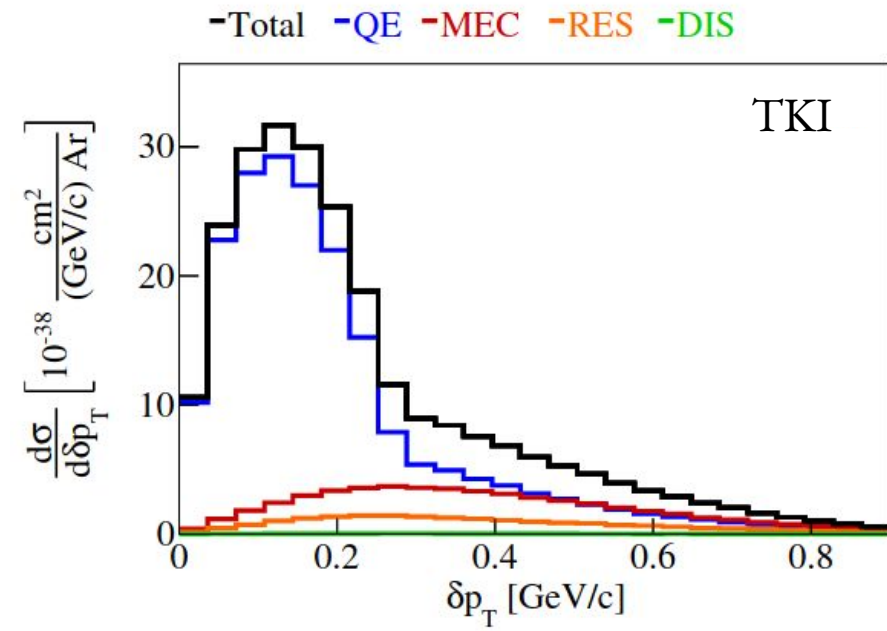
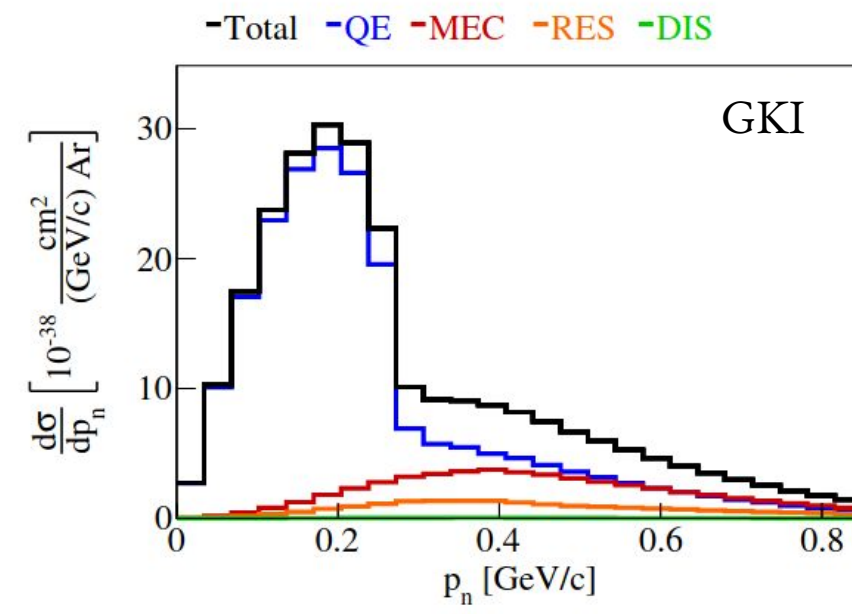
We should expect an additional dimension to add extra information - does this result in better sensitivity to nuclear effects?



# Missing momentum

arXiv:2310.06082

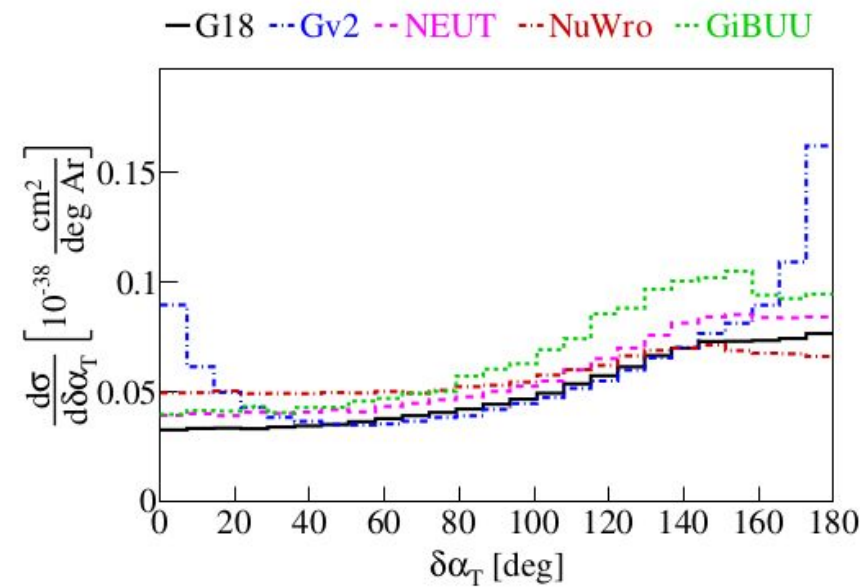
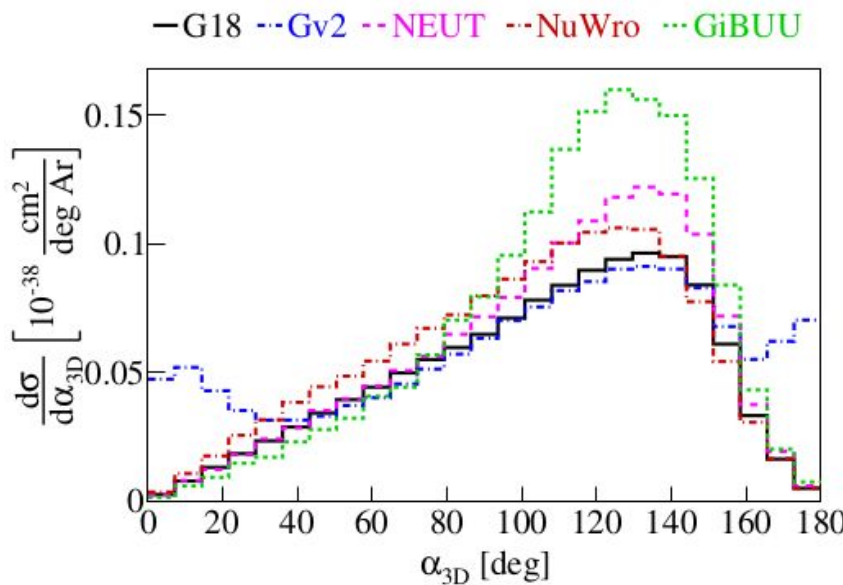
GENIE v3.0.6 G18\_10a\_02\_11a (no tune)



- QE dominance due to CC1p0 $\pi$  signal definition
- $p_n$  pushes non-QE component to higher values

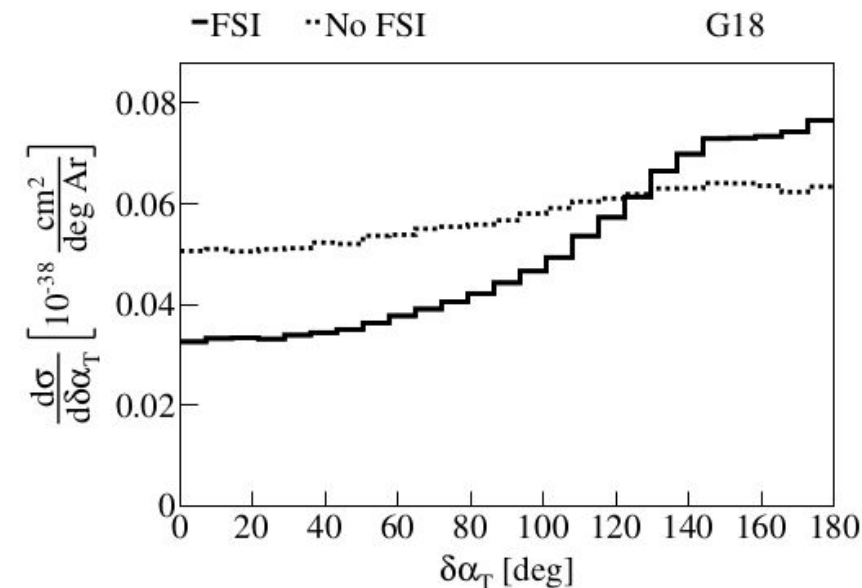
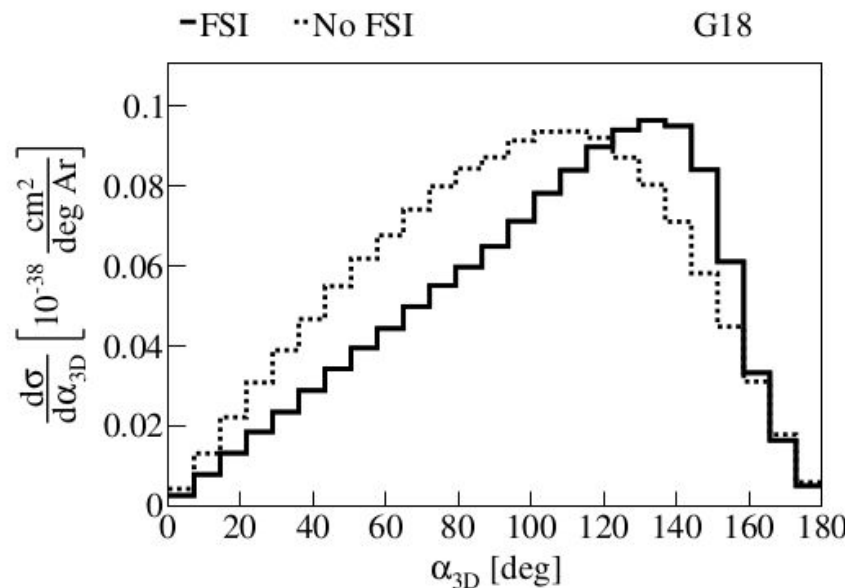
# GKI angles

- Difference between generators is larger for the GKI variables than the TKI variables



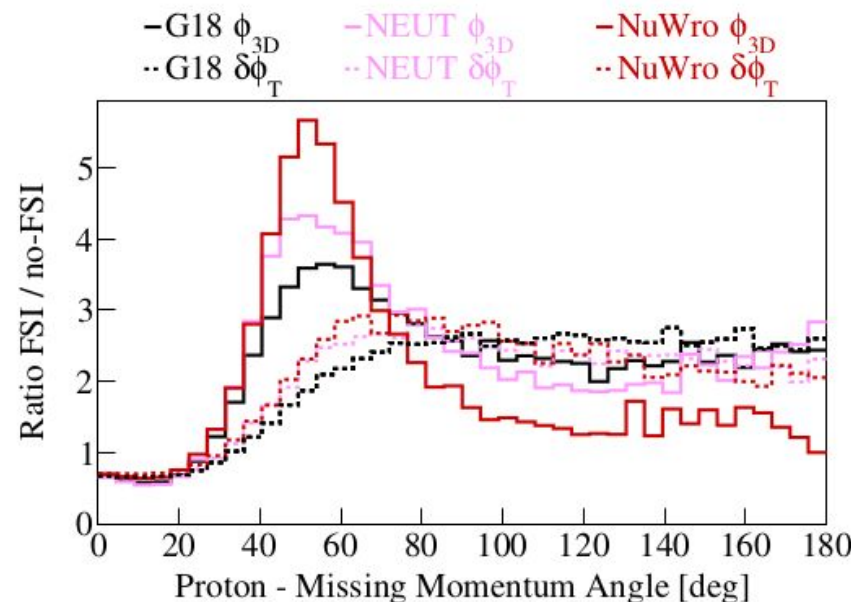
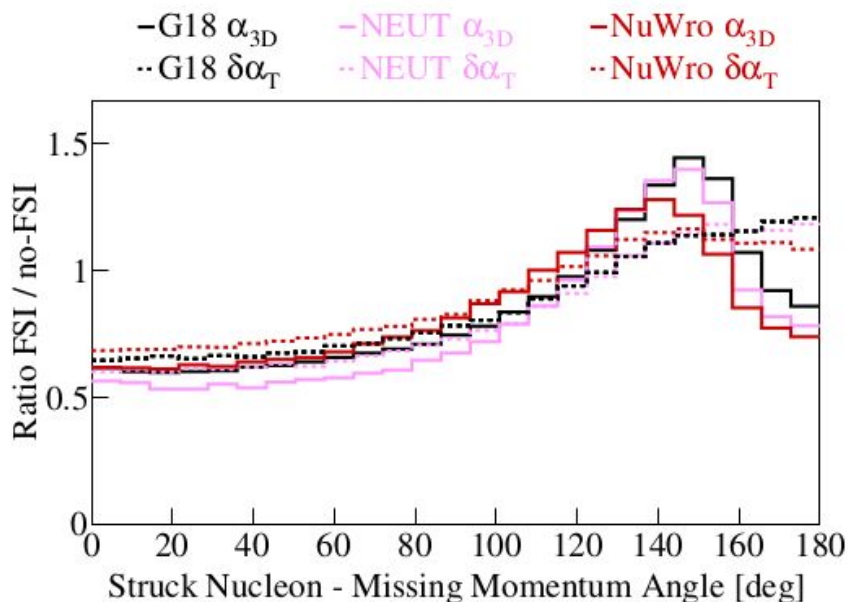
# GKI angles

- Impact of FSI is larger for GKI than TKI



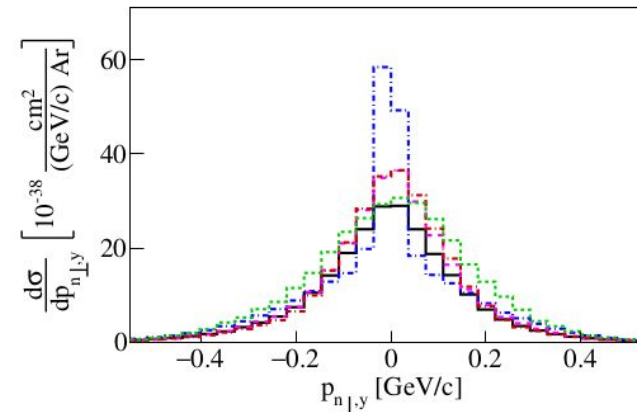
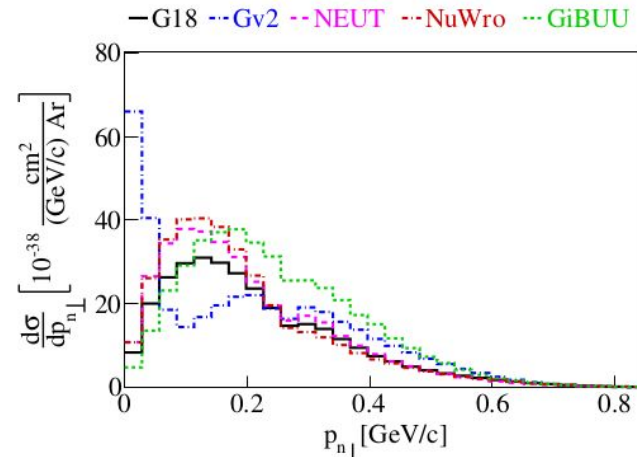
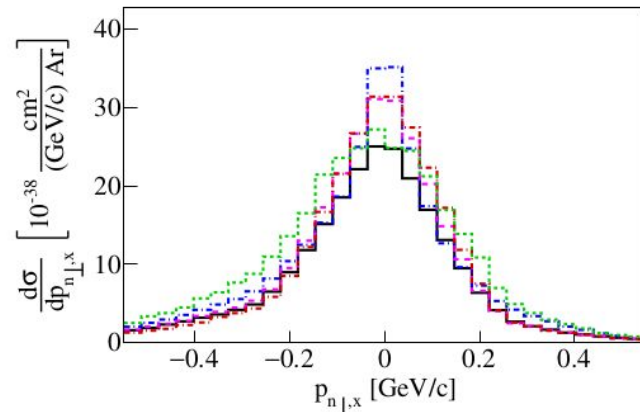
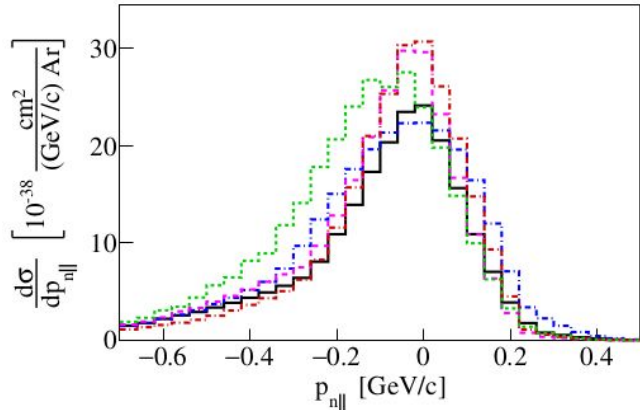
# GKI angles

- Larger ratio of FSI/no-FSI means FSI has a larger impact
- Not only do the GKI variables show larger FSI impact, they show more generator variation in FSI impact



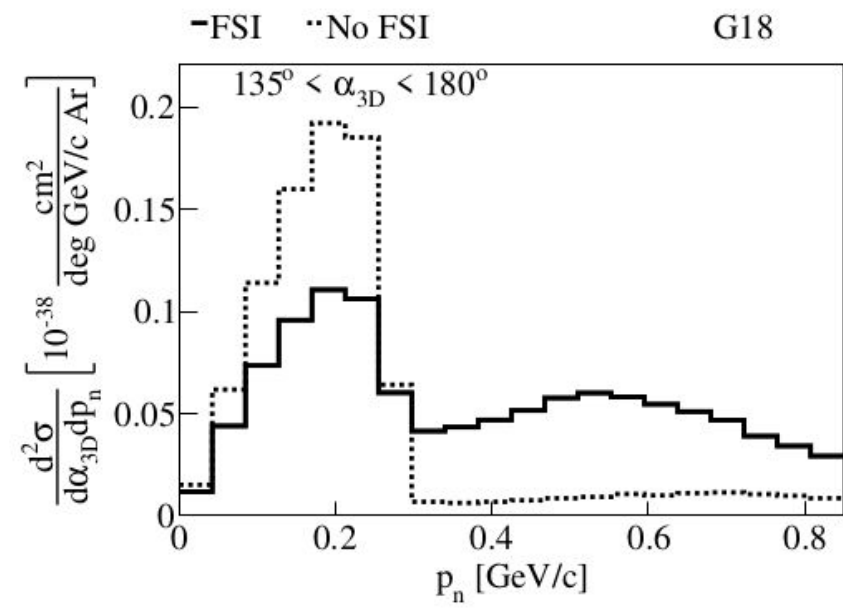
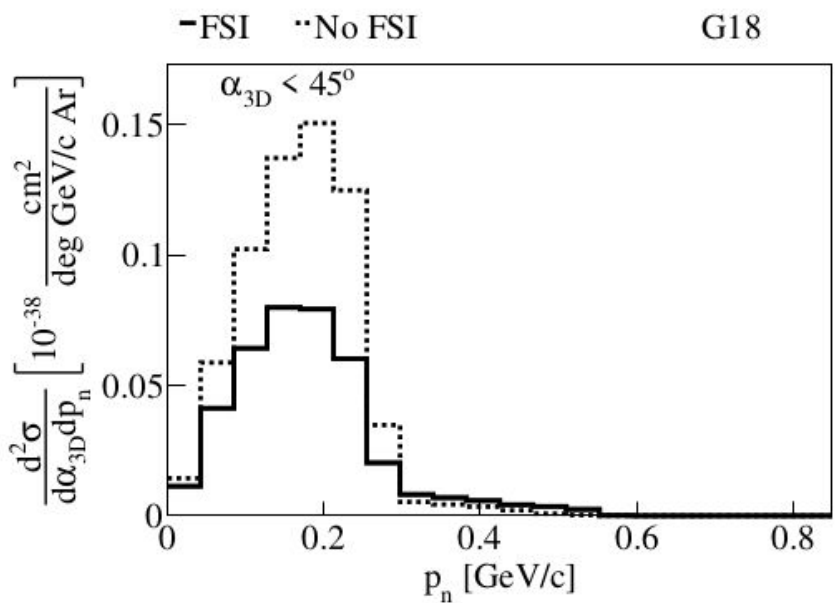
# GKI projection variables

- Parallel component of  $p_n$  picks up asymmetry due to FSI slowing protons
- Perpendicular components much more symmetric



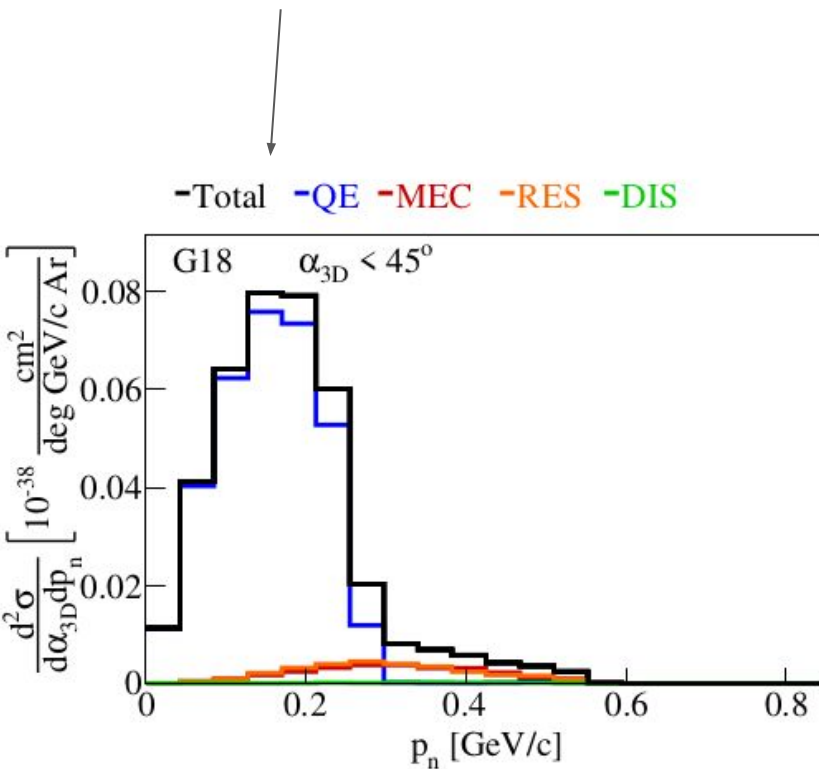
# GKI - into the multiverse!

- Divide the GKI variables just like we did for TKI
- High  $\alpha_{3D}$  significantly enhances tail of  $p_n$

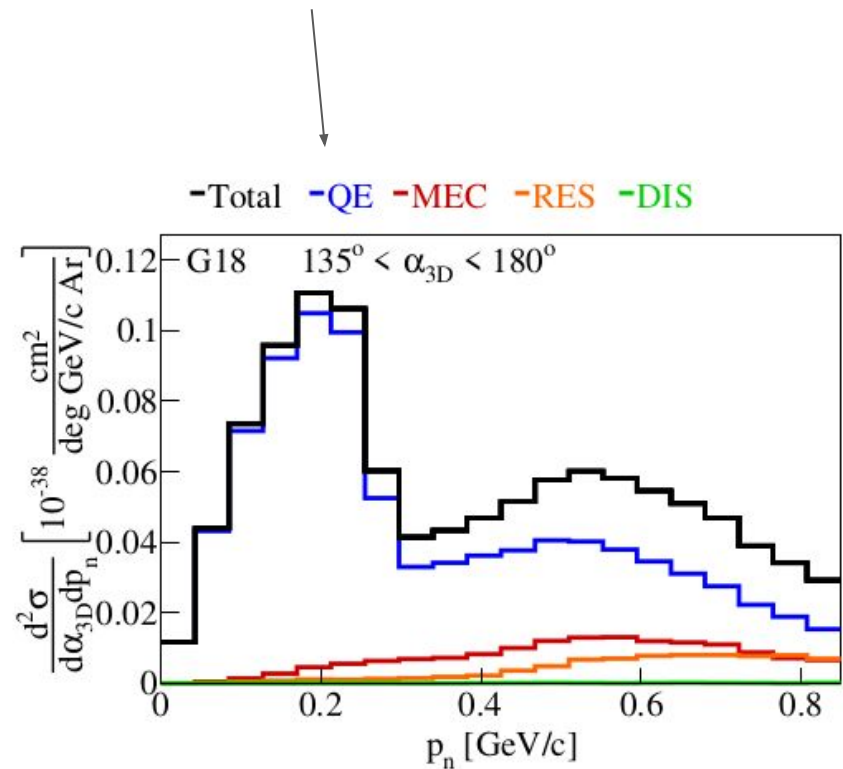


# GKI - into the multiverse!

At low  $\alpha_{3D}$ , tail is mainly MEC and RES

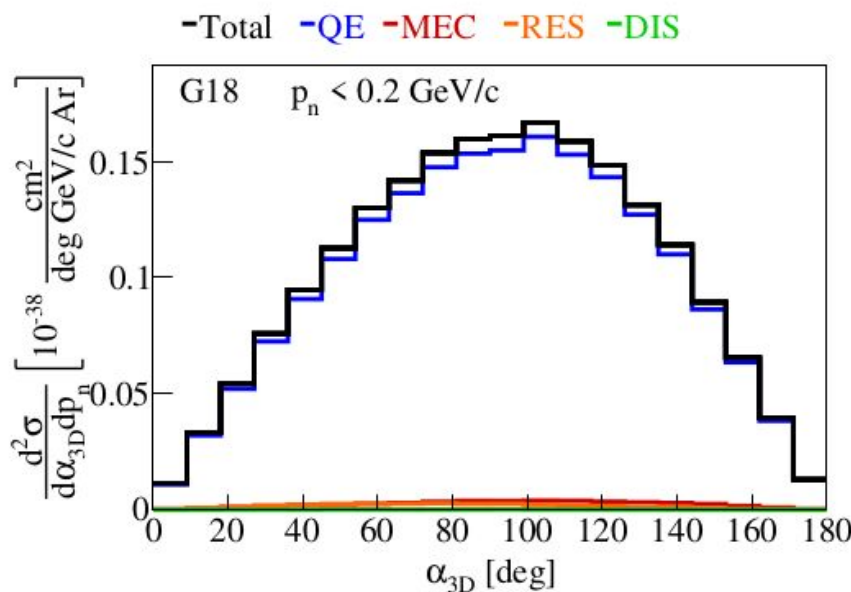


At high  $\alpha_{3D}$ , tail is mainly QE with FSI

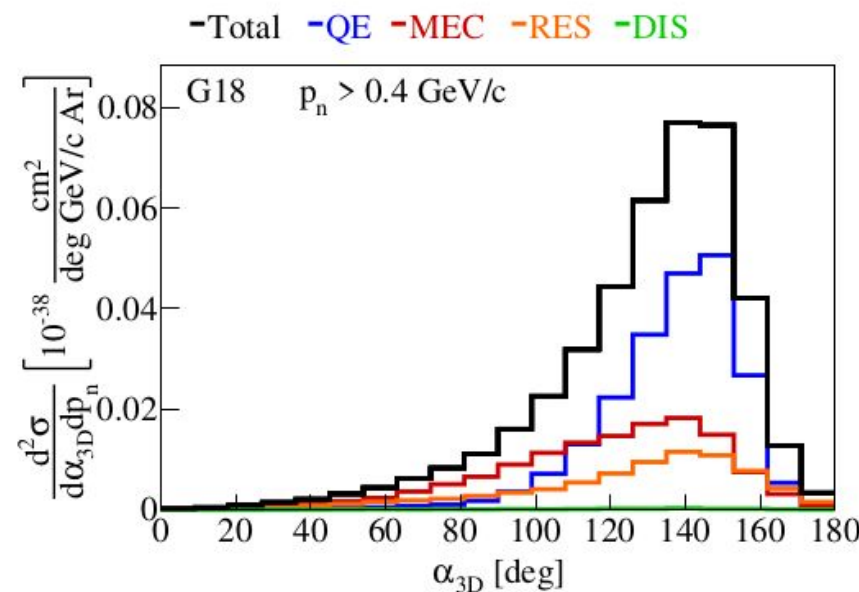


# GKI - into the multiverse!

At low  $p_n$  we see a sine function (this is 3D phase space)



At high  $p_n$ , tail is enhanced. Low  $\alpha_{3D}$  is now primarily MEC

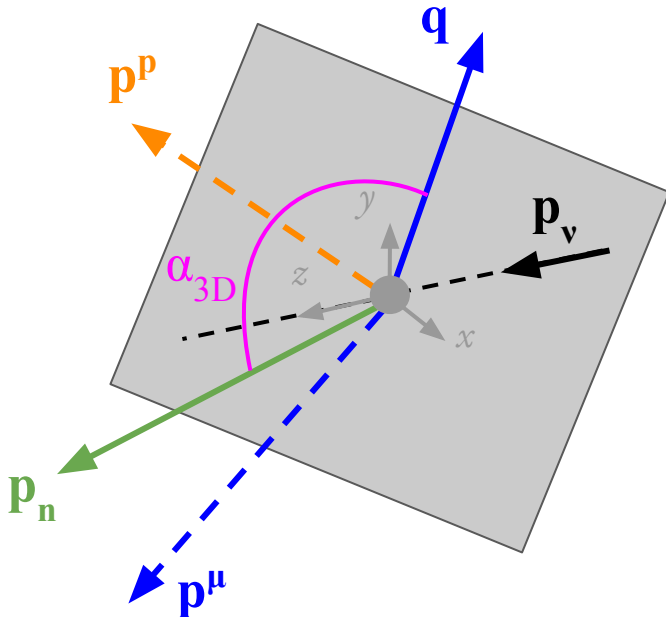


# Generalized Kinematic Imbalance (GKI)

[Phys. Rev. C 95, 065501 \(2017\)](#)

[arXiv:2310.06082](#)

- Extension to 3D by considering longitudinal component of missing momentum and calorimetric assumption on the incoming energy
- Extensively tested again several event generators and model configurations



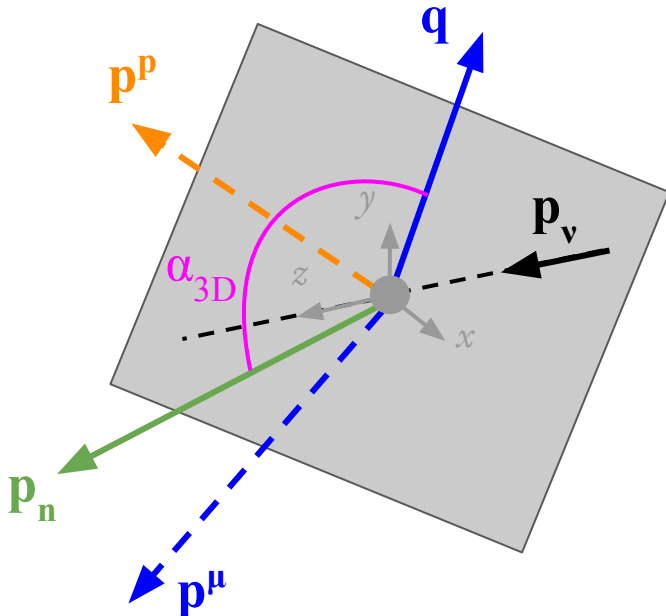
Name	Generator / Configuration
Gv2	GENIE v2.12.10
G18	GENIE v3.0.6 G18_10a_02_11a
G18T	G18 with tune
G21	GENIE v3.2.0 G21_11b_00_000
GiBUU	GiBUU 2021
NuWro	NuWro v19.02.1
NEUT	NEUT v5.4.0

# Generalized Kinematic Imbalance (GKI)

[Phys. Rev. C 95, 065501 \(2017\)](#)

[arXiv:2310.06082](#)

- Extension to 3D by considering longitudinal component of missing moment and calorimetric assumption on the incoming energy
- Extensively tested again several event generators and model configurations

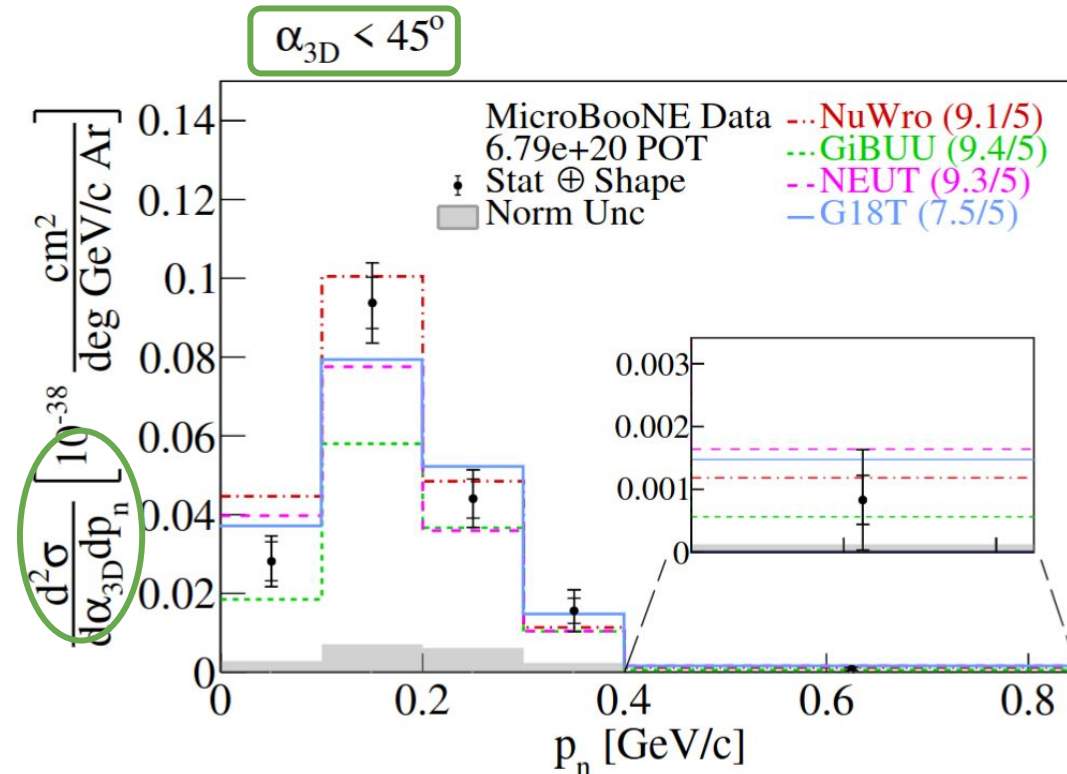


Name	Generator / Configuration
Gv2	GENIE v2.12.10
G18	GENIE v3.0.6 G18_10a_02_11a
G18T	G18 with tune
G21	GENIE v3.2.0 G21_11b_00_000
GiBUU	GiBUU 2021
NuWro	NuWro v19.02.1
NEUT	NEUT v5.4.0

Selected comparisons shown next  
using same CC1p0π selection

# GKI confronted with data!

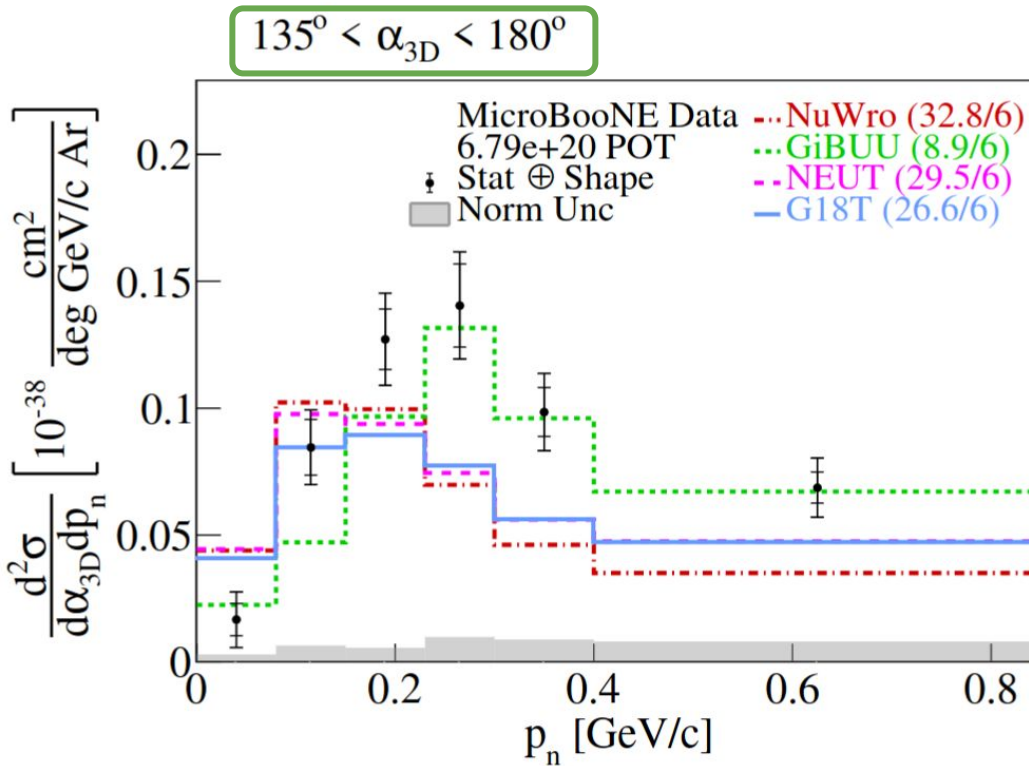
low-FSI region



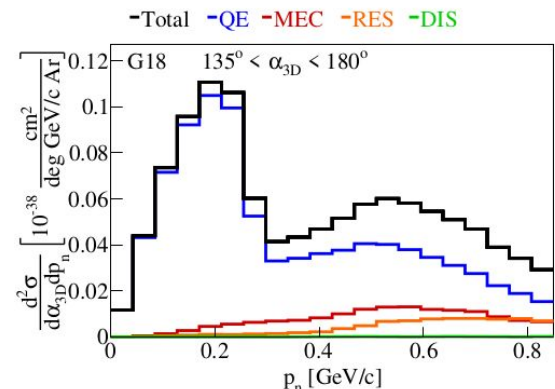
- Most models use LFG, with good agreement
- Large spread of predictions in tail
  - Unfortunately large uncertainties currently
- GiBUU underpredicts peak
- G18T provides best agreement

# GKI confronted with data!

high-FSI region

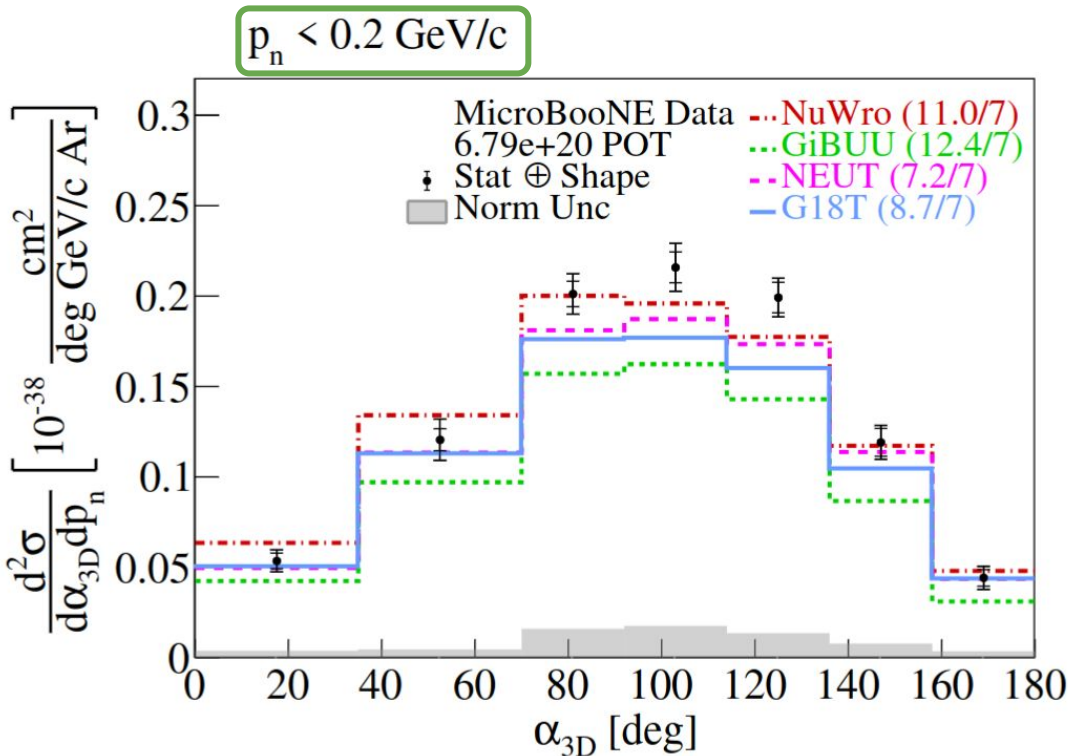


- FSI-driven tail very large in data
- GiBUU yields best result
- Can't resolve double peak - statistics and resolution



# GKI confronted with data!

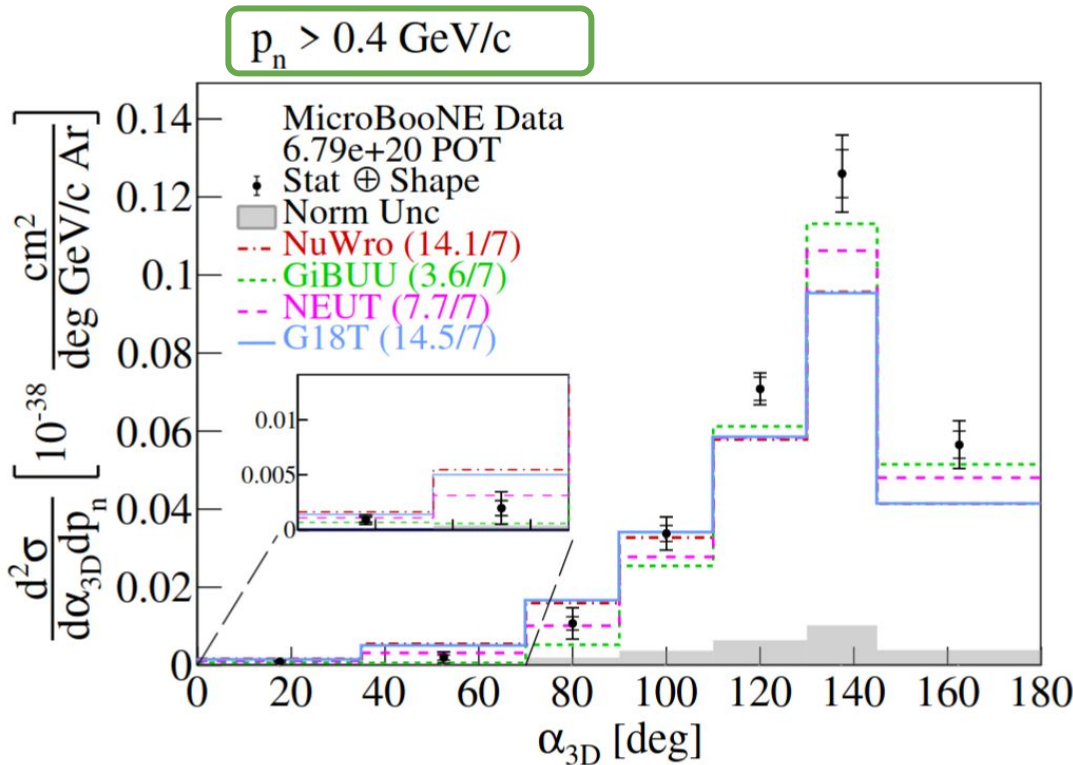
QE-dominated region



- Most generators agree well
- GiBUU normalisation too low

# GKI confronted with data!

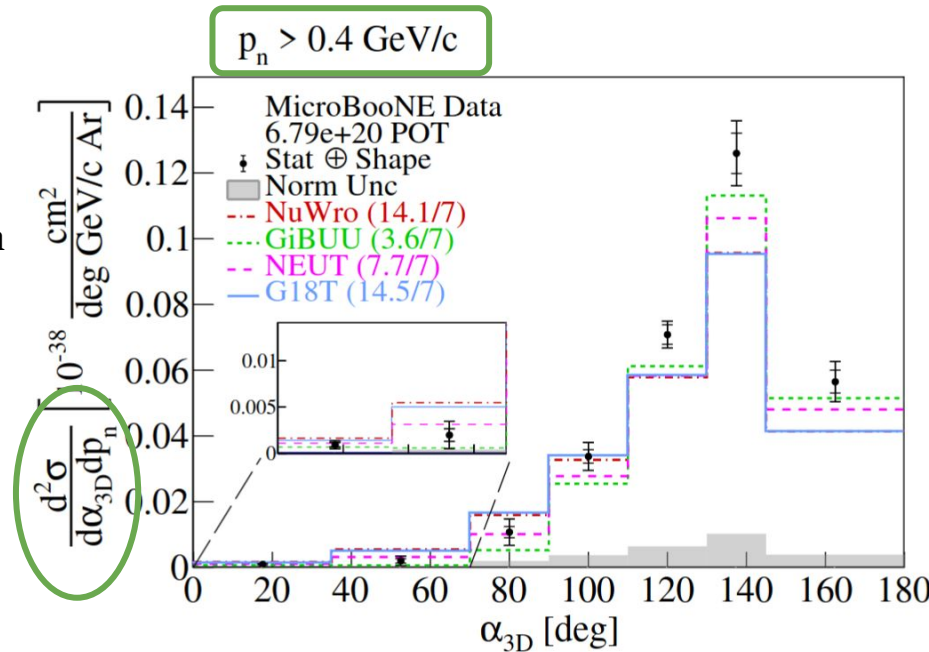
MEC/RES/FSI dominated region



- GiBUU describes high-FSI region well
- low- $\alpha_{3D}$  MEC-dominated. Significant variation in predictions.
- Again, uncertainties comparable with spread

# CC1p0 $\pi$ GKI Summary

- Introduction of generalized kinematic imbalance (GKI) variables in 3D space
- Enhanced sensitivity to nuclear effects
- First single- and double-differential cross section GKI measurement ever with MicroBooNE
- **G18T** results in good description in QE-dominated regions
- **GiBUU** yields best performance in FSI-dominated regions
- Way more results in [arXiv:2310.06082](https://arxiv.org/abs/2310.06082)!





Thank you!

# Backup Slides

# Backup Slides: Table of Contents

MicroBooNE / Unfolding: 66-77

TKI PRD: 78-127

TKI PRL: 128-159

GKI arxiv: 160-182

e4v: 183-280

### 3.6.3 Effect of Variation in Uncertainty

Figure 3.23 shows DUNE sensitivity to determination of neutrino mass hierarchy and discovery of CP violation as a function of exposure for several levels of signal normalization uncertainty. As seen in Figure 3.23, for early phases of DUNE with exposures less than  $100 \text{ kt} \cdot \text{MW} \cdot \text{year}$ , the experiment will be statistically limited. The impact of systematic uncertainty on the CP-violation sensitivity for large exposure is obvious in Figure 3.23; the  $\nu_e$  signal normalization uncertainty must be understood at the level of  $5\% \oplus 2\%$  in order to reach  $5\sigma$  sensitivity for 75% of  $\delta_{CP}$  values with exposures less than  $\sim 900 \text{ kt} \cdot \text{MW} \cdot \text{year}$  in the case of the Optimized Design. Specifically, the absolute normalization of the  $\nu_\mu$  sample must be known to  $\sim 5\%$  and the normalization of the  $\nu_e$  sample, relative to the  $\bar{\nu}_e$ ,  $\nu_\mu$ , and  $\bar{\nu}_\mu$  samples after all constraints from external, near detector, and far detector data have been applied, must be determined at the few-percent level. This level of systematic uncertainty sets the capability and design requirements for all components of the experiment, including the beam design and the near and far detectors.

Volume 2: The Physics Program for DUNE at LBNF

LBNF/DUNE Conceptual Design Report

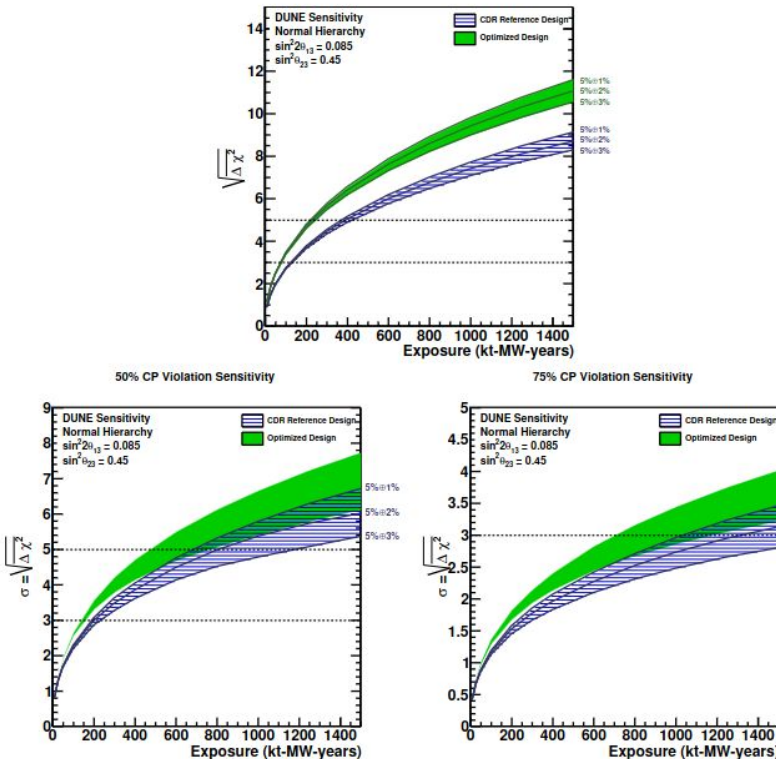
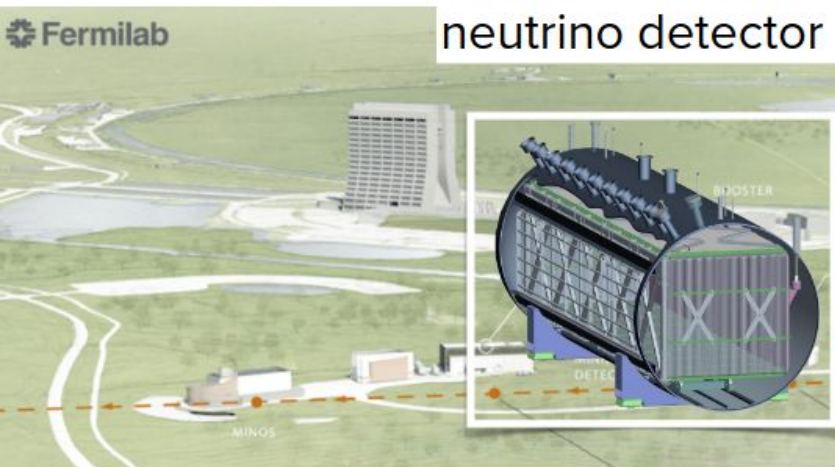
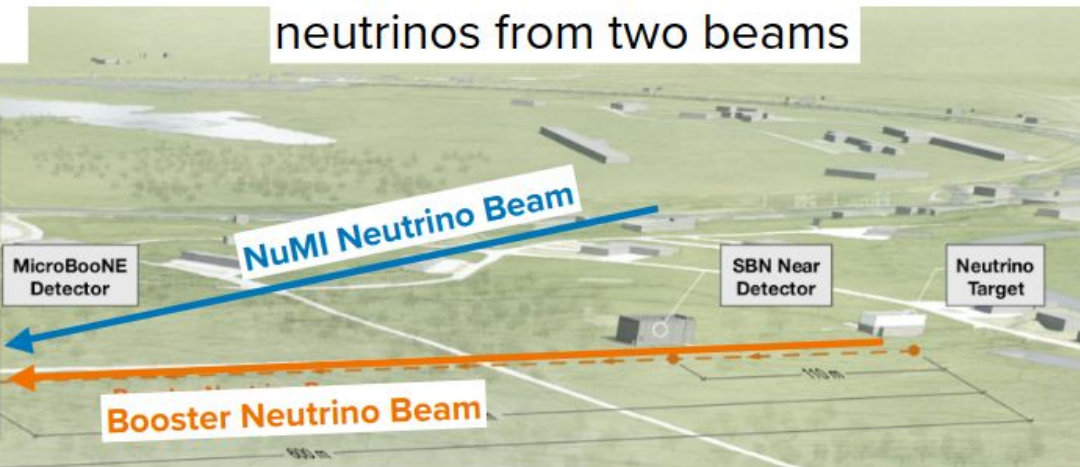


Figure 3.23: Expected sensitivity of DUNE to determination of the neutrino mass hierarchy (top) and discovery of CP violation, i.e.,  $\delta_{CP} \neq 0$  or  $\pi$ , (bottom) as a function of exposure in  $\text{kt} \cdot \text{MW} \cdot \text{year}$ , assuming equal running in neutrino and antineutrino mode, for a range of values for the  $\nu_e$  and  $\bar{\nu}_e$  signal normalization uncertainties from  $5\% \oplus 3\%$  to  $5\% \oplus 1\%$ . The sensitivities quoted are the minimum sensitivity for 100% of  $\delta_{CP}$  values in the case of mass hierarchy and 50% (bottom left) or 75% (bottom right) of  $\delta_{CP}$  values in the case of CP violation. The two bands on each plot represent a range of potential beam designs: the blue hashed band is for the CDR Reference Design and the solid green band is for the Optimized Design. Sensitivities are for true normal hierarchy; neutrino mass hierarchy and  $\theta_{23}$  octant are assumed to be unknown.

## A short baseline neutrino detector



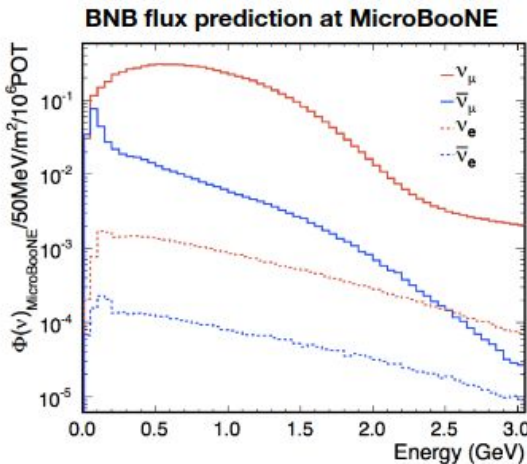
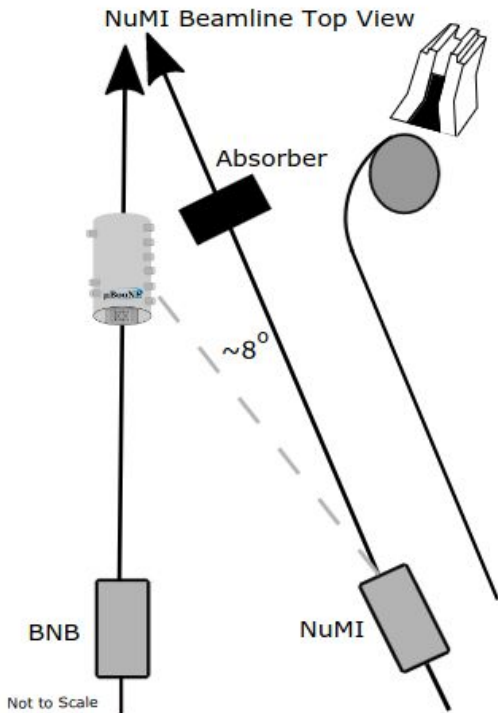
## Studying accelerator neutrinos from two beams



### MicroBooNE's physics program

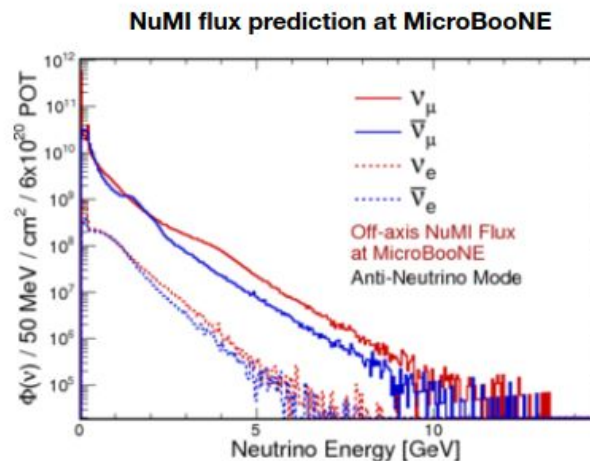
Non-standard neutrino oscillations	Cross-section measurements	Detector physics, R&D
---------------------------------------	-------------------------------	--------------------------

**Beyond Standard Model physics!**

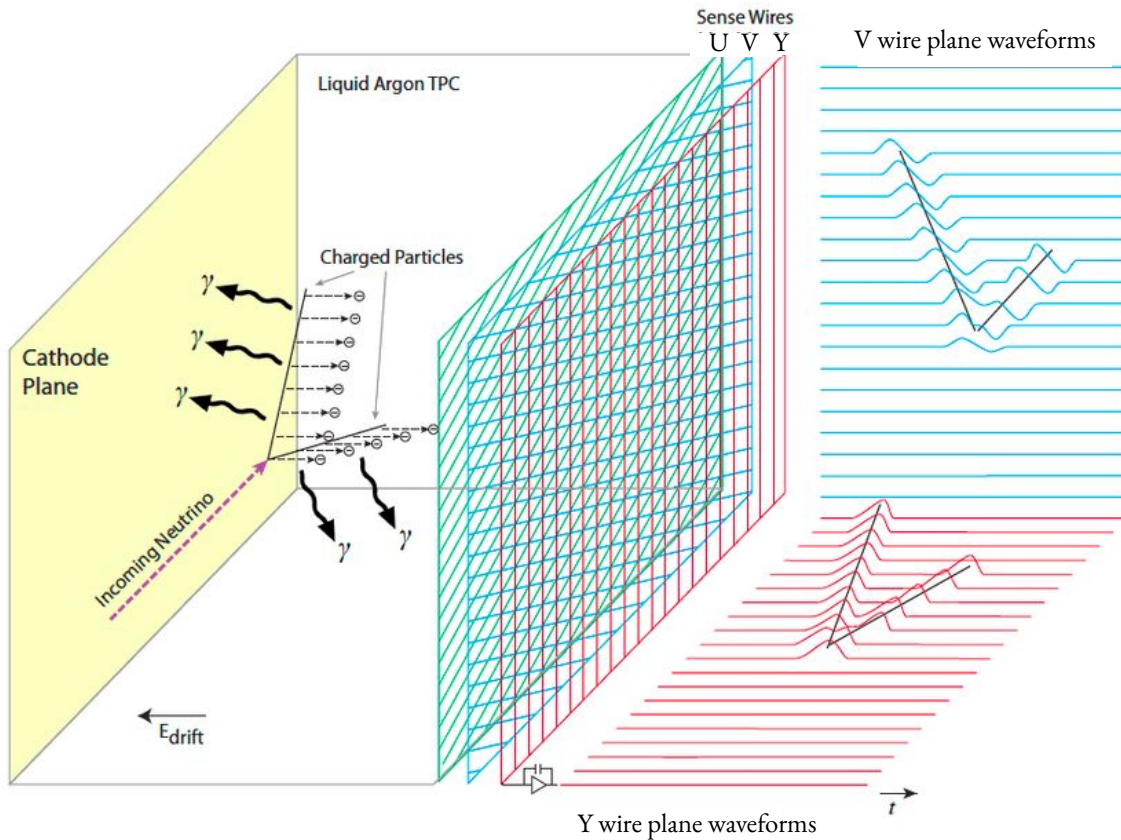


- 8 GeV protons
- $\sim 470$  m from MicroBooNE
- On-axis

- 120 GeV protons
- $\sim 680$  m from MicroBooNE
- $\sim 8^\circ$  off-axis from MicroBooNE



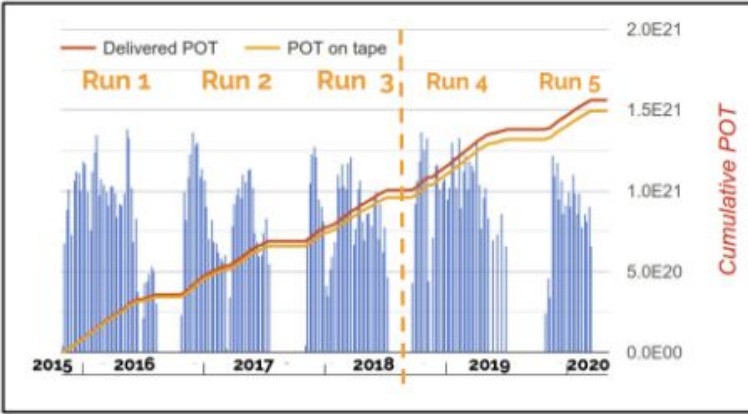
# LArTPC Operation Principle



## MicroBooNE

- 3 wire planes
- 8192 gold coated wires
- 3 mm wire spacing
- 32 PMTs

- MicroBooNE collected BNB and NuMI data between 2015 and 2020
- ~50% of the dataset (Runs 1-3) used in first wave of results



First results

POT: Protons on Target

From raw hits to  
particle reconstruction

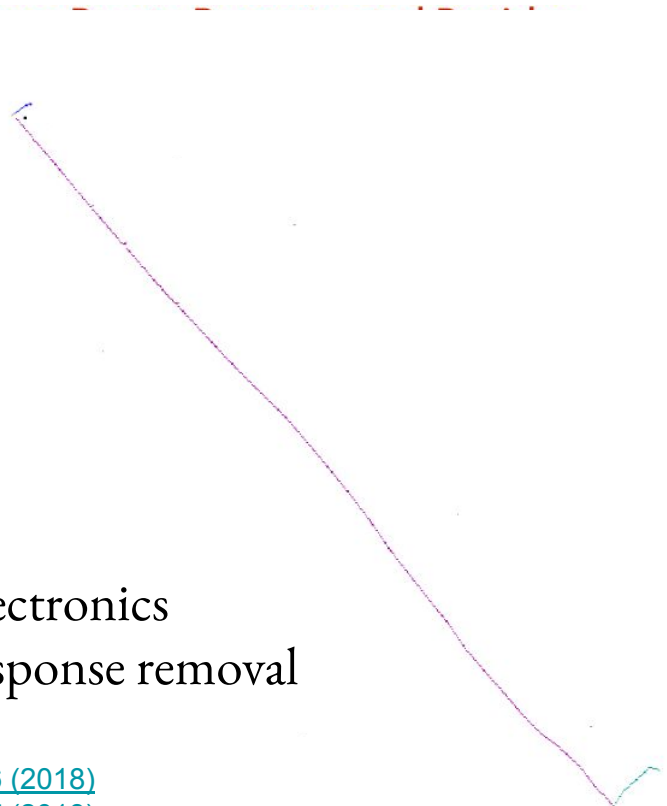
## Pandora Pattern Recognition

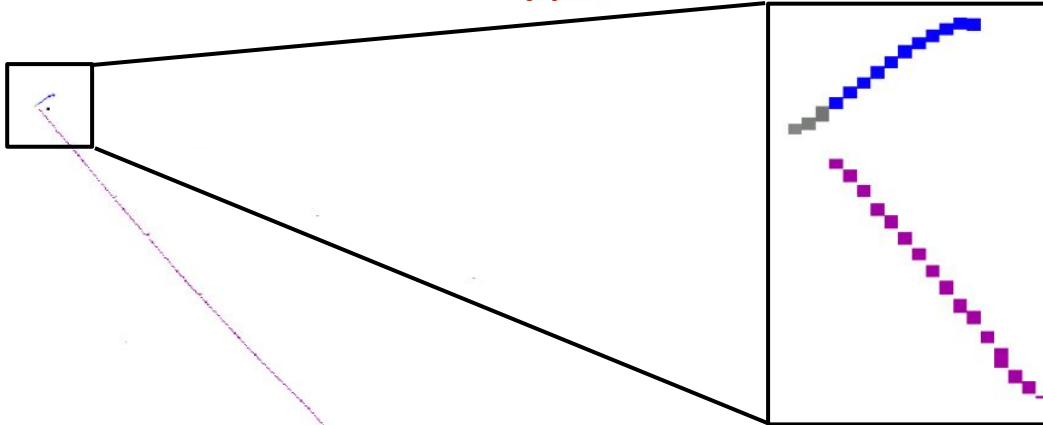
• Eur. Phys. J. C78, 1, 82 (2018)

Readout electronics  
and field response removal

[JINST 13, P07006 \(2018\)](#)

[JINST 13, P07007 \(2018\)](#)



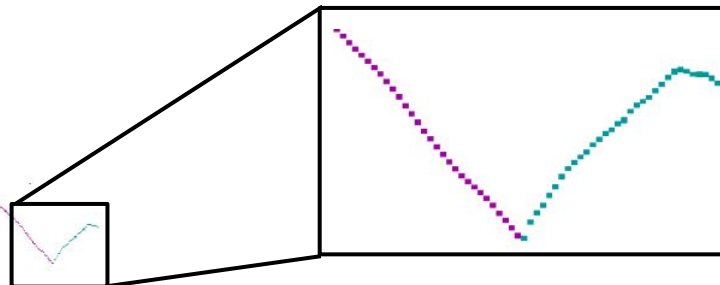


From raw hits to  
particle reconstruction

## Pandora Pattern Recognition

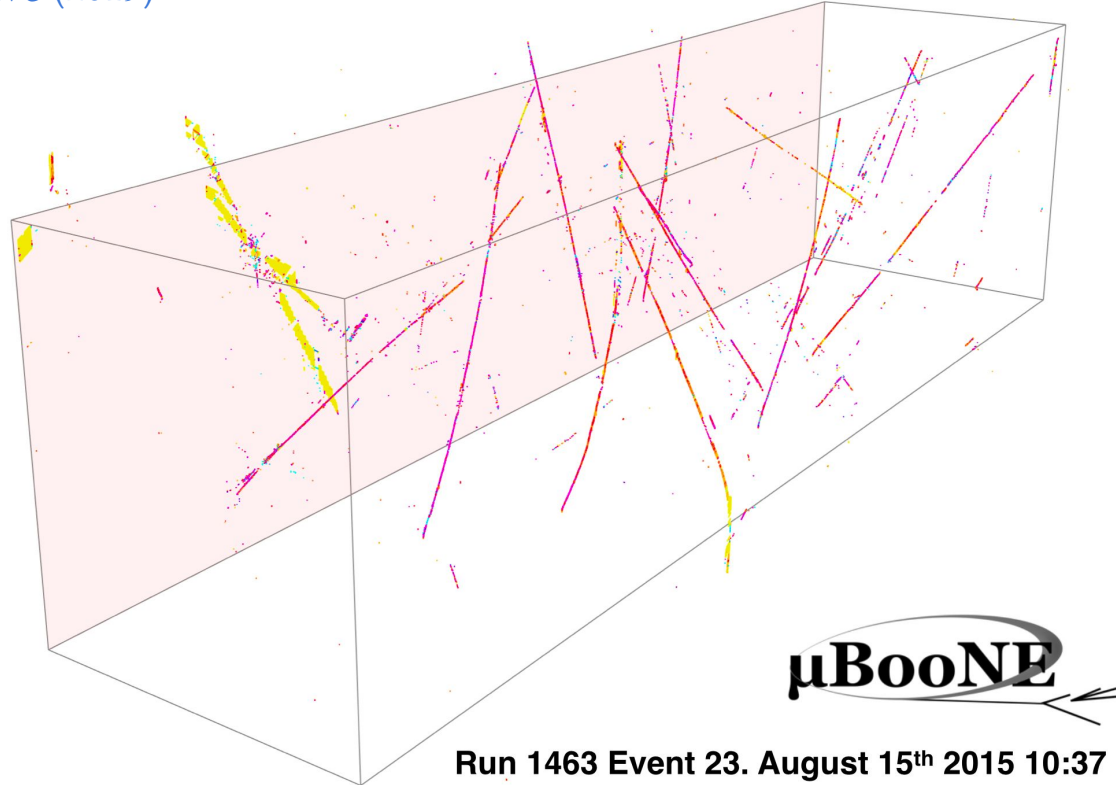
Eur. Phys. J. C78, 1, 82 (2018)

Readout electronics  
and field response removal



[JINST 13, P07006 \(2018\)](#)  
[JINST 13, P07007 \(2018\)](#)

Eur. Phys. J. C 79 673 (2019)



Readout window of 2.3 ms

- ~20 cosmic interactions
- ~0.0017  $\nu$  interactions

Significant reduction using optical information  
to 1  $\nu$  interaction in ~10 events

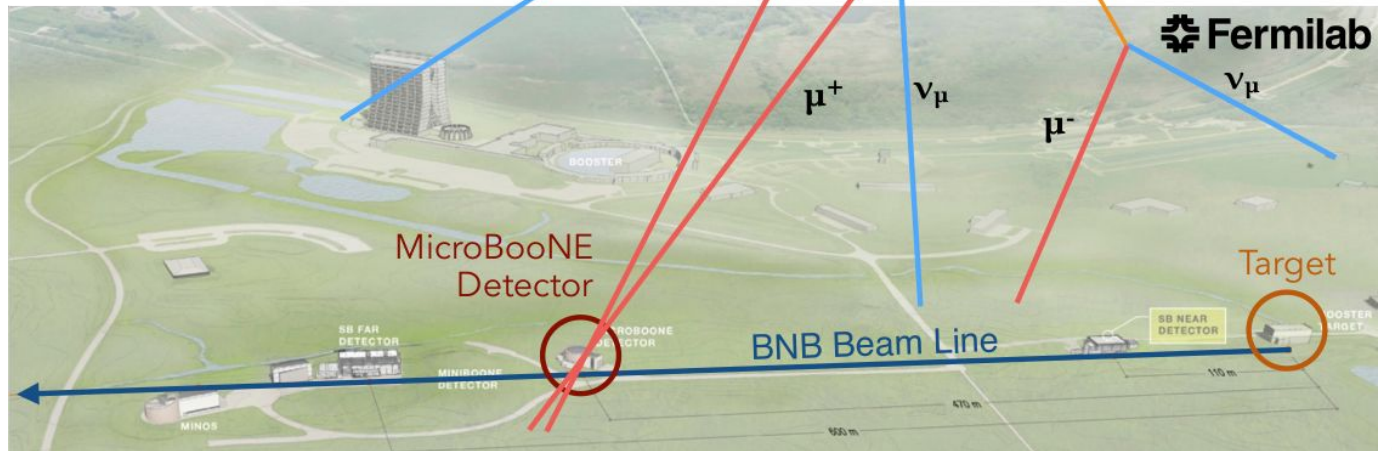
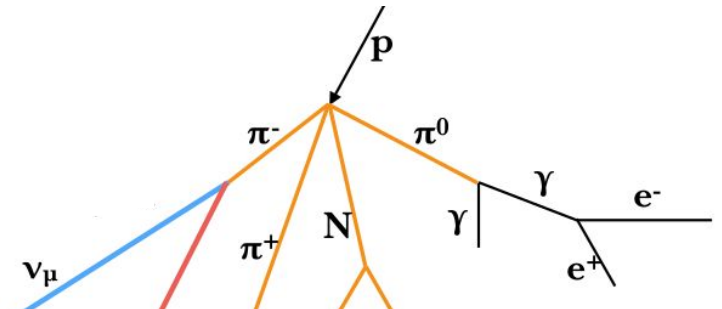


TABLE IV. Tuned parameter values and uncertainties after fitting to T2K CC0 $\pi$  data for the nominal simulation and three tunes that build to the final four parameter tune. Note that postfit  $\chi^2$  values are quoted here only for the 58 bins included in the fit (excluding the highest muon momentum bin in each  $\cos \theta$  bin), and using diagonal elements of the covariance matrix only. In the text and figures, pre- and postfit  $\chi^2$  comparisons are also quoted for the full T2K dataset of 67 bins. “Norm.” is an abbreviation for normalization.

	MaCCQE fitted value	CC2p2h Norm. fitted value	CCQE RPA Strength fitted value	CC2p2h Shape fitted value	T2K $\chi^2_{\text{diag}}/\text{N}_{\text{bins}}$
Nominal (untuned)	0.961242 GeV	1	100%	0	106.7/58
Fit MaCCQE + CC2p2h Norm.	$1.14 \pm 0.07$ GeV	$1.61 \pm 0.19$	100% (fixed)	0 (fixed)	71.8/58
Fit MaCCQE + CC2p2h Norm + CCQE RPA Strength	$1.18 \pm 0.08$ GeV	$1.12 \pm 0.38$	$(64 \pm 23)\%$	0 (fixed)	69.7/58
Fit MaCCQE + CC2p2h Norm + CCQE RPA Strength + CC2p2h Shape	$1.10 \pm 0.07$ GeV	$1.66 \pm 0.19$	$(85 \pm 20)\%$	$1^{+0}_{-0.74}$	52.5/58

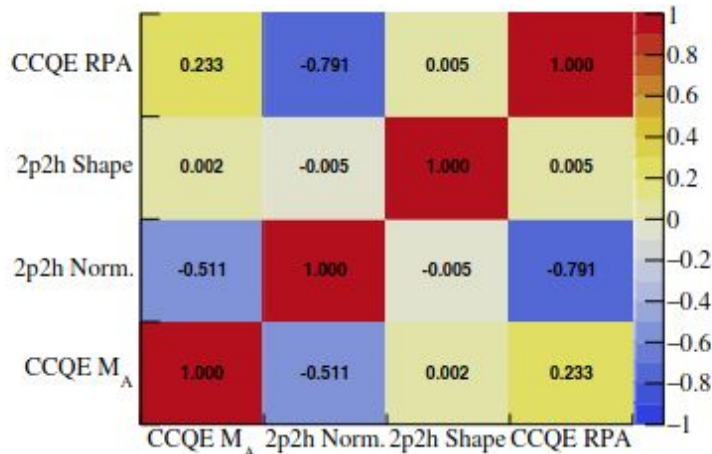
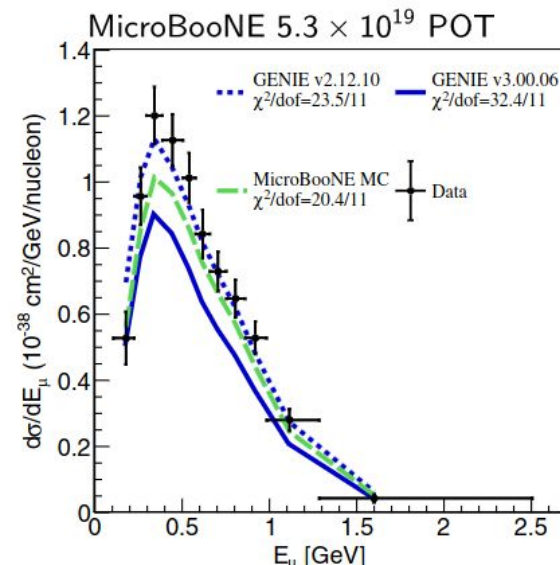


FIG. 7. Correlations between parameters after fitting to T2K CC0 $\pi$  data.



# Unfolding problem

- In practice, the data unfolding problem starts with

$$\chi^2(s) = (\mathbf{m} - \mathbf{r} \cdot s)^T \text{Cov}^{-1}(\mathbf{m} - \mathbf{r} \cdot s)$$

- $\mathbf{m}$  : measured spectrum,  $m$ -dimensional vector
- $\mathbf{s}$  : unknown spectrum, to be unfolded,  $n$ -dimensional vector
- $\mathbf{r}$  : smearing (response) matrix,  $m \times n$  and  $m \geq n$
- $\text{Cov}$  : covariance matrix containing all statistical and systematic uncertainties associated with  $\mathbf{m}$  and  $\mathbf{r}$ .

- Cholesky decomposition:  $\text{Cov}^{-1} = Q^T Q$ ,  $Q$  is a lower triangular matrix

$$\chi^2(s) = (M - R \cdot s)^T \cdot (M - R \cdot s)$$

## Pre-scaling

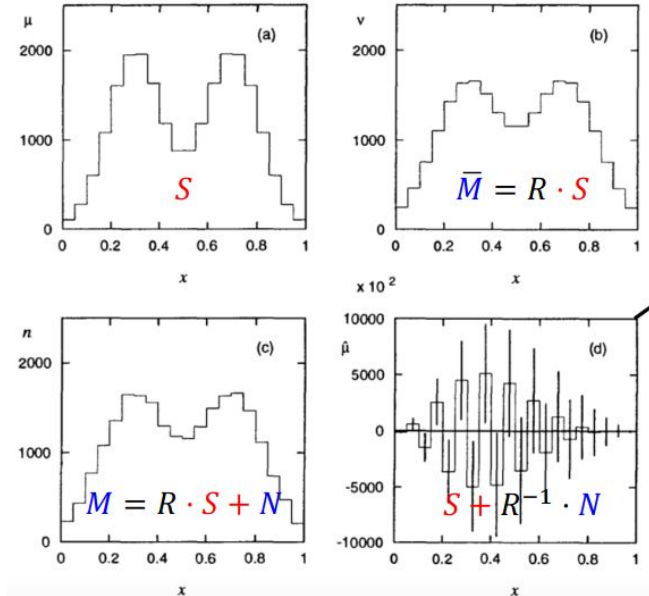
- $M := Q \cdot \mathbf{m}$
- $R := Q \cdot \mathbf{r}$

## Solution (direct inversion)

$$\begin{aligned}\hat{s} &= (R^T R)^{-1} R^T M \\ \hat{s} &= (R^T R)^{-1} R^T (R \cdot s_{true} + N)\end{aligned}$$

The response matrix  $R$  is unnecessary to be a square matrix

# Unfolding problem



This is one unbiased solution (direct inversion) to an unfolding problem. However, it has catastrophic oscillations, i.e. huge variance, in the unfolded spectrum.

- Decrease the number of bins to suppress the “oscillation” --> Nyquist theorem
- Trade-off **bias** and **variance** to suppress the “oscillation” --> e.g. **regularization [unfolding method]**

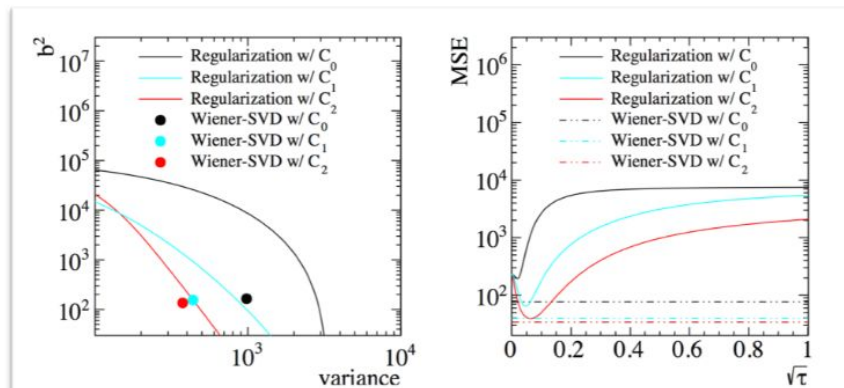
# Wiener-SVD unfolding

- To automatically minimize the Mean Square Error (MSE) given a model  $S$

$$\begin{aligned}
 MSE &= E \left[ (\hat{S} - S)^2 \right] = E \left[ \left( F \cdot \frac{M}{R} - S \right)^2 \right] = E \left[ \left( F \cdot S + F \cdot \frac{N}{R} - S \right)^2 \right] \\
 &= E \left[ ((\mathbf{F} - \mathbf{I}) \cdot \mathbf{S})^2 + \left( \mathbf{F} \cdot \frac{\mathbf{N}}{R} \right)^2 \right]
 \end{aligned}$$

↑ Bias      ↑ Variance

$F$  = “filter” = additional smearing  
matrix = regularization



Given one model  $S$

- General regularization, e.g. Tikhonov regularization, needs to “tune” a regularization strength parameter [curve in the left plot]
- Wiener-SVD regularization corresponds to a fixed point in the phase space of bias versus variance with **minimum MSE**

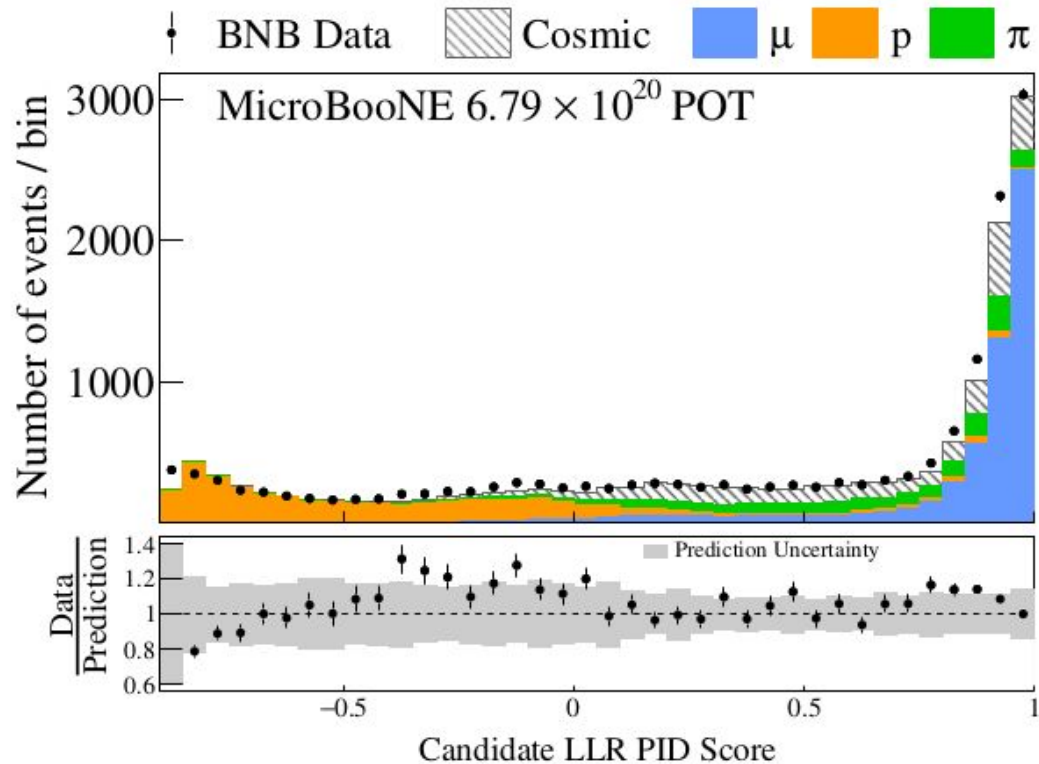


FIG. 1. The log-likelihood ratio (LLR) particle identification (PID) score distribution used to tag the muon and proton candidates.

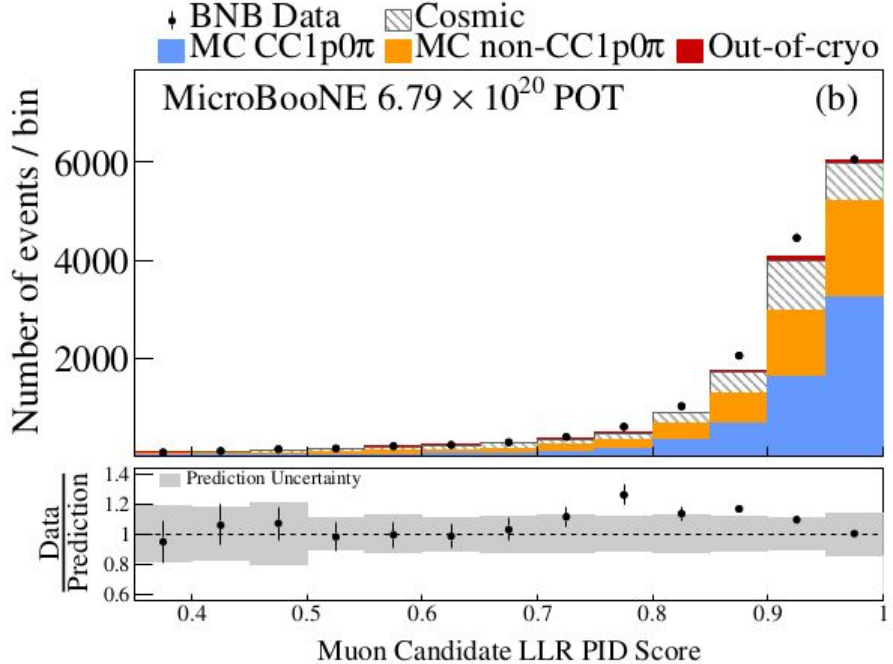
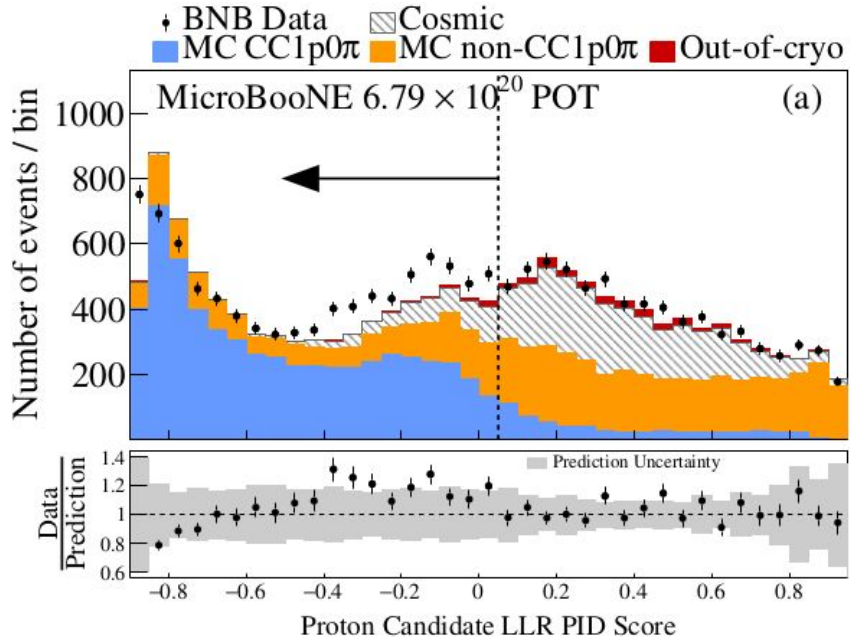


FIG. 2. (Top) the proton candidate LLR PID score distribution, illustrating the fitness of a cut at LLR PID  $< 0.05$  to reject cosmic and non-CC1p0 $\pi$  background events. (Bottom) the muon candidate LLR PID score distribution, illustrating a peak close to one. Only statistical uncertainties are shown on the data. The bottom panel shows the ratio of data to prediction.

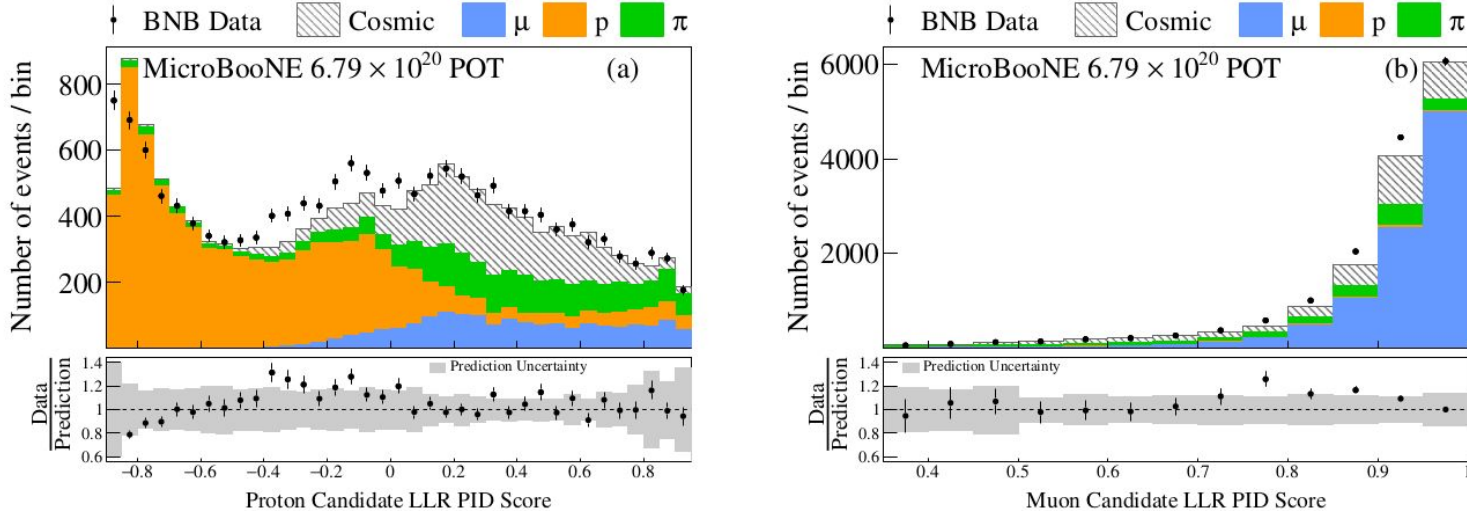


FIG. 1. (Left) the proton candidate LLR PID score distribution, illustrating the particle composition of the variable. (Right) the muon candidate LLR PID score distribution, illustrating a peak close to one. Only statistical uncertainties are shown on the data. The bottom panel shows the ratio of data to prediction.

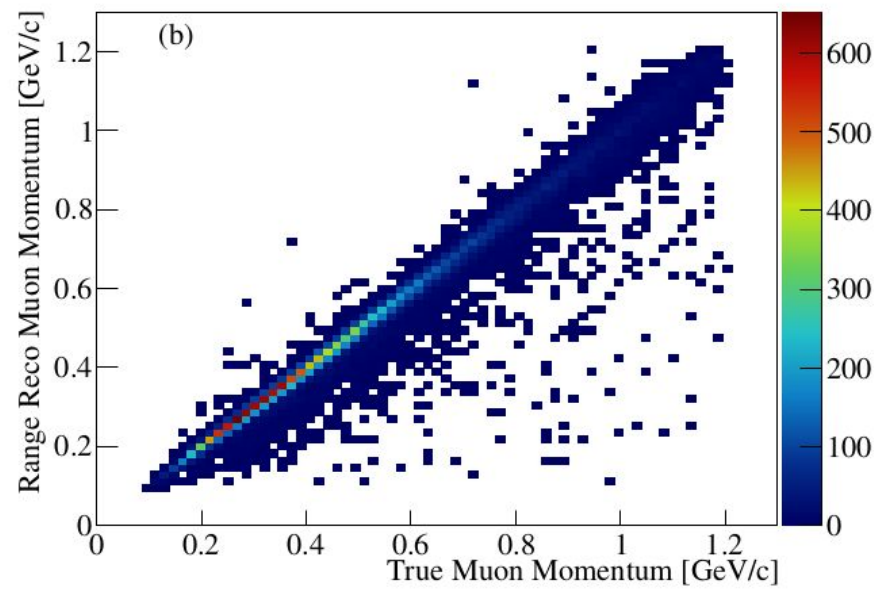
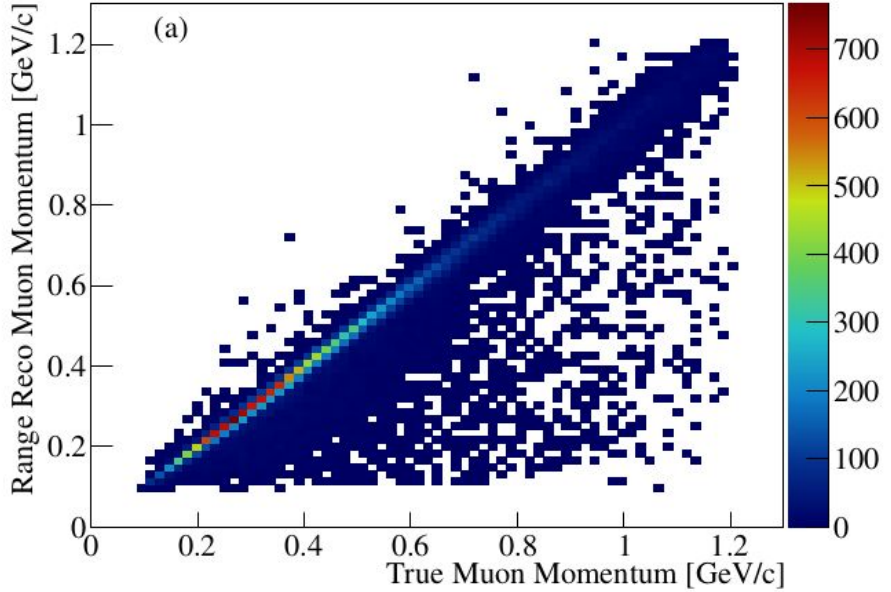
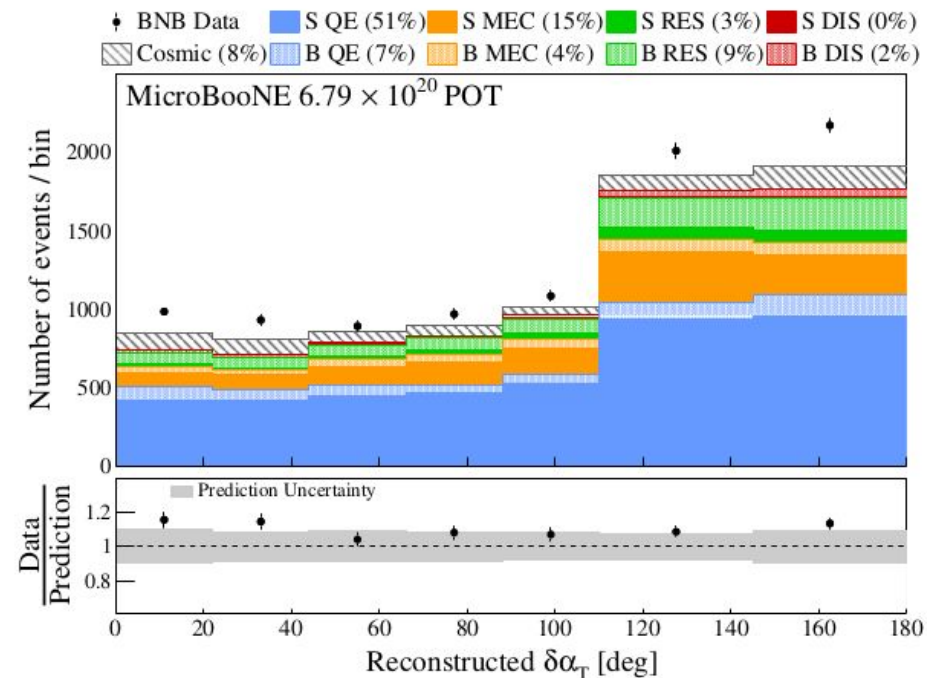
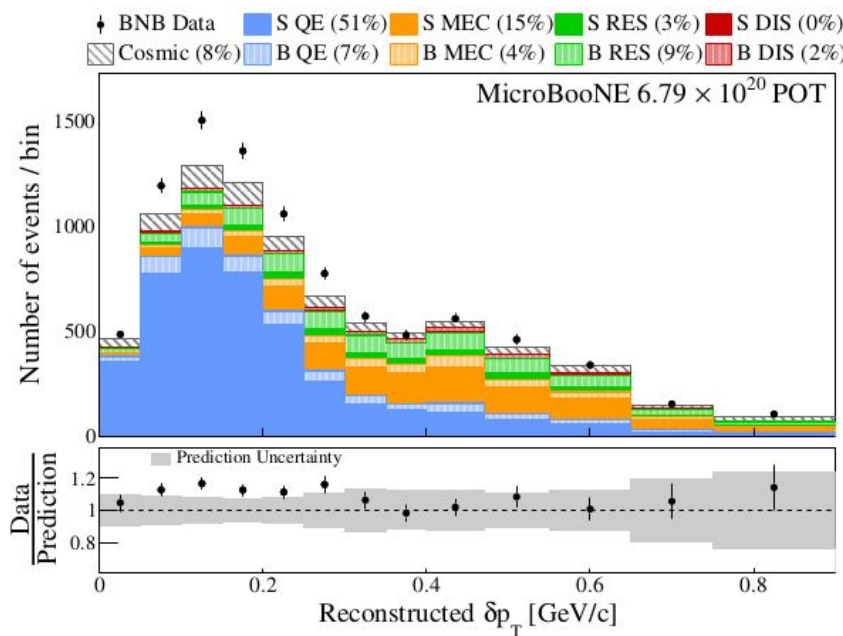
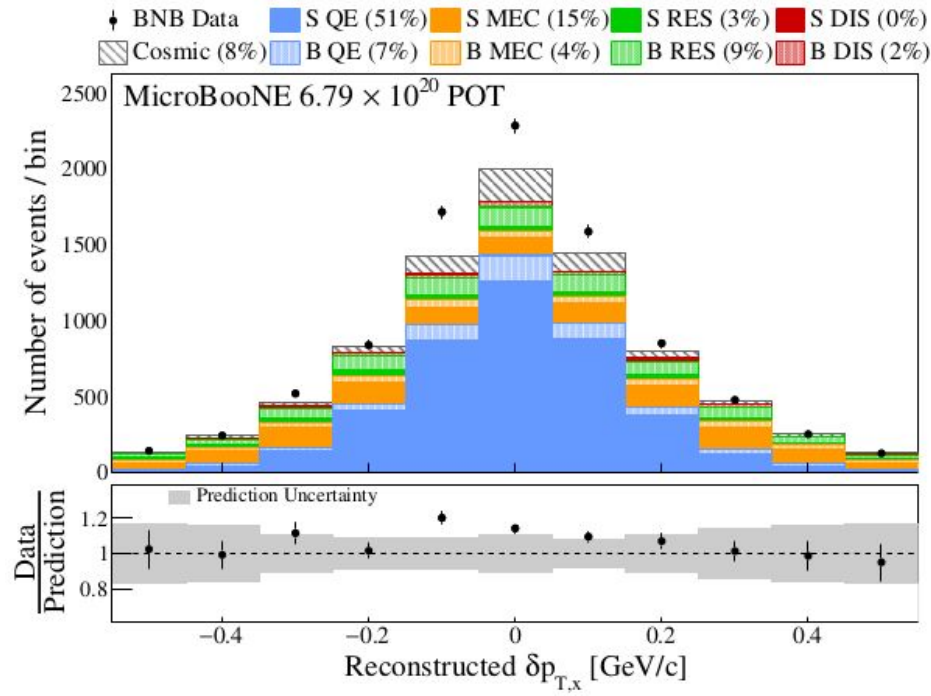
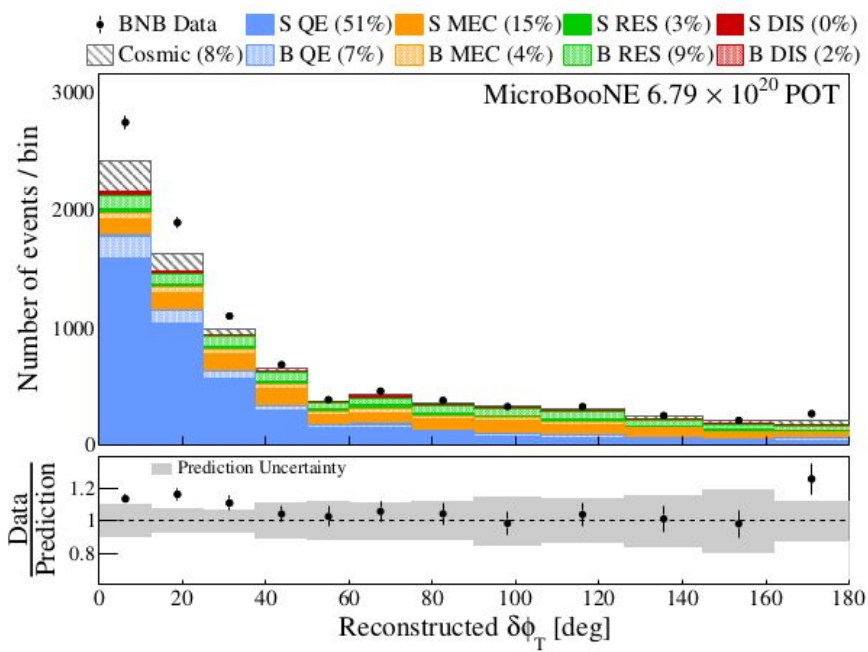
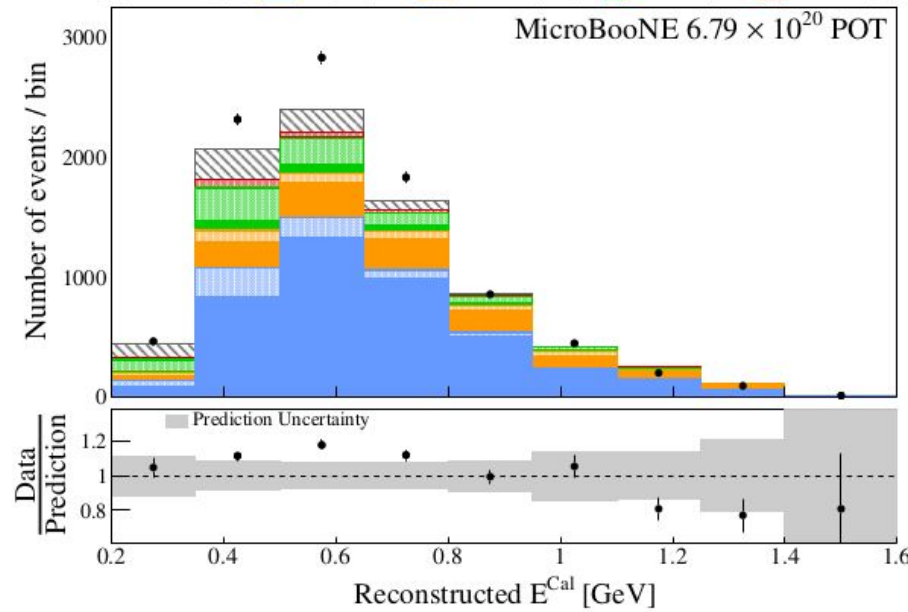
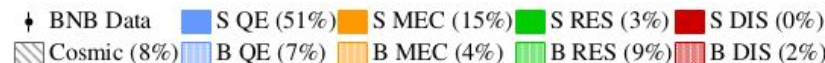
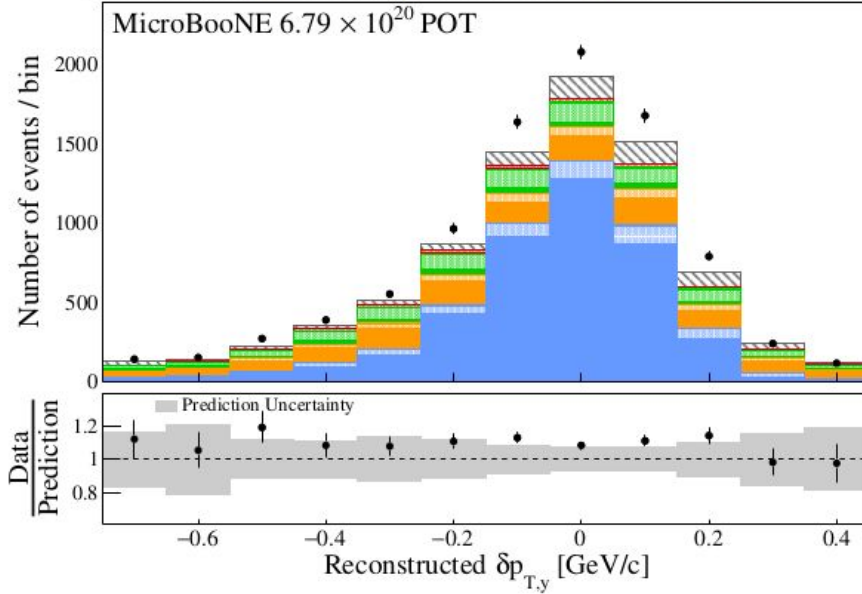
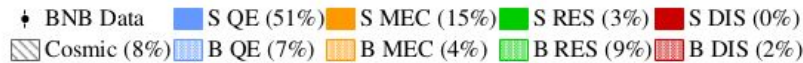
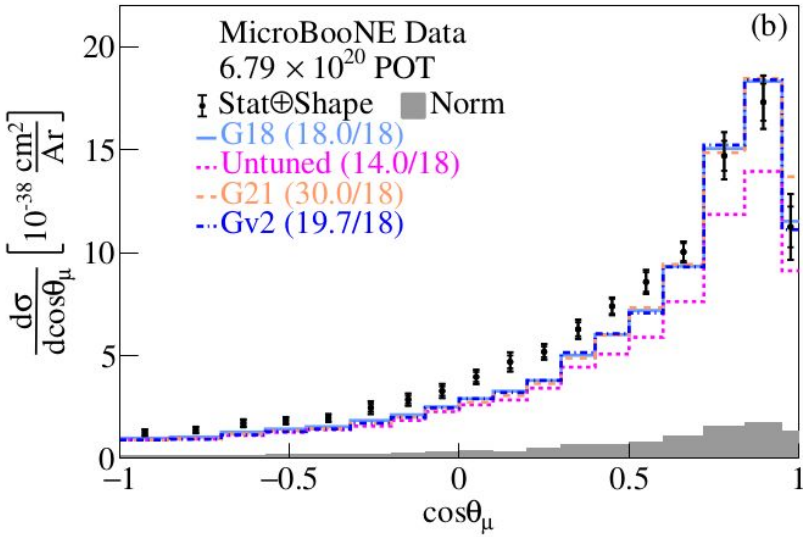
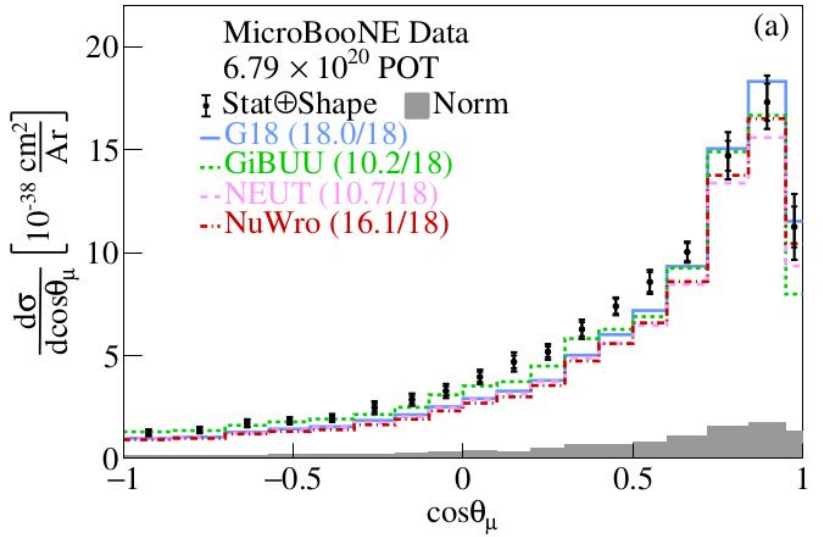


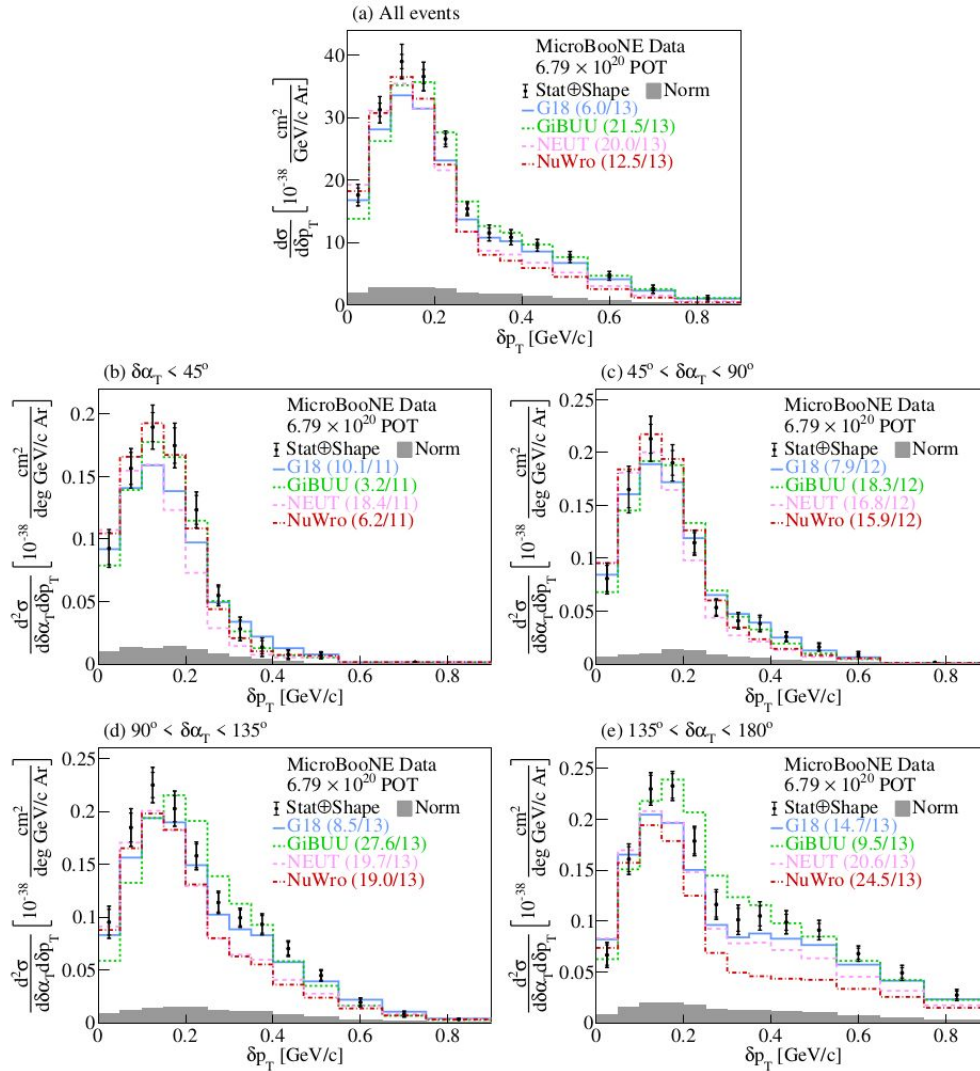
FIG. 3. Muon momentum reconstruction (top) before and (bottom) after the application of the muon momentum quality cut using contained muon tracks.

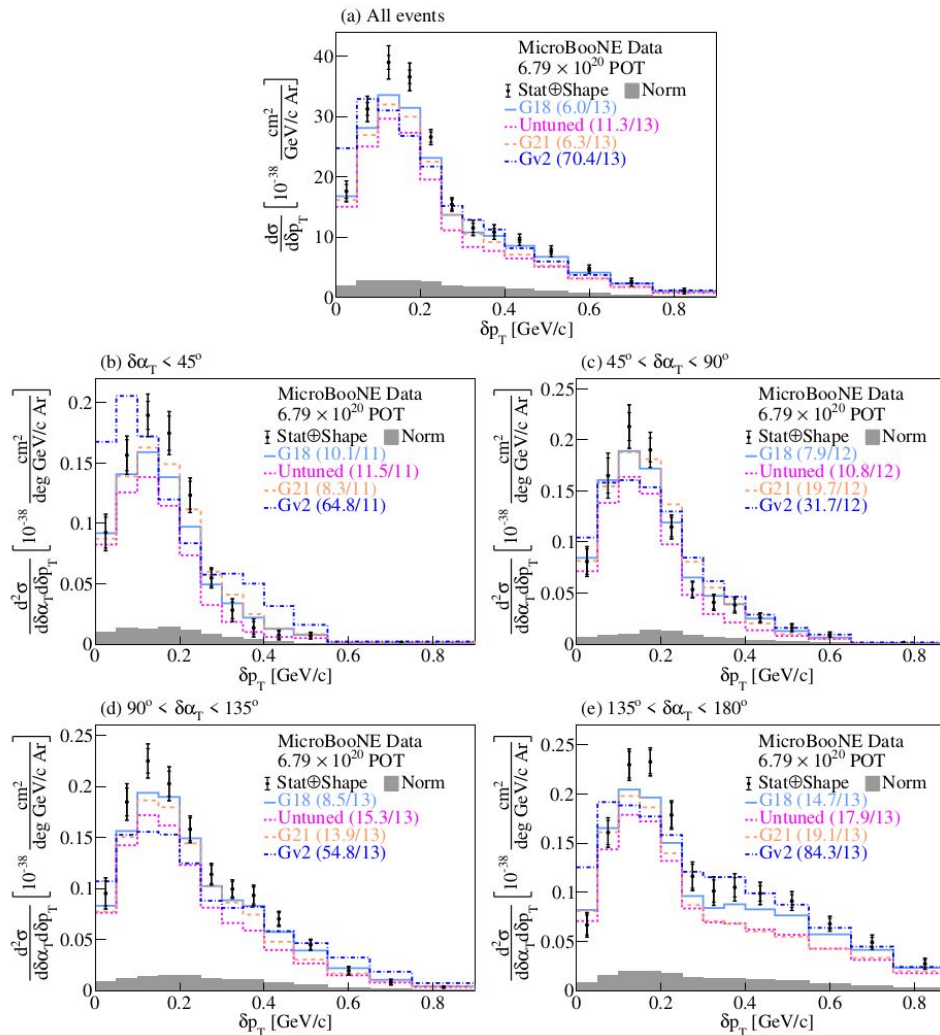


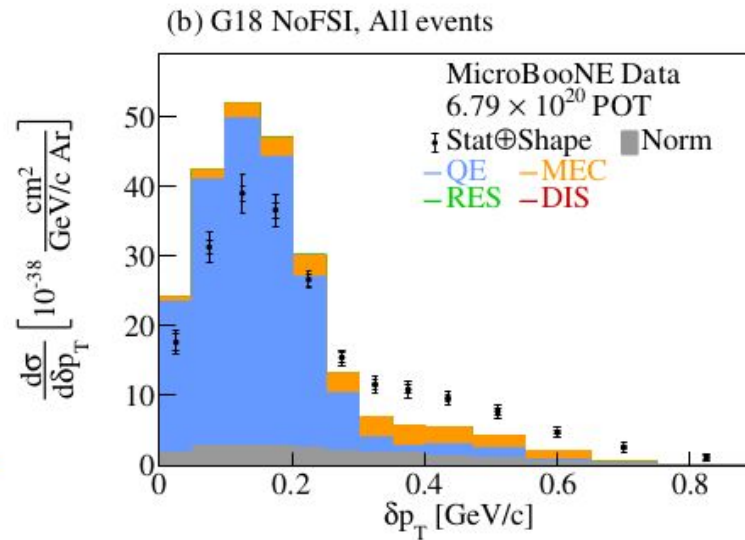
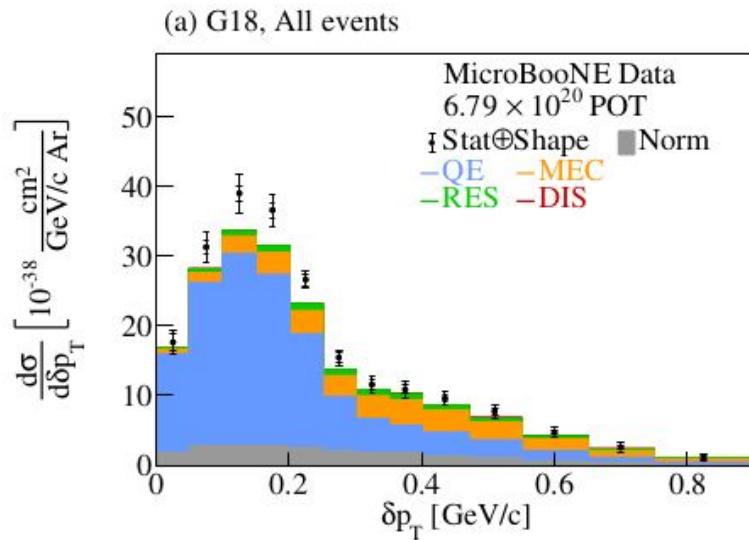


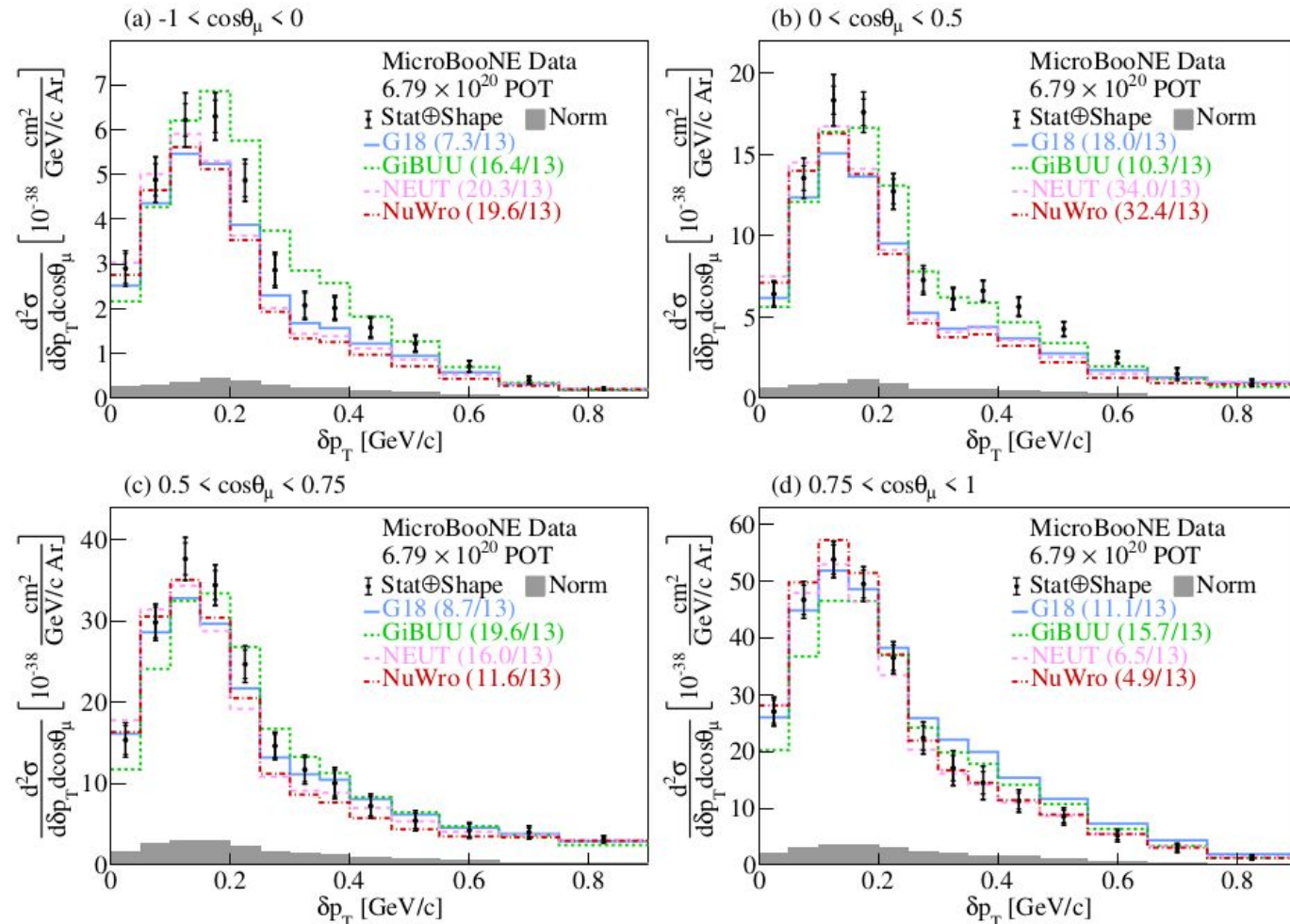


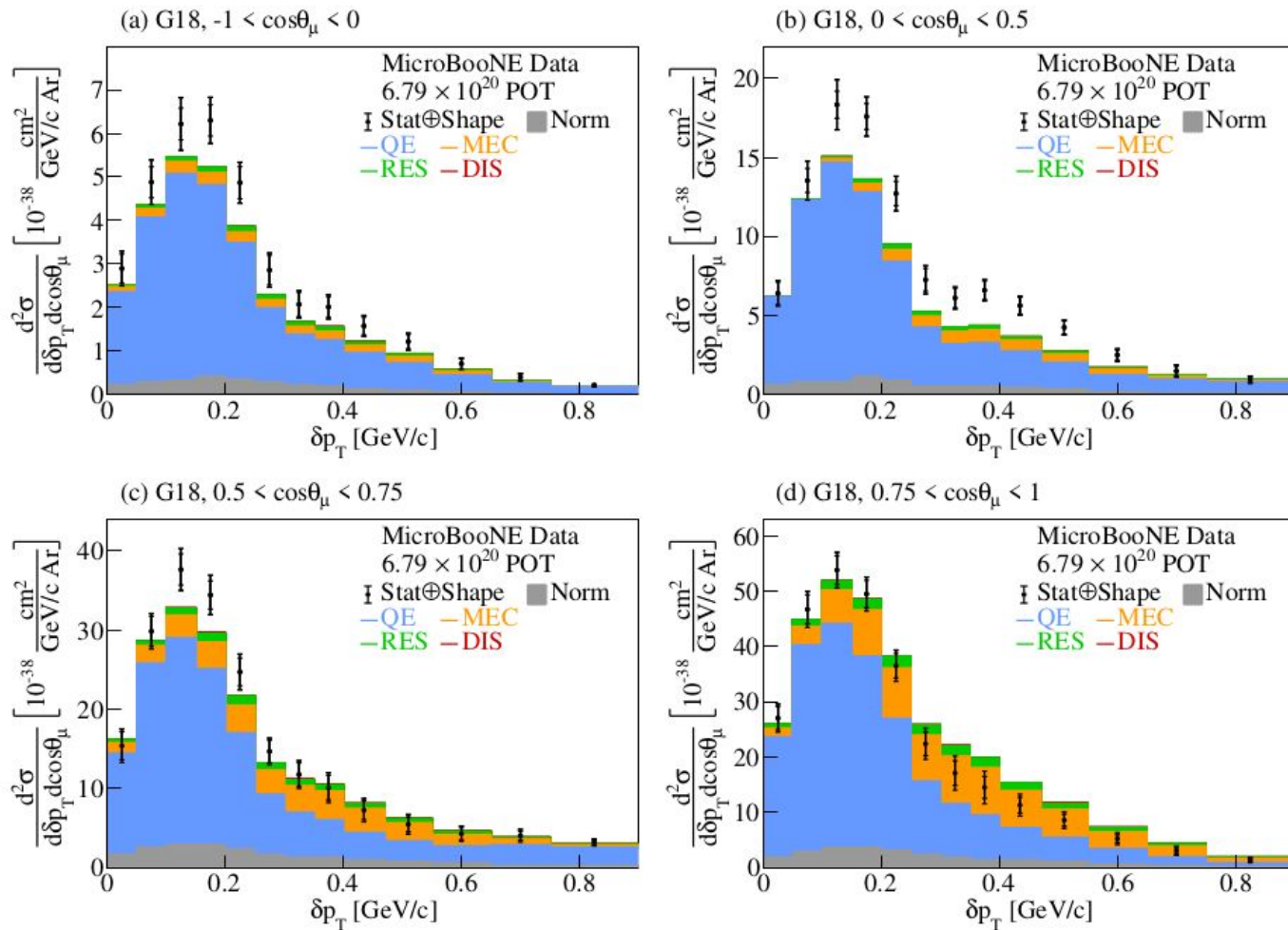


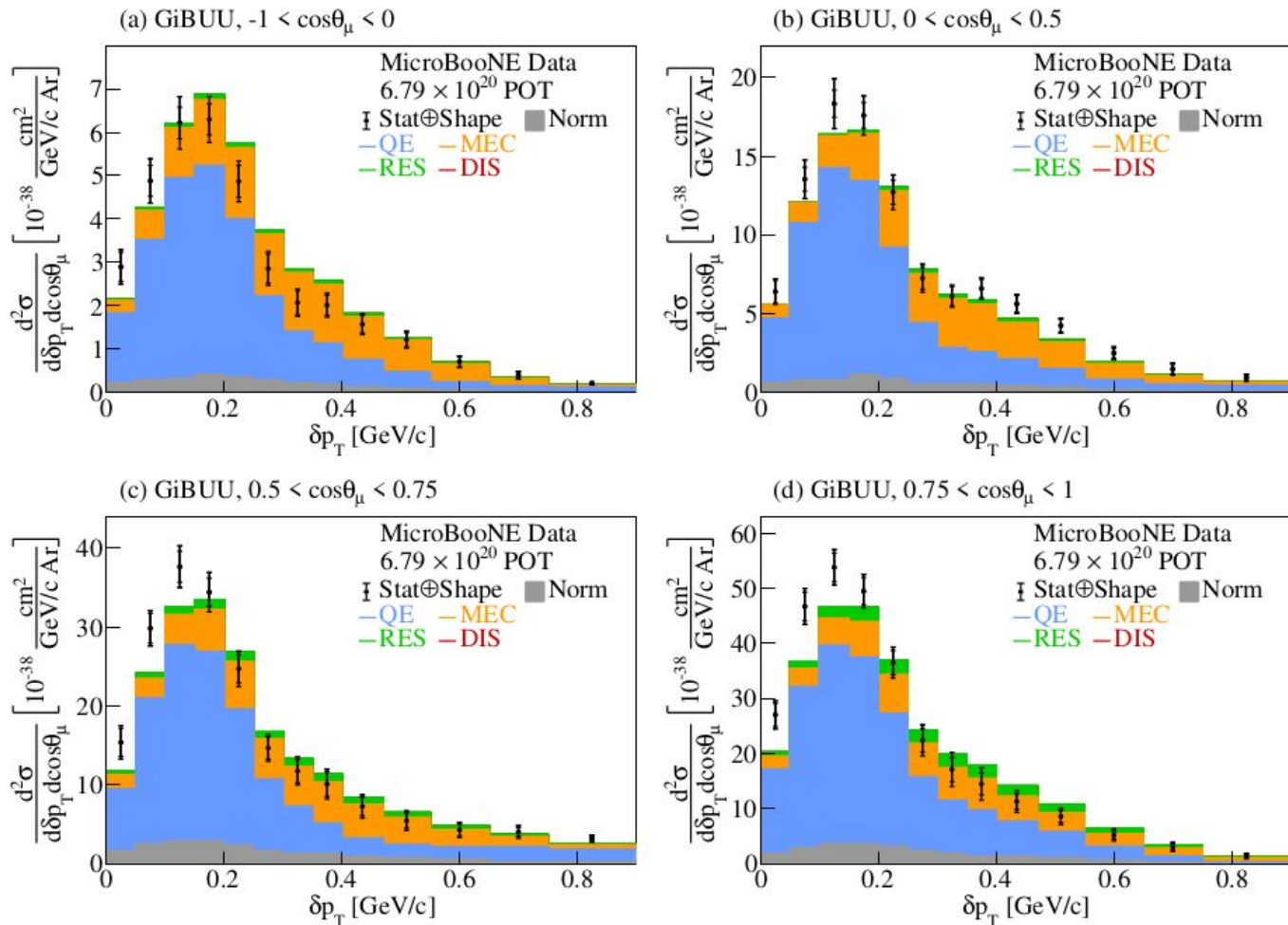


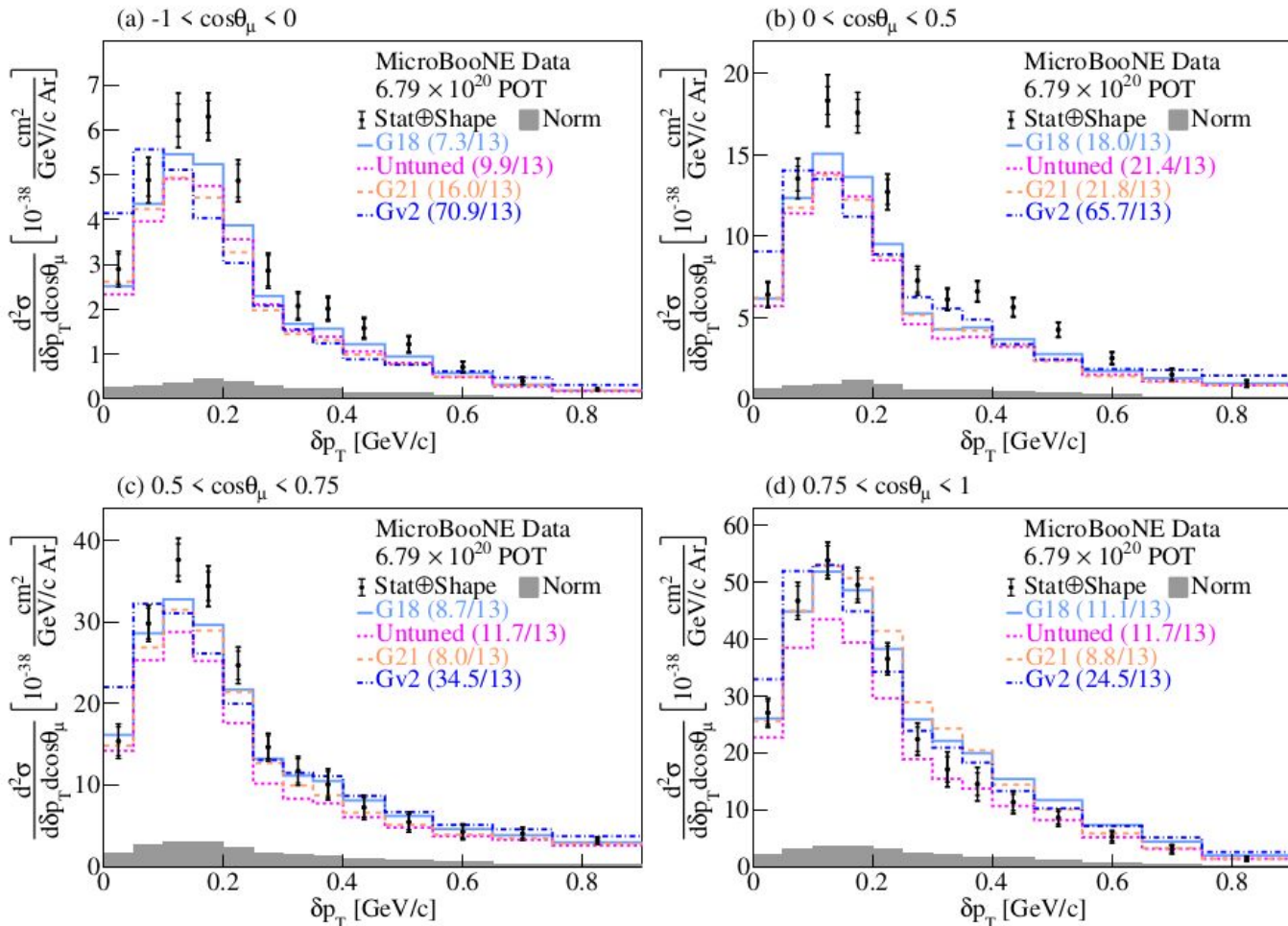


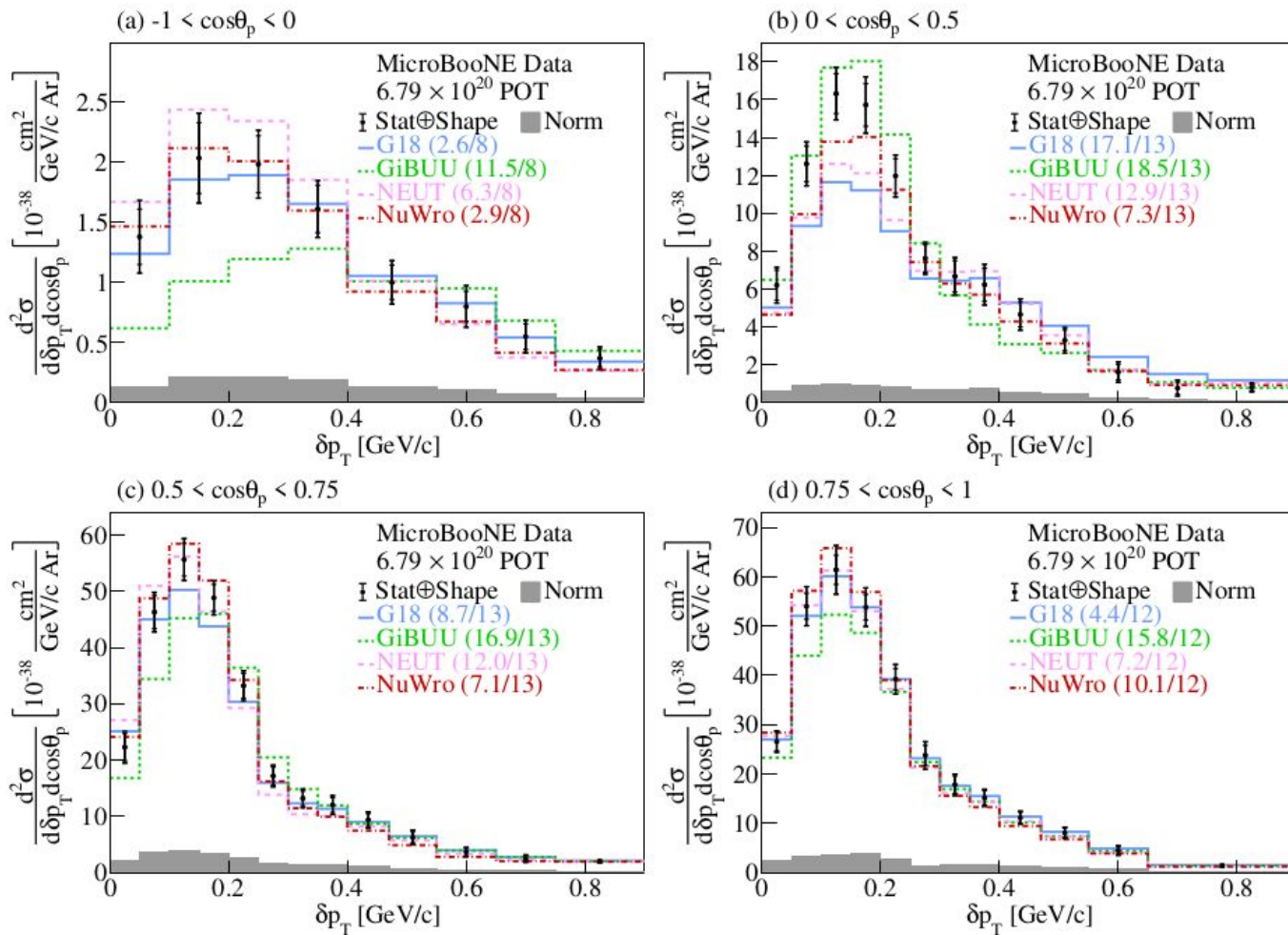


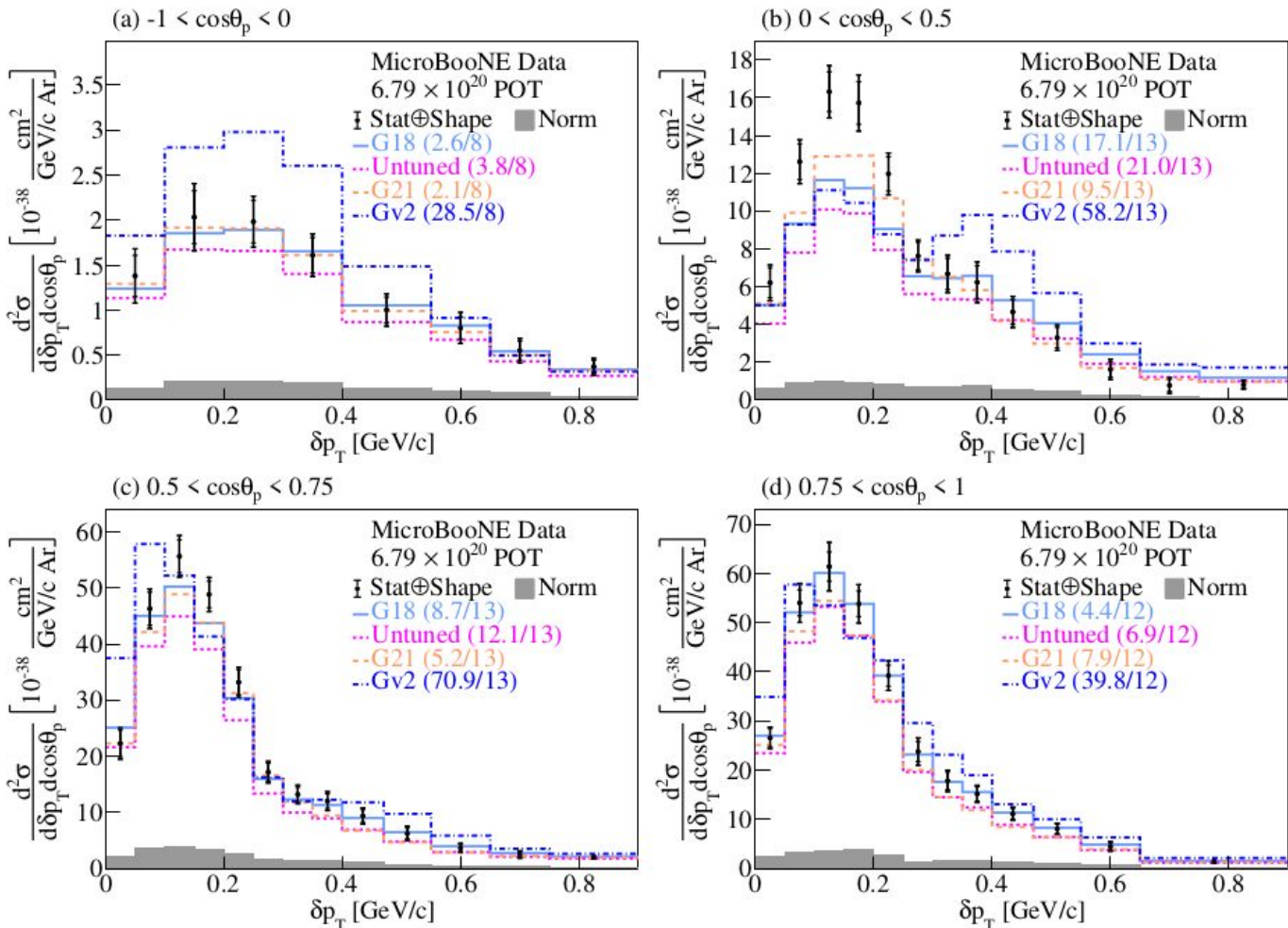


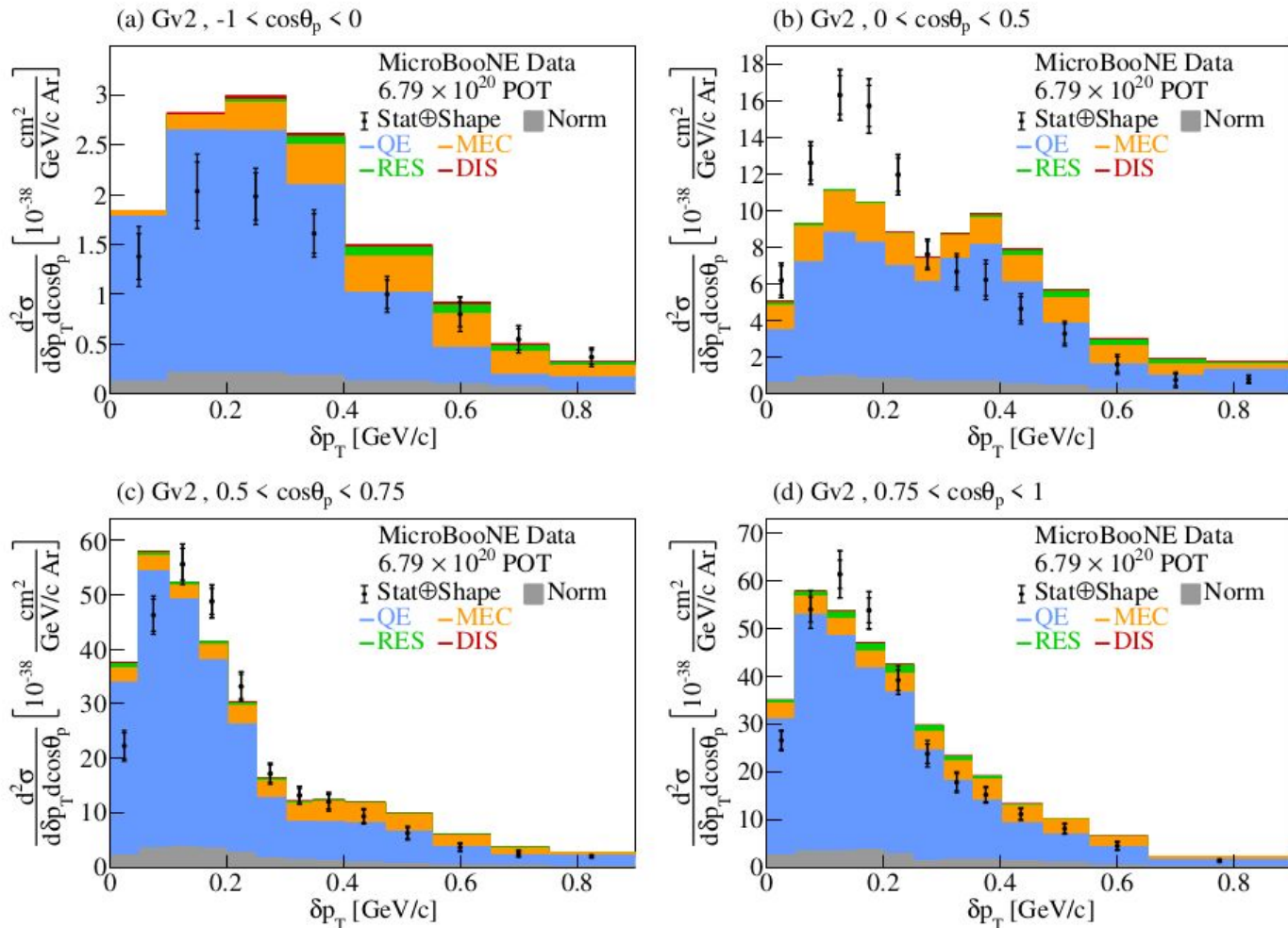


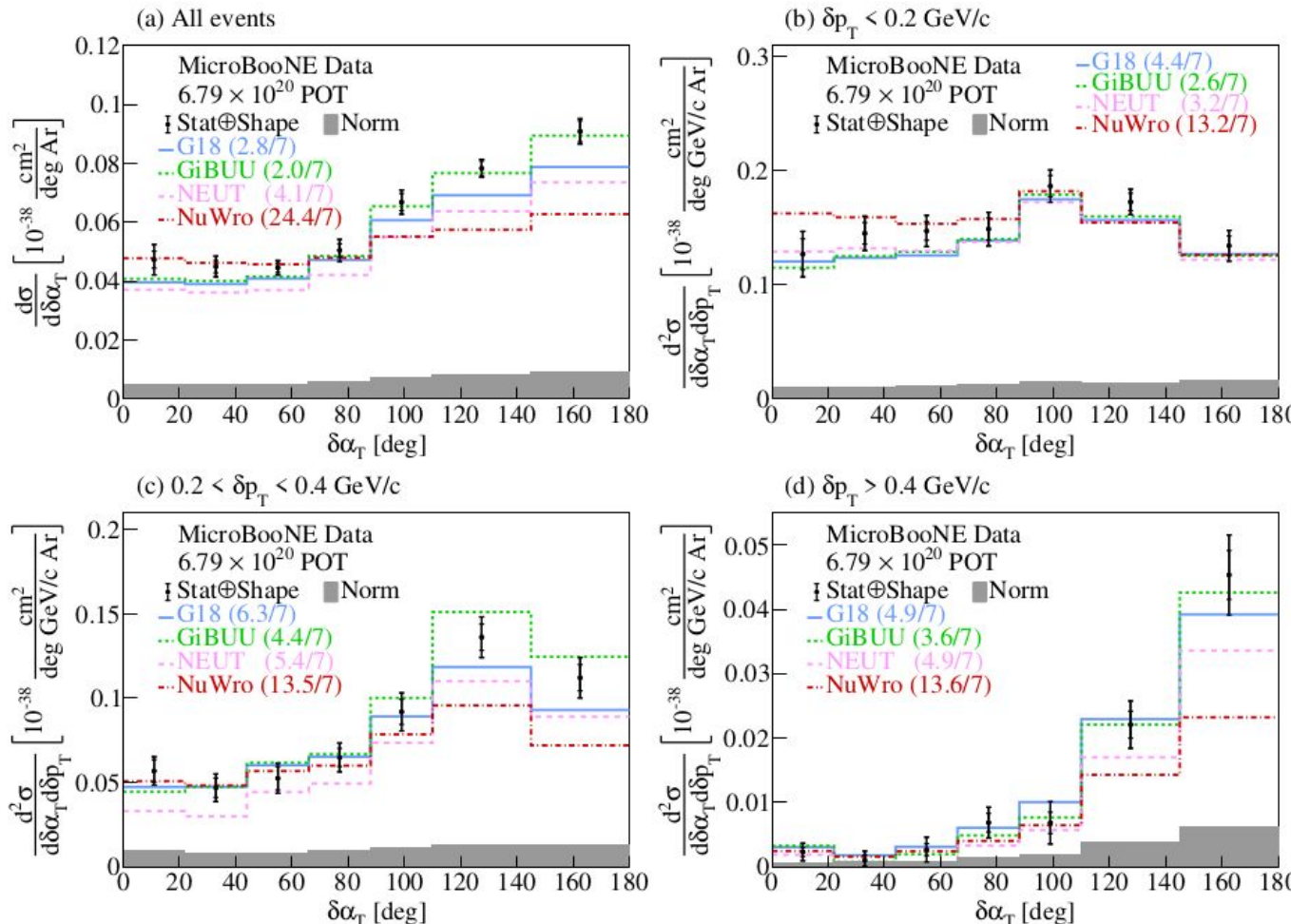


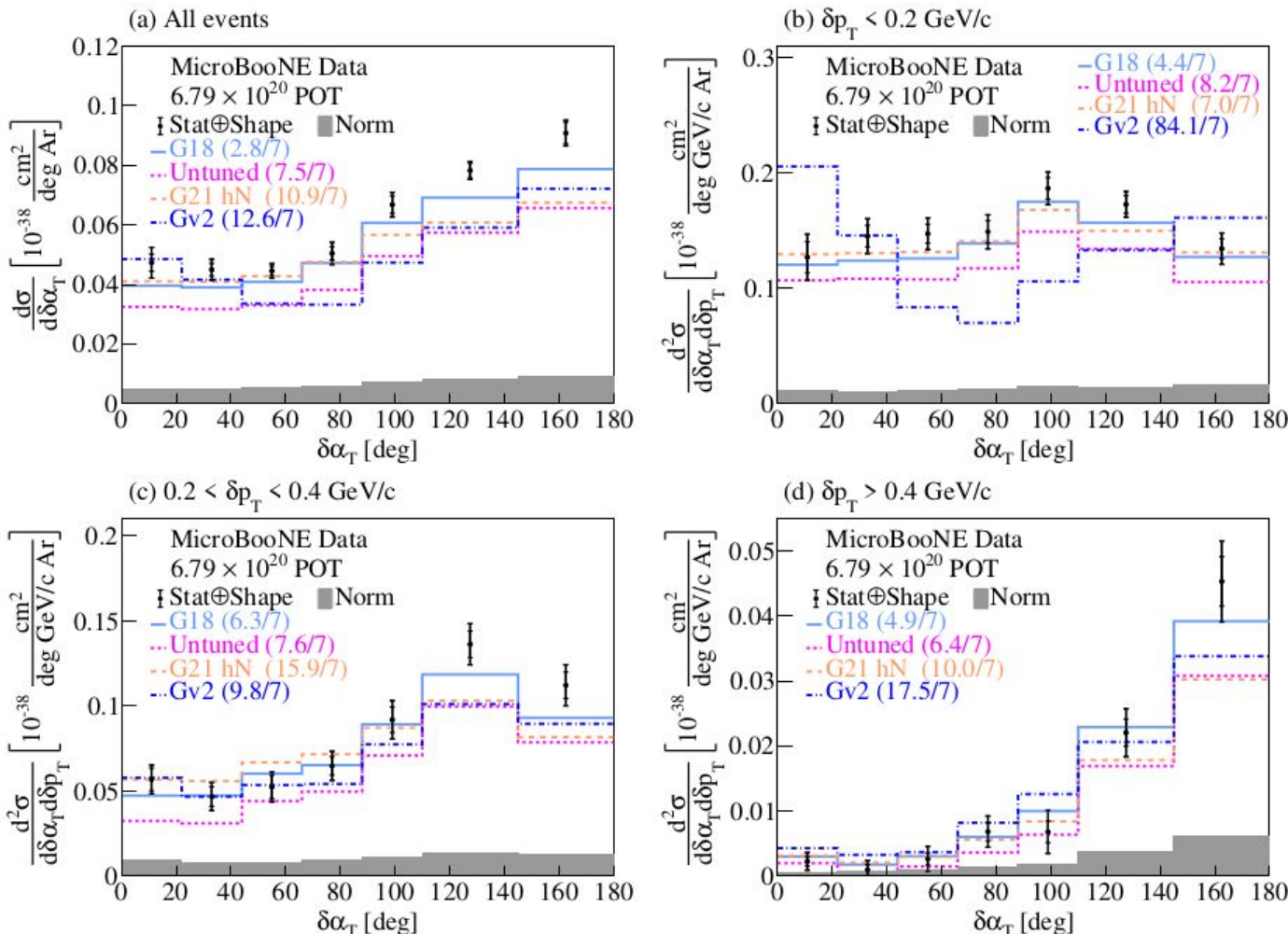


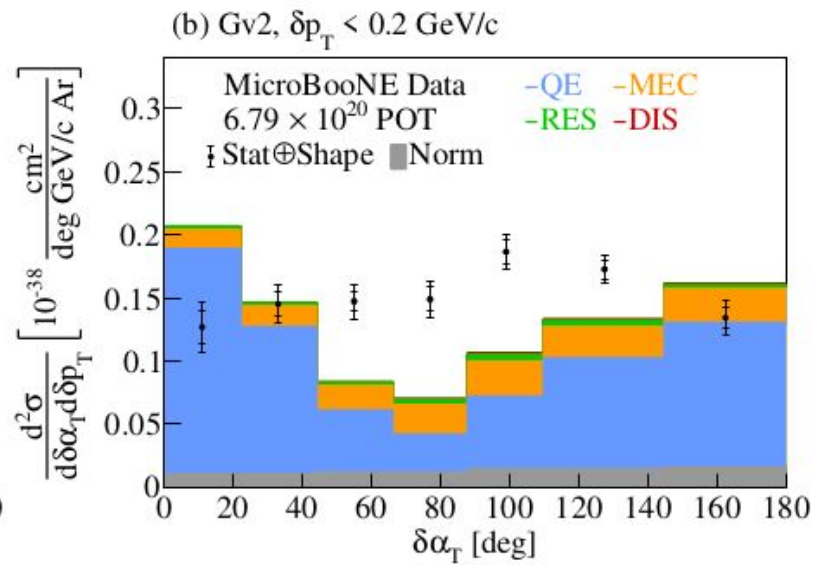
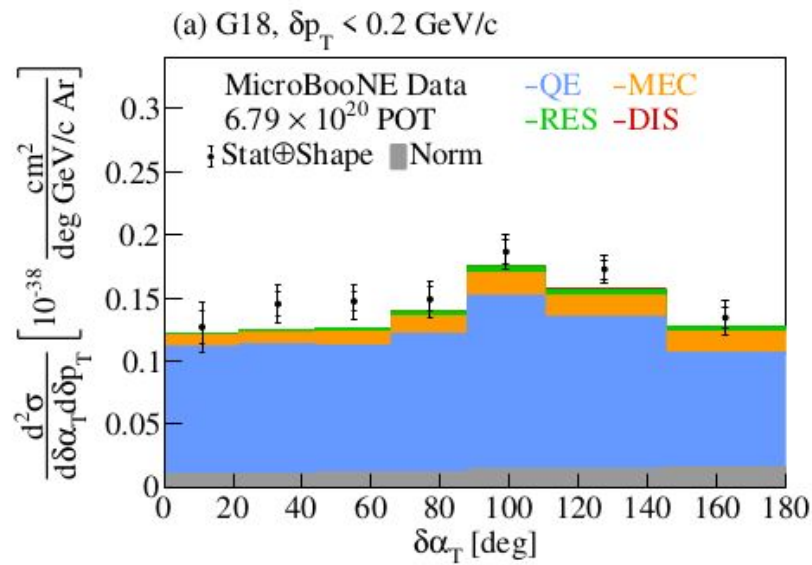


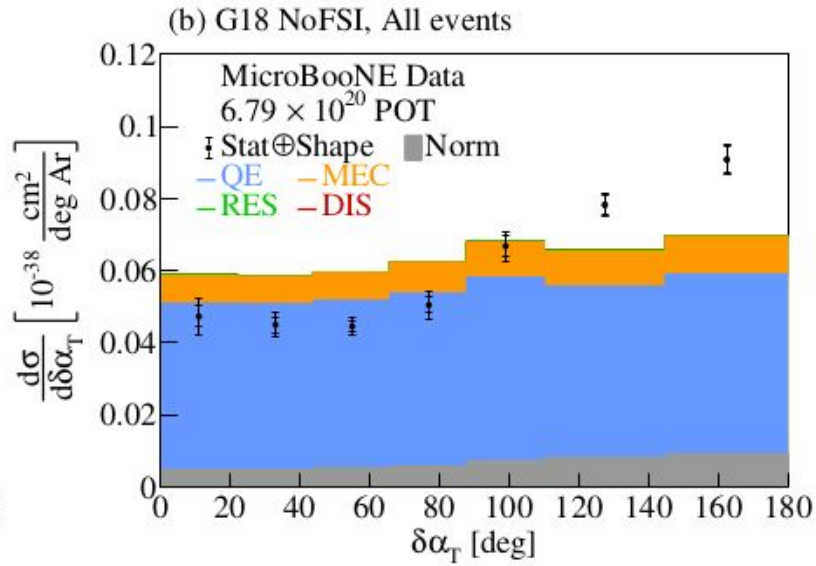
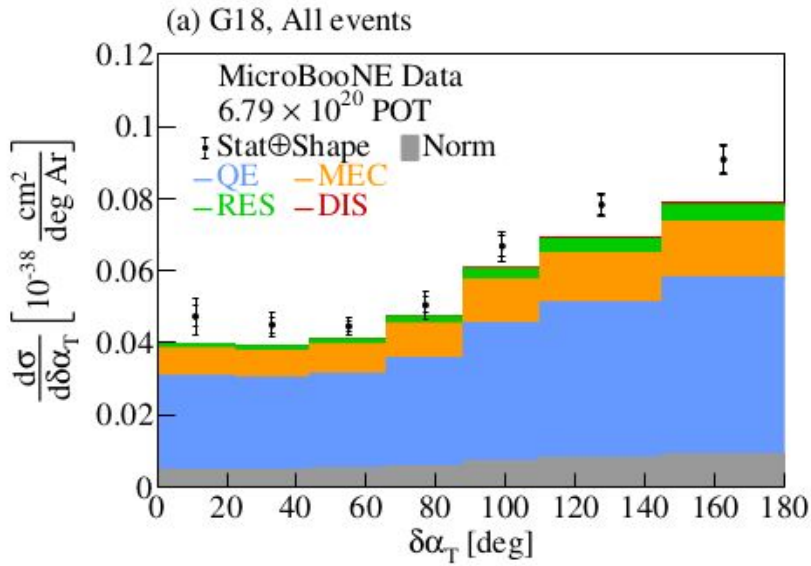


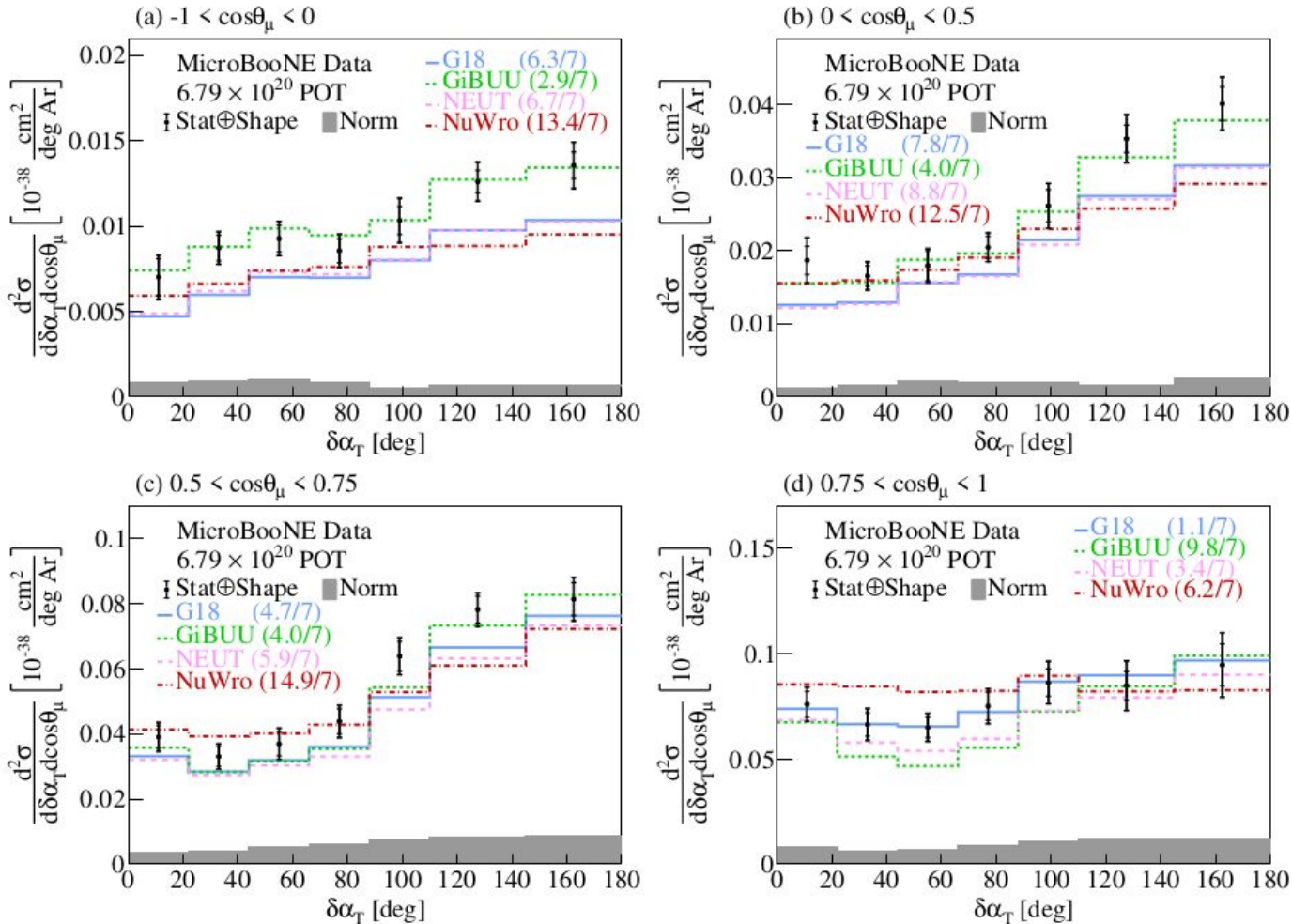


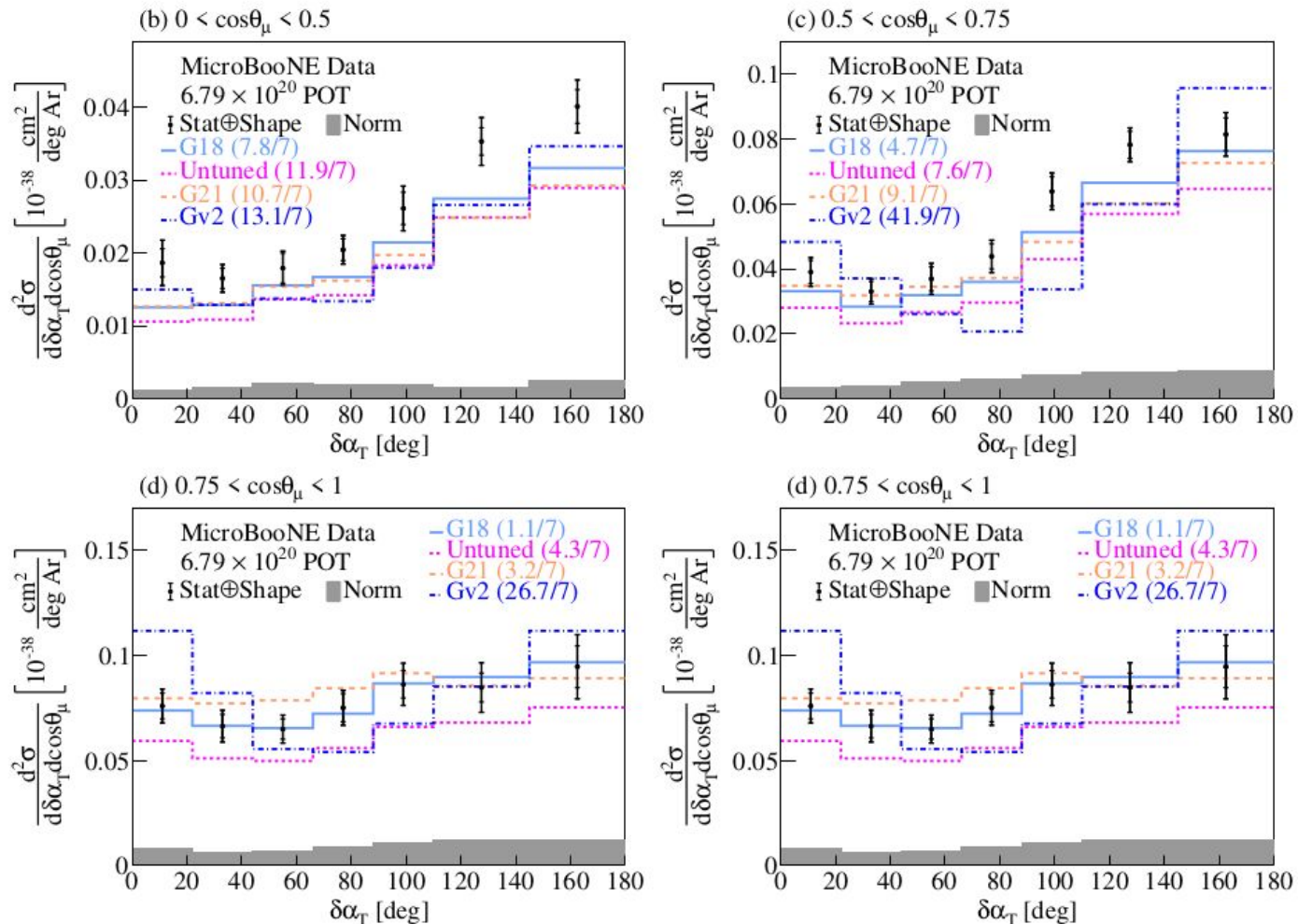


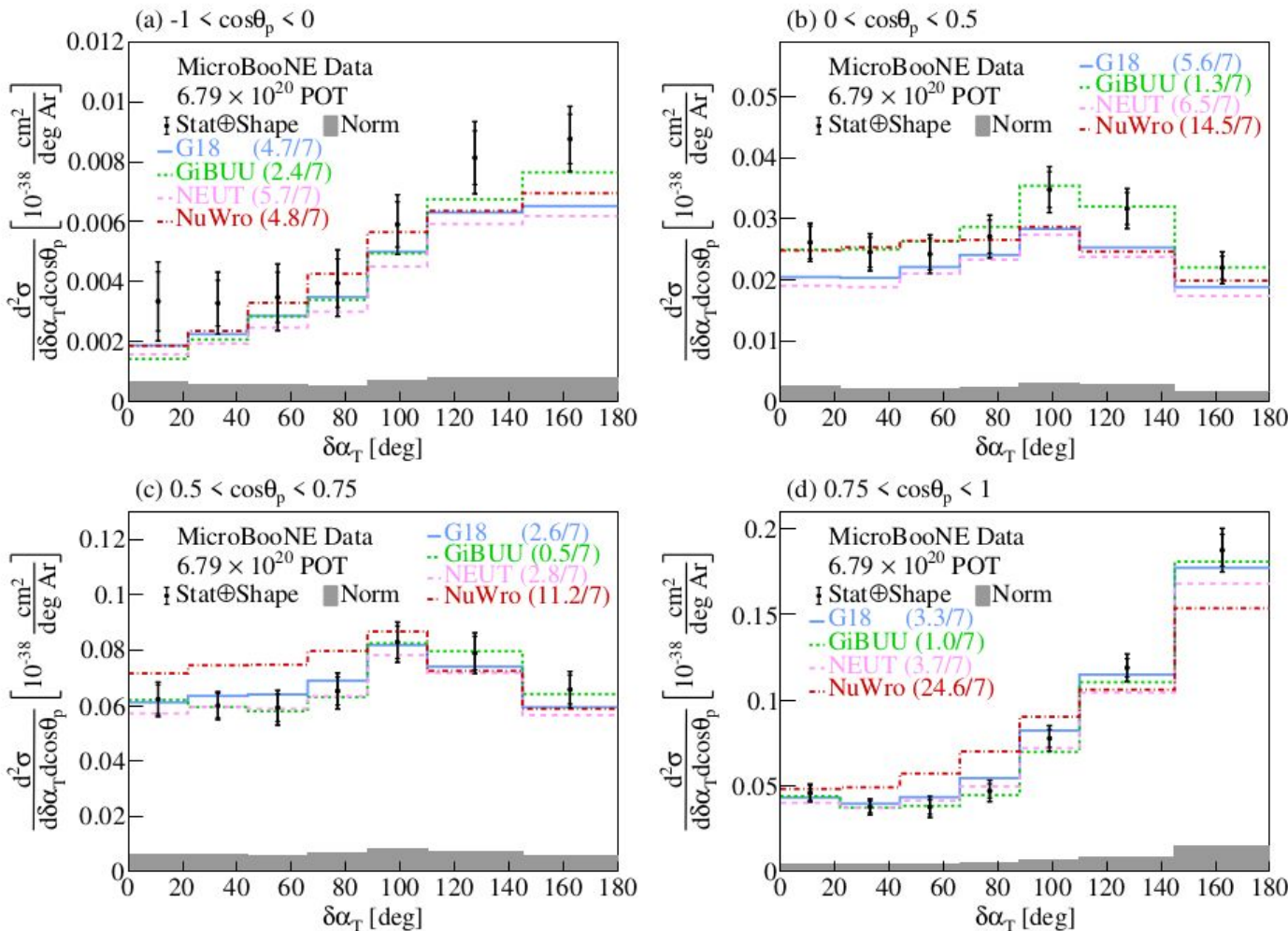


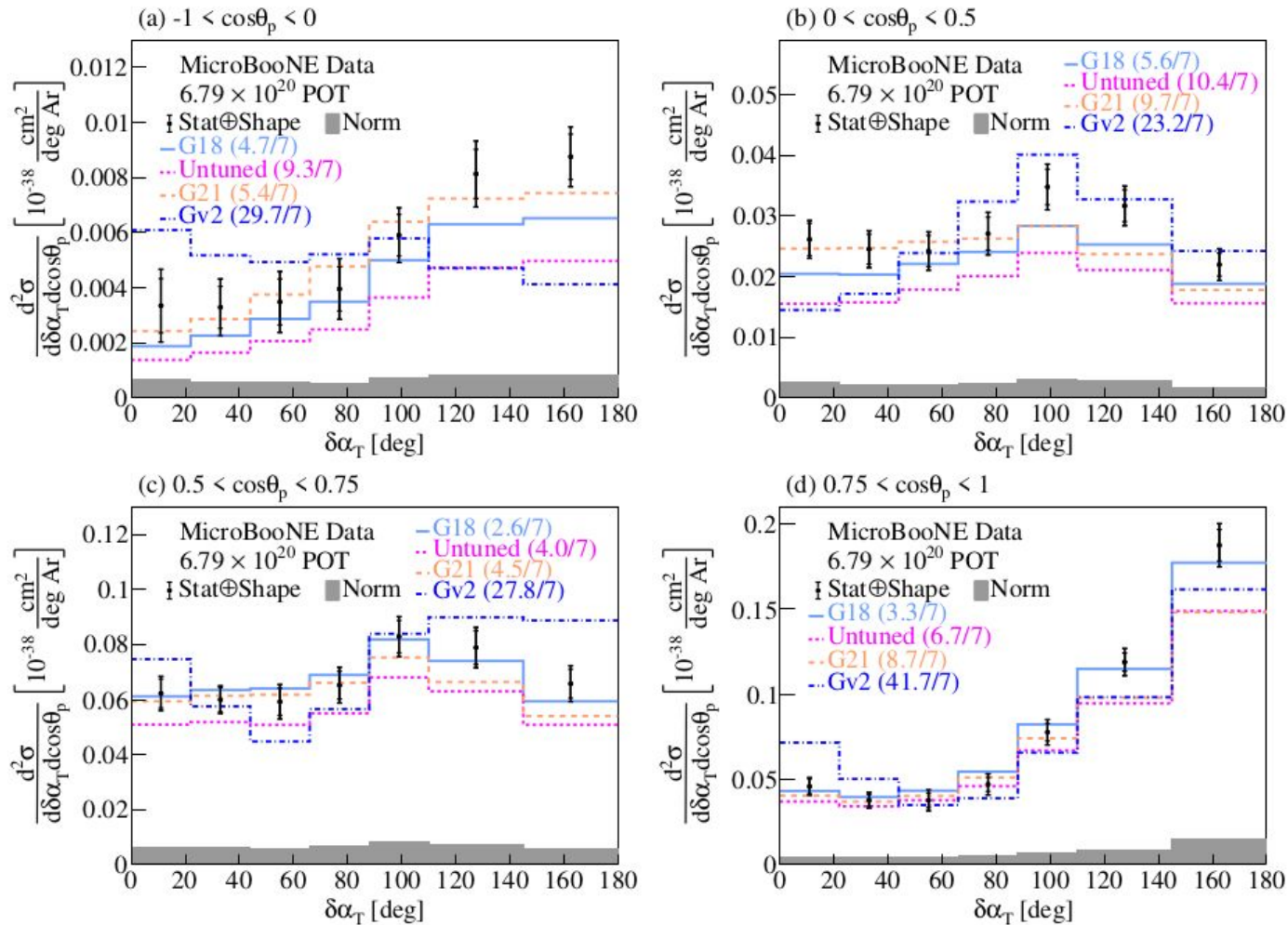


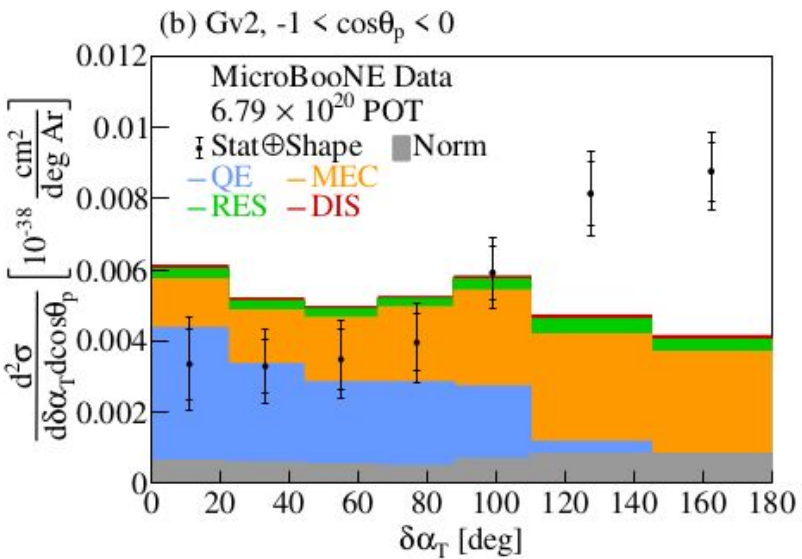
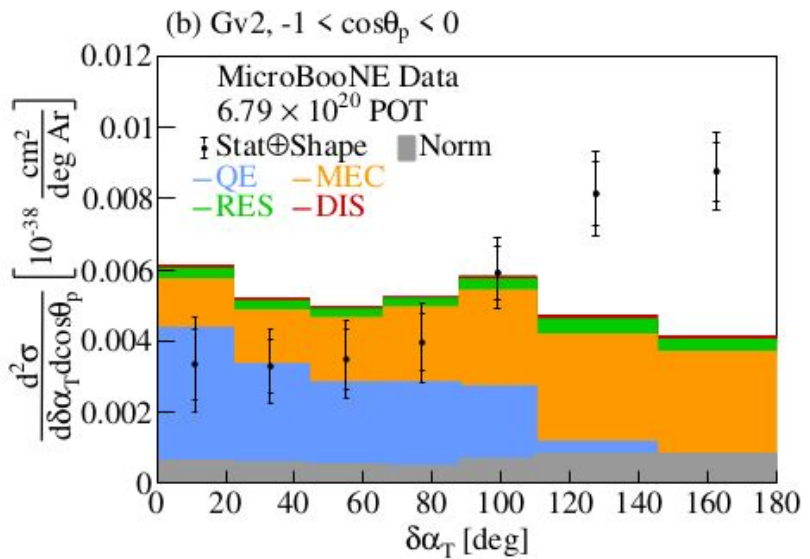


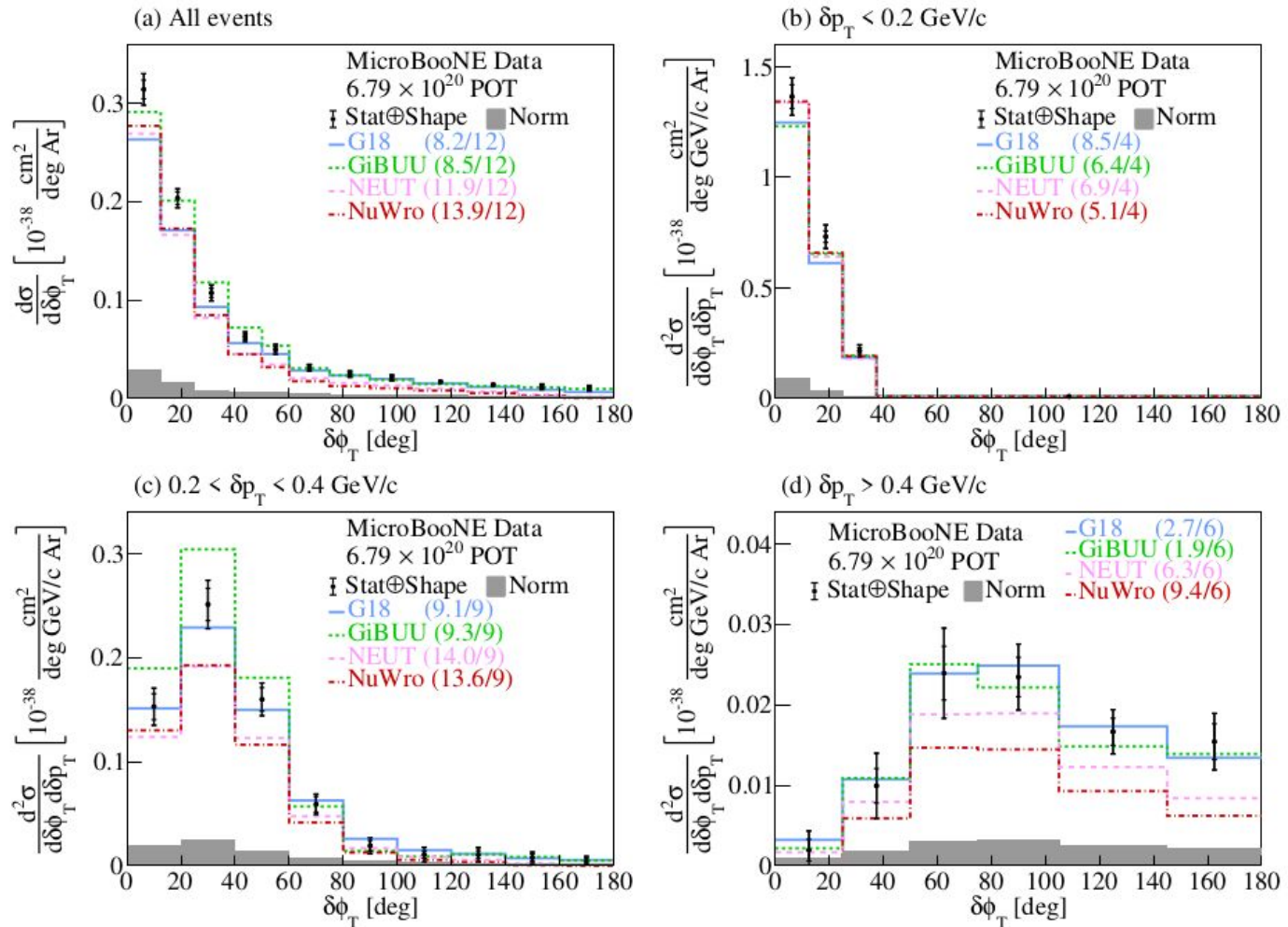


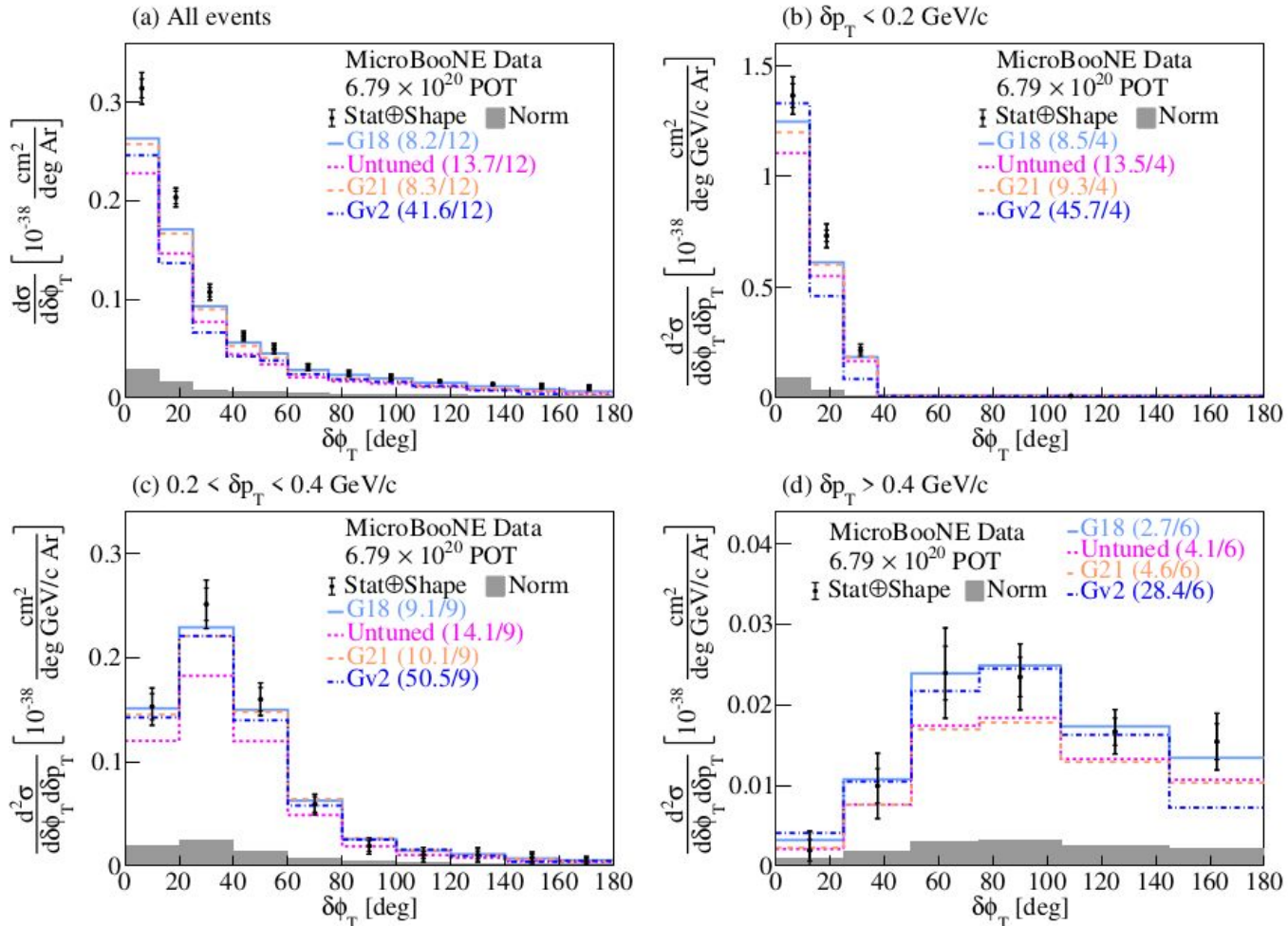


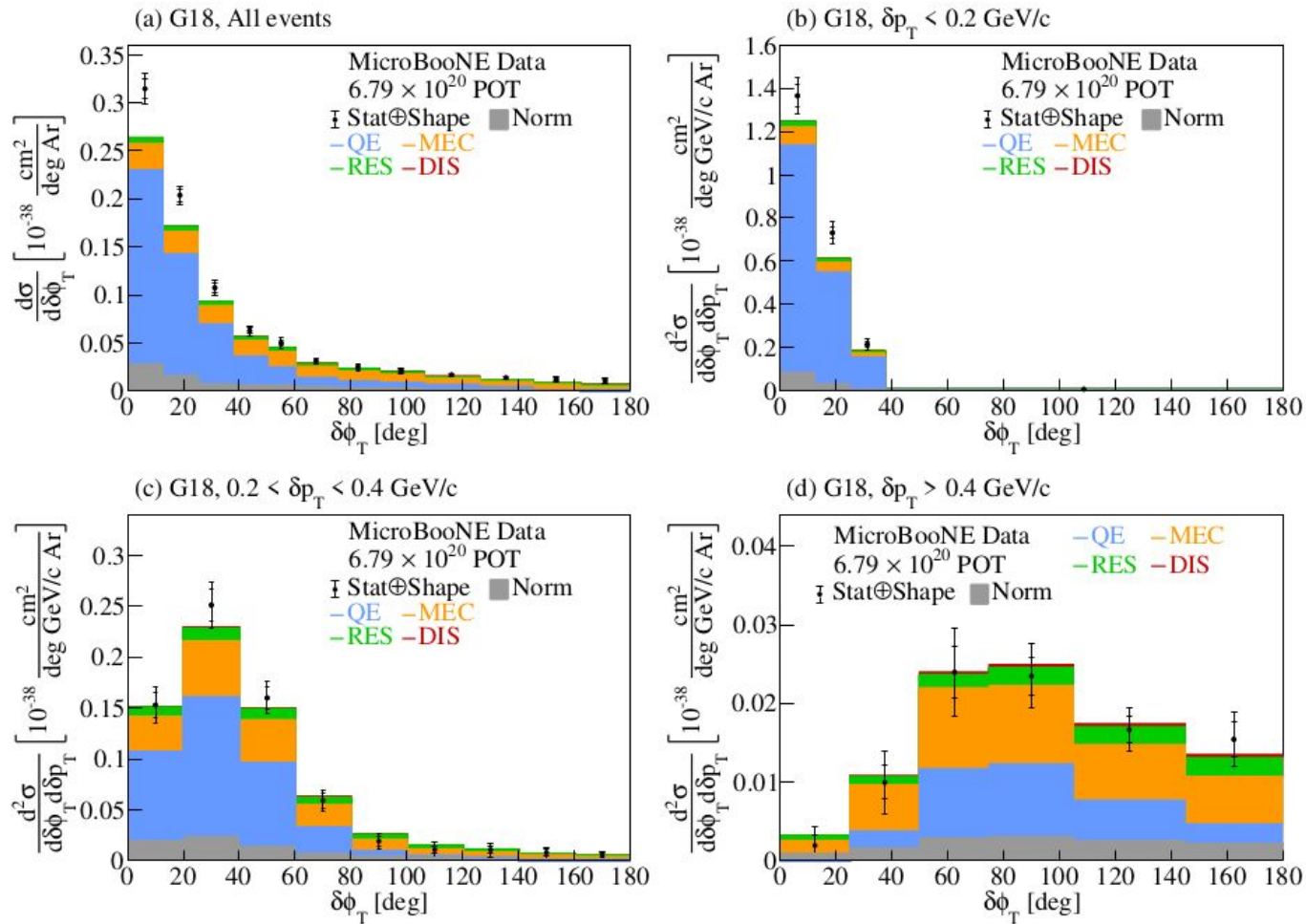


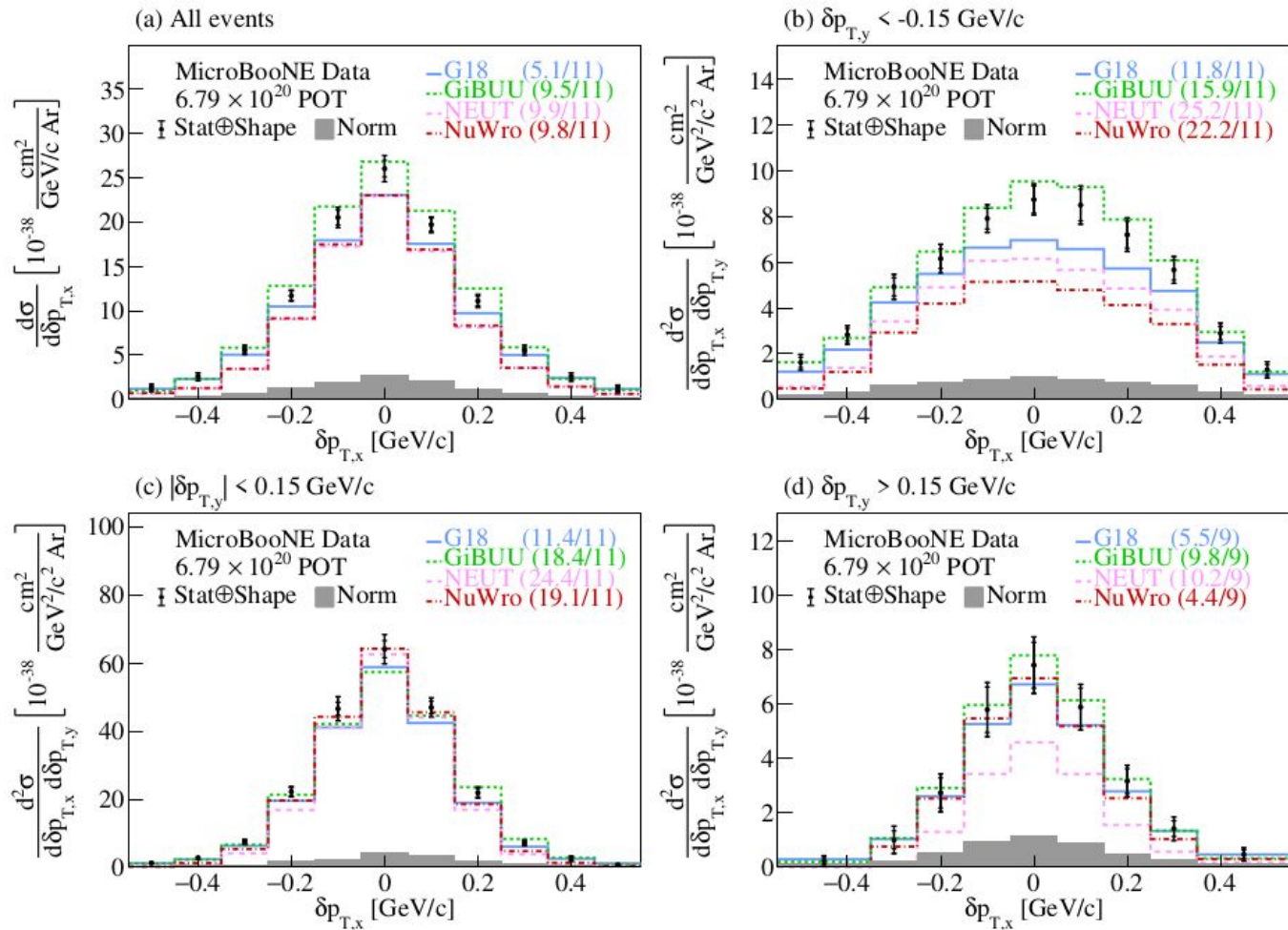


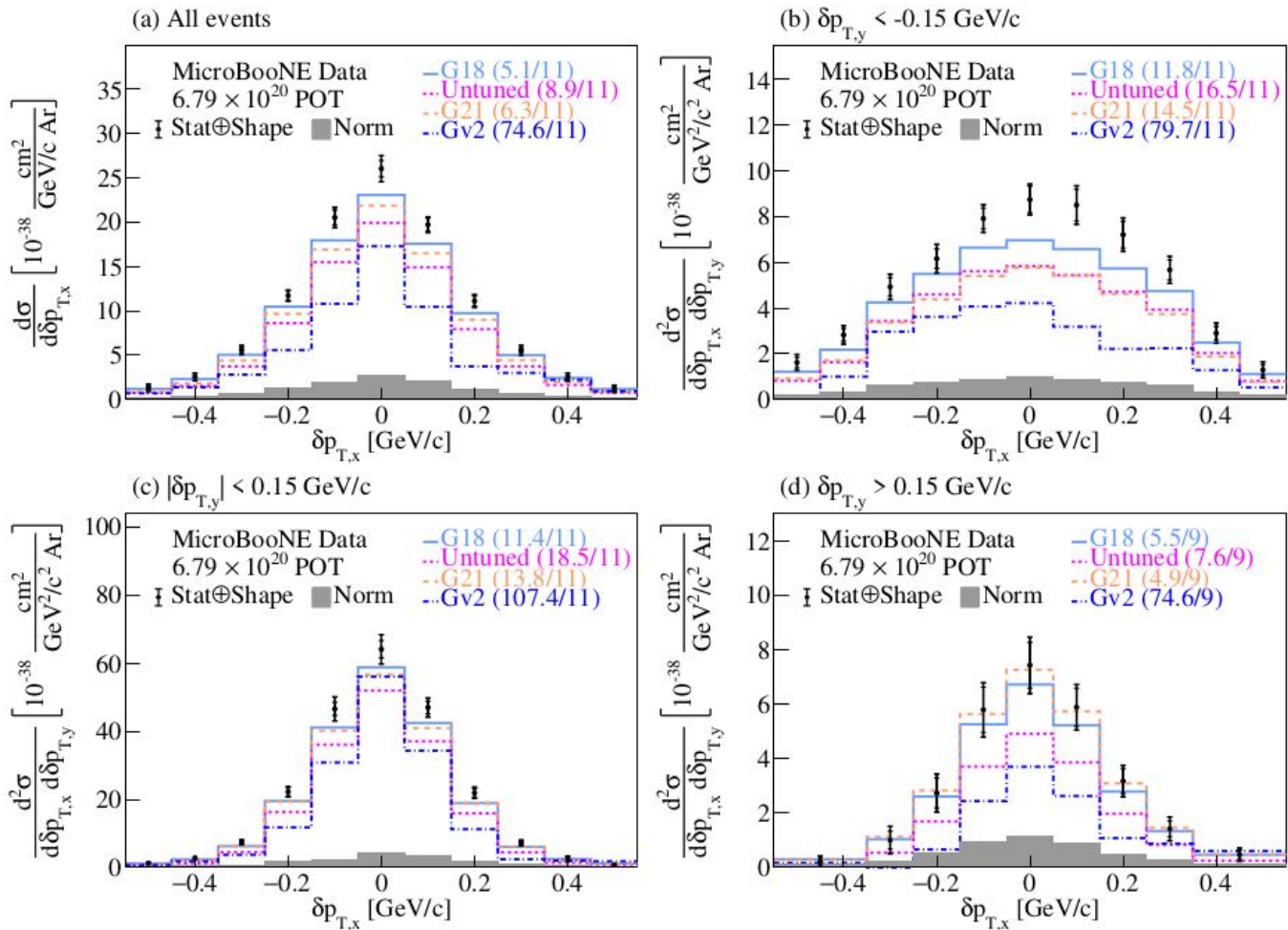


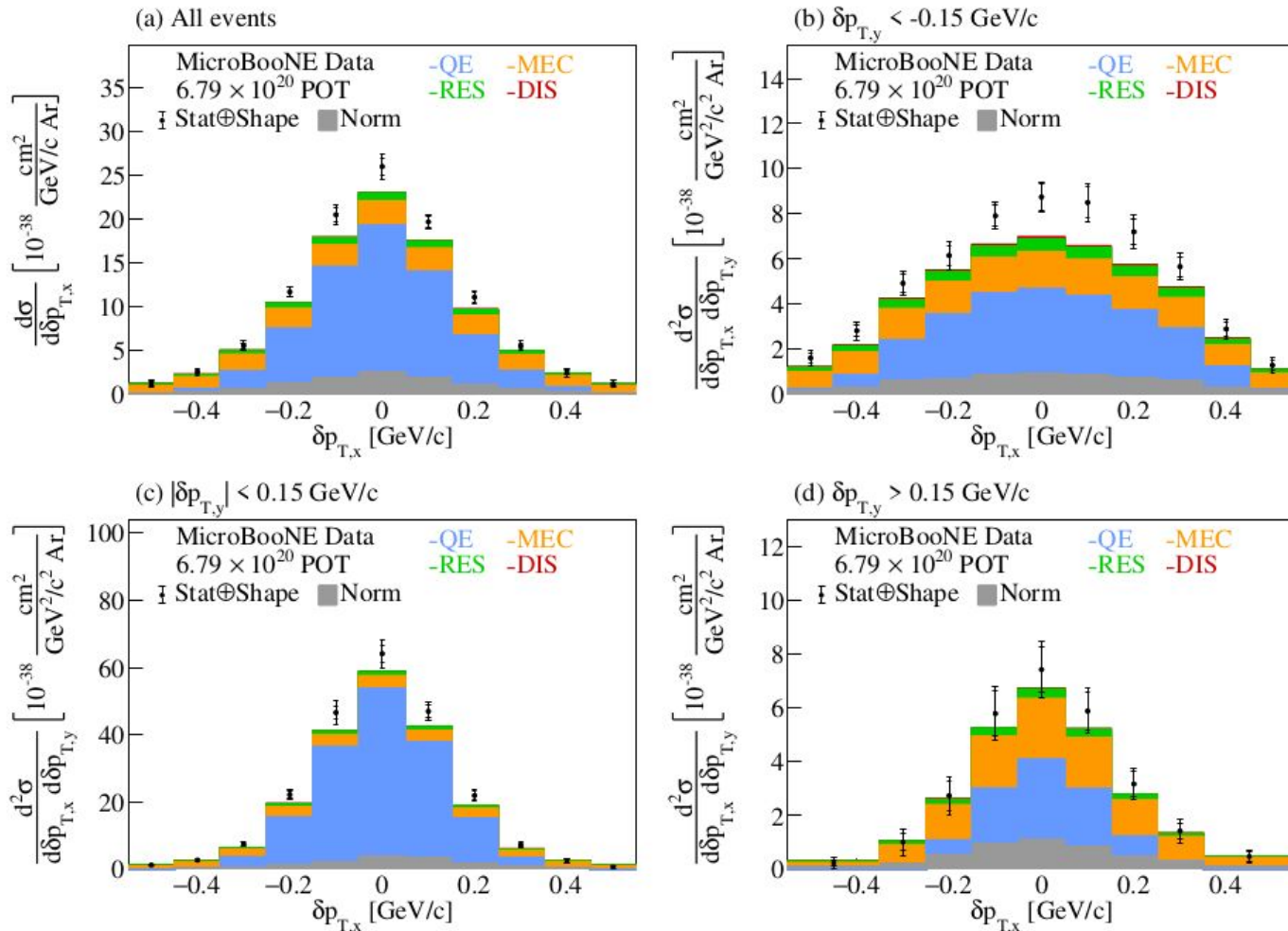


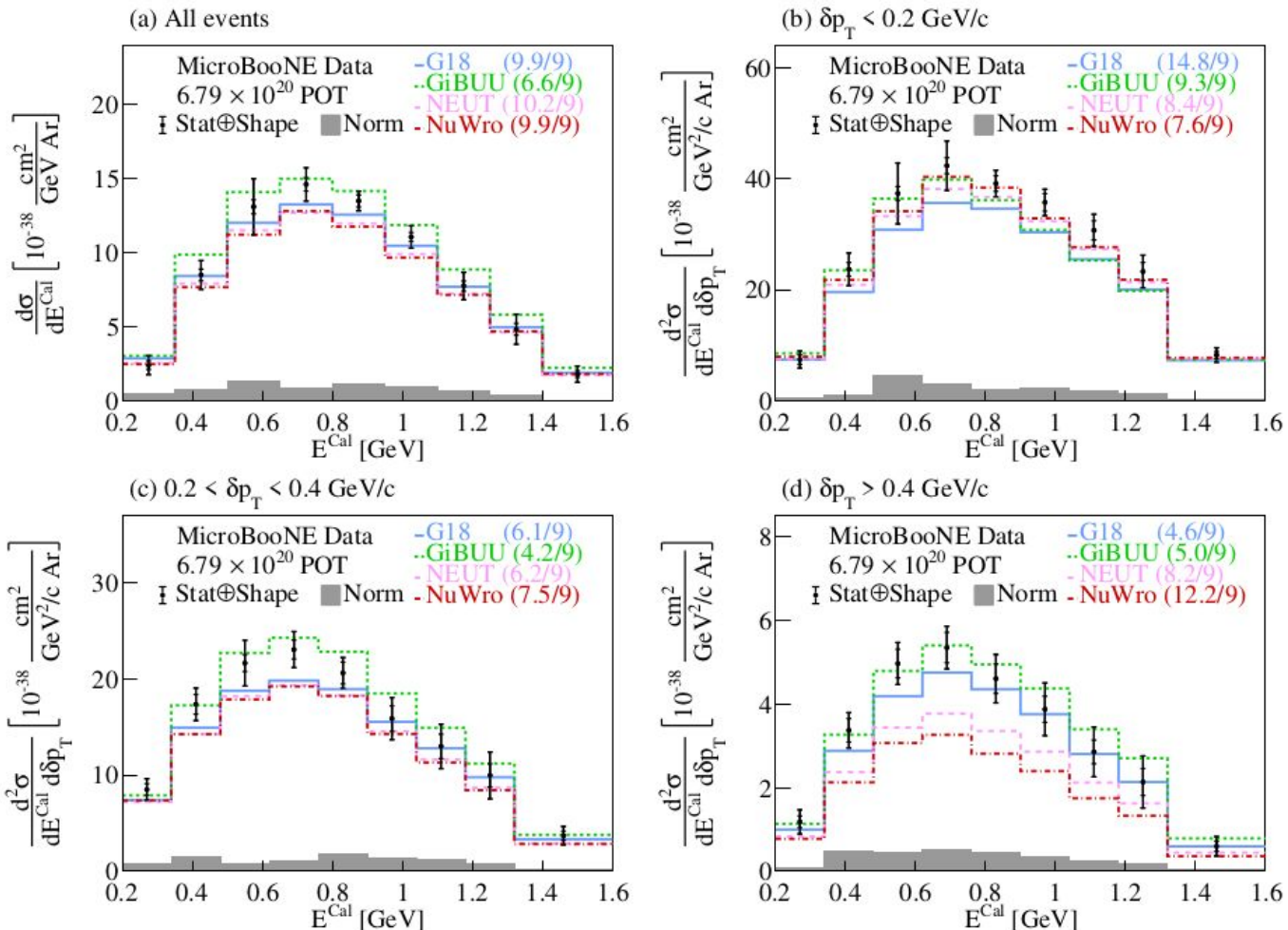


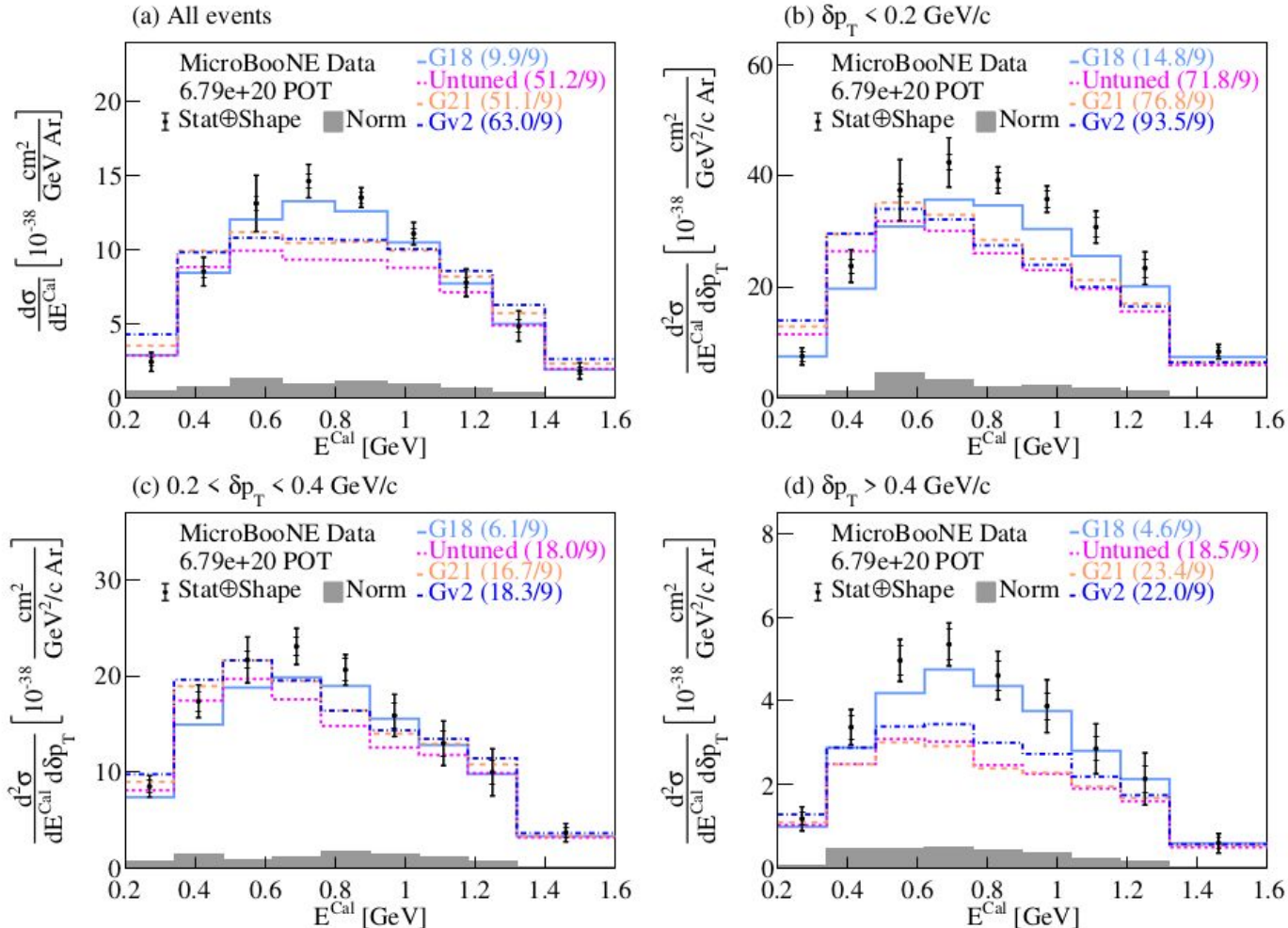


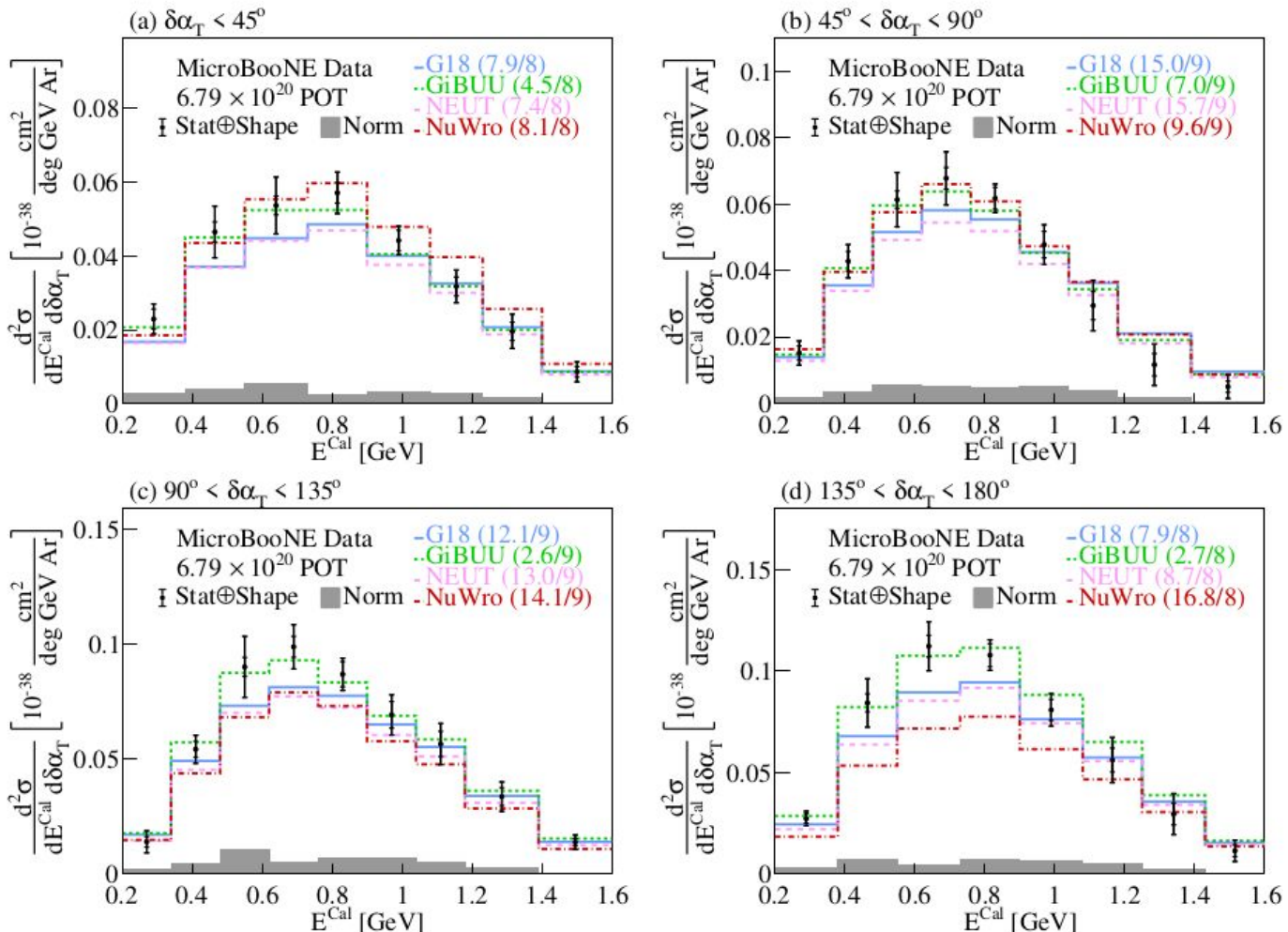


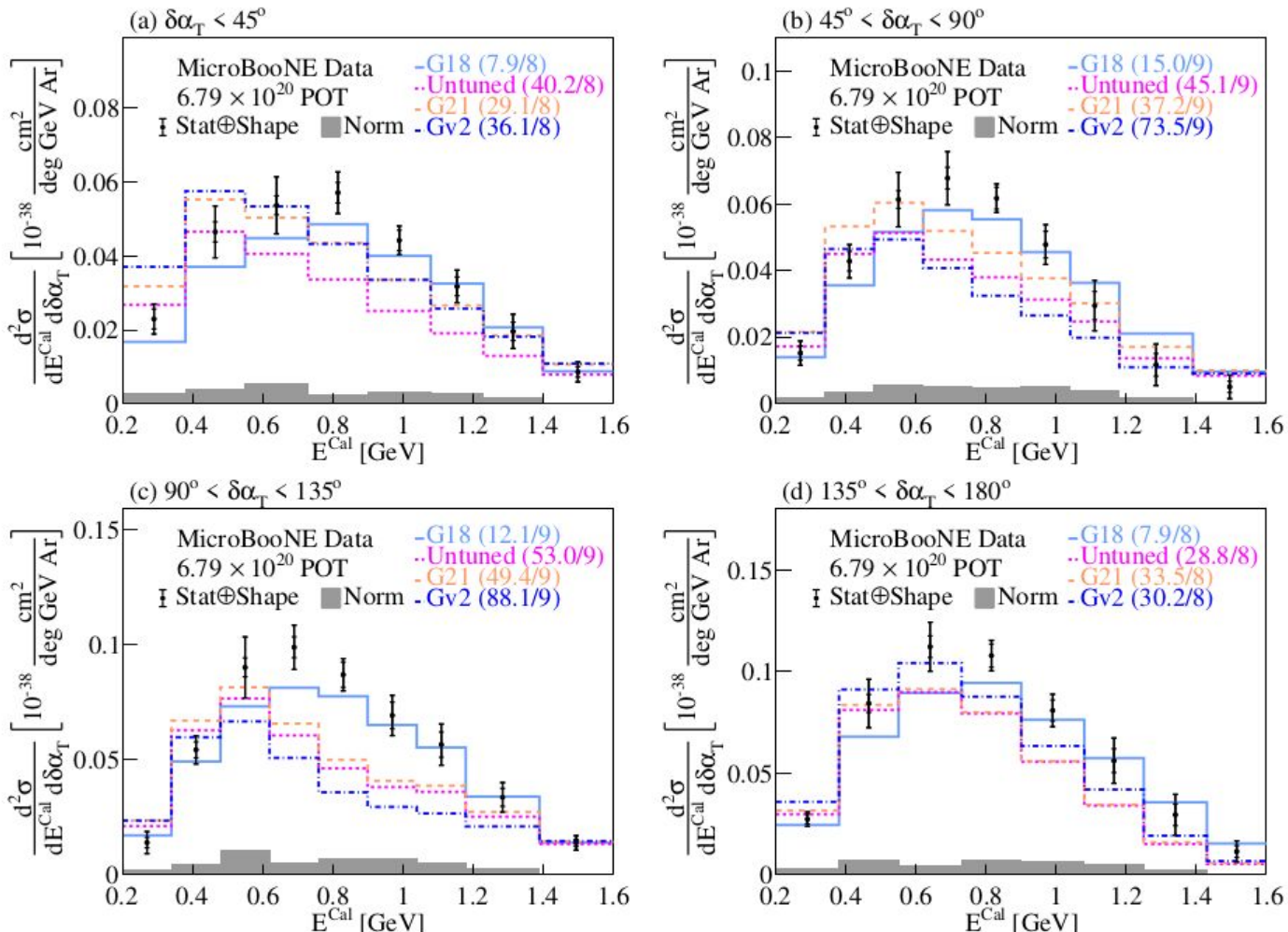


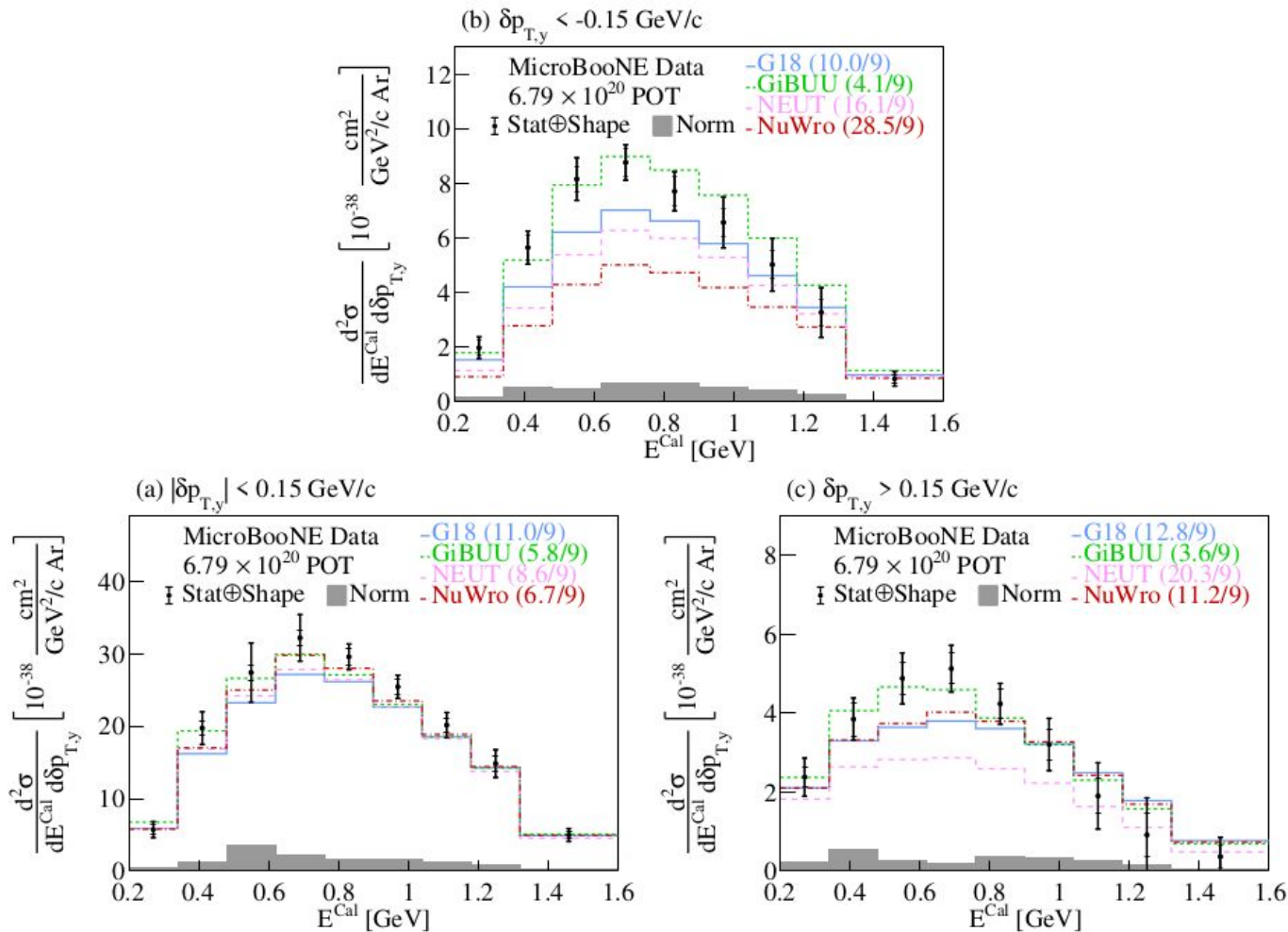


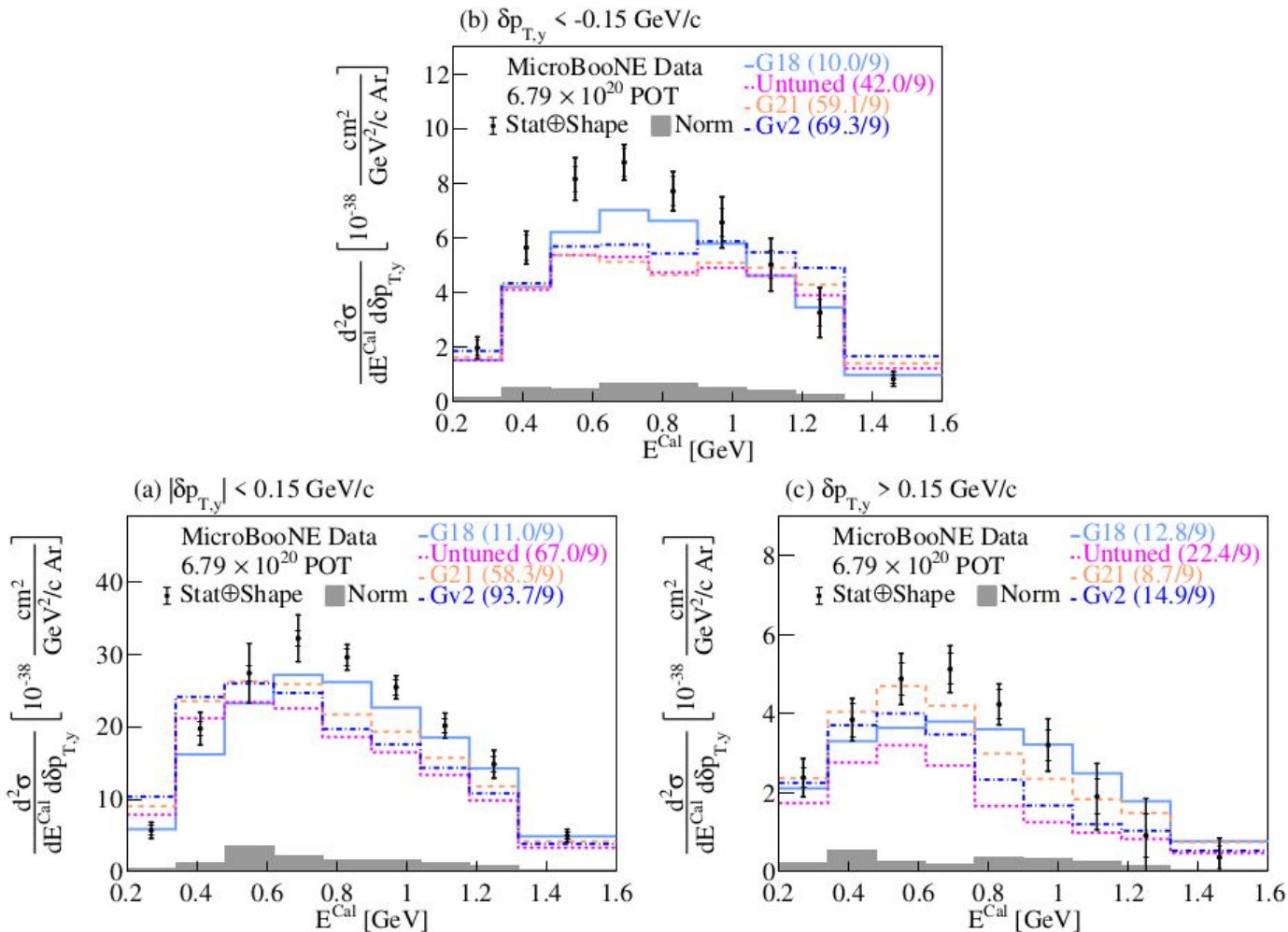




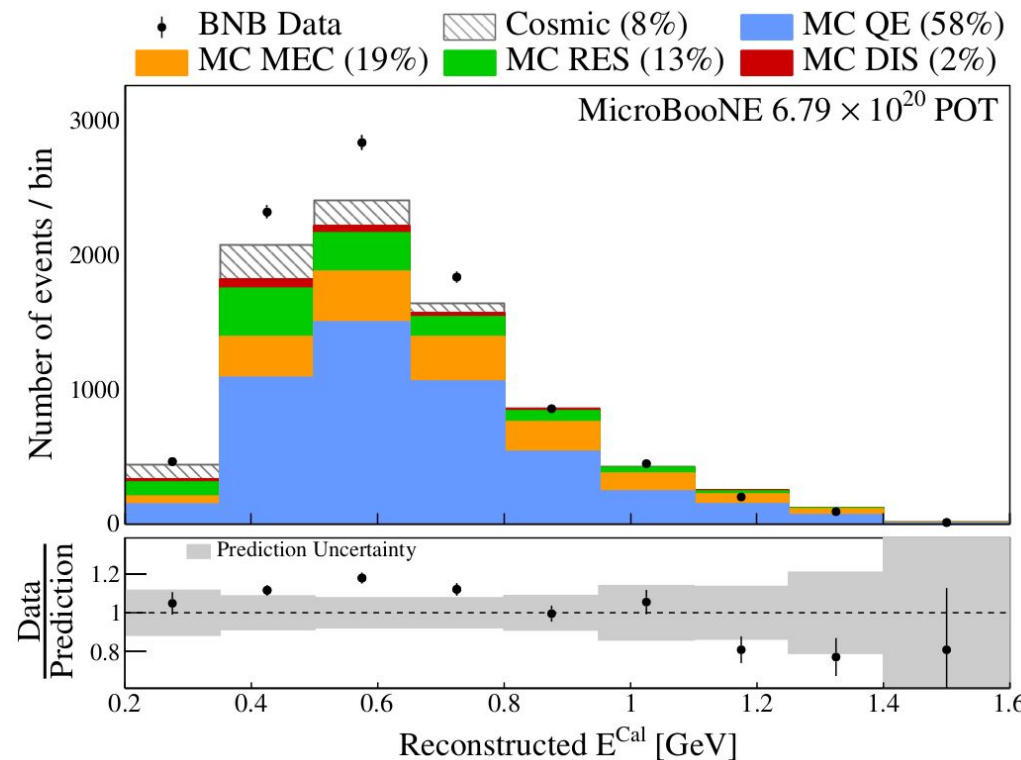








# Calorimetric Energy

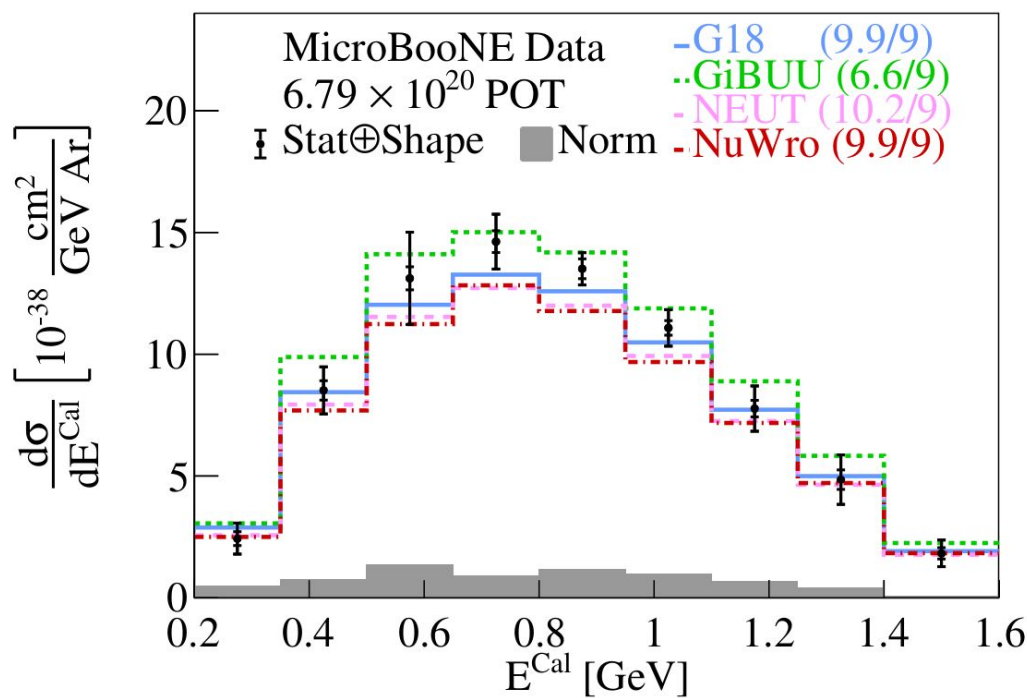


$$E^{Cal} = E_\mu + T_p + BE$$

- $E_\mu$  = muon energy
- $T_p$  = proton kinetic energy
- $BE = 40$  MeV binding energy
- Peak at  $\sim 0.7$  GeV

# Calorimetric Energy Cross Section

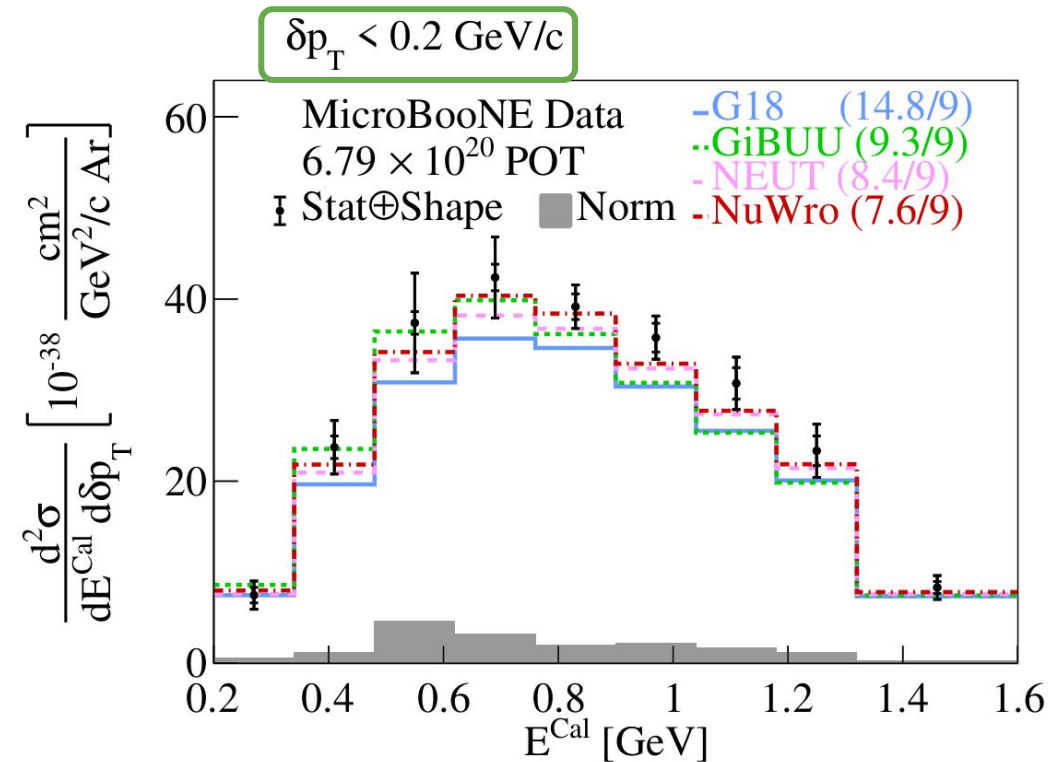
All events



$$E^{\text{Cal}} = E_\mu + T_p + BE$$

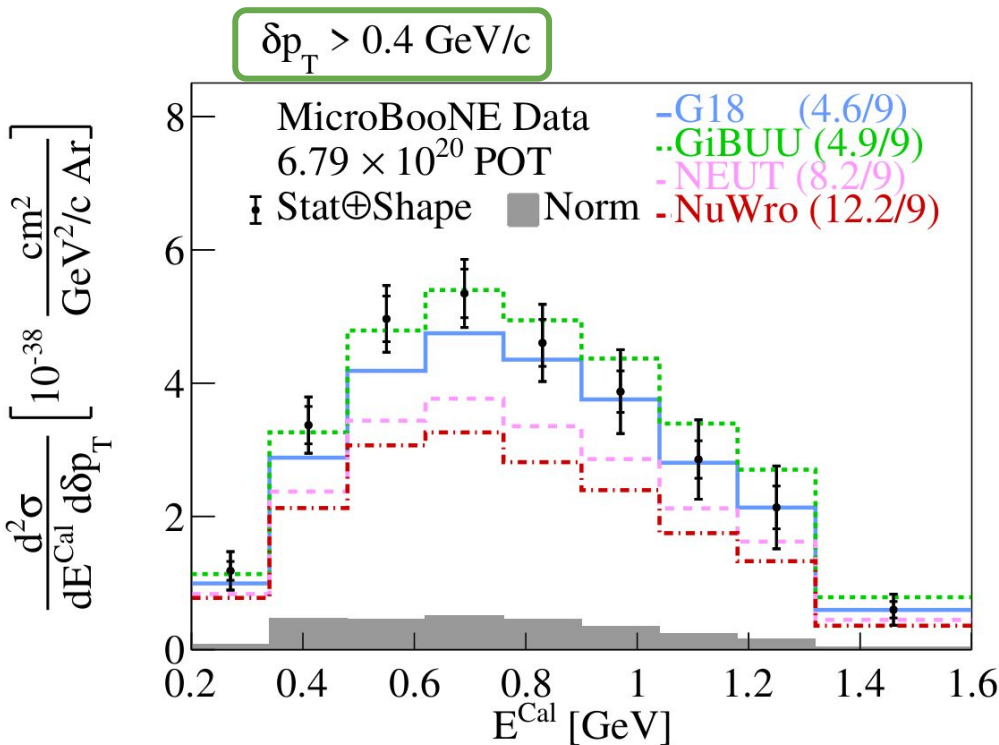
- $E_\mu$  = muon energy
- $T_p$  = proton kinetic energy
- BE = 40 MeV binding energy
- All generators yield good agreement

# High Statistics→Into the Multiverse!



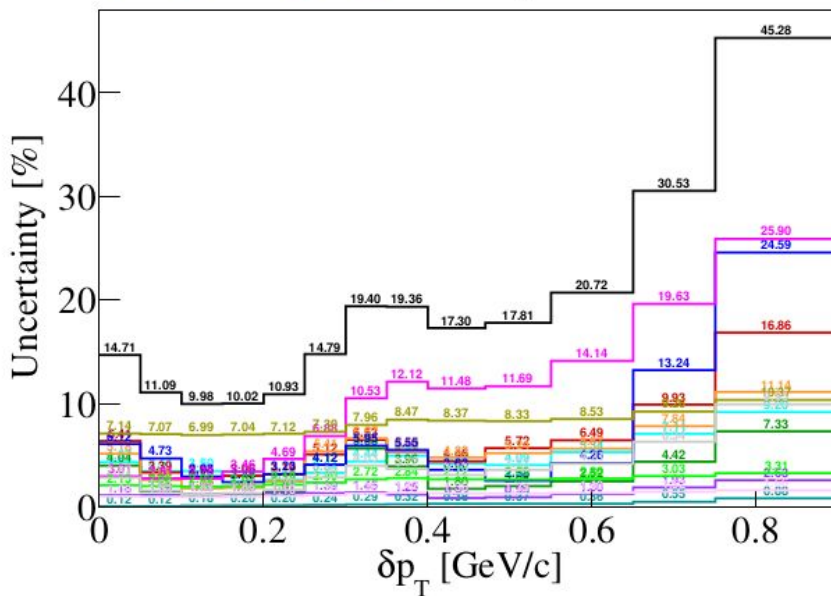
- QE dominated region
- All generators yield good agreement

# High Statistics→Into the Multiverse!

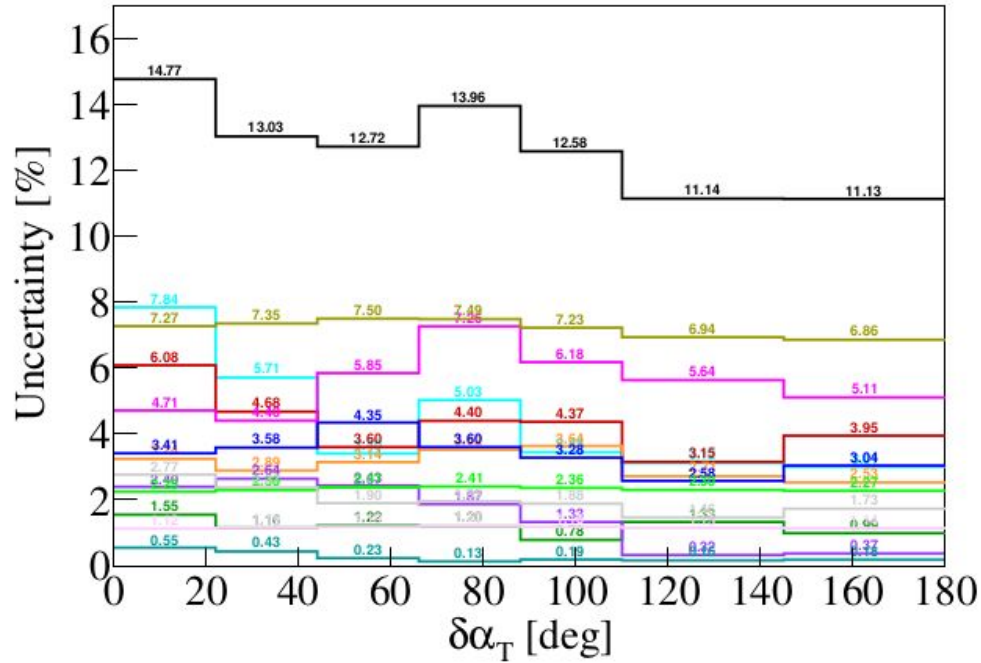


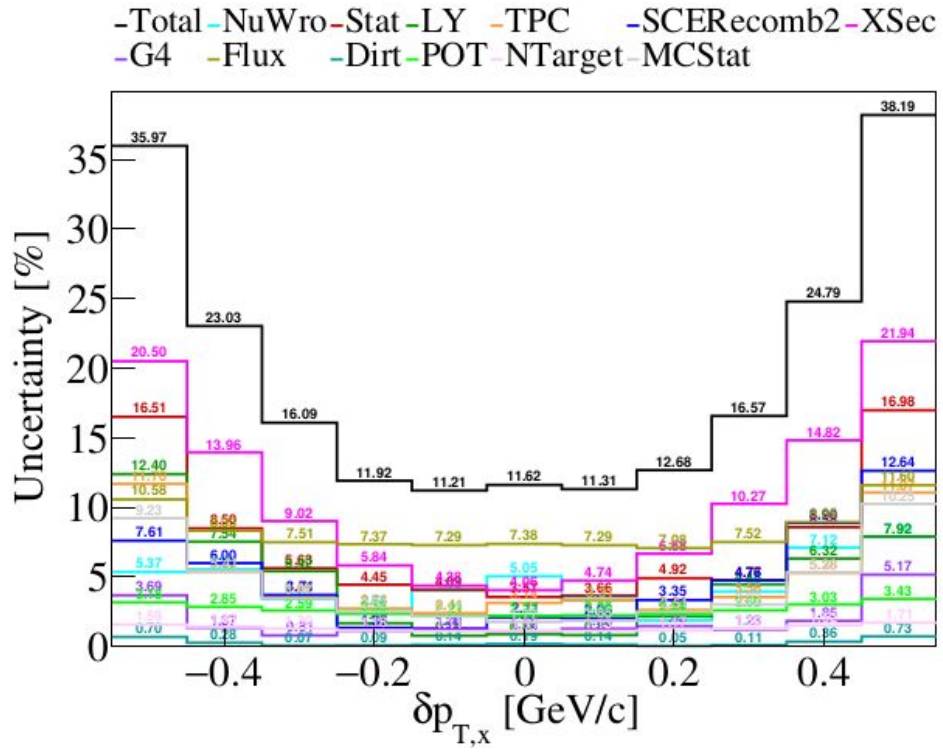
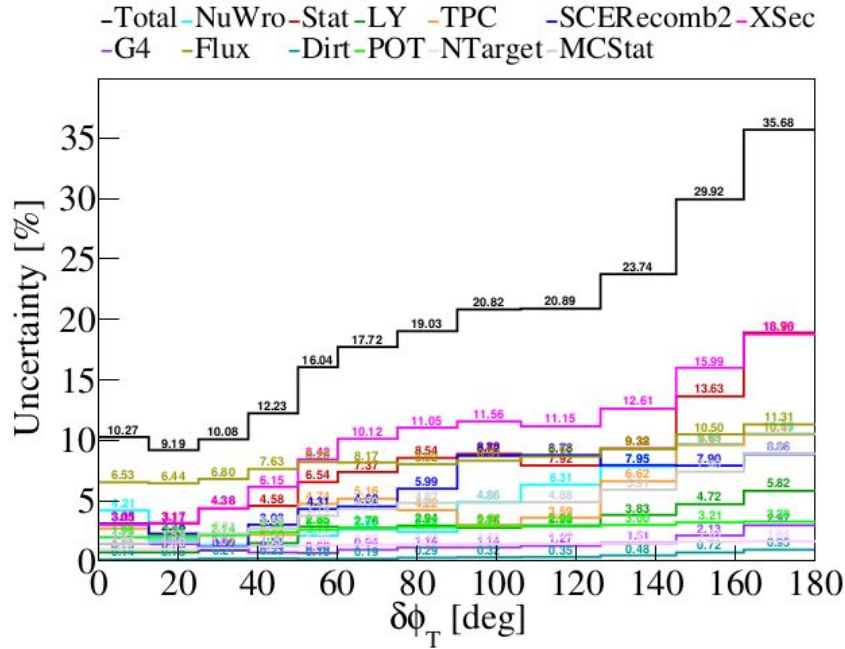
- MEC/RES dominated region
- Similar shapes
- Normalization differences
- Still reasonable  $\chi^2$ !

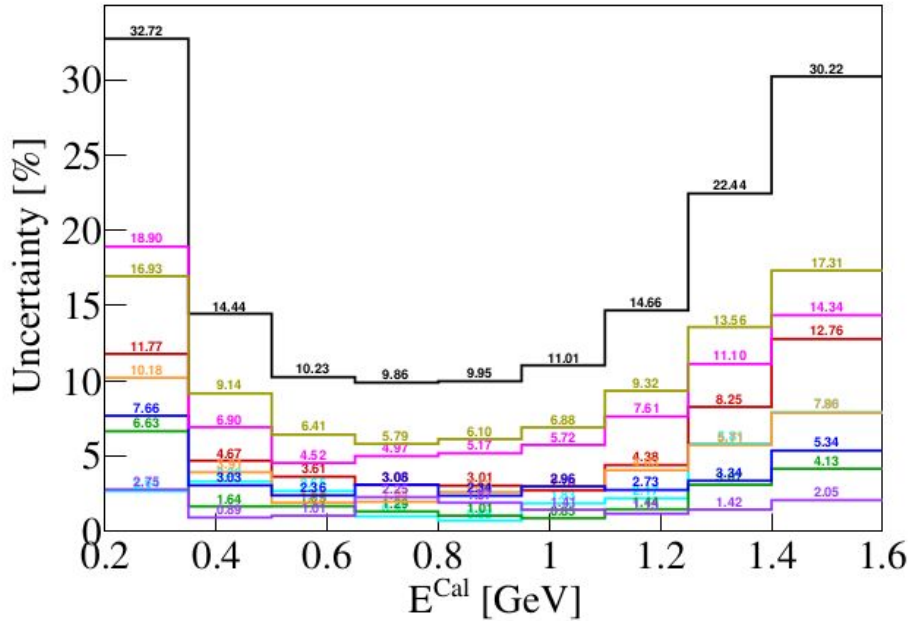
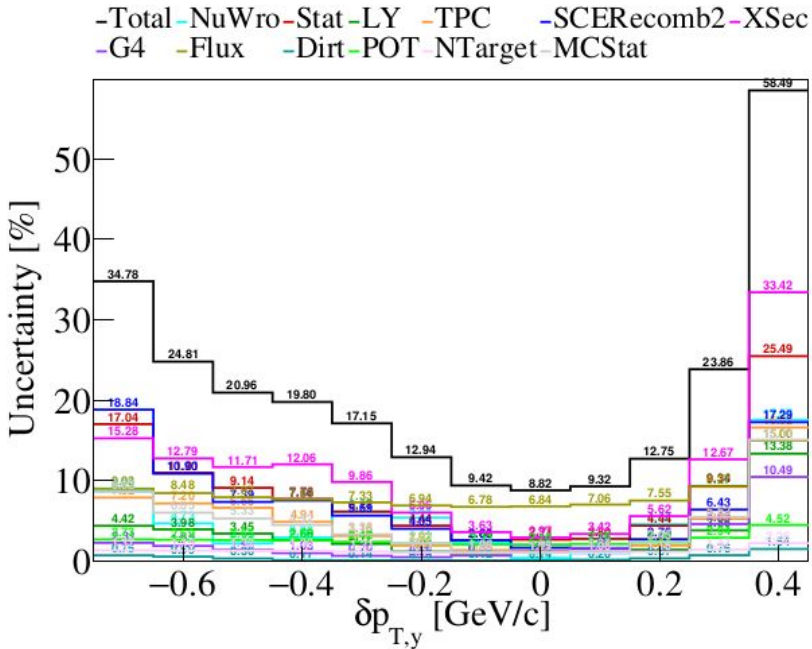
-Total -NuWro -Stat -LY -TPC -SCERecomb2 -XSec  
 -G4 -Flux -Dirt -POT -NTarget -MCStat



-Total -NuWro -Stat -LY -TPC -SCERecomb2 -XSec  
 -G4 -Flux -Dirt -POT -NTarget -MCStat







Parameter	Description	CV	$1\sigma$ Uncertainty	Contributing Uncertainty (%)
<b>Quasi-Elastic Parameters</b>				
MaCCQE	CCQE axial mass	1.10 GeV	$\pm 0.1$ GeV	0.038
RPA CCQE	Strength of the RPA correction	0.151	$\pm 0.4$	2.094
MaNCEL	Axial mass for NCEL	0.961242 GeV	$\pm 25\%$	0.348
EtaNCEL	Empirical parameter used to account for sea quark contribution to NCEL form factor	0.12	$\pm 30\%$	0.010
AxFCCQEshape	Parametrisation of the nucleon axial form factor	Dipole	z-expansion	0.022
VecFCCQEshape	Parametrisation of the nucleon vector form factors	BBA07	Dipole	0.051
<b>MEC Parameters</b>				
NormCCMEC	Energy-independent normalization for CCMEC	1.66	$\pm 0.5$	1.832
NormNCMEC	Energy-independent normalization for NCMEC	1	$\pm 20\%$	0.129
FracPNCCMEC	Fraction of initial nucleon pairs that are pn (0 = Valencia)	0	$\pm 20\%$	0.041
FracDeltaCCMEC	Relative contribution of $\Delta$ diagrams to total MEC cross section (0 = Valencia)	0	$\pm 30\%$	0.124
XSecShape CCMEC	Changes shape of differential cross section	1.0	0.0	2.273
DecayAngMEC	Changes angular distribution of nucleon cluster	Isotropic	$\cos^2 \vartheta$ in rest frame	0.693
<b>Resonant Parameters</b>				
MaCCRES	CCRES axial mass	1.120 GeV	$\pm 0.2$	0.986
MvCCRES	Shape-only CCRES axial mass	0.840 GeV	$\pm 0.1$	0.775
MaNCRES	NCRES axial mass	1.120 GeV	$\pm 0.2$	0.969
MvNCRES	NCRES vector mass.	0.840 GeV	$\pm 0.1$	0.395
ThetaDelta2Npi	Interpolates angular distribution for $\Delta \rightarrow N + \pi$	Rein-Sehgal	Isotropic	1.533
ThetaDelta2NRad	Interpolates angular distribution for $\Delta \rightarrow N + \gamma$	Rein-Sehgal	$\cos^2 \vartheta$	0.016

Parameter	Description	CV	$1\sigma$ Uncertainty	Contributing Uncertainty (%)
<b>Non-Resonant Parameters</b>				
NonRESBGvpNC1pi	Non-resonant background normalization for $\nu p$ NC1 $\pi$	0.1	$\pm 0.5$	0.041
NonRESBGvpNC2pi	Non-resonant background normalization for $\nu p$ NC2 $\pi$	1	$\pm 0.5$	0.096
NonRESBGvnNC1pi	Non-resonant background normalization for $\bar{\nu} n$ NC1 $\pi$	0.3	$\pm 0.5$	0.390
NonRESBGvnNC2pi	Non-resonant background normalization for $\bar{\nu} n$ NC2 $\pi$	1	$\pm 0.5$	0.022
NonRESBGvbarpNC1pi	Non-resonant background normalization for $\bar{\nu} p$ NC1 $\pi$	0.3	$\pm 0.5$	0.010
NonRESBGvbarpNC2pi	Non-resonant background normalization for $\bar{\nu} p$ NC2 $\pi$	1	$\pm 0.5$	0.010
NonRESBGvbarnNC1pi	Non-resonant background normalization for $\bar{\nu} n$ NC1 $\pi$	0.1	$\pm 0.5$	0.010
NonRESBGvbarnNC2pi	Non-resonant background normalization for $\bar{\nu} n$ NC2 $\pi$	1	$\pm 0.5$	0.010
NonRESBGvpCC1pi	Non-resonant background normalization for $\nu p$ CC1 $\pi$	0.007713	$\pm 0.5$	0.014
NonRESBGvpCC2pi	Non-resonant background normalization for $\nu p$ CC2 $\pi$	0.787999	$\pm 0.5$	0.059
NonRESBGvnCC1pi	Non-resonant background normalization for $\bar{\nu} n$ CC1 $\pi$	0.127858	$\pm 0.5$	0.217
NonRESBGvnCC2pi	Non-resonant background normalization for $\bar{\nu} n$ CC2 $\pi$	2.11523	$\pm 0.5$	0.079
NonRESBGvbarpCC1pi	Non-resonant background normalization for $\bar{\nu} p$ CC1 $\pi$	0.127858	$\pm 0.5$	0.013
NonRESBGvbarpCC2pi	Non-resonant background normalization for $\bar{\nu} p$ CC2 $\pi$	2.11523	$\pm 0.5$	0.010
NonRESBGvbarnCC1pi	Non-resonant background normalization for $\bar{\nu} n$ CC1 $\pi$	0.007713	$\pm 0.5$	0.010
NonRESBGvbarnCC2pi	Non-resonant background normalization for $\bar{\nu} n$ CC2 $\pi$	0.787999	$\pm 0.5$	0.010
AhtBY	AHT higher-twist parameter in the Bodek-Yang model scaling variable $\xi_w$	0.538	$\pm 0.25$	0.010
BhtBY	BHT higher-twist parameter in the Bodek-Yang model scaling variable $\xi_w$	0.305	$\pm 0.25$	0.010
CV1uBY	CV1u valence GRV98 PDF correction parameter in the Bodek-Yang model	0.291	$\pm 0.3$	0.010
CV2uBY	CV2u valence GRV98 PDF correction parameter in the Bodek-Yang model	0.189	$\pm 0.4$	0.010

**Hadronisation Parameters**

AGKYxF1pi	Hadronization parameter, applicable to true DIS interactions only	-0.385	$\pm 0.2$	0.108
AGKYpT1pi	Hadronization parameter, applicable to true DIS interactions only	1/6.625	$\pm 0.03$	0.034

**Final State Interaction Parameters**

MFP <sub><math>\pi</math></sub>	$\pi$ mean free path	0	$\pm 0.2$	0.032
MFP <sub>N</sub>	Nucleon mean free path	0	$\pm 0.2$	1.212
FrCEx <sub><math>\pi</math></sub>	Fractional cross section for $\pi$ charge exchange	0	$\pm 0.5$	0.159
FrInel <sub><math>\pi</math></sub>	Fractional cross section for $\pi$ inelastic scattering	0	$\pm 0.4$	0.133
FrAbs <sub><math>\pi</math></sub>	Fractional cross section for $\pi$ absorption	0	$\pm 0.3$	0.906
FrCEx <sub>N</sub>	Fractional cross section for nucleon charge exchange	0	$\pm 0.2$	0.953
FrInel <sub>N</sub>	Fractional cross section for nucleon inelastic scattering	0	$\pm 0.5$	0.289
FrAbs <sub>N</sub>	Fractional cross section for nucleon absorption	0	$\pm 0.4$	0.906

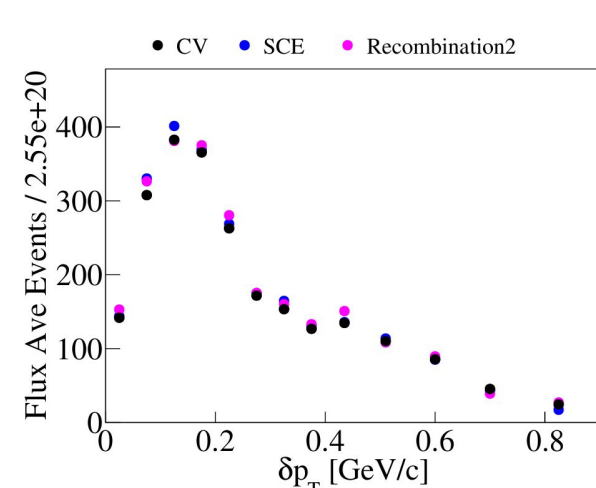
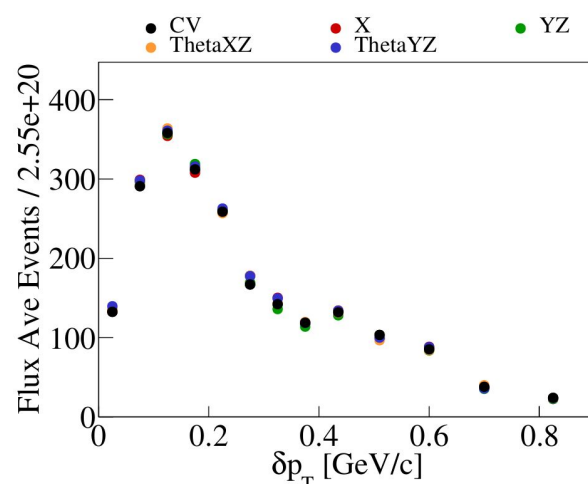
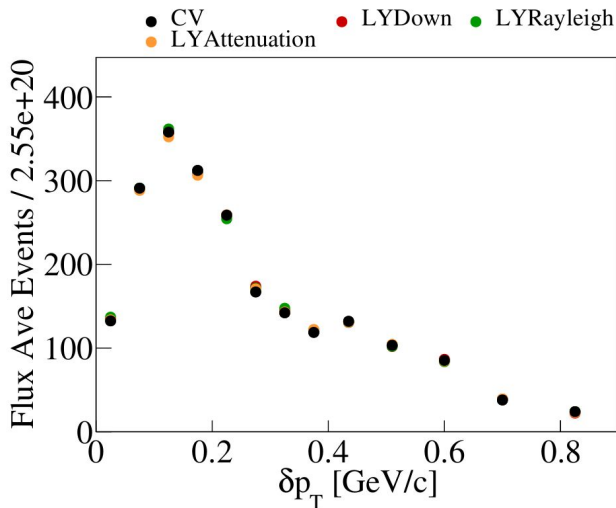
**Delta Resonant Decay Parameters**

RDecBR1gamma	Normalization for $\Delta \rightarrow \gamma$ decays	Nominal BR	$\pm 0.5$	0.042
RDecBR1eta	Normalization for $\Delta \rightarrow \eta$ decays	Nominal BR	$\pm 0.5$	0.513

**Coherent Parameters**

NormCCCOH	Scaling factor for CCCOH $\pi$ production total cross section	Nominal	100% increase	0.027
NormNCCOH	Scaling factor for NCCOH $\pi$ production total cross section	Nominal	100% increase	0.016

Variation	Description
Wire Mod x position	Wire modification of x position
Wire Mod (y,z) position	Wire modification of (y,z) position
Wire Mod $\theta_{XZ}$	Wire modification of angle in XZ plane
Wire Mod $\theta_{YZ}$	Wire modification of angle in YZ plane
Light Yield Attenuation	Attenuation of LY response in detector over time
Light Yield Down	Turn down the light yield in the detector by 25%
Light Yield Rayleigh	Increase Rayleigh scattering length from 60 cm to 90 cm
Recombination	Reduce value of $\beta'$ in the Modified Box Model
SCE	Use an alternative Space Charge Map



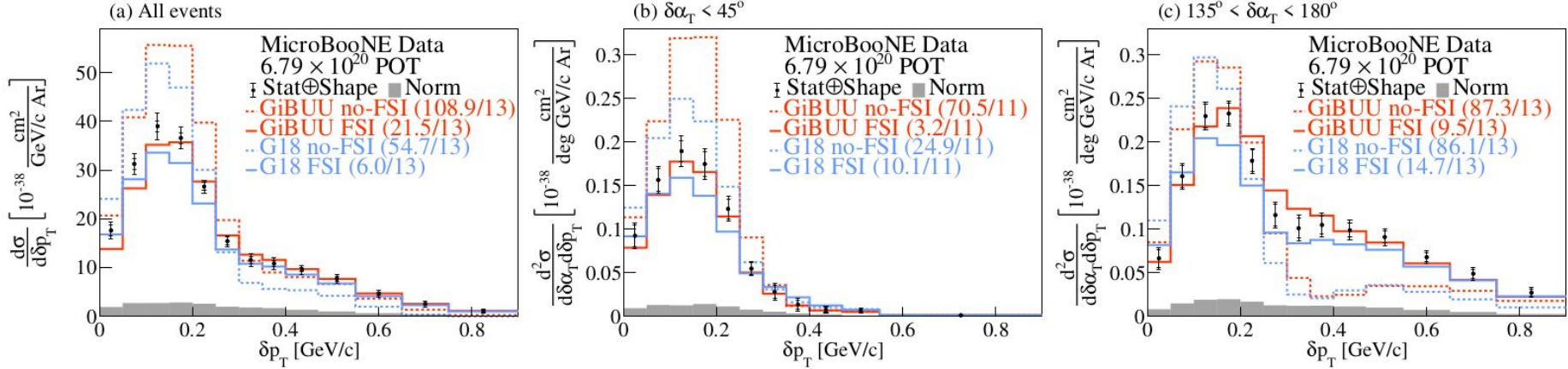


FIG. 1. The flux-integrated (a) single- and (b-c) double- (in  $\delta\alpha_T$  bins) differential CC1p0 $\pi$  cross sections as a function of the transverse missing momentum  $\delta p_T$ . Inner and outer error bars show the statistical and total (statistical and shape systematic) uncertainty at the  $1\sigma$ , or 68%, confidence level. The gray band shows the separate normalization systematic uncertainty. Colored lines show the results of theoretical cross section calculations with (solid line) and without (dashed line) FSI based on the `GENIE` (blue) and `GiBUU` (orange) event generators.

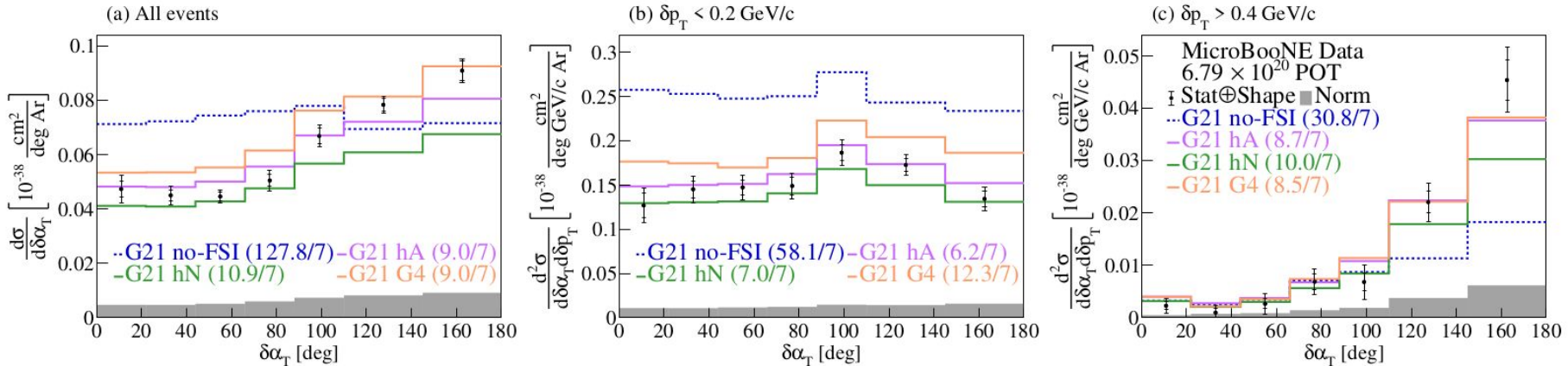


FIG. 2. The flux-integrated (a) single- and (b-c) double- (in  $\delta p_T$  bins) differential CC1p0 $\pi$  cross sections as a function of the angle  $\delta\alpha_T$ . Inner and outer error bars show the statistical and total (statistical and shape systematic) uncertainty at the  $1\sigma$ , or 68%, confidence level. The gray band shows the separate normalization systematic uncertainty. Colored lines show the results of theoretical cross section calculations with a number of FSI-modeling choices based on the GENIE event generator.

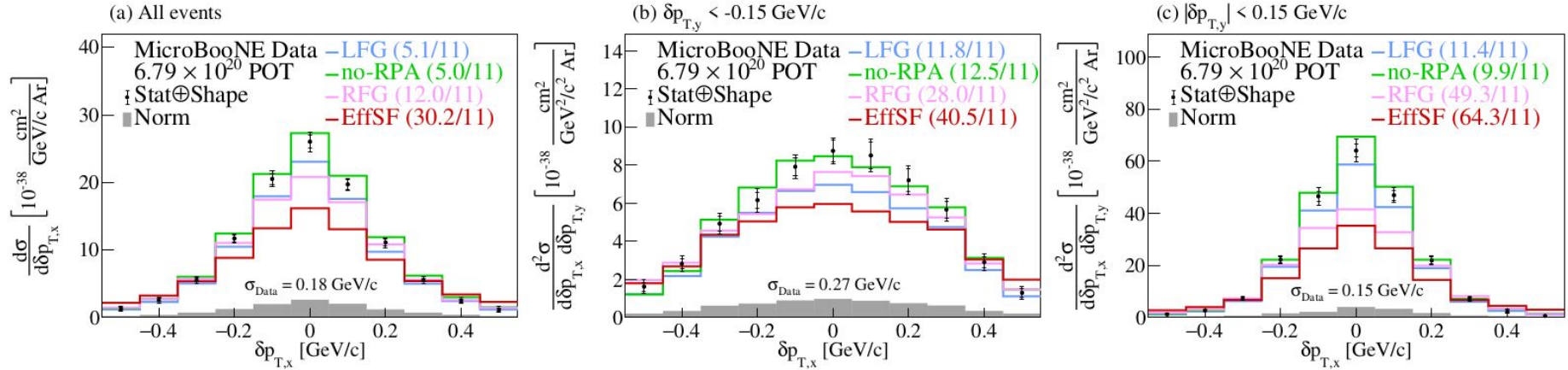
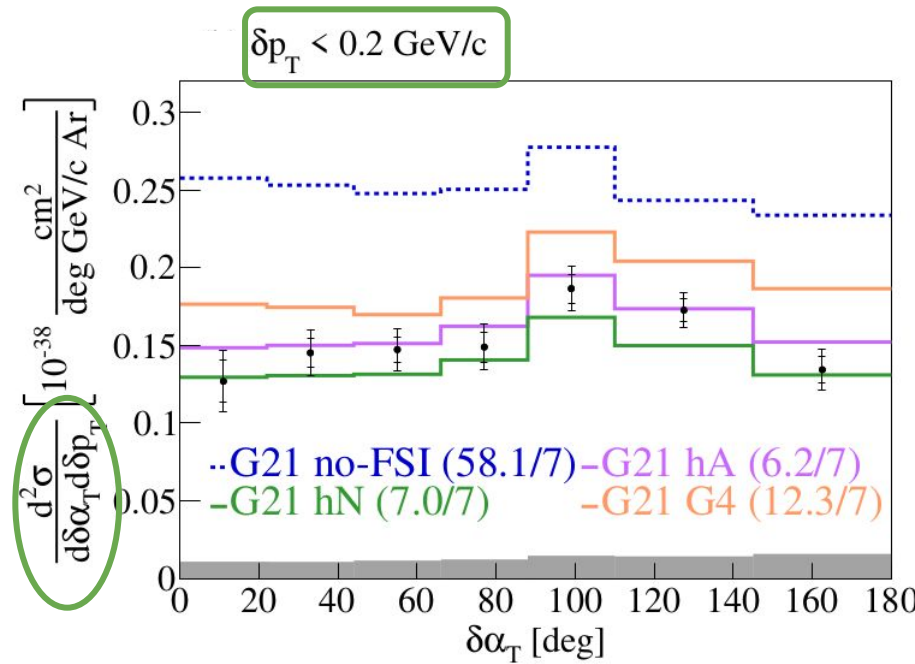


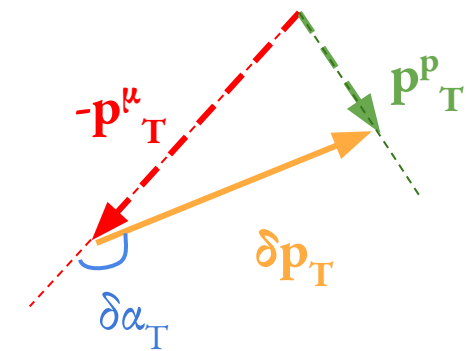
FIG. 3. The flux-integrated (a) single- and (b-c) double- (in  $\delta p_{T,y}$  bins) differential CC1p0 $\pi$  cross sections as a function of the transverse three-momentum transfer component,  $\delta p_{T,x}$ . Inner and outer error bars show the statistical and total (statistical and shape systematic) uncertainty at the  $1\sigma$ , or 68%, confidence level. The gray band shows the separate normalization systematic uncertainty. Colored lines show the results of theoretical cross section calculations with a number of event generators. The standard deviation ( $\sigma_{\text{Data}}$ ) of a Gaussian fit to the data is shown on each panel.

# High Statistics → Into the Multiverse!

QE-dominated region

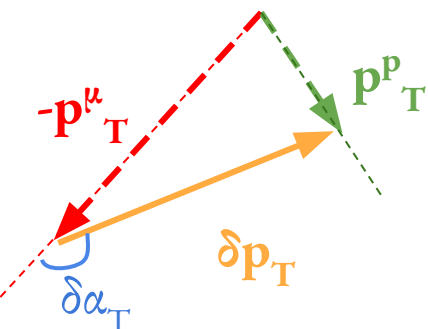
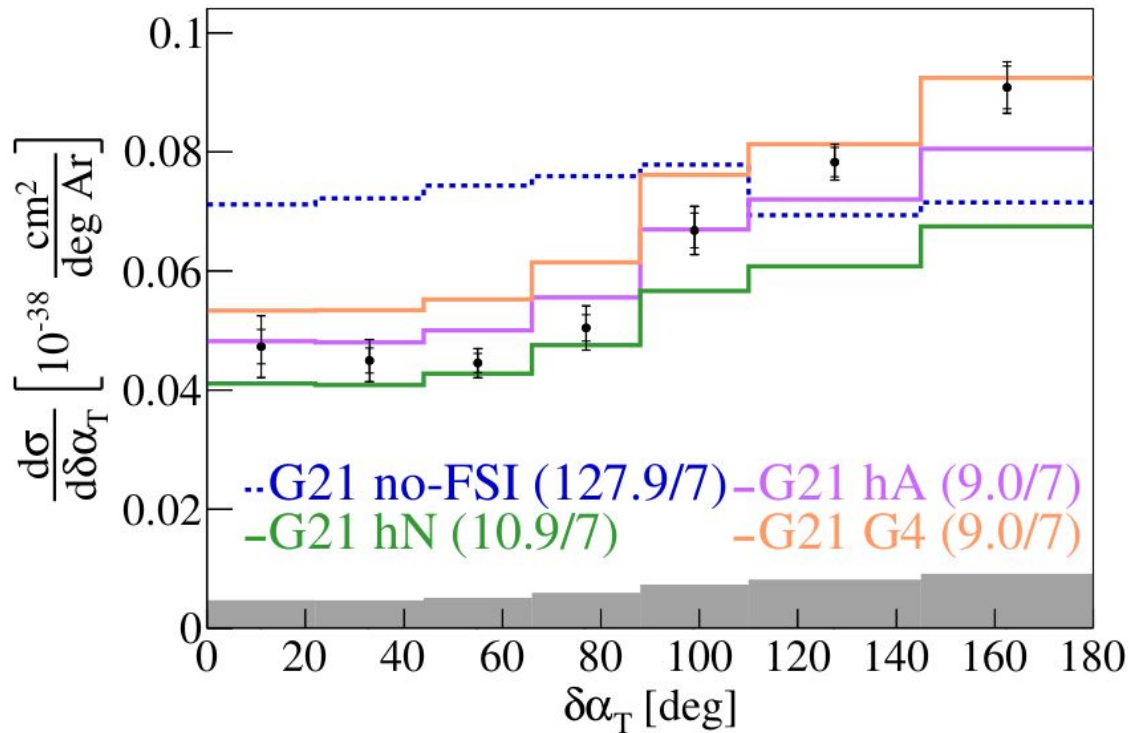


- Flat distribution indicative of absence of proton FSI
- Shape and normalization differences across FSI models



# Transverse Orientation $\delta\alpha_T$ Cross Section

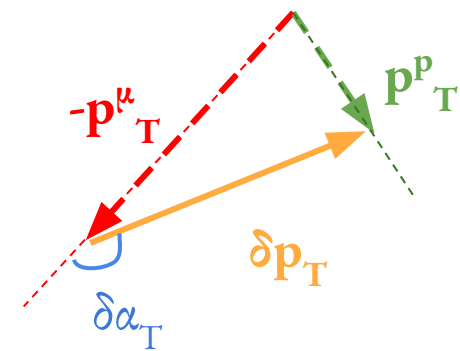
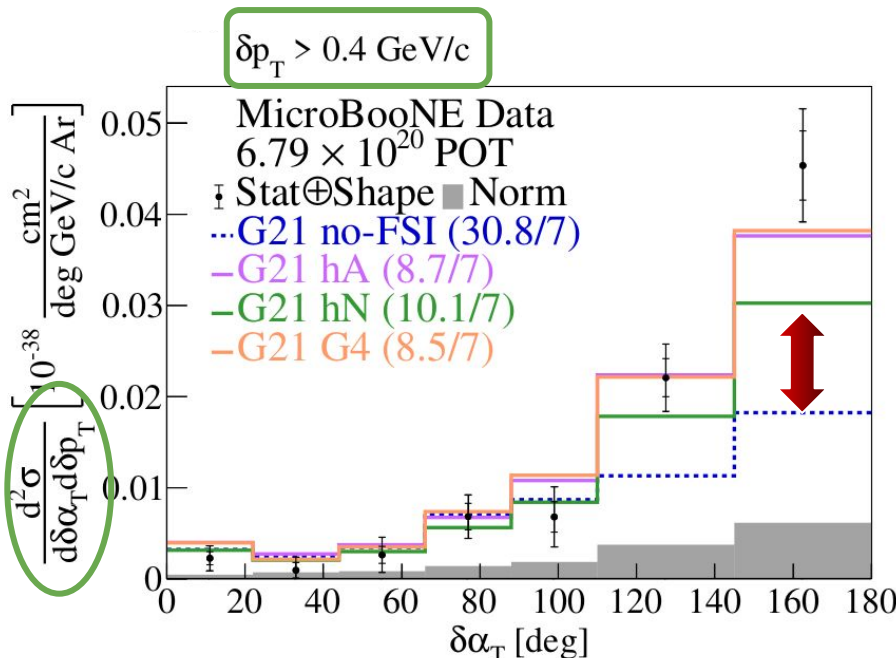
All events



- First neutrino-argon differential cross section in  $\delta\alpha_T$
- Sensitive to proton FSI modeling
- Data favors FSI addition
- Shape differences observed

# High Statistics→Into the Multiverse!

- Extension to 2D for the first time on argon
- Probe regions with greater model discrimination power



- Primarily contributions from MEC/RES & QE events undergoing FSI
- More asymmetric behavior compared to 1D result
- No-FSI contribution lower than FSI ones
- High  $\delta\alpha_T$  & high  $\delta p_T$  part of phase-space ideal to test FSI / multinucleon effect sensitivity

G21 = GENIE v3.0.6 G21\_11b\_00\_000

SuSAv2 QE & MEC\*, hA/hN/G4 = FSI modeling options <sup>120</sup>

## VI. MODELING CONFIGURATIONS

The nominal MC neutrino interaction prediction (**G18**) uses the local Fermi gas (LFG) model [50], the Nieves CCQE scattering prescription [51] which includes Coulomb corrections for the outgoing muon [52] and random phase approximation (RPA) corrections [53]. Additionally, it uses the Nieves MEC model [54], the KLN-BS RES [55–58] and Berger-Sehgal coherent (COH) [59] scattering models, the hA2018 FSI model [60], and MicroBooNE-specific tuning of model parameters [38].

Our results are also compared to a number of alternative event generators. **GiBUU** 2021 (**GiBUU**) uses similar models, but they are implemented in a coherent way by solving the Boltzmann-Uehling-Uhlenbeck transport equation [61]. The modeling includes the LFG model [50], a standard CCQE expression [62], an empirical MEC model and a dedicated spin dependent resonance amplitude calculation following the MAID analysis [61]. The DIS model is from PYTHIA [63]. **GiBUU**'s FSI treatment propagates the hadrons through the residual nucleus in a nuclear potential which is consistent with the initial state. **NuWro** v19.02.2 (**NuWro**) uses the LFG model [50], the Llewellyn Smith model for QE events [64], the Nieves model for MEC events [65], the Adler-Rarita-Schwinger formalism to calculate the  $\Delta$  resonance explicitly [58], the BS COH [59] scattering model and an intranuclear cascade model for FSI [65]. **NEUT** v5.4.0 (**NEUT**) uses the LFG model [50], the Nieves CCQE scattering prescription [51], the Nieves MEC model [54], the BS RES [55–58] and BS COH [59] scattering models, and FSI with Oset medium corrections for pions [35, 36].

In addition to the alternative event generators, our results are compared to a number of different **GENIE** configurations. These include an older version, **GENIE** v2.12.10 (Gv2) [35, 36], which uses the Bodek-Ritchie Fermi Gas model, the Llewellyn Smith CCQE scattering prescription [64], the empirical MEC model [66], a Rein-Sehgal RES and COH scattering model [67], and a data driven FSI model denoted as “hA” [68]. Another model, “Untuned”, uses the **GENIE** v3.0.6 G18\_10a\_02\_11a configuration without additional MicroBooNE-specific tuning. Finally, the newly added theory-driven **GENIE** v3.2.0 G21\_11b\_00\_000 configuration (**G21**) is shown. This includes the SuSAv2 prediction for the QE and MEC scattering parts [69] and the hN2018 FSI model [70]. The modeling options for RES, DIS, and COH interactions are the same as for **G18**.

To quantify the data-simulation agreement, the  $\chi^2/\text{bins}$  ratio data comparison for each generator is shown on all the figures and is calculated by taking into account the total covariance matrix. Ratios close to unity are indicative of a sufficiently accurate modeling performance. Theoretical uncertainties on the models themselves are not included.

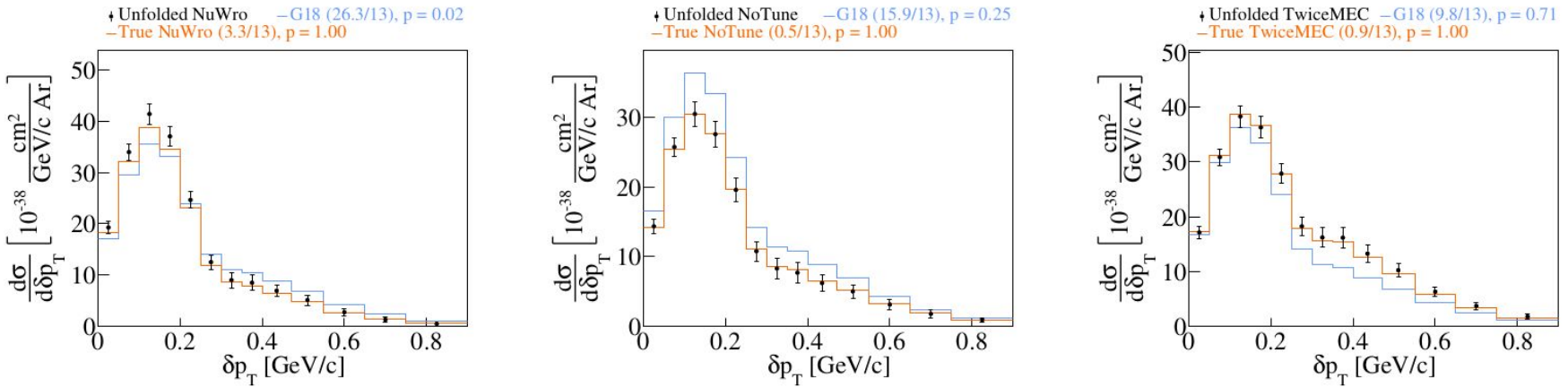


FIG. 1. Fake data studies for  $\delta p_T$  using (left) NuWro, (center) GENIE without the MicroBooNE tune (NoTune), and (right) twice the weights for MEC events (TwiceMEC) as fake data samples.

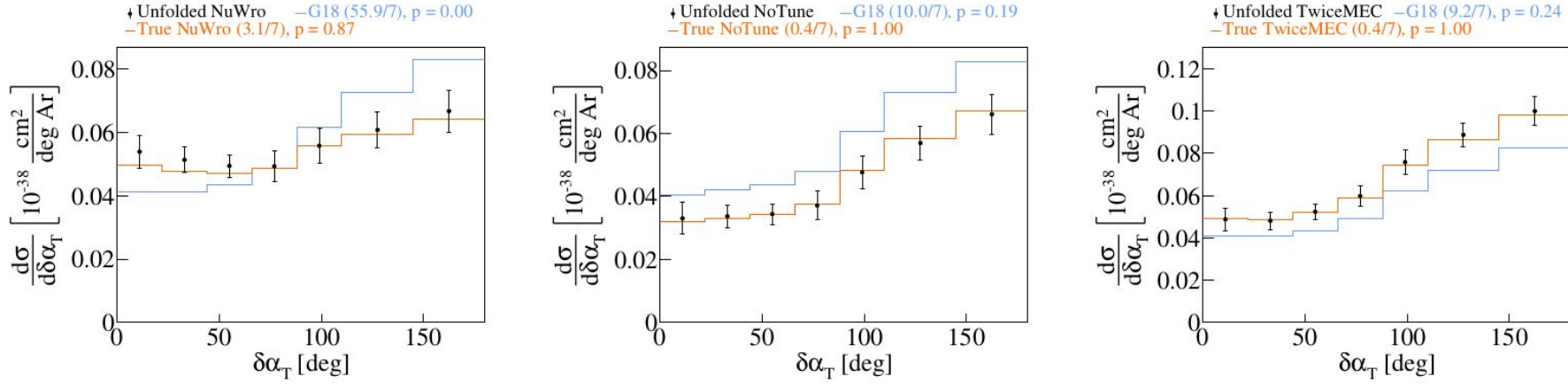


FIG. 2. Fake data studies for  $\delta\alpha_T$  using (left) NuWro, (center) GENIE without the MicroBooNE tune (NoTune), and (right) twice the weights for MEC events (TwiceMEC) as fake data samples.

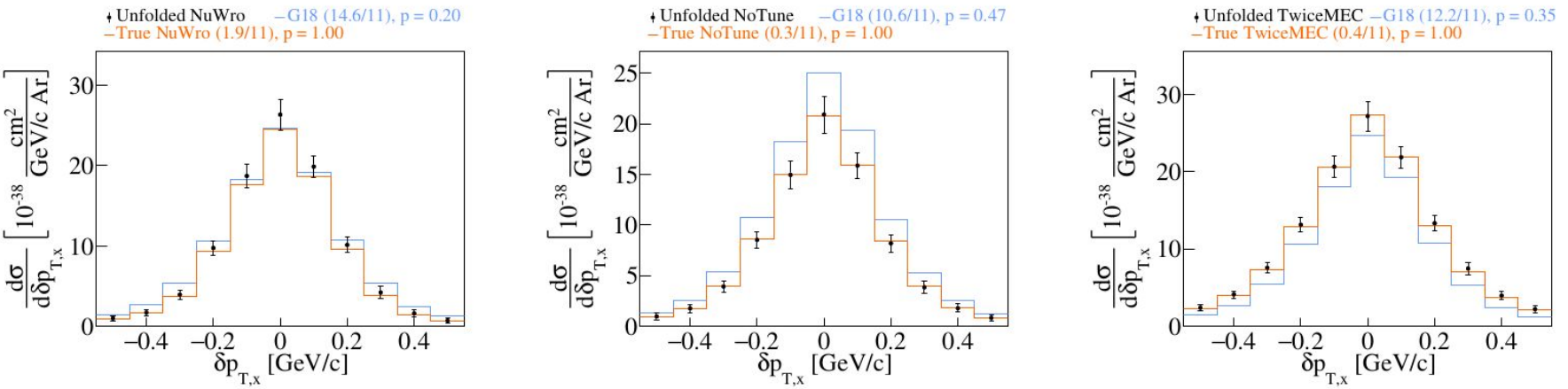


FIG. 3. Fake data studies for  $\delta p_{T,x}$  using (left) NuWro, (center) GENIE without the MicroBooNE tune (NoTune), and (right) twice the weights for MEC events (TwiceMEC) as fake data samples.

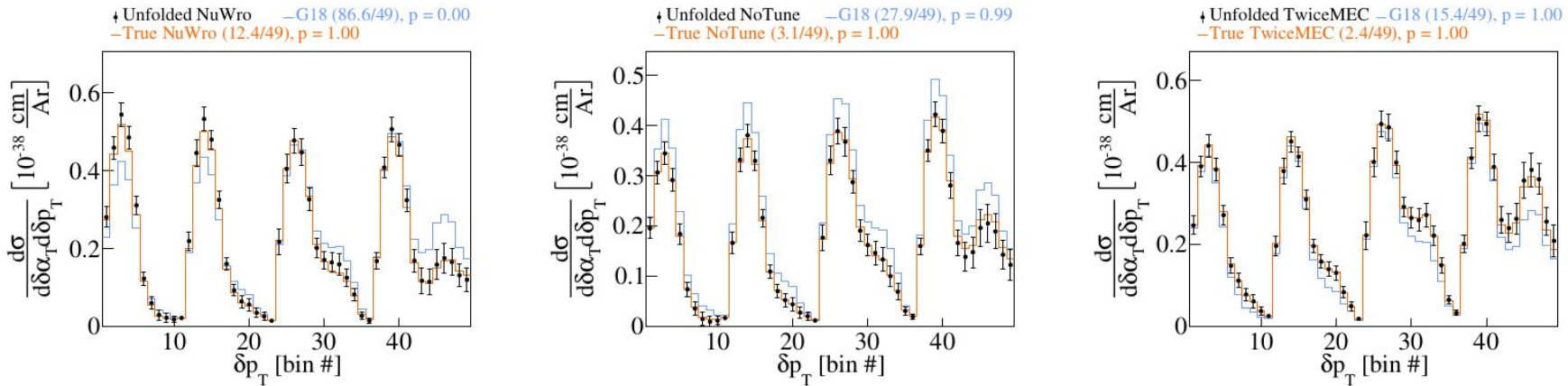


FIG. 4. Fake data studies for  $\delta p_T$  in  $\delta\alpha_T$  bins using (left) NuWro, (center) GENIE without the MicroBooNE tune (NoTune), and (right) twice the weights for MEC events (TwiceMEC) as fake data samples.

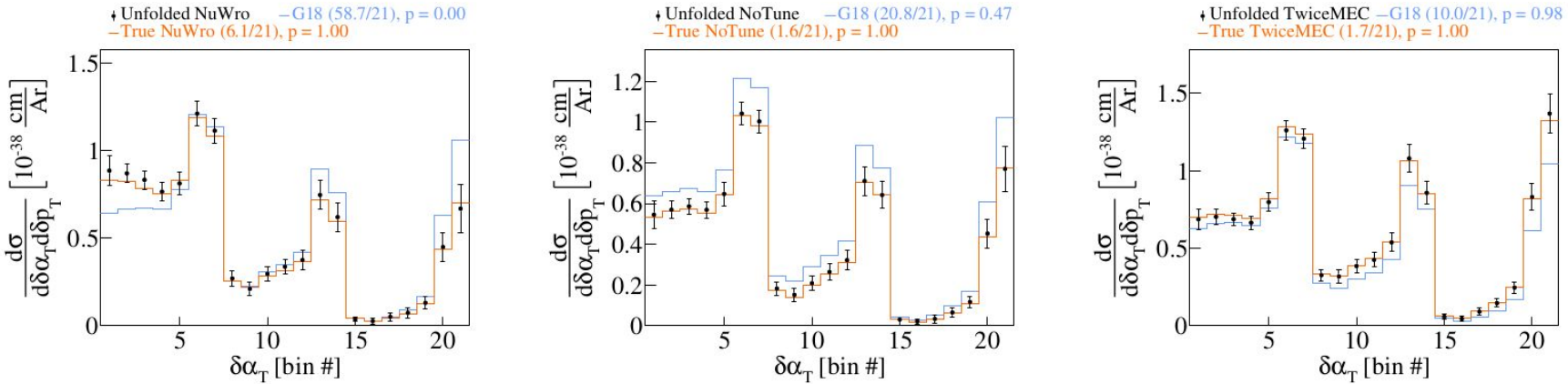


FIG. 5. Fake data studies for  $\delta\alpha_T$  in  $\delta p_T$  bins using (left) NuWro, (center) GENIE without the MicroBooNE tune (NoTune), and (right) twice the weights for MEC events (TwiceMEC) as fake data samples.

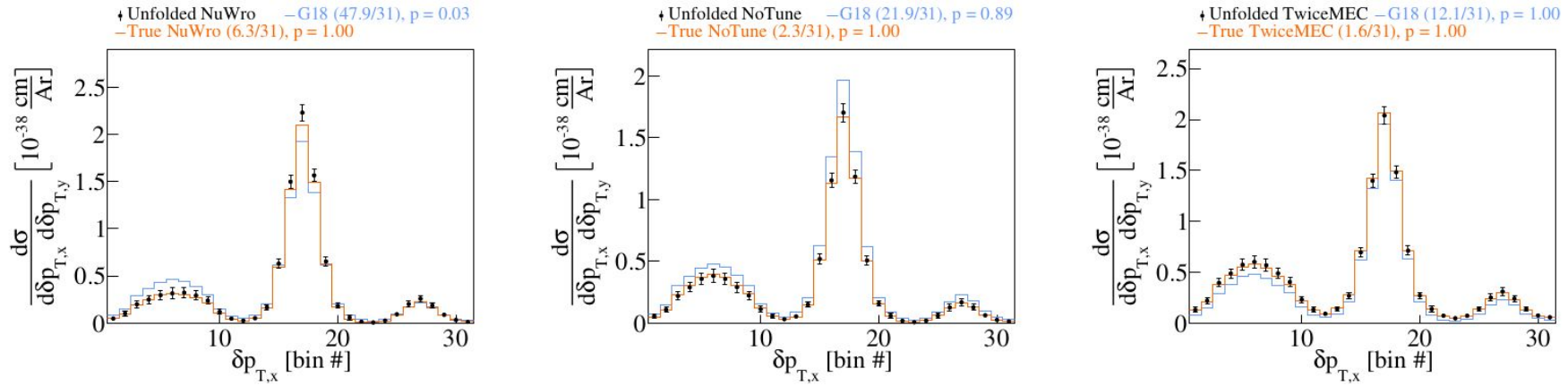


FIG. 6. Fake data studies for  $\delta p_{T,x}$  in  $\delta p_{T,y}$  bins using (left) NuWro, (center) GENIE without the MicroBooNE tune (NoTune), and (right) twice the weights for MEC events (TwiceMEC) as fake data samples.

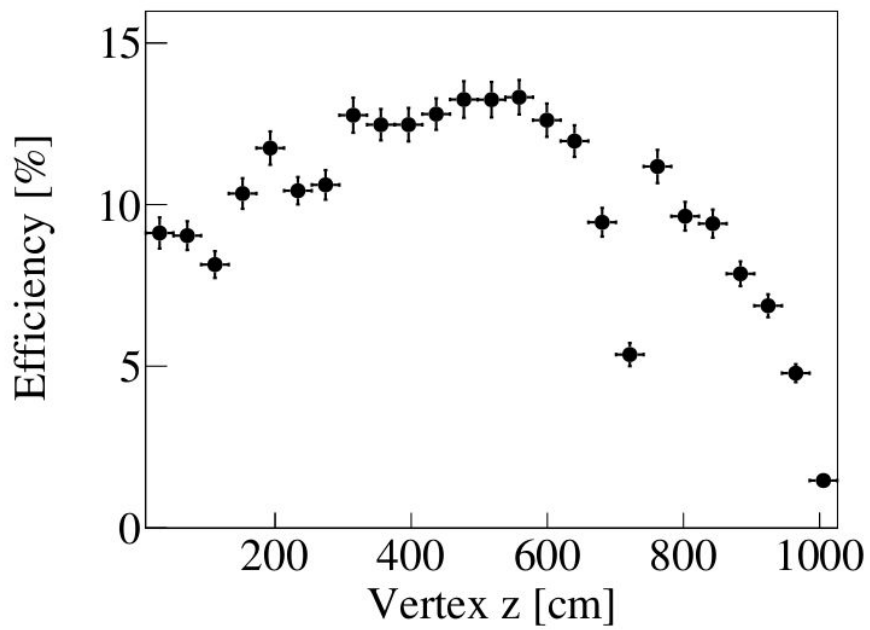
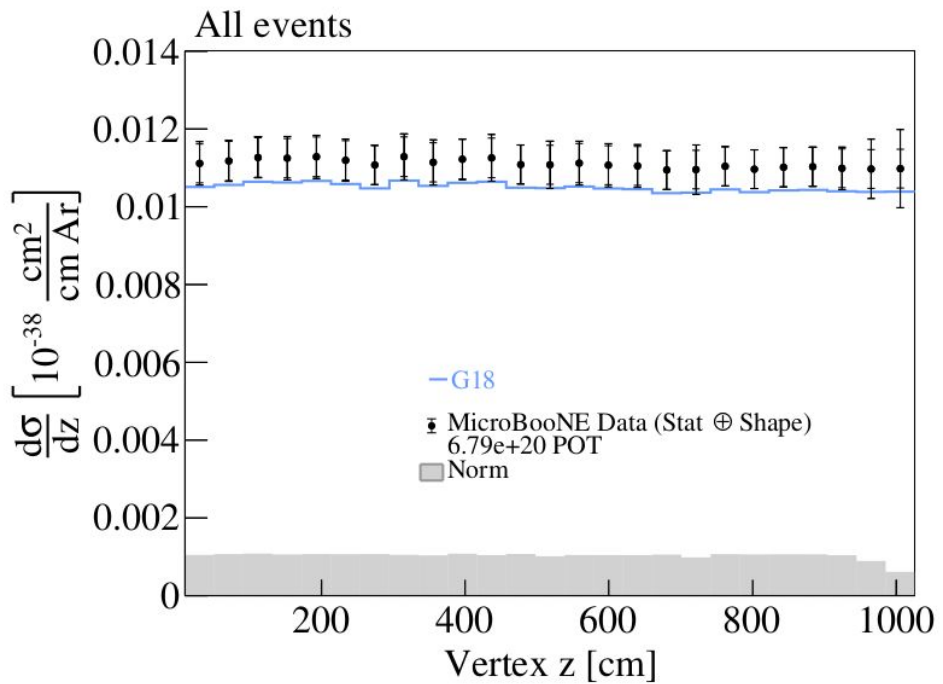


FIG. 7. (Left) extracted cross section as a function of the vertex z distribution. (Right) vertex z efficiency function.

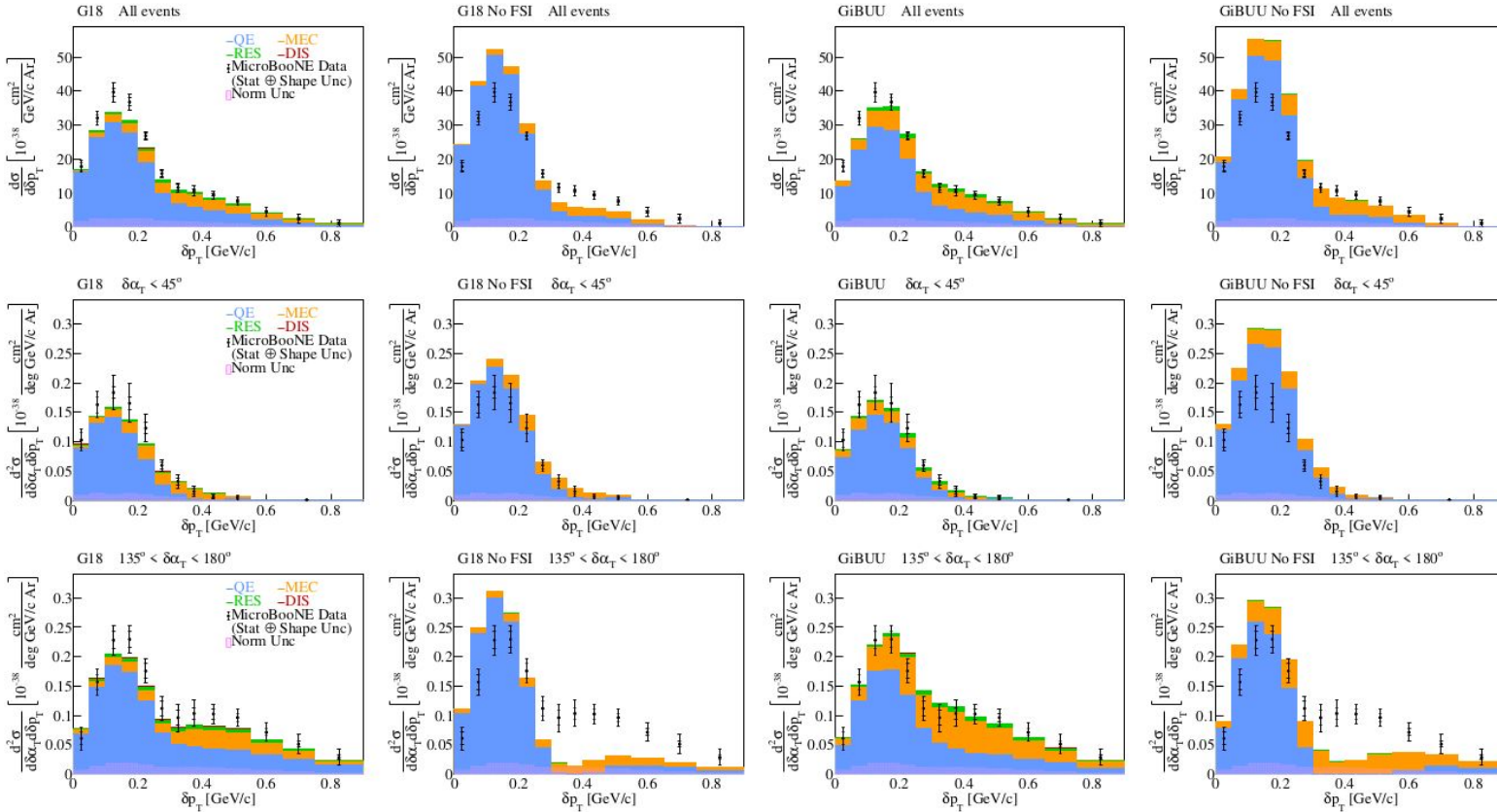


FIG. 8. Cross section interaction breakdown for (top) all the selected events, (middle) events with  $\delta\alpha_T < 45^\circ$ , and (bottom) events with  $135^\circ < \delta\alpha_T < 180^\circ$ . The breakdown is shown for (first column) the G18 configuration with FSI effects, (second column) the G18 configuration without FSI effects, (third column) GiB with FSI effects, and (forth column) GiB without FSI effects.

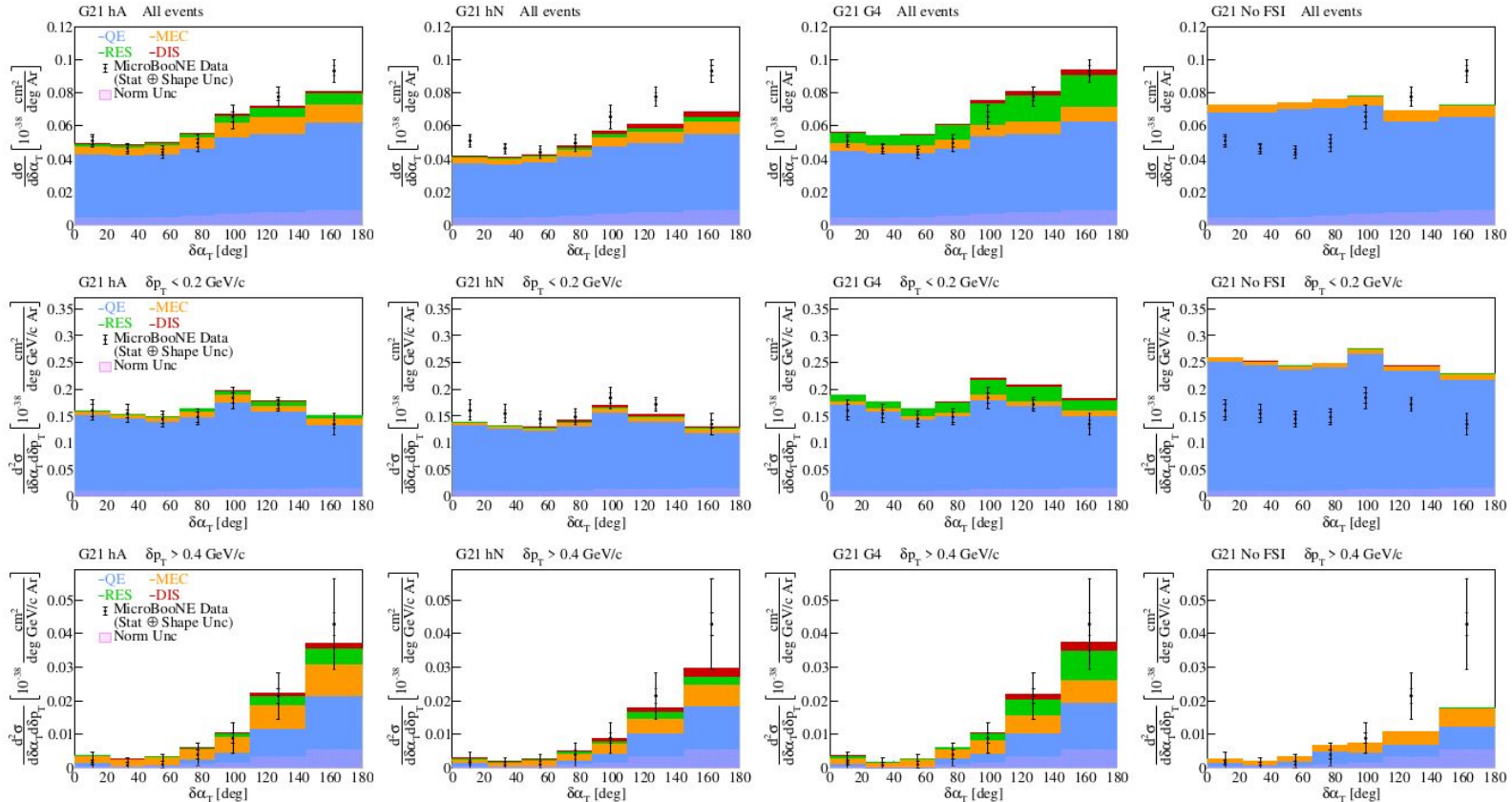


FIG. 9. Cross section interaction breakdown for (top) all the selected events, (middle) events with  $\delta p_T < 0.2 \text{ GeV}/c$ , and (bottom) events with  $\delta p_T > 0.4 \text{ GeV}/c$ . The breakdown is shown for (first column) the G21 hA configuration with the hA2018 FSI model, (second column) the G21 hN configuration with the hN FSI model, (third column) the G21 G4 configuration with the G4 FSI model, and (forth column) the G21 No FSI configuration without FSI effects.

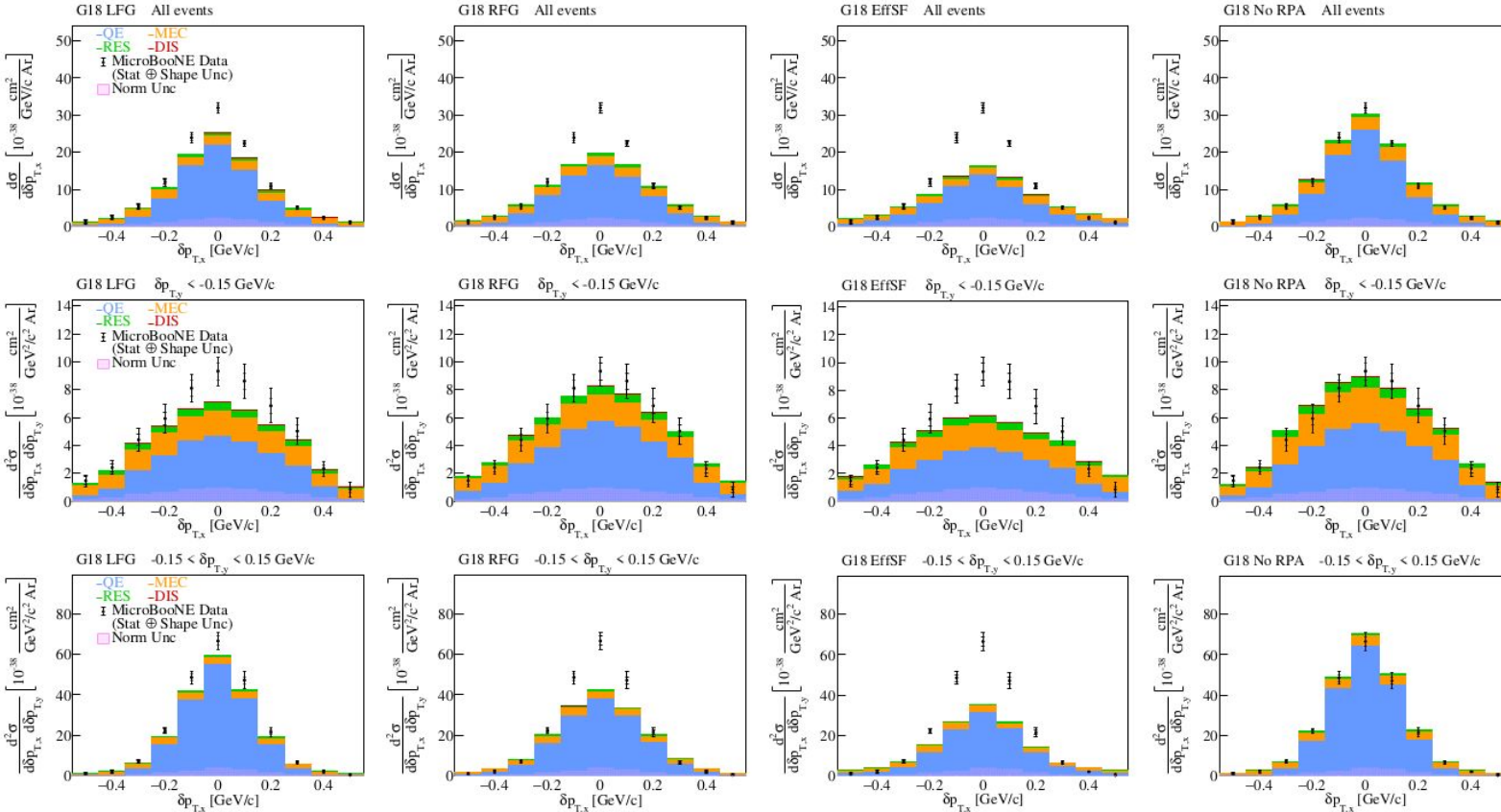


FIG. 10. Cross section interaction breakdown for (top) all the selected events, (middle) events with  $\delta p_{T,y} < -0.15 \text{ GeV}/c$ , and (bottom) events with  $-0.15 < \delta p_{T,y} < 0.15 \text{ GeV}/c$ . The breakdown is shown for (first column) the G18 LFG configuration, (second column) the G18 RFG configuration, (third column) the G18 EffSF configuration, and (forth column) the G18 No RPA configuration.

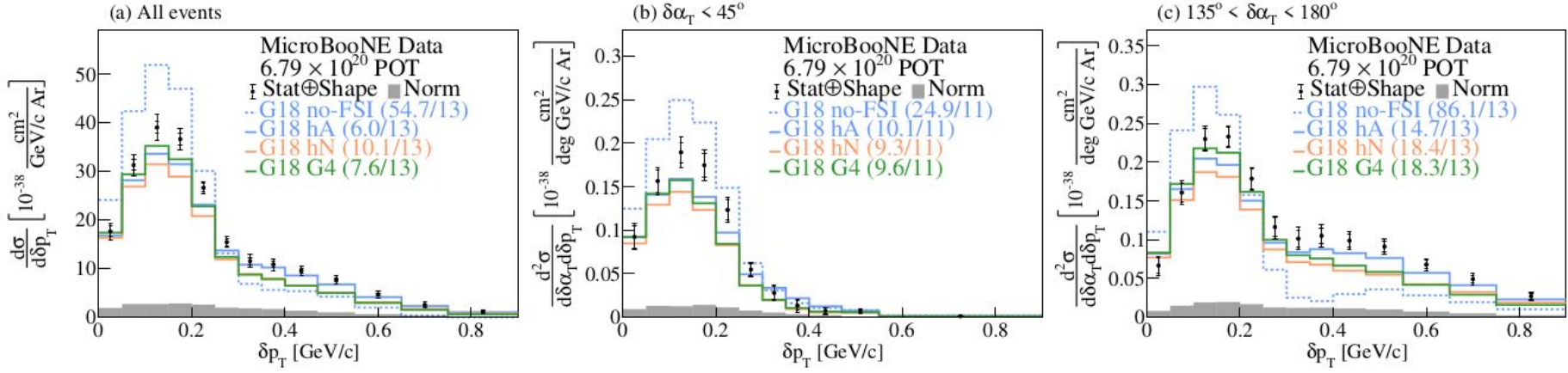


FIG. 11. The flux-integrated (a) single- and (b-c) double- (in  $\delta\alpha_T$  bins) differential CC1p0 $\pi$  cross sections as a function of the transverse missing momentum,  $\delta p_T$ . Inner and outer error bars show the statistical and total (statistical and shape systematic) uncertainty at the  $1\sigma$ , or 68%, confidence level. The gray band shows the separate normalization systematic uncertainty. Colored lines show the results of theoretical cross section calculations with a number of G21 FSI modeling variations.

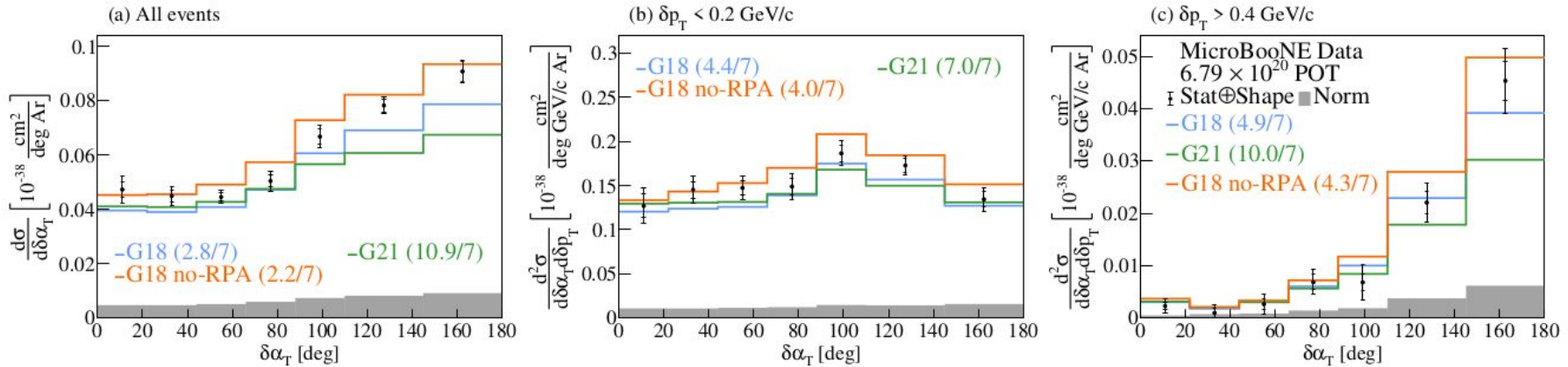


FIG. 12. The flux-integrated (a) single- and (b-c) double- (in  $\delta p_T$  bins) differential CC1p0 $\pi$  cross sections as a function of the angle  $\delta\alpha_T$ . Inner and outer error bars show the statistical and total (statistical and shape systematic) uncertainty at the  $1\sigma$ , or 68%, confidence level. The gray band shows the separate normalization systematic uncertainty. Colored lines show the results of theoretical cross section calculations with a number of QE-modeling choices based on the GENIE event generator.

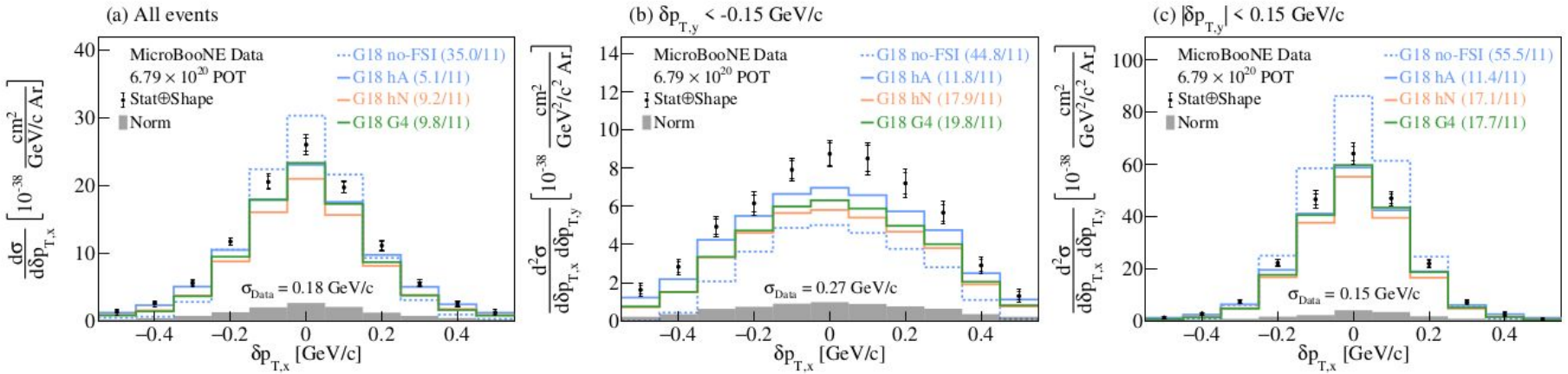
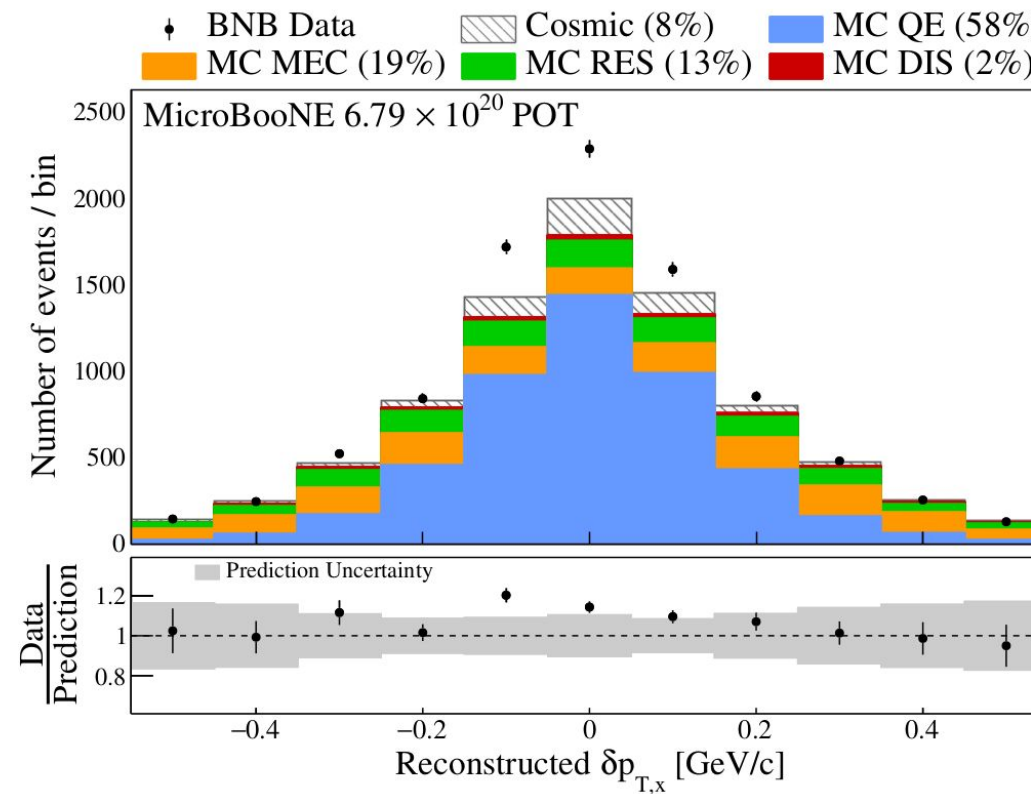
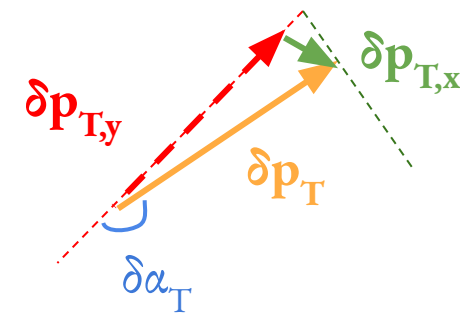


FIG. 13. The flux-integrated (a) single- and (b-c) double- (in  $\delta p_{T,y}$  bins) differential CC1p0 $\pi$  cross sections as a function of the transverse three-momentum transfer component,  $\delta p_{T,x}$ . Inner and outer error bars show the statistical and total (statistical and shape systematic) uncertainty at the  $1\sigma$ , or 68%, confidence level. The gray band shows the separate normalization systematic uncertainty. Colored lines show the results of theoretical cross section calculations with a number of G18 FSI modeling variations. The standard deviation ( $\sigma_{\text{Data}}$ ) of a Gaussian fit to the data is shown on each panel.

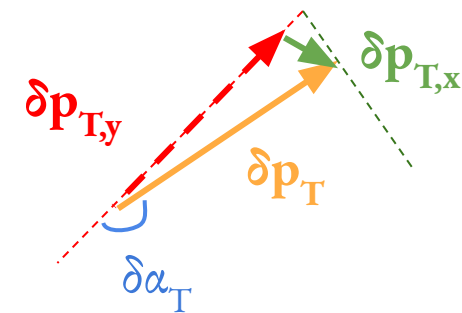
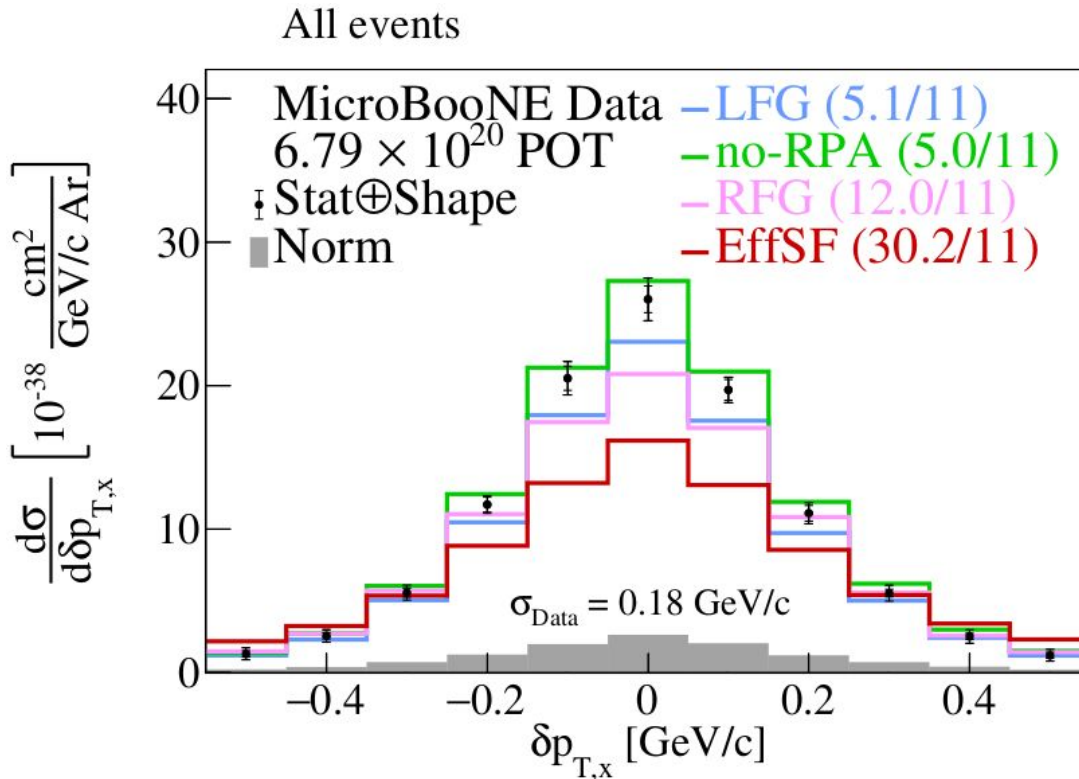
# Transverse Component $\delta p_{T,x}$



$$\delta p_{T,x} = \delta p_T \cdot \sin \delta \alpha_T$$

- Symmetric around 0 GeV/c
- **QE** dominance in central region
- **MEC/RES** events primarily in the tail

# Transverse Component $\delta p_{T,x}$ Cross Section

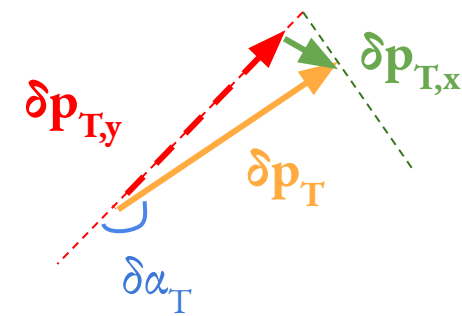
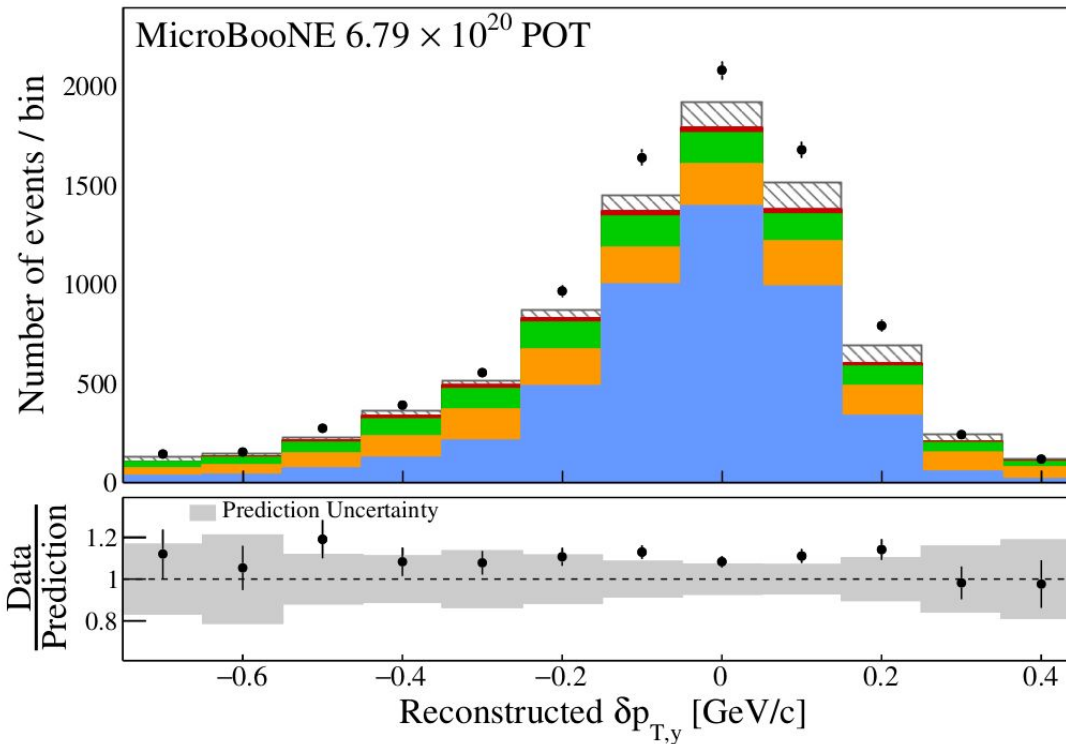


$$\delta p_{T,x} = \delta p_T \cdot \sin \delta \alpha_T$$

- G18 LFG = GENIE v3.0.6  
G18\_10a\_02\_11a (G18) + uB Tune  
with local Fermi gas
- G18 no-RPA = G18 w/o RPA effects
- G18 RFG = G18 with relativistic  
Fermi gas (RFG)
- G18 EffSF = G18 with spectral  
function (EffSF)

# Longitudinal Component $\delta p_{T,y}$

◆ BNB Data      Cosmic (8%)      MC QE (58%)  
■ MC MEC (19%)      MC RES (13%)      MC DIS (2%)

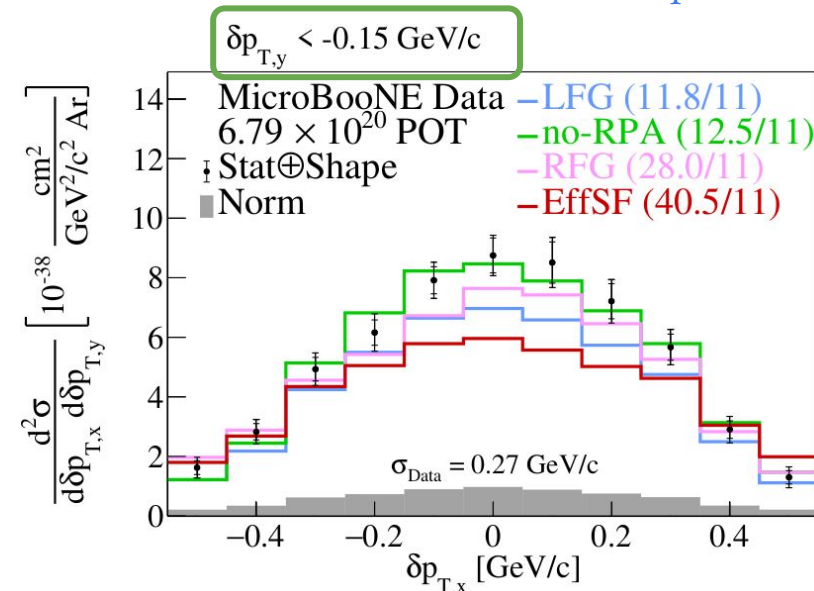
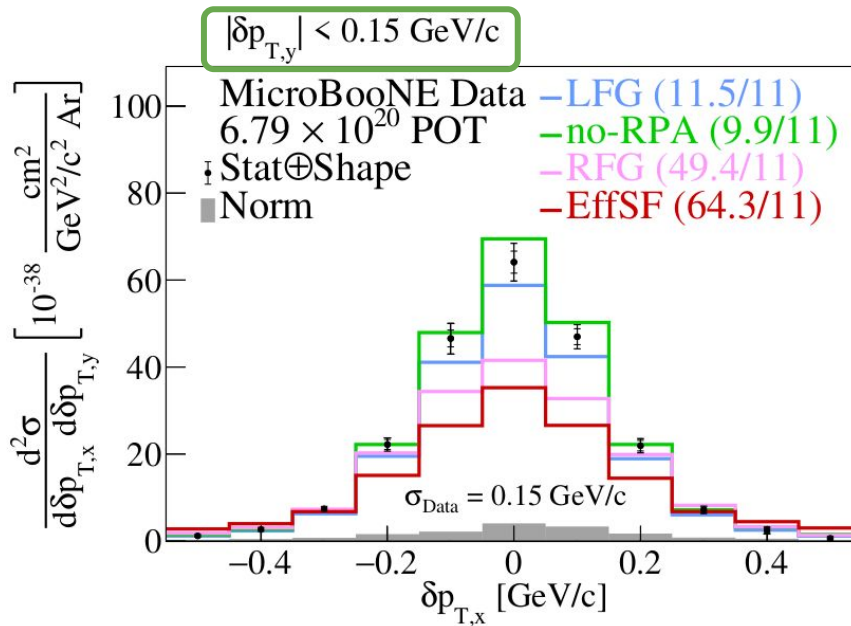
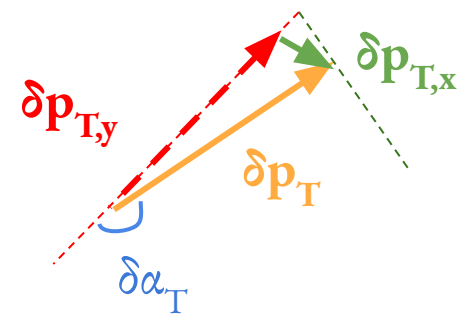


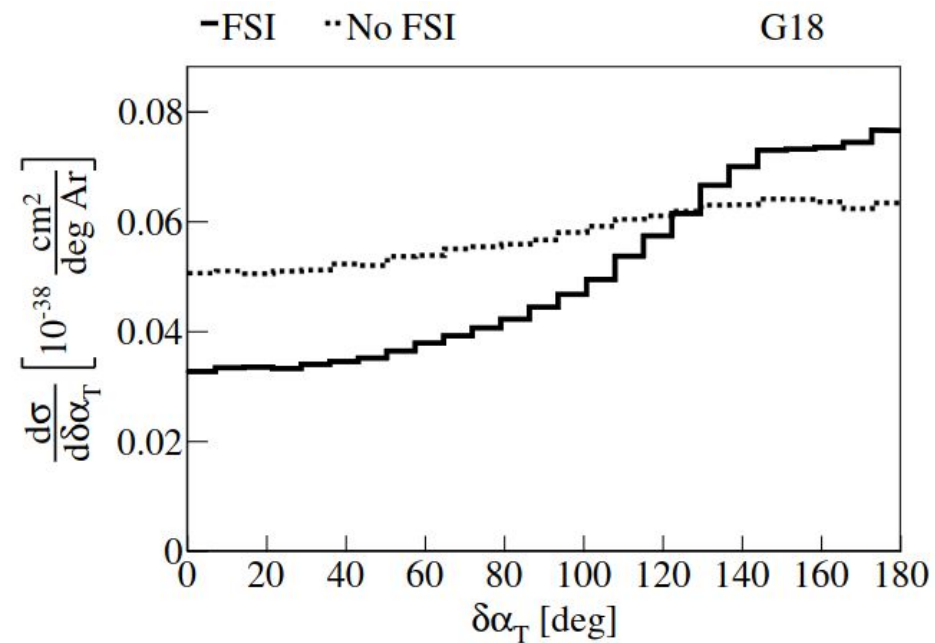
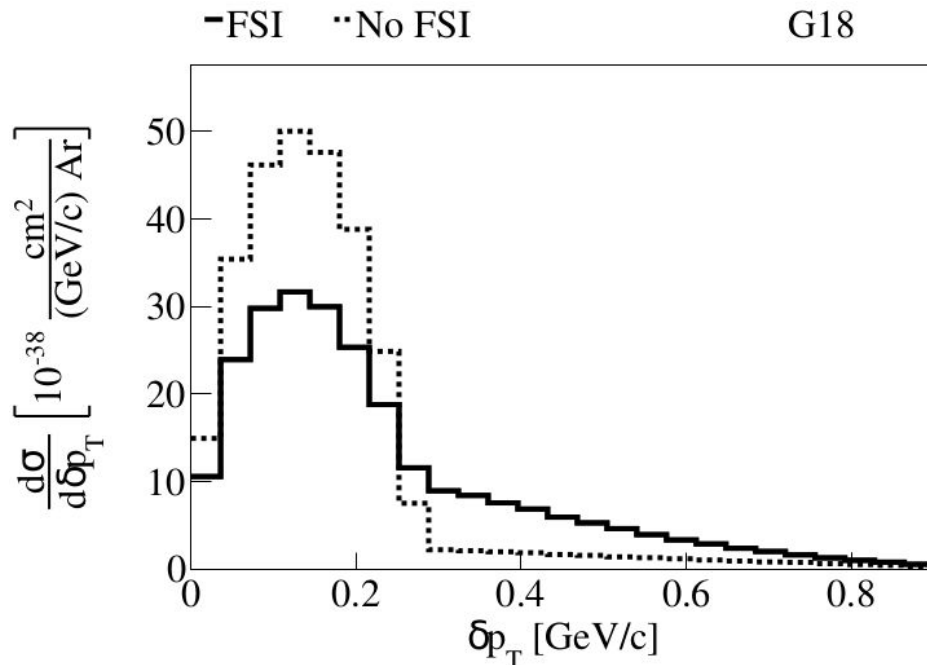
$$\delta p_{T,y} = \delta p_T \cdot \cos\delta\alpha_T$$

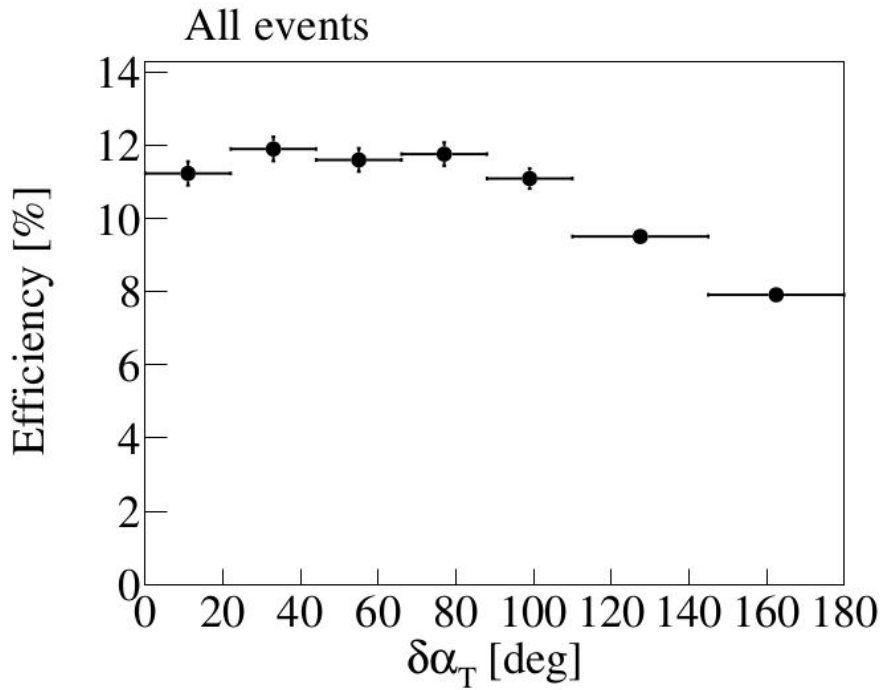
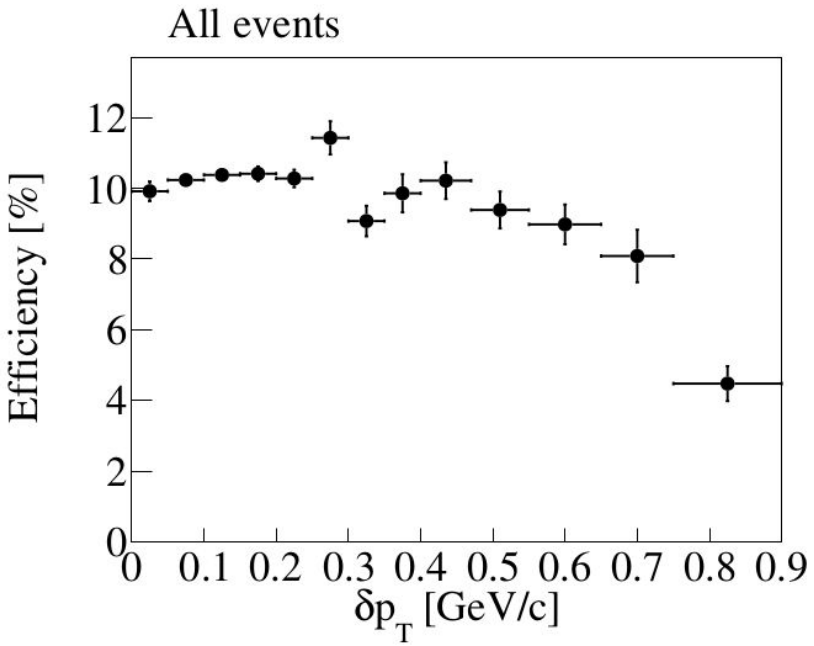
- Asymmetric due to  $\delta\alpha_T$  enhancement at  $\sim 180^\circ$
- **QE** dominance in central region
- Spread of tail sensitive to FSI strength & **MEC/RES**

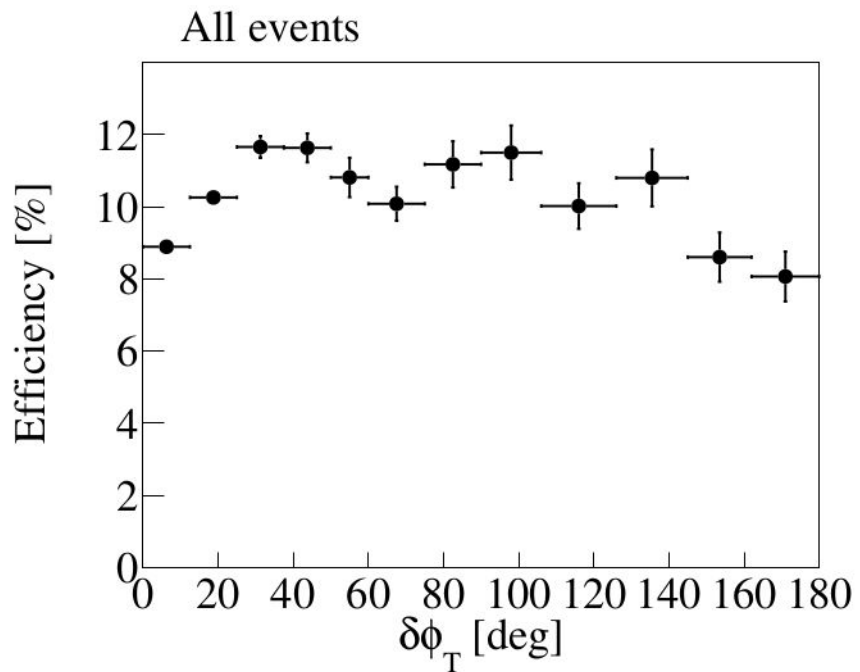
# High Statistics → Into the Multiverse!

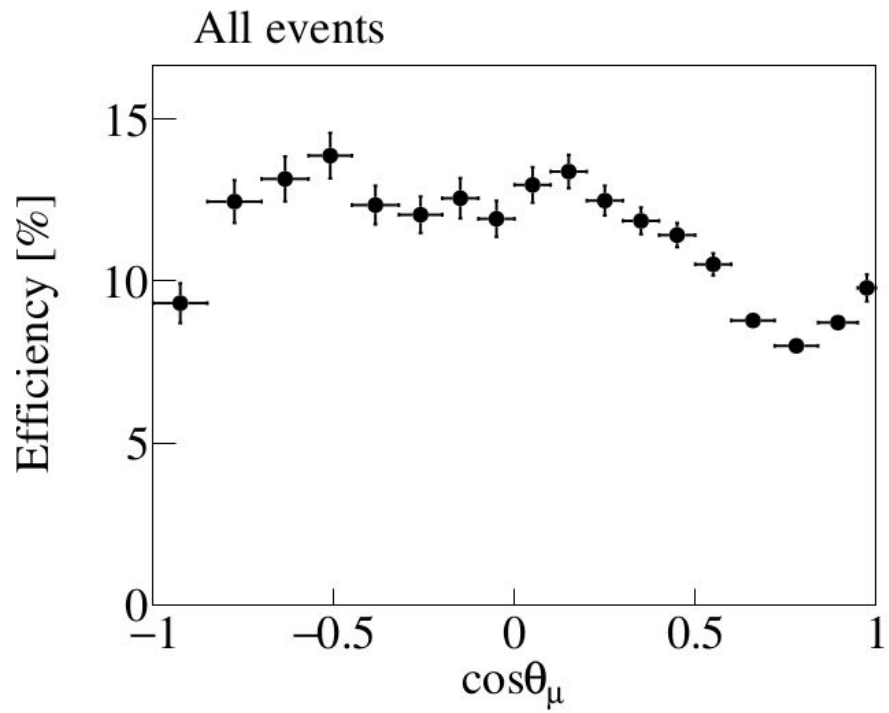
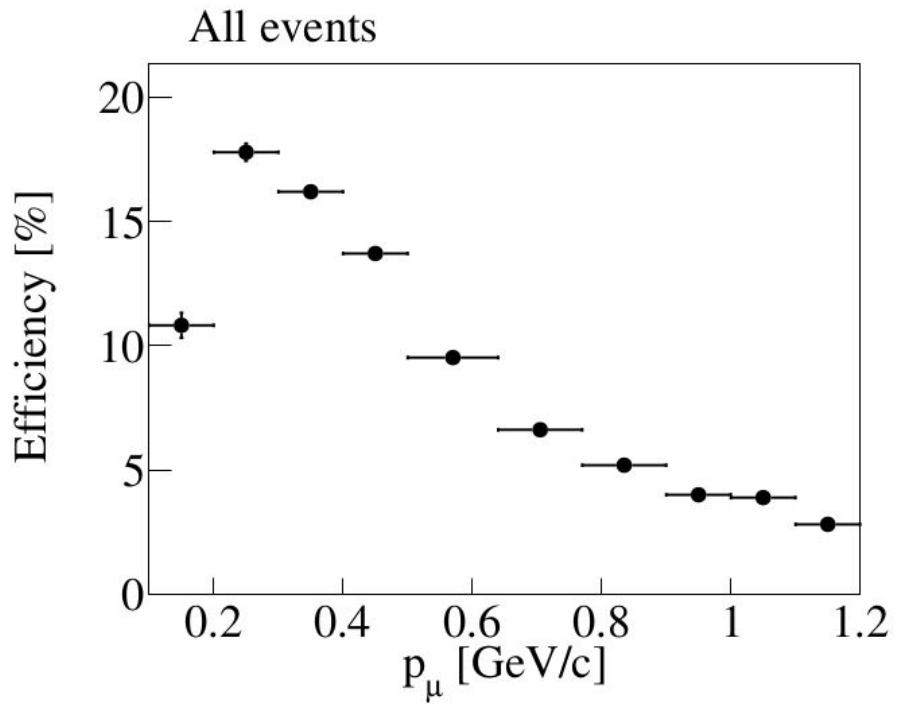
- First neutrino-argon differential cross section in TKI variables
- Sensitive to initial nucleon motion & proton FSI modeling

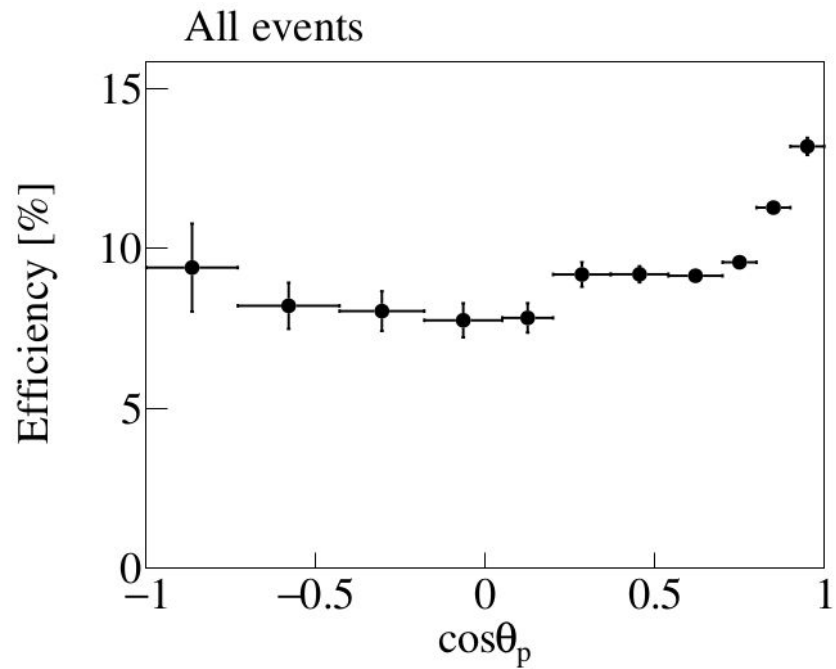
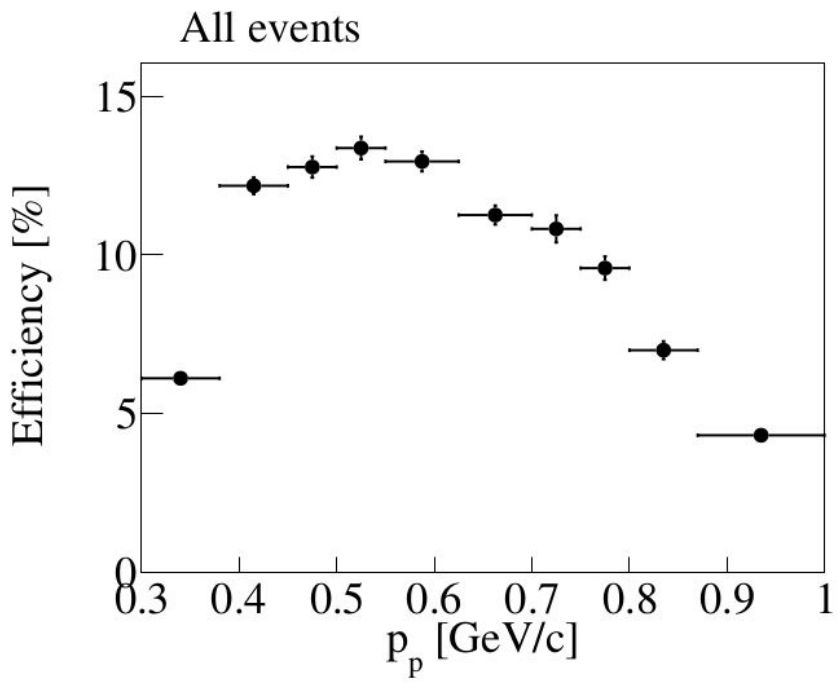


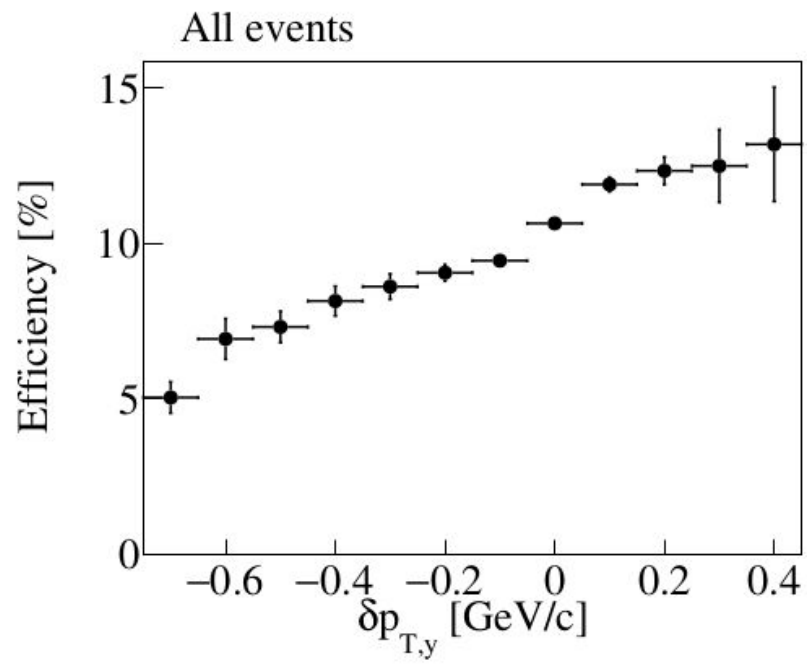
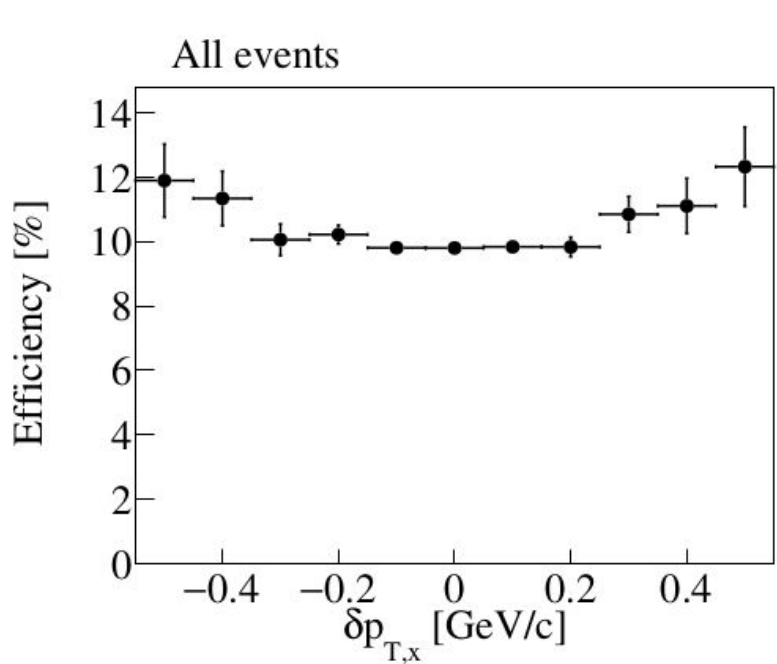












• MicroBooNE Data 6.79e+20 POT  
— MC uB Tune

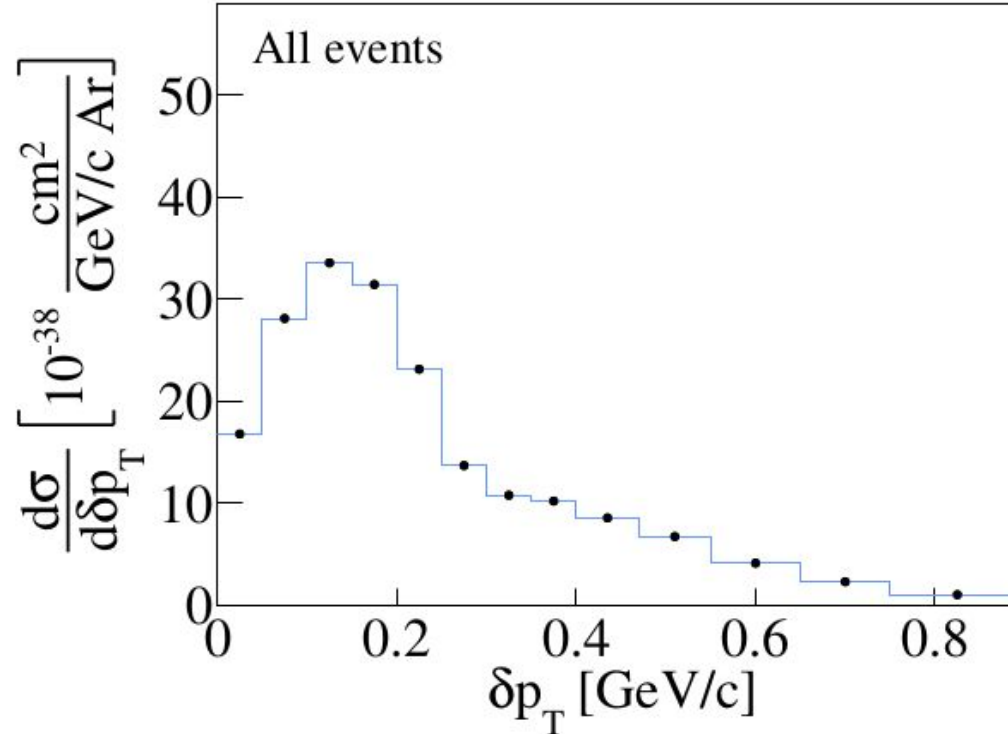
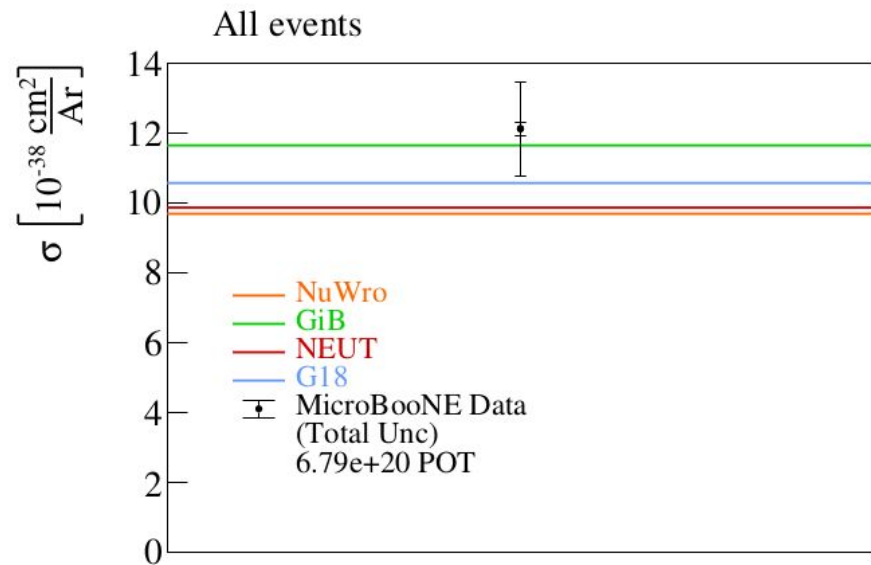
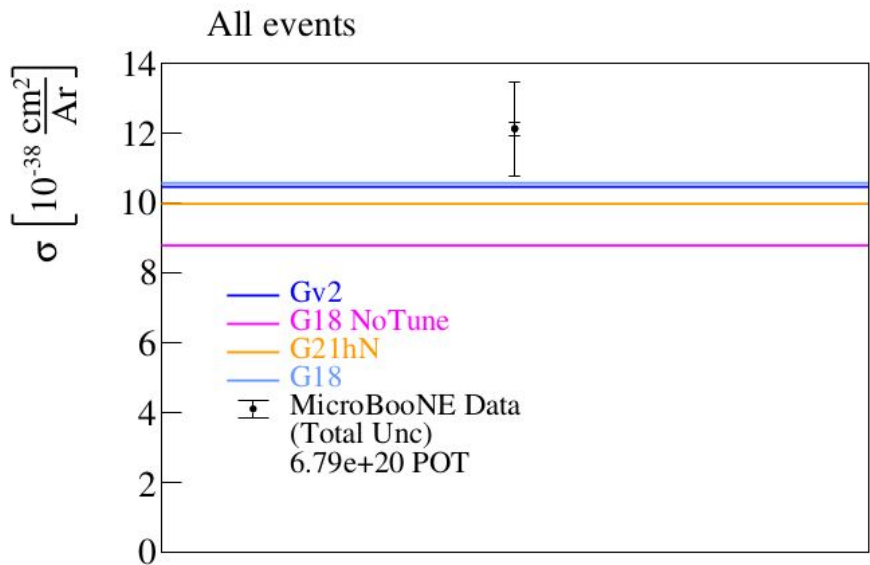


Figure 56: Closure test for  $\delta p_T$ .



# Generalized Kinematic Imbalance (GKI)

Straightforward extension to 3D by considering longitudinal component of missing moment

However, an assumption on the incoming energy has to be made

First attempt in [Phys. Rev. C 95, 065501 \(2017\)](#) using CCQE interactions off a bound stationary neutron

Leveraging calorimetric energy estimator definition

$$E_{\text{cal}} = E_\mu + K_p + B$$

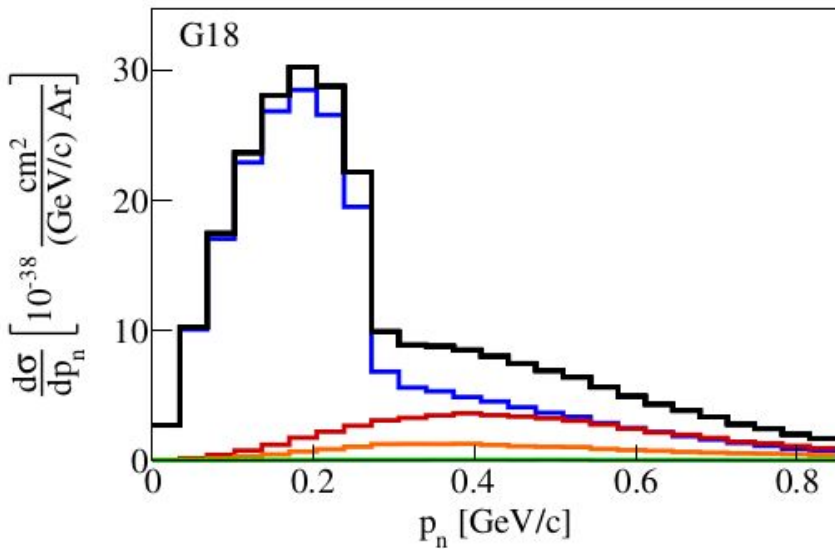
to obtain the longitudinal component of missing momentum

$$p_L = p_L^\mu + p_L^p - E_{\text{cal}}$$

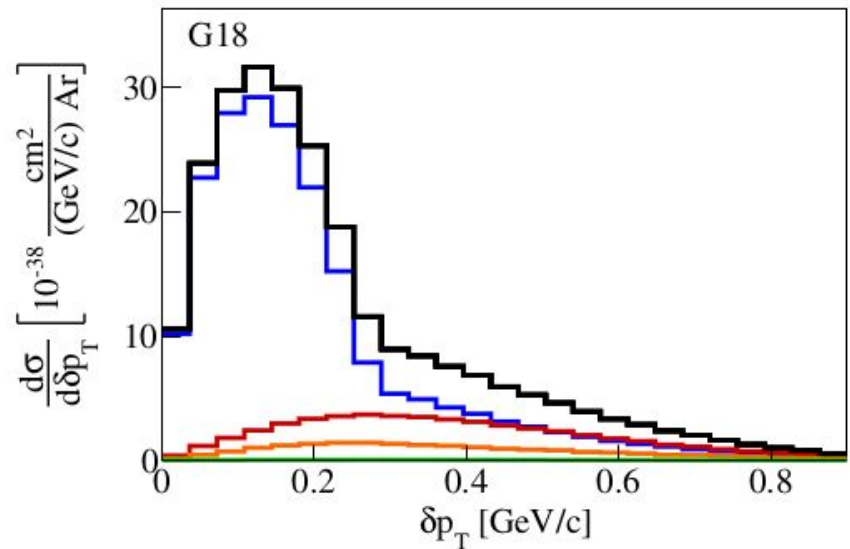
and the energy transfer vector

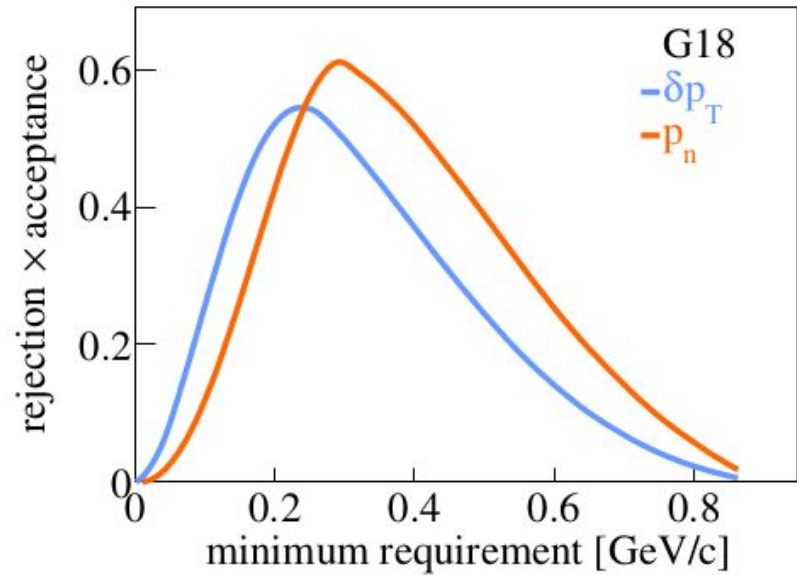
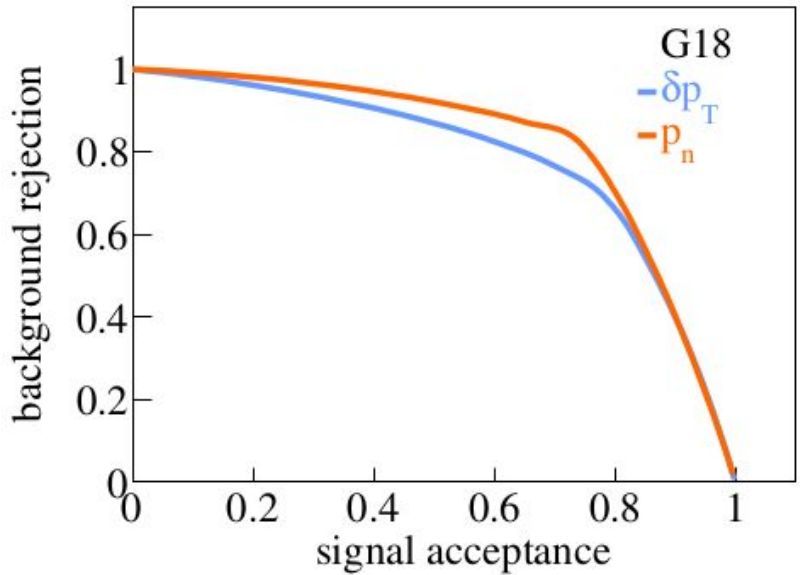
$$\vec{q} = E_{\text{cal}} \hat{z} - \vec{p}_\mu$$

-Total -QE -MEC -RES -DIS



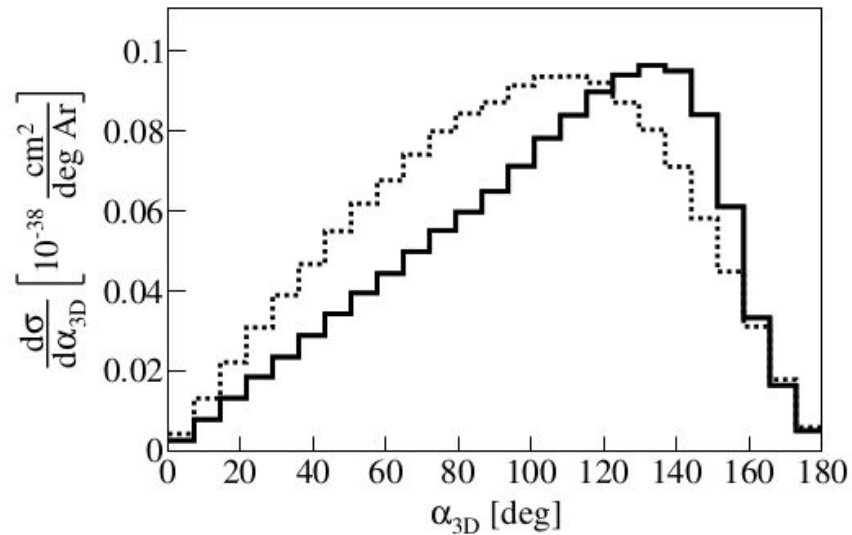
-Total -QE -MEC -RES -DIS





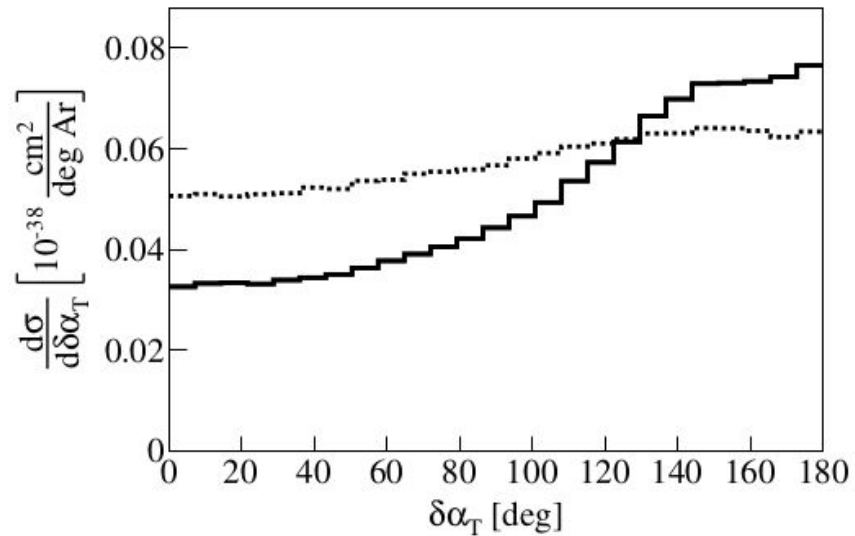
-FSI    ..No FSI

G18

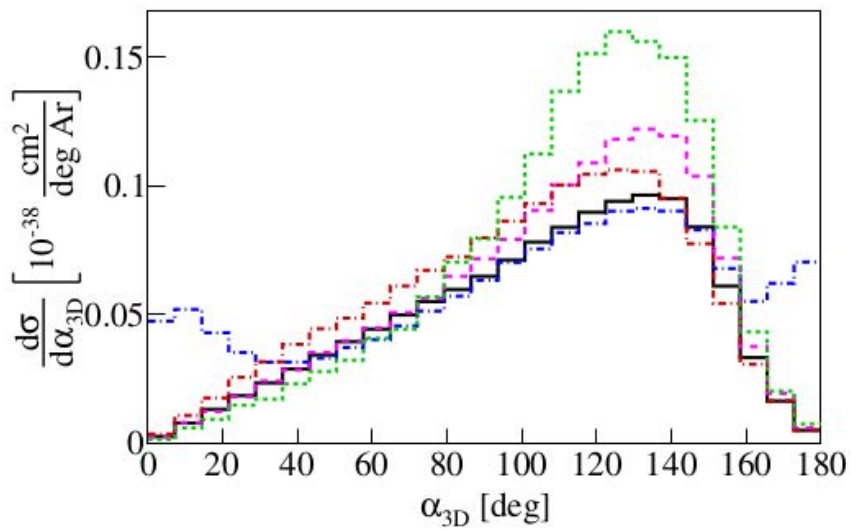


-FSI    ..No FSI

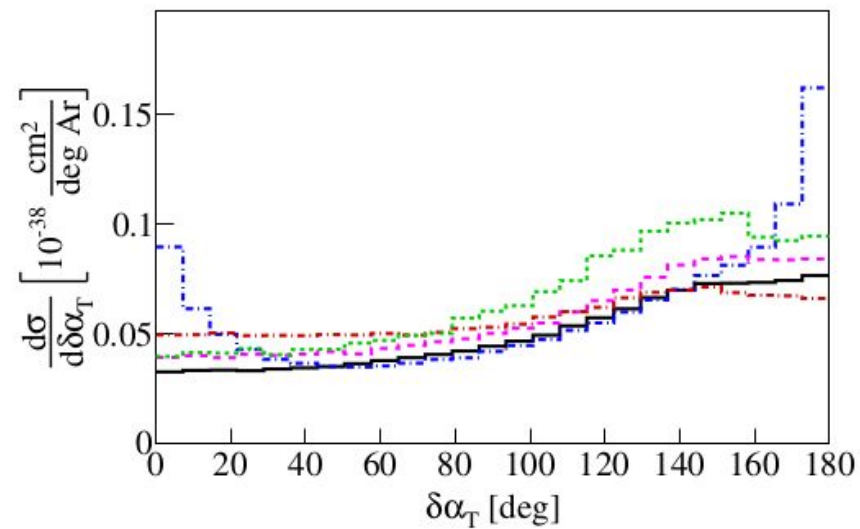
G18



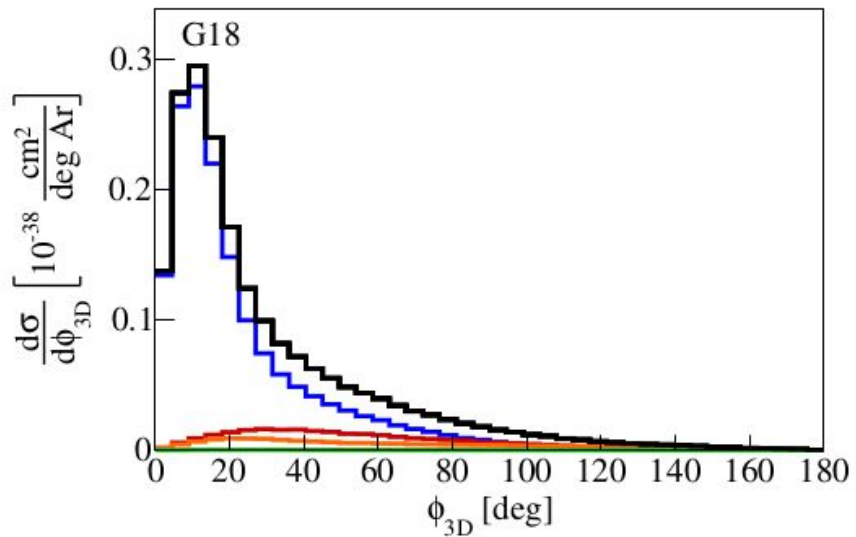
— G18 ⋯ Gv2 ⋯ NEUT ⋯ NuWro ⋯ GiBUU



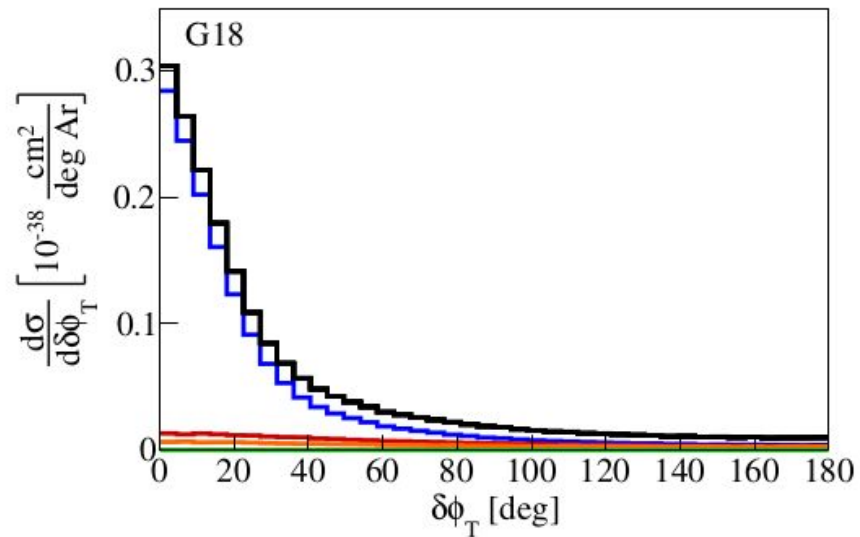
— G18 ⋯ Gv2 ⋯ NEUT ⋯ NuWro ⋯ GiBUU

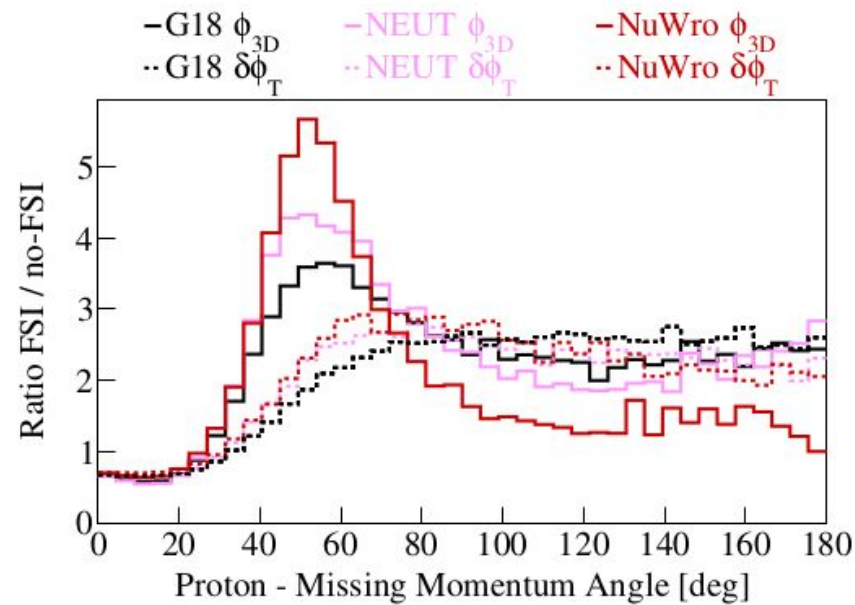
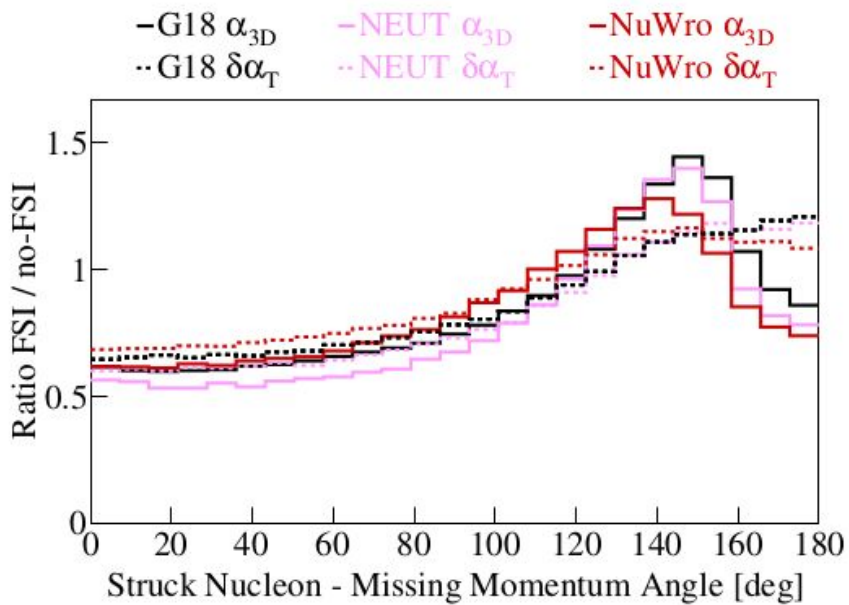


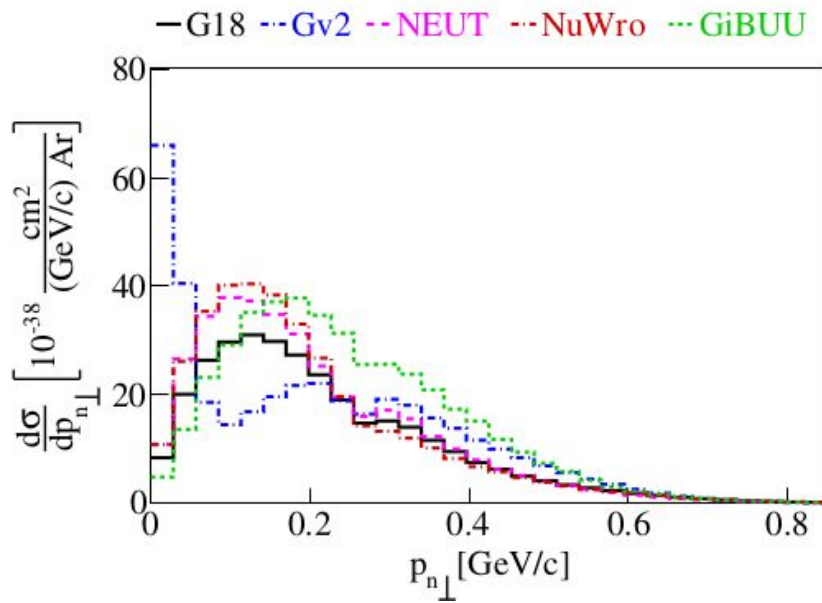
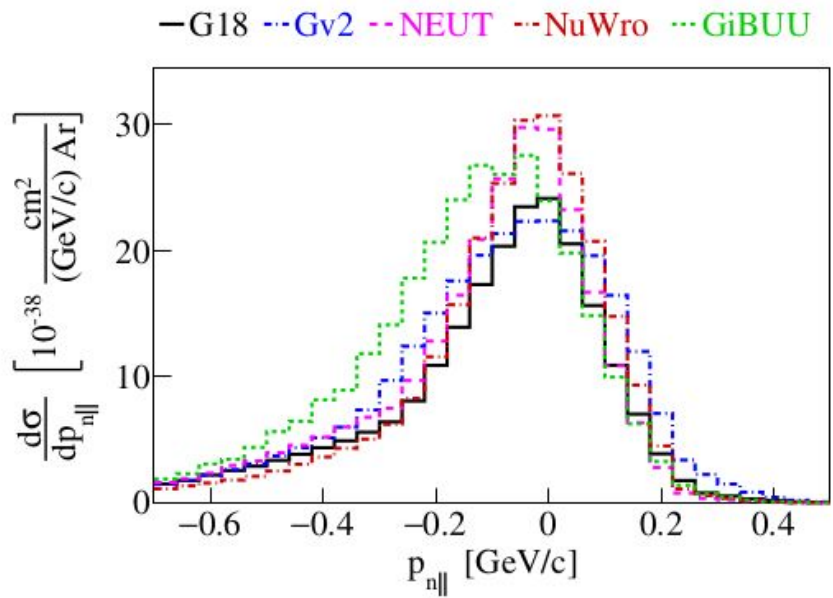
-Total -QE -MEC -RES -DIS



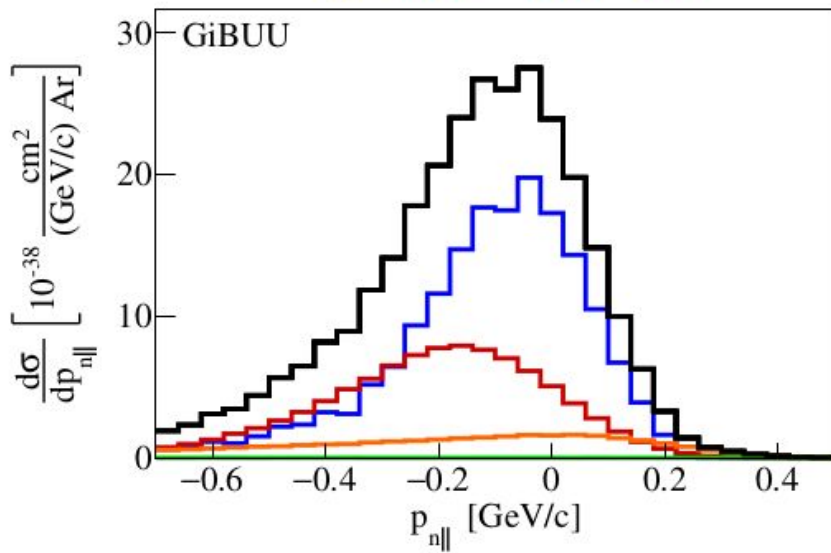
-Total -QE -MEC -RES -DIS



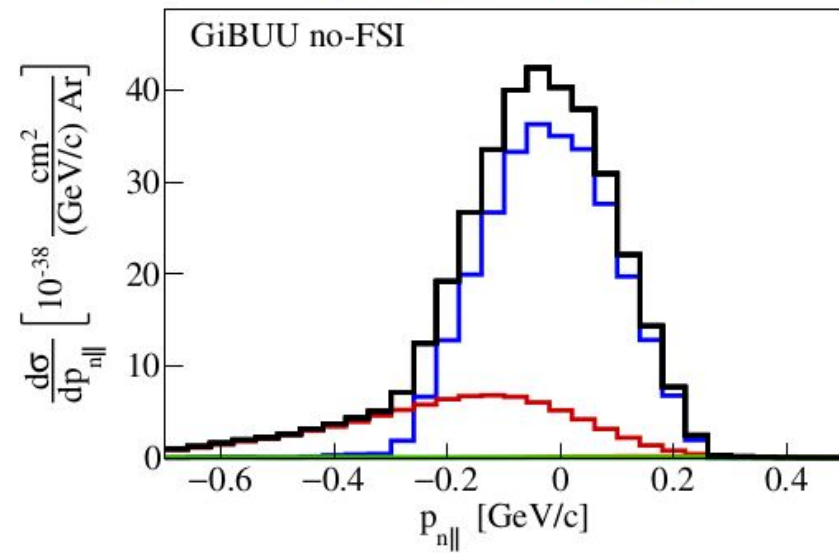


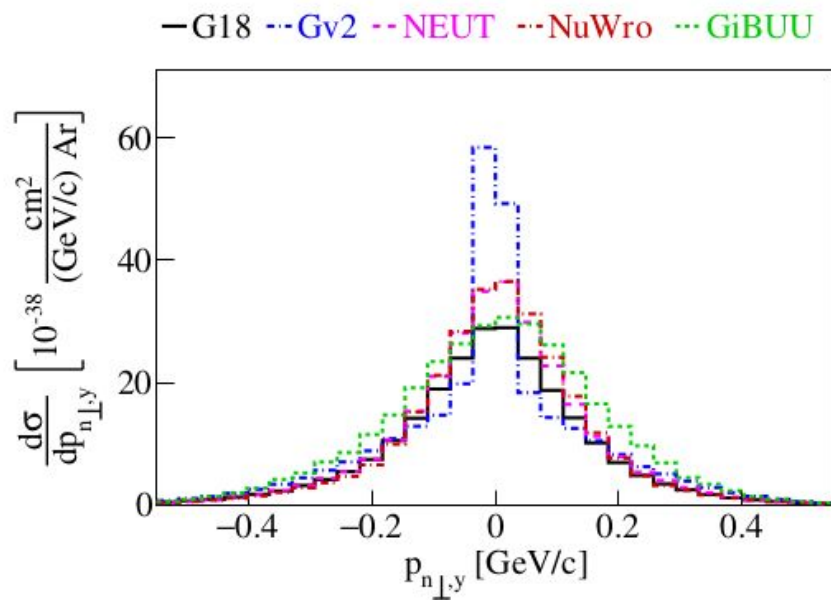
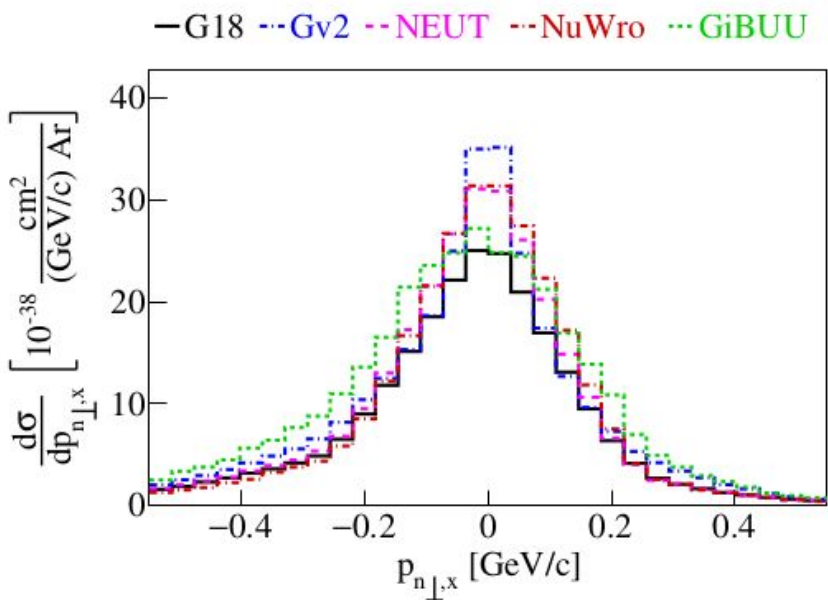


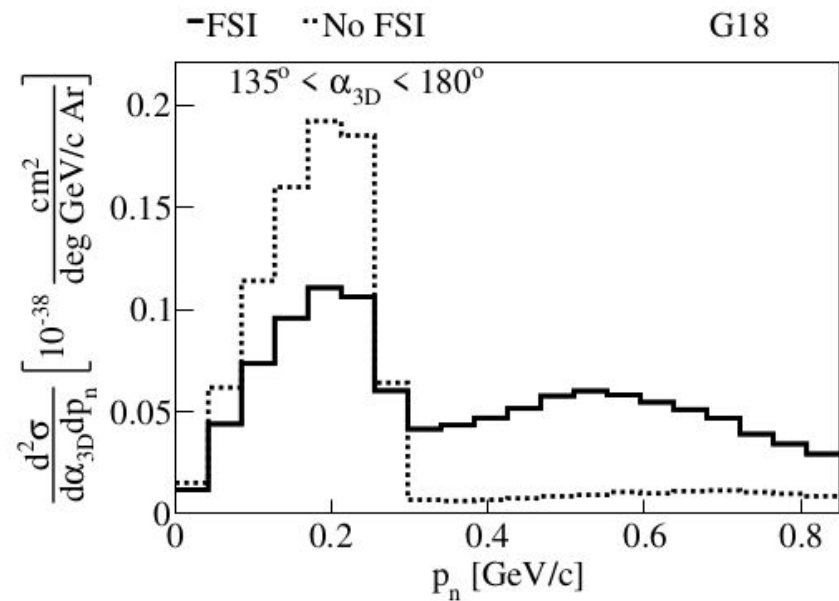
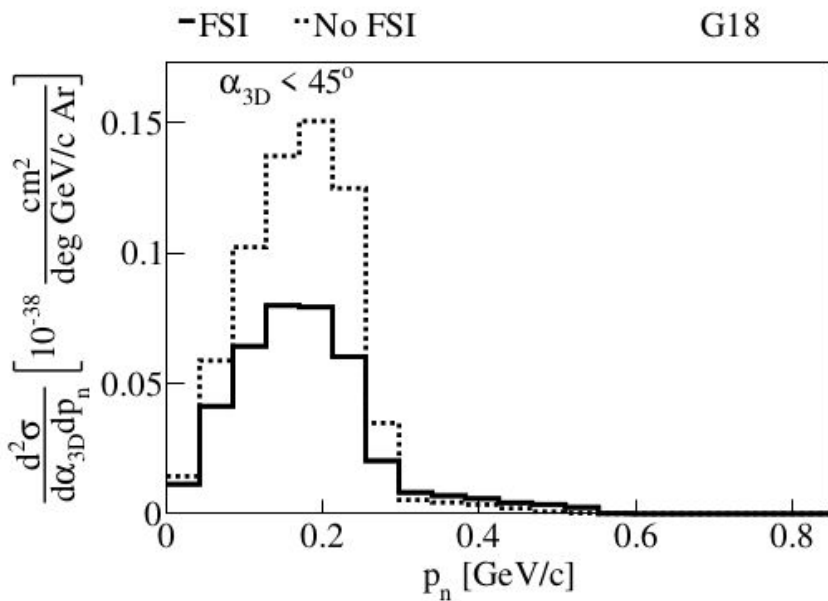
-Total -QE -MEC -RES -DIS

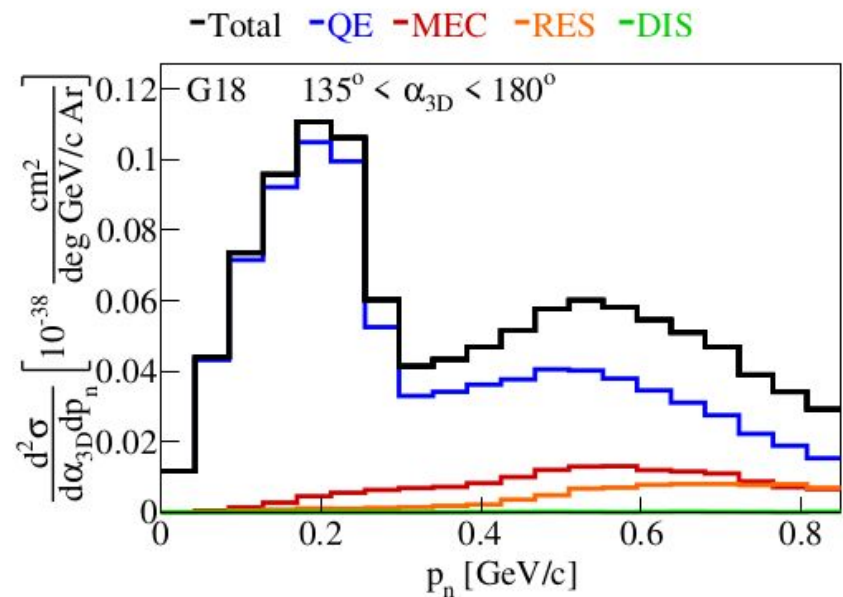
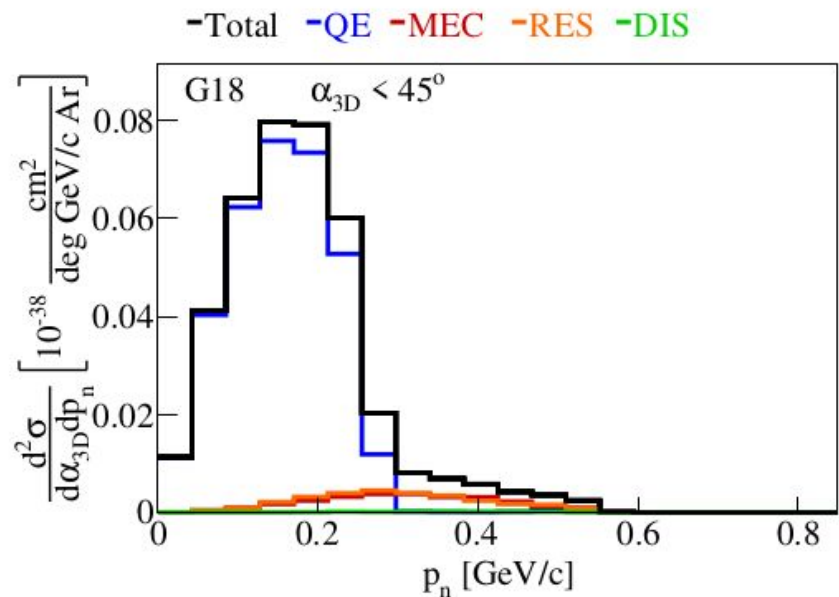


-Total -QE -MEC -RES -DIS

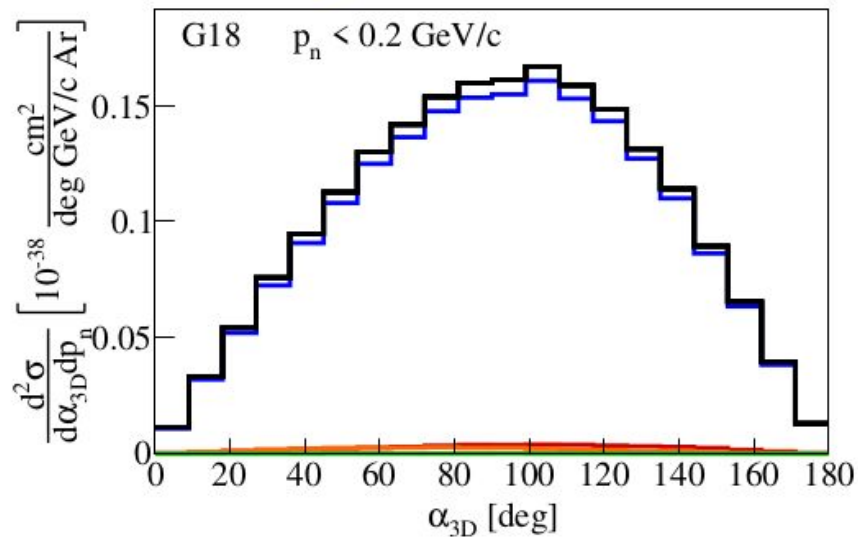




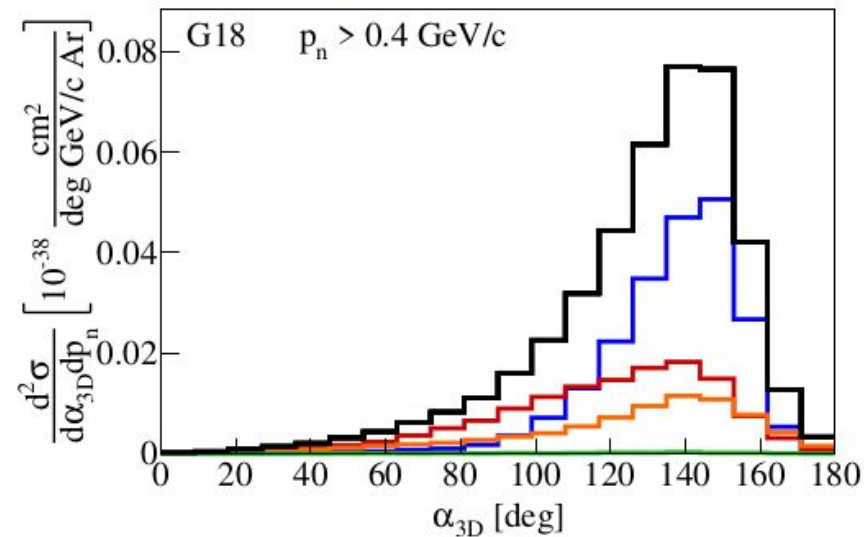


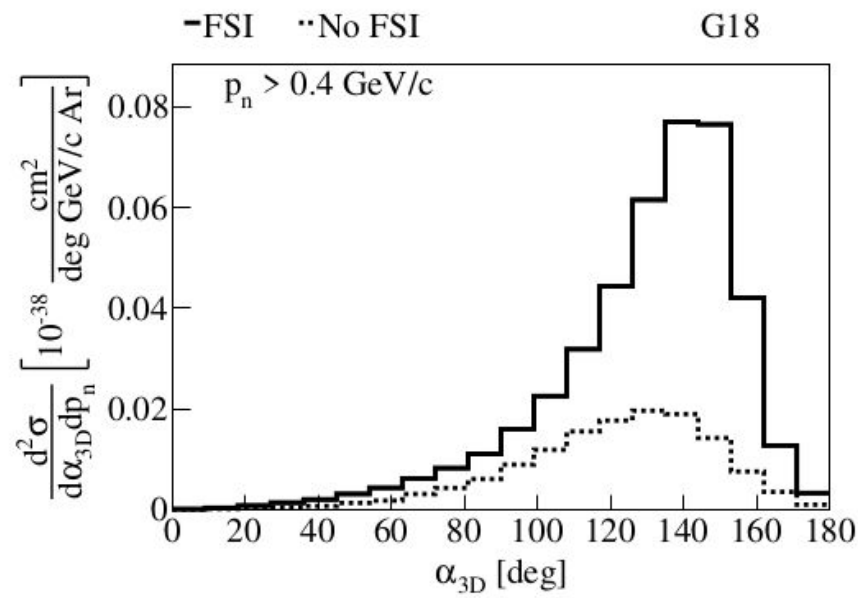
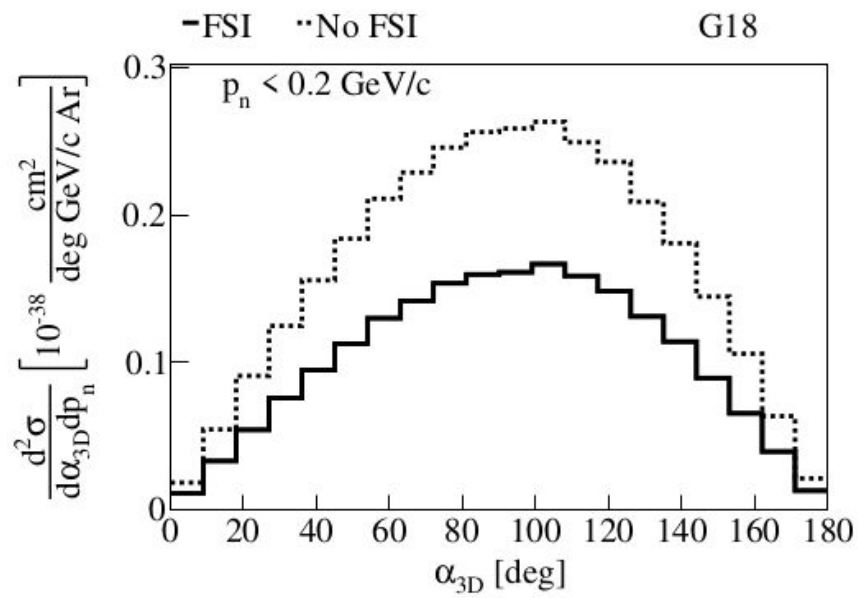


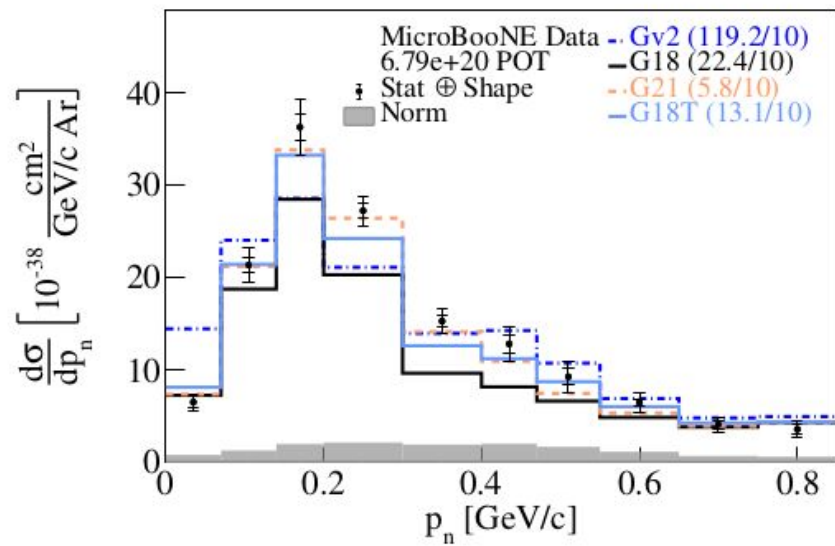
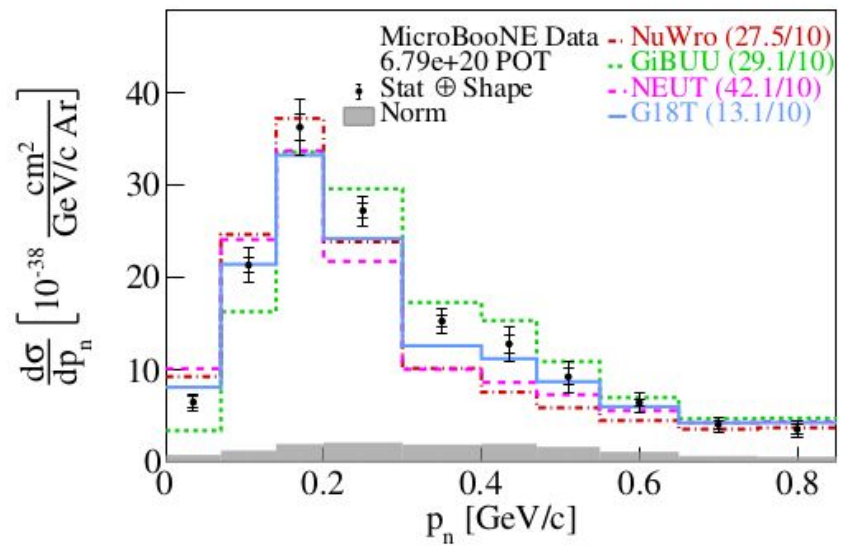
-Total -QE -MEC -RES -DIS

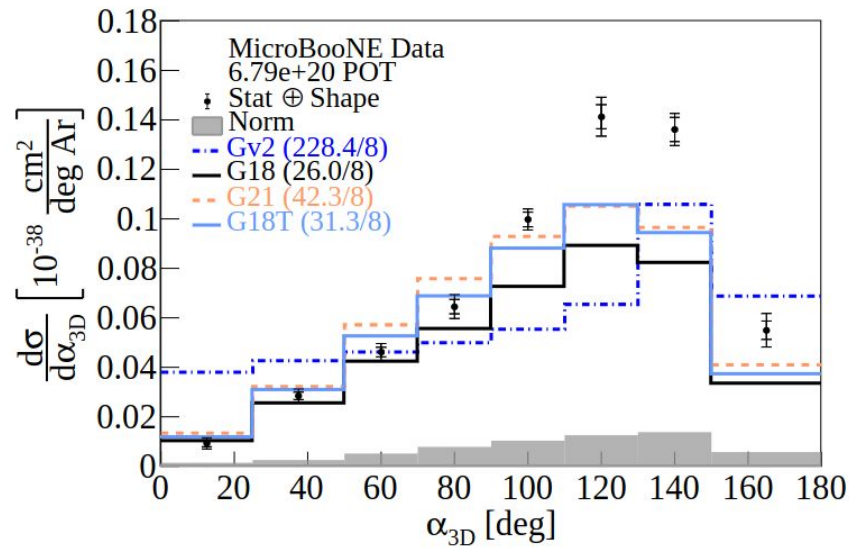
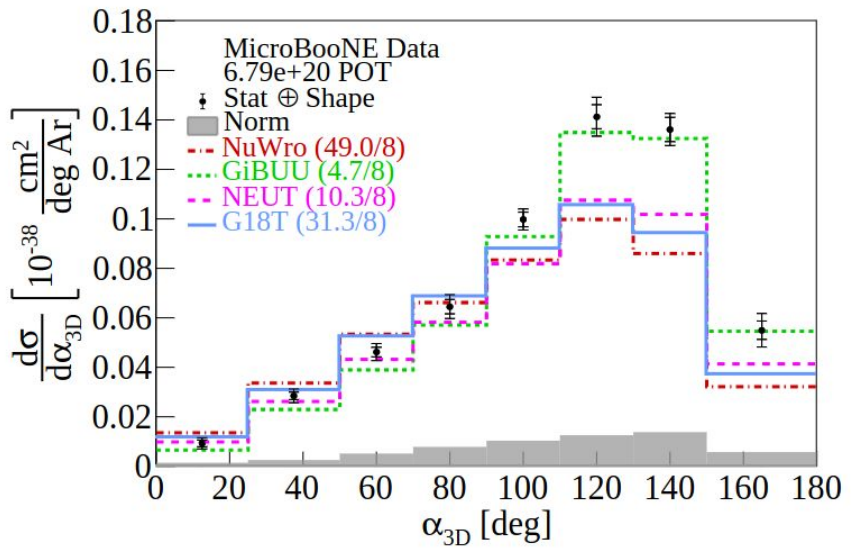


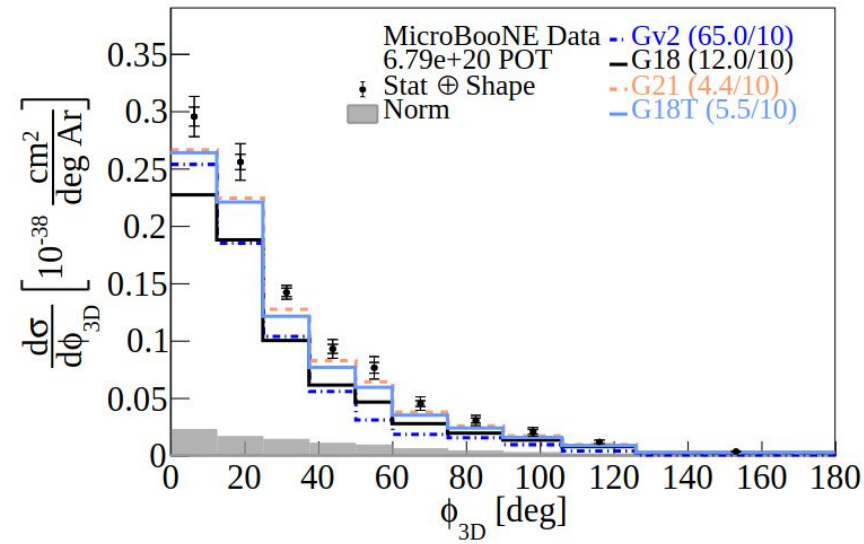
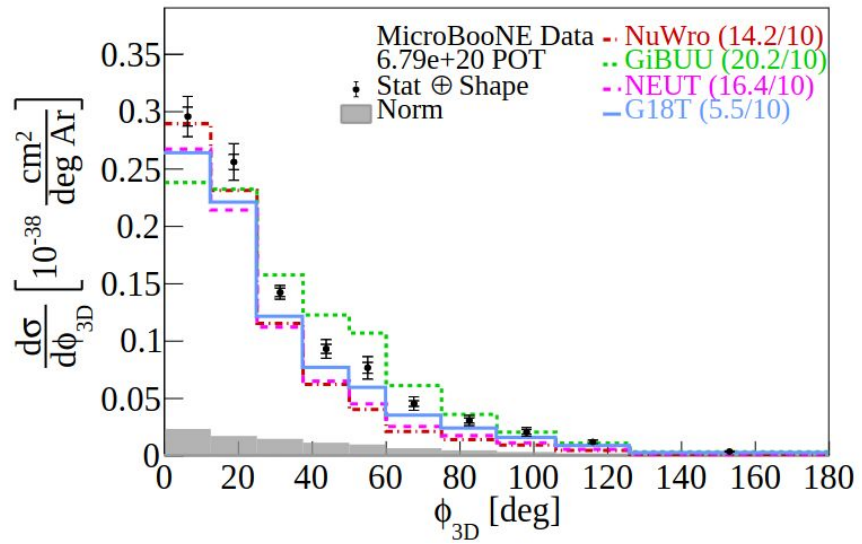
-Total -QE -MEC -RES -DIS

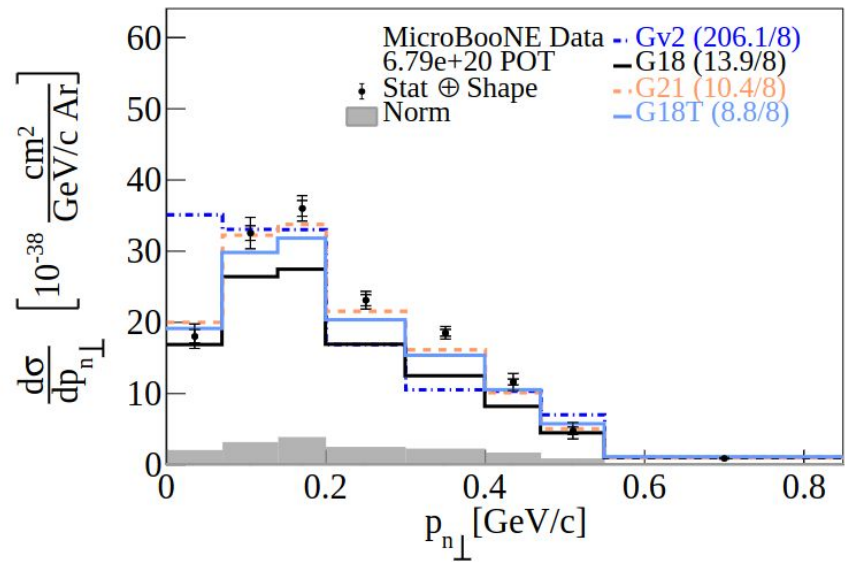
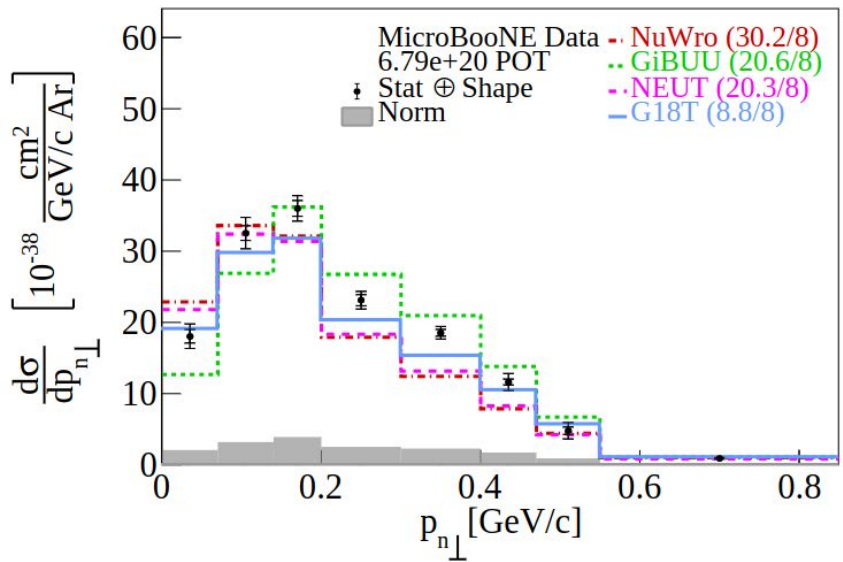


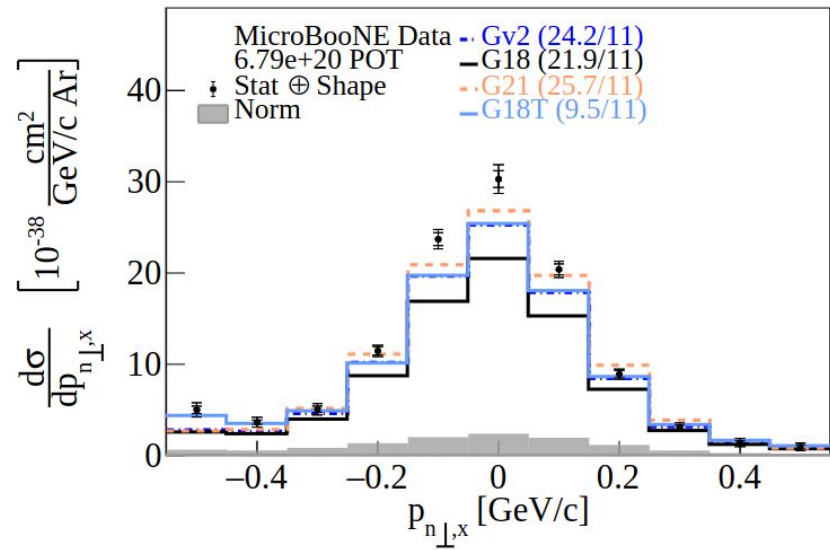
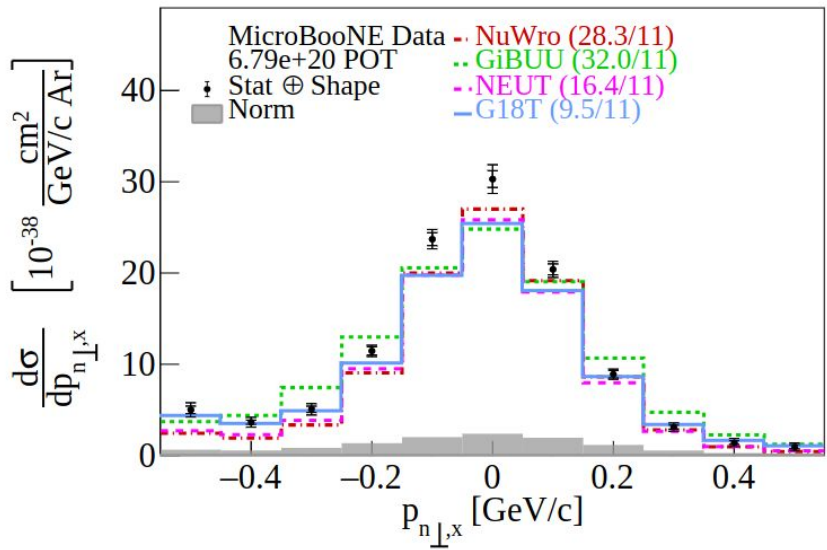


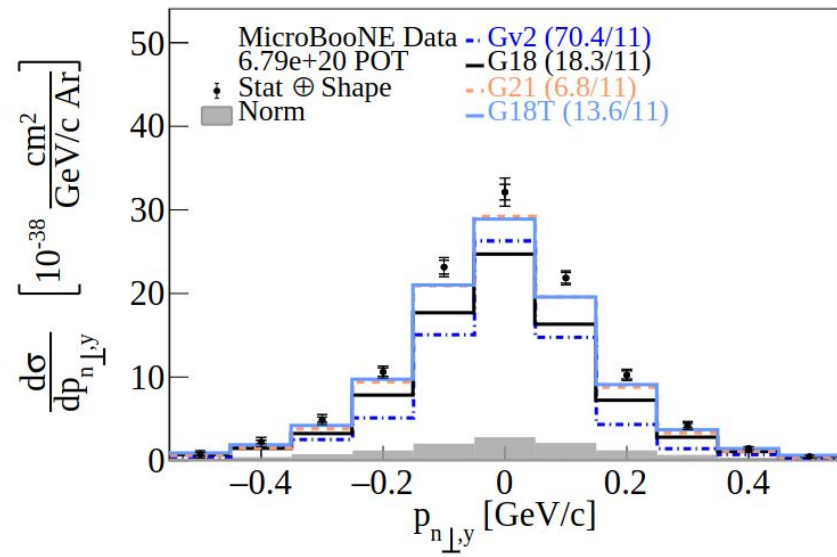
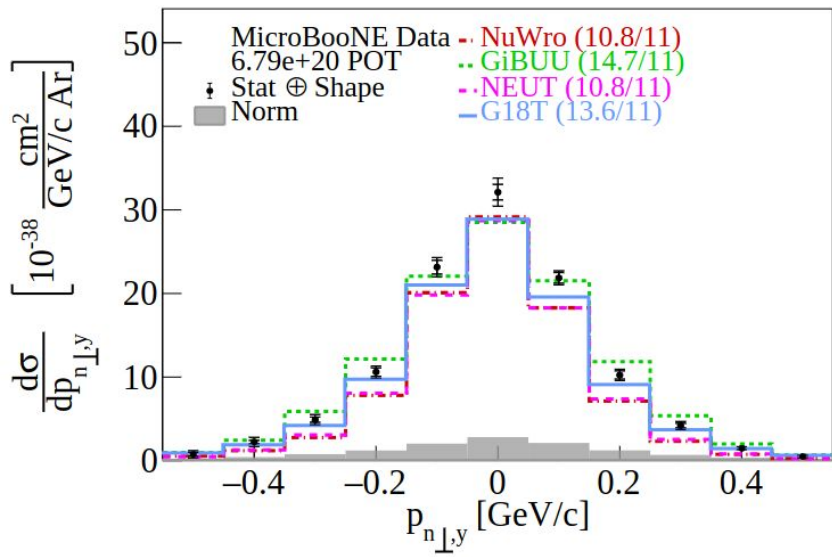


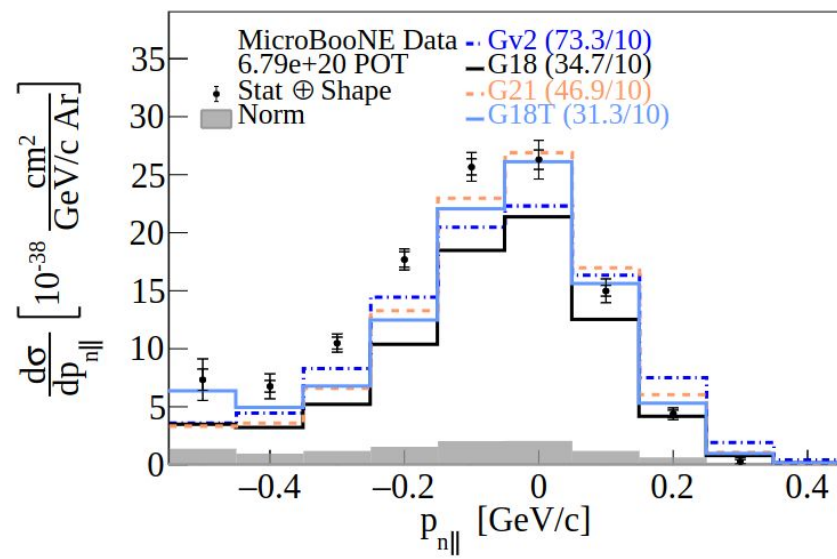
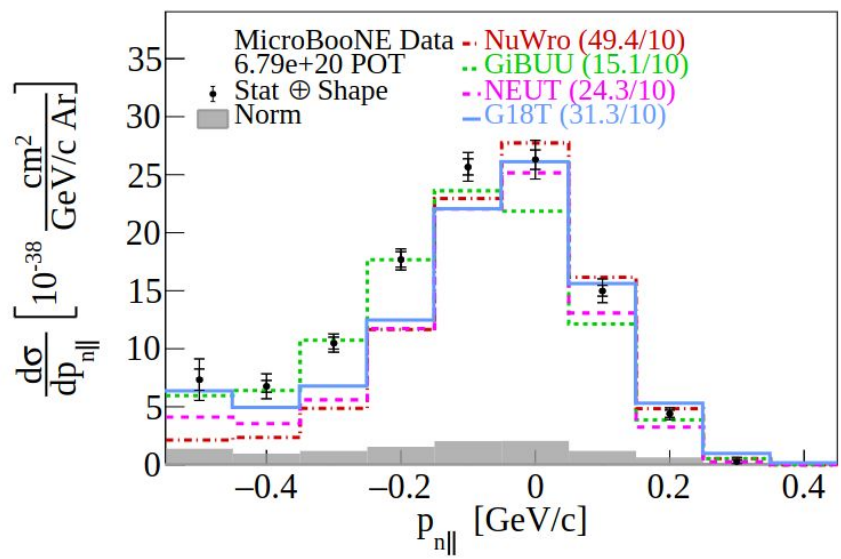




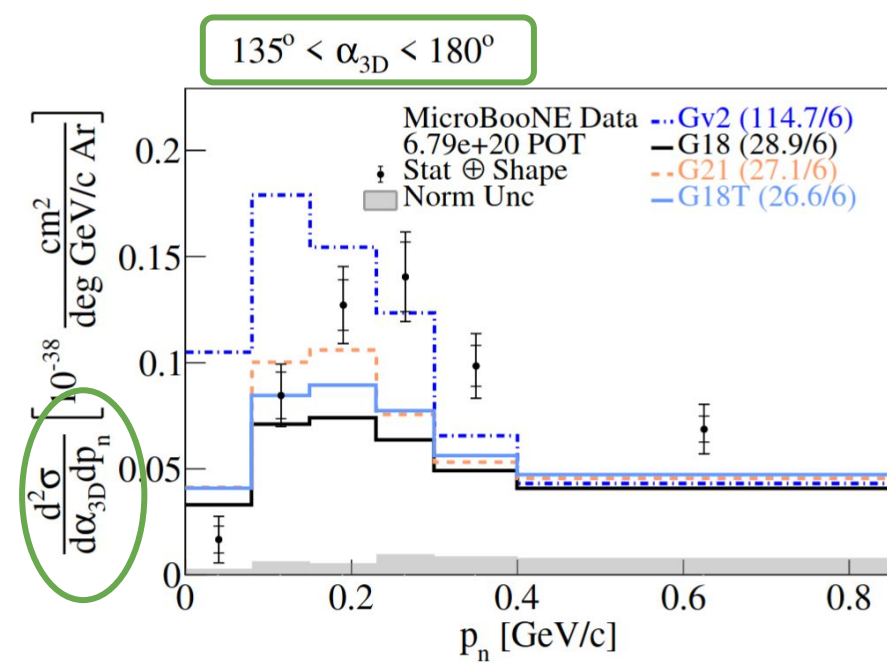
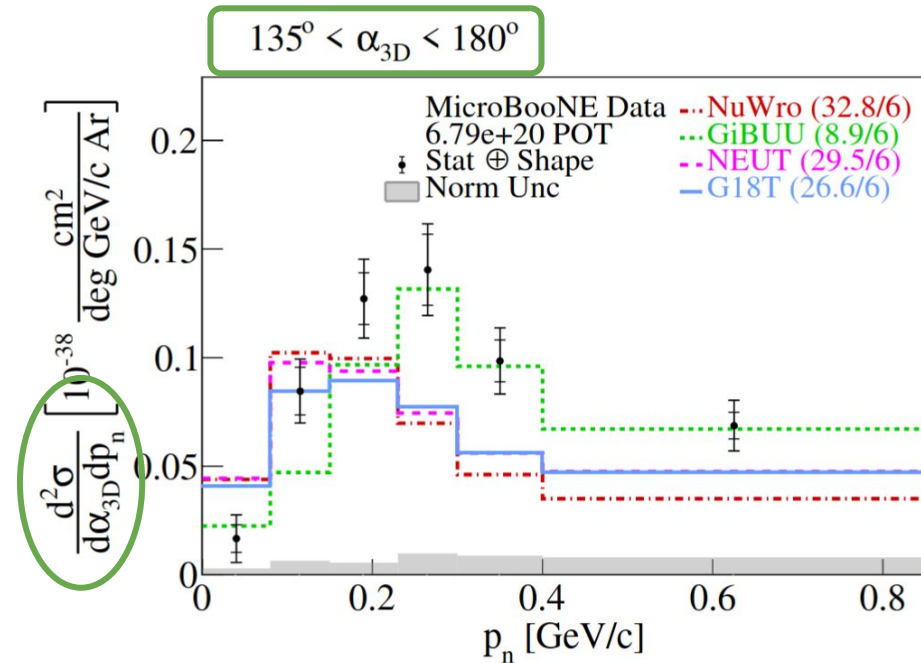








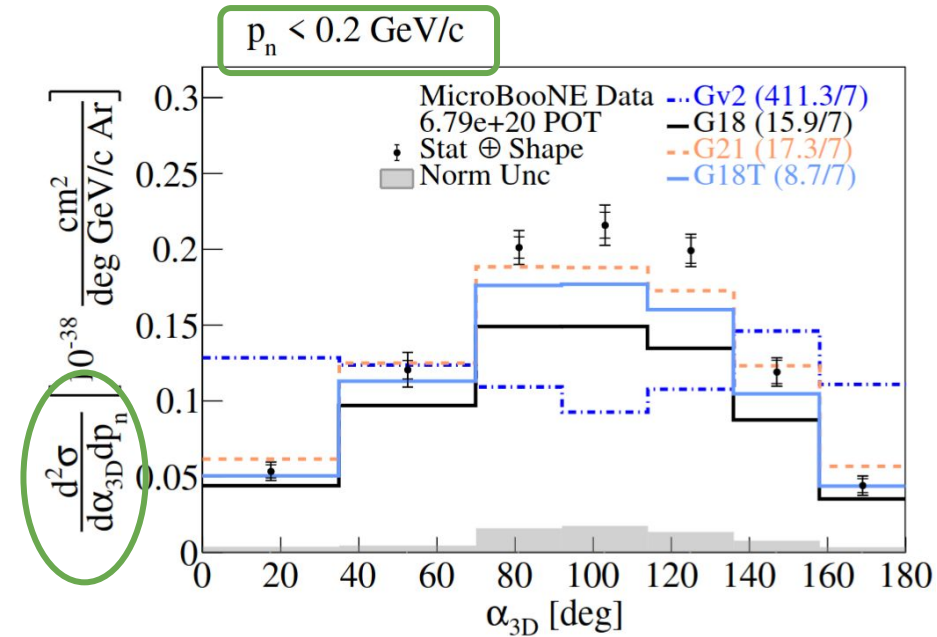
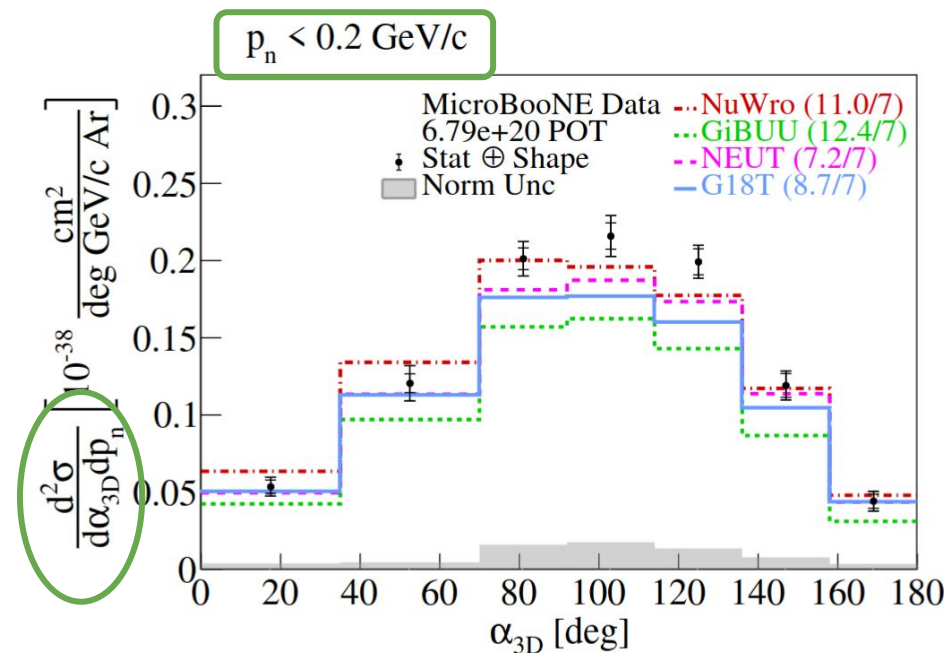
# Into the GKI multiverse!



- Extended tail to higher values
- FSI-dominated region

- GiBUU shift to the right, yet lowest  $\chi^2$
- Gv2 yields worst agreement
- Other generators yield comparable ratios

# Into the GKI multiverse!



- QE-dominated region
- Most generators result in comparable results

- **Gv2** yields worst agreement
- **G18T** results in good agreement